

eman ta zabal zazu



Universidad
del País Vasco

Euskal Herriko
Unibertsitatea

**Synthesis of N-glycan mimetics and their evaluation as
C-type lectin receptor (CLR) antagonists using
microarray technology**

Anna Cioce

2018



Synthesis of N-glycan mimetics and their evaluation as
C-type lectin receptor (CLR) antagonists using microarray
technology

Anna Cioce

Glycotechnology Laboratory, CIC BiomaGUNE

2018

The research was carried out within the international training network Immunoshape in the Glycotechnology Laboratory at the Centre for Cooperative Research in Biomaterials, CIC BiomaGUNE, San Sebastián, País Vasco, Spain.

This project received funding from the European Union's Horizon 2020 research and innovation program under the Marie Curie-Sklodowska grant agreement No 642870.

Resumen tesis

Los N-glicanos son una clase de oligosacáridos complejos con un cuerpo común de $\text{Man}\alpha 1-6(\text{Man}\alpha 1-3)\text{Man}\beta 1-4\text{GlcNAc}\beta 1-4\text{GlcNAc}\beta 1$. Estos compuestos están presentes en células y tejidos normalmente unidos a glicoproteínas a través de un enlace N-glicosídico con asparaginas (Asn) en una secuencia Asn-X-Ser/Thr.

Cada N-glicano tiene una forma específica, una orientación en el espacio y una composición química útiles para su reconocimiento por lectinas de tipo C (C-type lectins) de manera altamente específica.

La interacción entre un N-glicano y una lectina está en la base de muchos procesos biológicos tales como la comunicación celular, la migración celular, la regulación de nivel de glicoproteínas y, de manera muy importante, en la base del reconocimiento y la neutralización de patógenos.

Ya que las interacciones glicanos-lectina son muy importantes para el sistema inmunológico, los glicanos se han convertido en una fuente muy apropiada para desarrollar nuevos fármacos. Sin embargo, el uso de N-glicanos naturales como medicamentos presenta algunas limitaciones: por ejemplo son inestables frente a enzimas de degradación endógenas, la preparación de tales estructuras complejas presenta un gran desafío y además, aunque cada lectina muestra alta selectividad para un monosacárido específico terminal del N-glicano, la afinidad entre ellos es muy débil.

Actualmente, para intentar desarrollar fármacos con estructura glicosídica hay dos estrategias: a) modificar la estructura de glicanos naturales para la preparación de nuevos glicomiméticos con una estabilidad y afinidad por lectinas mejoradas; b) preparar estructuras multivalentes de ligandos con tamaño, forma y propiedades físicas adecuadas.

En cualquier caso, la preparación de nuevos glicomiméticos o estructuras multivalentes exige mucho trabajo de síntesis debido a las numerosas reacciones de protección/desprotección y largos pasos de purificación requeridos; Además, las técnicas de rutina para el estudio de la interacción glicano-lectina como XPS, ELISA (enzyme-linked immunosorbent assay), SPR (surface plasmon resonance) y otros, necesitan elevada cantidad de compuesto y de proteína.

En el desarrollo de nuevos ligandos para lectinas de tipo C, los microarrays de carbohidratos se están convirtiendo en una técnica consolidada tanto para analizar

interacciones glicano-proteína como para sintetizar, a través de reacciones químicas y/o enzimáticas, nuevos ligandos con afinidades mejoradas por las lectinas.

Los microarrays son una novedosa tecnología que consiste en el uso de una superficie, debidamente funcionalizada, sobre la cual es posible inmovilizar un gran número de muestras en cantidades muy pequeñas (nano litros) y luego realizar reacciones o análisis biológicos. Como resultado es posible preparar en paralelo un gran número de nuevos ligandos y después evaluar su interacción con lectinas. Además la limpieza de la superficie después de los ensayos con proteínas y/o modificaciones químico-enzimáticas se realiza a través de un simple lavado con una disolución acuosa adecuada. Este conjunto de características hace de los microarrays una técnica sencilla que se puede utilizar para múltiples objetivos con ahorro de tiempo y de muestra.

En esta tesis doctoral vamos a producir una superficie hidrofóbica novedosa sobre la que se pueden realizar análisis de fluorescencia, con la ayuda de lectinas marcadas con sonda fluorescente, y además analizar a través espectroscopia de MALDI-TOF la masa de los compuestos unidos sobre la superficie tras cada modificación realizada.; La posibilidad de usar diferentes métodos de detección sobre una superficie de microarray implica también una ventaja importante.

Aunque entre los distintos tipos de superficies que se han desarrollado en las últimas décadas hay pocas que admiten el uso de MALDI-TOF la posibilidad de efectuar el análisis de masas es muy importante sobre todo cuando se van a modificar compuestos sobre la superficie. Conocer la composición química real después de una reacción ayuda a mejorar el rendimiento de la reacción misma así como a evaluar la formación de eventuales subproductos.

Por otro lado, el uso de una superficie hidrofóbica tiene la desventaja de no ser tan estable cuando se usan los disolventes orgánicos y/o detergentes normalmente usados en los procesos de limpieza o cuando precipita una proteína o un reactivo sobre la superficie. Este inconvenientes se han solucionado a través de la reducción del tiempo de reacción sin sacrificar el rendimiento, y disminuyendo el porcentaje de disolvente orgánico en las disoluciones de lavado.

La primera parte de esta tesis se ha centrado en el uso de una superficie hidrofóbica activada con un grupo N-Hidroxisuccinimídico, para la inmovilización de distintos

N-glicanos. Estos sustratos fueron modificados a través de reacciones químico-enzimáticas para la preparación de una librería ampliada de glicomiméticos.

El primer paso para la preparación de glicomiméticos sobre una superficie de microarray, consiste en una reacción enzimática con el uso de la enzima doble mutante de la galactosiltransferasa para instalar residuos de azido-N-acetilgalactosamina sobre antenas de N-acetilglucosamina a través de un enlace β -1,4-glicosídico.

Una vez que se ha introducido la función azida en cada N-glicano, se va a realizar una reacción de CuAAC (Copper-(I) catalyzed Azide Alkyne cycloaddition), también llamada “click chemistry”, con diferentes alquinos terminales.

Para cada modificación sobre los N-glicanos inmovilizados, se ha realizado el análisis de masas a través MALDI-Tof para estimar el rendimiento de la reacción y comprobar la composición química de los compuestos sintetizados. El análisis de masas ha sido útil para excluir de la estrategia a aquellos alquinos que reaccionan con rendimiento demasiado bajo o que forman subproductos.

A final, se ha probado la nueva librería de glicomiméticos en ensayos de interacción con distintas lectinas de tipo C para encontrar los mejores ligandos para cada proteína y al mismo tiempo evaluar como las modificaciones sobre una pequeña porción del N-glicano pueden afectar, de manera positiva o negativa, su interacción con la proteína. Este tipo de test ha sido hecho empleando espectroscopía de fluorescencia mediante el marcaje directo de la proteína con sonda fluorescente.

Como resultado importante, en los ensayos biológicos sobre la librería de nuevos glicomiméticos se observó que es posible influir sobre la interacción de cada ligando con una lectina a través de la modificación de su epítipo o de aquellos monosacáridos que se encuentran en la proximidad del mismo.

La segunda parte de esta tesis se enfocó en el uso de la misma superficie hidrofóbica para la preparación, sobre ella glicodendrones de diferente valencia. El objetivo de este proyecto fue evaluar de qué manera el número de ligandos y su presentación sobre la superficie pueden influir en la interacción ligando-lectina.

En principio, los dendrones de ciclooctino con distinta valencia, se sintetizaron en el IIQ-CSIC en Seville por Antonio Di Maio, un estudiante de doctorado del grupo del Dr. Javier Rojo.

Esos dendrones se inmovilizaron sobre la superficie hidrofóbica para la preparación de arrays estando caracterizados por distintos números de residuo de ciclooctinos y diferentes presentaciones en el espacio.

Los arrays de ciclooctino fueron usados para realizar reacciones de cicloadición libre de metal (Strain-Promoted Alkyne Azide Cycloaddition, SPAAC) con glicanos funcionalizados con un brazo azido. En principio se utilizaron glicanos simples para establecer las condiciones óptimas de reacción y luego el procedimiento se extendió a estructuras glicomiméticas más complejas preparadas en el laboratorio de la profesora Anna Bernardi de la Universidad de Milán.

Los glicodendrones preparados sobre la superficie con una cantidad muy pequeña de reactivos, se probaron en ensayos de interacción con distintas lectinas de tipo C marcadas con sonda fluorescente. Como resultado se observó que, en general, la señal fluorescente aumentaba al aumentar de número de ligandos sobre el array. Esta tendencia no se logra para todos los ligandos ya que para alguno no se observó ningún efecto relacionado con el aumento de valencia. Estos resultados demuestran que el solo aumento del número de ligandos no es suficiente para mejorar la interacción con la proteína ya que otros elementos, como la forma de presentación, la movilidad del ligando y su accesibilidad estérica para interactuar con la proteína etc., contribuyen también en la interacción.

La tercera parte de esta tesis propone, en principio, la síntesis de la estructura de la glucosamina simple y de la glucosamina con un grupo de fosforilcolina unida al carbono C6, ambas funcionalizadas con un brazo amino. Con estos compuestos, a través de la activación con grupo N-Hidroxisuccinimídico, se han preparado glicoconjugados con la proteína antigénica ovoalbúmina (OVA) con distinto número de ligandos pegados sobre su superficie.

La fosforilcolina (PC) es un componente abundante en las células eucariotas donde se encuentra formando parte de los fosfolípidos, fosfatidilcolina y esfingomiélin. En ciertas bacterias, hongos e invertebrados inferiores, incluidos los nematodos filariales, se ha encontrado PC asociada de manera diferente, específicamente a los carbohidratos (glicoproteínas o glicolípidos). Los estudios con parásitos que emplean moléculas que contienen PC indican que este grupo funcional posee una gran cantidad de actividades inmunomoduladoras que podrían ser beneficiosas para ambos, para el parásito al promover su supervivencia, y para el organismo anfitrión, al limitar la patología.

Todo eso hace que los derivados de fosforilcolina sean muy interesantes para la manipulación de respuestas inmunes en el tratamiento de enfermedades autoinmunes. Sin embargo, el hecho de que la PC parece tener una gran cantidad de actividades inmunomoduladoras, algunas de las cuales parecen ser pro-inflamatorias, sugiere que se debe realizar mucha más investigación sobre esta molécula antes de considerar su uso terapéutico.

Un primer objetivo de este proyecto ha sido la evaluación, a través de ensayos de captación directa de glicoconjugados de OVA en células dendríticas (CDs) de origen murino, del efecto de la fosforilcolina para mejorar la captación de la glicoproteína en la célula dendrítica. Este ensayo se hizo a través de la cuantificación del marcador CD11c por citometría de flujo.

En estos ensayos se observó como la presencia de un grupo de fosforilcolina, así como el aumento del número de ligandos unidos a la ovoalbúmina, no contribuyen a lograr una internalización más efectiva de la OVA en la célula.

Paralelamente a este estudio, los glicoconjugados de glucosamina simple y de glucosamina funcionalizada con fosforilcolina se ensayaron en un co-cultivo de CDs y linfocitos T, para evaluar la activación de las células dendríticas y su posterior diferenciación en células efectoras. Esto se hizo a través de la cuantificación del marcador CD69 por citometría de flujo y de la expresión de interleuquina 2 (IL-2) e interferón gamma (IFN γ) mediante ELISA. En estos experimentos tampoco se observó, ningún tipo de diferencia entre los glicoconjugados con OVA.

Por lo tanto, desde estos ensayos preliminares, parece que la presencia de un grupo de fosforilcolina, sobre un pequeño y simple glicano unido a una OVA, no tiene ningún efecto ni sobre el proceso de internalización en las células dendríticas ni sobre la activación de los linfocitos T.

Sin embargo, merece la pena continuar el estudio de este tipo de grupo funcional que ha demostrado ser un valioso inmunomodulador. Alternativamente, se puede intentar introducirlo sobre otro tipo de glicanos y/o proteínas y, al mismo tiempo, explorar otra tipología de ensayos biológicos para evaluar mejor su función en el sistema inmunitario.

List of abbreviations

AAL	Auleria Aurantia Lectin
AcCN	Acetonitrile
Ac₂O	Acetic anhydride
Asn	Asparagine
Asp	Aspartic acid
b	broad
Bis-MPA	2,2-Bis(hydroxymethyl)propionic acid
BF₃OEt₂	Boron trifluoride diethyl etherate
BCN-cyclooctyne	(<i>N</i> -[(1 <i>R</i> ,8 <i>S</i> ,9 <i>S</i>)-Bicyclo[6.1.0]non-4-yn-9-ylmethoxy carbonyl]-1,8-diamino3,6-dioxa-octane)
Brine	Saturated solution of sodium chloride
BSA	Bovine serum albumin
BuOH	Buthanol
ConA	Concanavalin A
CRD	Carbohydrate Recognition Domain
CuAAC	Copper(I)-catalyzed Azide Alkyne cycloaddition
δ	Chemical shift
d	doublet
DAMPs	Damage Associated Molecular Patterns
DCM	Methylene chloride
DC SIGN (R)	Dendritic Cell Specific Intercellular adhesion molecule-3-Grabbing Non Integrin (R)
DCs	Dendritic Cells
dd	doublet of doublets
DHB	2,5-Dihydroxybenzoic acid
DIPEA	4-(Dimethylamino)pyridine
DMF	Dimethylformamide
DMSO	Dimethyl sulfoxide
DOL	Degree of labelling
DSC	<i>N,N'</i> -Disuccinimidyl carbonate
DSS	Disuccinimidyl suberate
ECD	Extracellular domain
EDTA	Ethylenediaminetetraacetic acid
eq	equivalent

List of abbreviations

Et₂O	Diethyl ether
EtOAc	Ethyl acetate
EtOH	Ethanol
EtSH	Ethanethiol
FACS	Fluorescence-activated cell sorting
FBS	Fetal Bovine Serum
FS	Forward Scatter
GBP	Glycan Binding protein
Glu	Glucose
Gal	Galactose
GalNac	N-Acetylgalactosamine
GlcNAc	N-Acetylglucosamine
GM-CSF	Granulocyte-macrophage colony-stimulating factor
HEPES	4-(2-hydroxyethyl)-1-piperazineethansulfonic acid
hMBL	<i>human</i> Mannose Binding Lectin
IMDM	Iscove's Modified Dulbecco's medium
IPTG	Isopropyl-β-D-1-thiogalattopyranoside
ITO	Indium tin oxide
<i>J</i>	Coupling constant
<i>m</i>	multiplet
MALDI	Matrix Assisted Laser Desorption Ionization
Man	Mannose
MeOH	Methanol
MGL	Macrophage Galactose Lectin
MS	Mass Spectroscopy
<i>m/z</i>	mass to charge ratio
NaOMe	Sodium methoxide
<i>nd</i>	not detected
NHS	<i>N</i> -Hydroxysuccinimide
NIS	<i>N</i> -iodosuccinimide
NMe₃	Trimethylamine
ODPA	Octadecylphosphonic acid
OVA	Ovalbumin
PA-I	<i>Pseudomonas aeruginosa</i>
PAMAM	Polyamidoamine

List of abbreviations

PAMPs	Pathogen Associated Molecular Patterns
Pen/Strep	Penicillin Streptomycin
Phth	Phthalimide
PMSF	Phenylmethylsulfonyl fluoride
ppm	parts per million
PPRs	Pattern recognition receptors
SAMDI	Self-Assembled Monolayer Desorption Ionization
SBA	Soybean agglutinin
Ser	Serine
SS	Side Scatter
SPAAC	Strain-Promoted Alkyne Azide Cycloaddition
t	triplet
TBAF	Tetrabutylammonium fluoride
TBDPSCI	<i>tert</i> -butyl(chloro)diphenylsilane
<i>t</i>-BuOOH	<i>tert</i> -Butyl hydroperoxide
THPTA	Tris(3-hydroxypropyltriazolylmethyl)amine
Thr	Threonine
TEA	Triethylamine
TFA	Trifluoroacetic acid
TfOH	Triflic acid
THF	Tetrahydrofuran
TMSOTf	Trimethylsilyl trifluoromethanesulphonate
TOF	Time-of-flight
Tris-HCl	Tris(hydroxymethyl)aminomethane hydrochloride
WFA	Wisteria floribunda agglutinin
WGA	Wheat Germ Agglutinin

Table of contents

1. Introduction.....	1
1.1 Human Immune System.....	1
1.2 C-type lectins.....	5
1.2.1 Mannose-type lectins (EPN-sequence).....	8
1.2.2 Galactose-type lectin (QPD-sequence).....	10
1.3 Carbohydrates lead for drug development.....	11
1.3.1 Glycomimetics.....	11
1.3.2 Multivalence.....	15
1.4 Carbohydrate microarrays technology in carbohydrate-lectin binding assays....	20
1.4.1 Fabrication of carbohydrate microarrays.....	22
1.4.3 Carbohydrates' presentation and effect of the epitope density on microarray-based binding events.....	25
1.5 Further carbohydrate microarrays applications.....	28
1.5.1 Assessment of enzymes specificity.....	28
1.5.2 Carbohydrate microarrays as synthetic tool for the preparation of novel ligands.....	29
2. Objectives.....	43
3. On-chip chemo-enzymatic synthesis of a N-glycan mimetics library.....	47
3.1 Development of NHS-activated hydrophobic ITO (Indium-Tin Oxide)-coated glass slide.....	51
3.1.1 ITO-glass slide modification with phosphonate-based hydrophobic monolayer.....	52
3.1.2 NHS-activation of hydrophobic ITO surface with linker 1 and linker 2.....	53
3.1.3 Optimized procedure to NHS-activation of hydrophobic ITO surface with linker 2.....	54
3.1.4 Surface characterization by contact angle measurement.....	55
3.2 N-glycans immobilization on NHS-activated ITO surface.....	56
3.3 On-chip enzymatic elongation with azido-N-acetyl-D-galactosamine and double mutant of β -1,4-galactosyltransferase I (C342T_Y289L).....	59
3.3.1 Double mutant of β -1,4-galactosyltransferase I (C342T_Y289L) and activity assays.....	59
3.3.2 Optimization of on-chip enzymatic protocol with DM-GalT1 and UDP-azido-N-acetyl-D-galactosamine.....	61
3.3.3 On-chip enzymatic elongations with UDP-GalNAc and UDP-Gal.....	67
3.4 On-chip Copper(I)-catalyzed Alkyne Azide Cycloaddition (CuAAC) on immobilized azide-N-glycan derivatives.....	68
3.4.1 Optimization of on-chip CuAAC.....	70

Table of contents

3.5	Microarray-based lectin-binding assays of N-glycan mimetics library.....	75
3.5.1	Binding assays with Wisteria Floribunda Agglutinin (WFA).....	76
3.5.2	Binding assays with Macrophage Galactose Lectin ECD (extracellular domain).....	79
3.5.3	Binding assays with Langerin ECD (extracellular domain)	82
3.6	Conclusion.....	85
4.	On-chip synthesis of multivalent constructs to strengthen carbohydrate-lectin binding	93
4.1	Cyclooctyne dendrons immobilization on NHS-activated hydrophobic ITO glass slide.....	96
4.1.1	Surface density quantification of Cyclooctyne-dendrons by MALDI-TOF detection	96
4.1.2	Preliminary glycodendrons binding assays with Concanavalin A (Con A)...	98
4.2	On-chip synthesis of glycondendrons.....	100
4.3	Binding assays with fluorescently labeled lectins	101
4.4	On-Chip synthesis of glycomimetic dendrons and role of ligand presentation in carbohydrate-lectin strength	105
4.4.1	On-chip synthesis of glycomimetic dendrons	107
4.4.2	Glycomimetics dendrons binding assays with plant and human lectins.....	108
4.5	Comparison of glycomimetic binding to tetrameric <i>DC-SIGN</i> on different array formats.....	118
4.6	Conclusion.....	124
5.	Synthesis of phosphorylcholine-containing OVA-glycoproteins for dendritic cells targeting.....	129
5.1	Immunomodulation by Phosphorylcholine	129
5.2	Synthesis of Phosphorylcholine (PC)-based sugars	131
5.3	Synthesis of OVA-based bioconjugates.....	132
5.4	OVA-based glycoproteins in dendritic cells targeting.....	136
5.4.1	Dendritic Cells uptake assays.....	136
5.4.2	In vitro stimulation and DCs/T cells co-culture	139
5.4.3	Enzyme-Linked Immunosorbent Assay (ELISA)	141
5.5	Conclusion.....	142

1. Introduction

1. Introduction

1.1 Human Immune System

Physical and chemical barriers are the first line of defense of the human body against infection.¹ One example of first defense is the skin which prevents access of microbes to the underlying tissue, or the gastric acid in the stomach which can kill many microbes that might be ingested with food. In addition, saliva, mucus and tears contain enzymes able to break down bacterial cell walls.²

When pathogens enter the blood stream, a second line of defense is activated; it is composed by immune cells that destroy or remove unwanted material from the body (*cell-mediated immunity*) and soluble molecules, which eliminate antigen without the need for cellular involvement (*humoral immunity*).

The immune cells responsible for *cell-mediated immunity* are called **leukocytes**, or white blood cells, that reside in tissues and specialized organs; these cells move around the body through blood circulation and a system of interconnected vessels called lymphatic system. On the other side, the soluble molecules responsible for *humoral immunity* are immunoglobulins or **antibodies** that are secreted by a particular type of leukocytes.

Both the production of antibodies and the activation of cell-mediated immune response depend on an elaborate signaling system regulated either by interactions involving leukocytes and other cell types in the body or by small secreted proteins called *cytokines*.²

The mammalian immune system can be classified in two types of immune responses: *innate* and *adaptive*.^{3,4}

Innate immune responses are generally active and can respond to pathogenic threats within minutes or hours. In contrast, the *adaptive immune response* is activated upon serious infection and requires several days to become effective. A major advantage of adaptive immune response is the generation of immune memory, resulting in rapid and more efficient response upon reiterated infection with the pathogen.

➤ The innate immune system

The *innate immune system* is composed of phagocytes like dendritic cells, macrophages and neutrophils that protect the body against infectious or non-infectious status. The innate response can be activated immediately either by recognition of conserved structures on pathogens, called pathogen-associated molecular patterns (PAMPs) or by

recognition of damage-associated molecular patterns (DAMPs), endogenous danger signals that alert the immune system to unscheduled cell death.⁵ (Figure 1.1)

The PAMPs and DAMPS recognition represents the first step of the immune response to promote degradative pathway.⁶

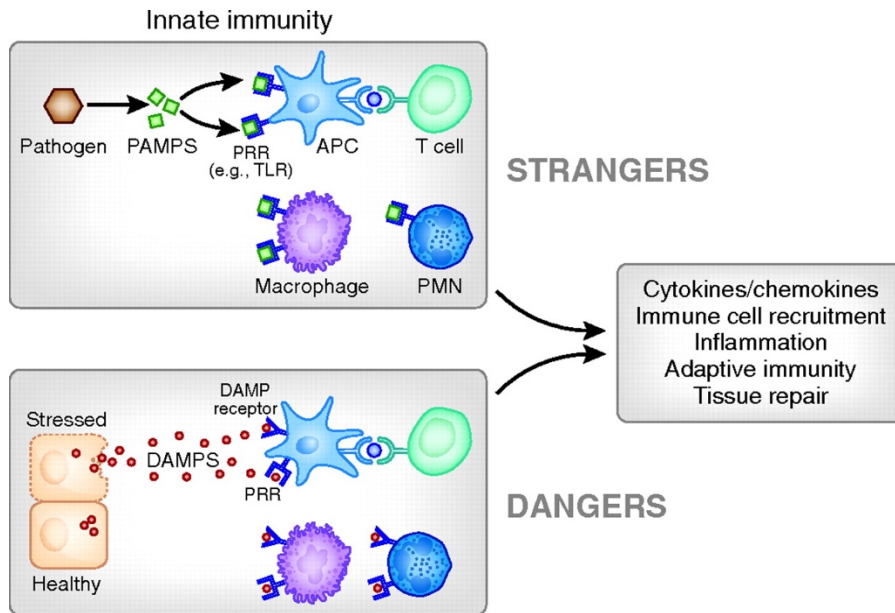


Figure 1.1 Picture taken from *J. Am. Soc. Nephrol.*, 2011.⁷

Professional antigen presenting cells (APCs), like dendritic cells (DCs), bridge both innate and adaptive immune systems since they are able to recognize PAMPs (or DAMPs) and to initiate adaptive immune responses (Figure 1.2).

Immature DCs in peripheral tissue can recognize PAMPs on pathogens (or DAMPS on host cells), via pattern-recognition receptors (PRRs); each PRR recognizes a DAMP or PAMP that is shared by different damaged cells or pathogens thus, PRRs make the innate immune response the feature of broad recognition.

The recognition event is followed by pathogen uptakes and subsequent cellular degradation and presentation of antigenic peptides via MHCs (major histocompatibility complexes). This process causes DCs maturation that undergo to a number of phenotypical and functional changes which include: morphological changes (e.g. formation of dendrites), secretion of chemokines, cytokines and proteases, and surface expression of co-stimulatory molecules.

Mature DCs migrate to the lymph nodes to interact with naïve T cells, through antigen peptide-MHCs, providing T cells activation in different T cell subsets: **cytotoxic T cells** (T_c), that kill infiltrated, cancerous and abnormal cells, and **helper T cells** (T_h) that

1. Introduction

mediate B cells activation in adaptive response. In addition, T-cells activation by DCs require co-stimulation and polarizing signals such as **chemokines** and **cytokines**.⁸

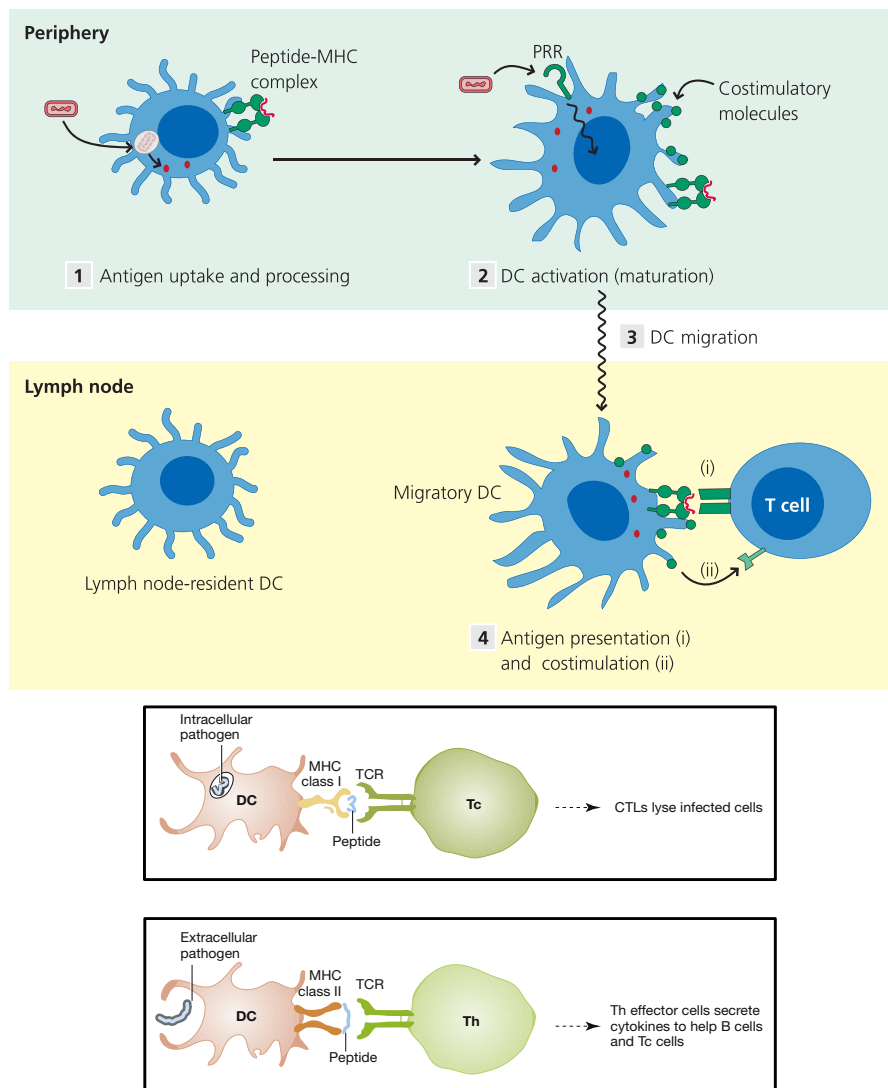


Figure 1.2 Innate immune response mediated by DCs. Picture modified from *Immunol. Concepts Evidence, 2012*.¹

➤ The adaptive immune system

The key components of the *adaptive immune system* are the lymphocytes; these subtypes of leukocytes are divided in two main groups: *T lymphocytes* (T cells) and *B lymphocytes* (B cells).

In contrast to the innate response, the recognition of molecules from infectious agents by lymphocytes is mediated by specialized antigen receptors. An antigen is a molecular structure against which a specific adaptive immune response can be made; the antigens

1. Introduction

are generally unique to particularly infectious agents and each lymphocyte expresses multiple copies of a receptor of only a single given specificity.¹

In the adaptive response, B cell receptors (BCRs) can bind directly to an intact antigen, which may be either a soluble molecule or a molecule attached on a pathogen surface; once the pathogen is recognized, it is internalized, processed and its derived peptides are presented via MHC molecules on B cells surface. To be effectively activated, the B cells need to interact with *helper T cells* (T_h), through MHCs, and receive co-stimulatory signals provided from *cytokines* (**Figure 1.3**).

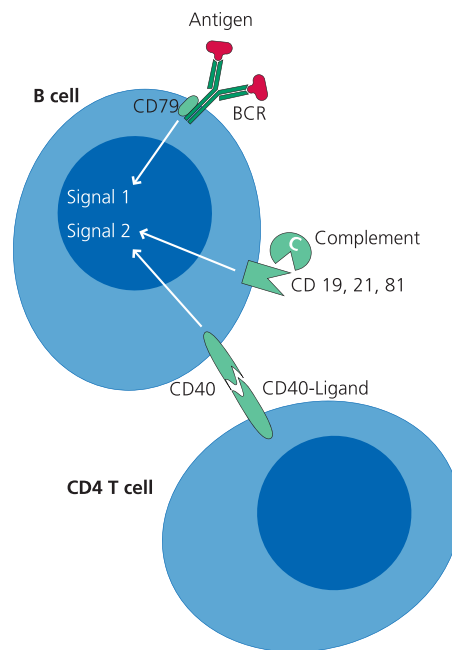


Figure 1.3 The binding between the B cell receptor (BCR) and the antigen (Signal 1) is not normally sufficient to induce full B cells activation; instead they need an additional signal (Signal 2) to provide co-stimulation. Picture modified from *Immunol. Concepts Evidence, 2012*.¹

As results of B cells activation, they proliferate and differentiate in *Plasma cells* and *Memory cells*; while the latter persist in the tissues in a resting mode until a subsequent exposure to the same pathogens, Plasma cells secrete specific antibody molecules. Each antibody has a unique binding site shape which recognizes a specific shape of the antigen thus, when antibodies are released into the host's circulation and tissues, they destroy the antigen (pathogen) which is then engulfed and digested by phagocytes.

1. Introduction

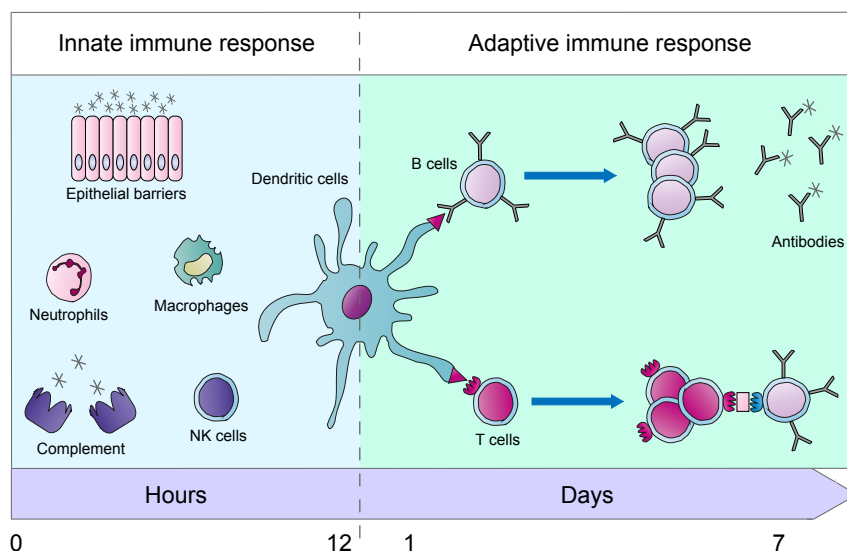


Figure 1.4 General overview of innate and adaptive immunity: *Innate immunity* has low specificity and affinity, but reacts within hours of an infection by the activation of phagocytic cells (macrophages and neutrophils) and natural killer (NK) cells through the recognition of common conserved bacterial and viral components. The *adaptive immune response* develops later upon the activation of T and B lymphocytes by the dendritic cells through antigen presentation on MHC. This process requires more time but results in a specific immune response, where the dendritic cells act as mediators between the innate and the adaptive immune systems; Moreover, the generation of T and B memory cells during adaptive immunity can aid in mounting a rapid immune response upon recurrent infection.

1.2 C-type lectins

Since the surface of nearly every pathogen is covered with glycoproteins or glycolipids, carbohydrates represent an important class of PAMPs.

Recognition of carbohydrate-containing PAMPs (or DAMPs) by DCs, in the innate immune response, is mediated by carbohydrates-binding proteins that function as PRRs; among them, C-type lectins are the most diverse and abundant family of proteins in animals.^{3,9}

C-type lectins contain an independently folding carbohydrate-recognition domain (CRD) that binds sugars in a calcium dependent chelation mode: Calcium crosslinks with conserved amino acids of the protein binding pocket and with the C3 and C4 hydroxyls of hexose units.¹⁰

In addition to the calcium ion complexation, other interactions including hydrogen bonding, hydrophobic C-H \cdots π stacking, van der Waals interactions and ionic interactions

are active. The network of all these interactions possesses all the energetic and geometrical features necessary to make carbohydrate-lectin complex stable; thus, the loss or the exchange of one or more of these interactions can dramatically affect the binding.¹¹

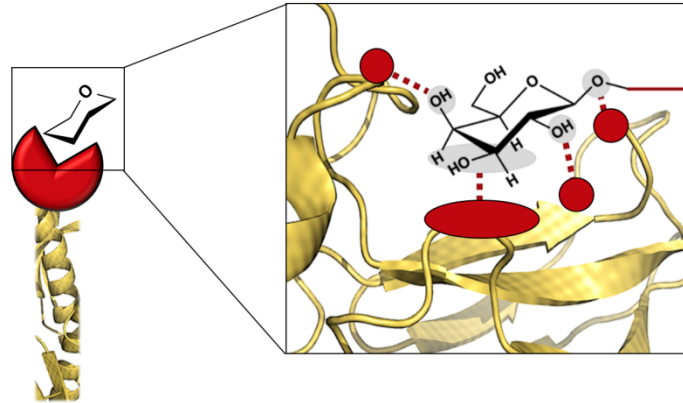


Figure 1.5 Binding of a hexose unit within the binding site of lectin (CRD).

In general, C-type lectins can be divided in two main groups based to amino-acid sequence involved in the sugar recognition and coordination of the Ca^{2+} ion:¹²

- 1) *Mannose-type* lectins, such as DC-SIGN and Langerin, are characterized by amino-acid sequence Glu-Pro-Asn (**EPN**) in the CRD showing specificity for sugars which possess adjacent equatorial C3 and C4 hydroxyl groups as mannose-, glucose- and N-acetylglucosamine-terminated.
- 2) *Galactose-type* lectins, as MGL (Macrophage Galactose Lectin), are characterized by amino-acid sequence Gln-Pro-Asp (**QPD**) in the CRD showing specificity for sugars bearing an axial C4 hydroxyl group like galactose and N-acetyl-D-galactosamine.

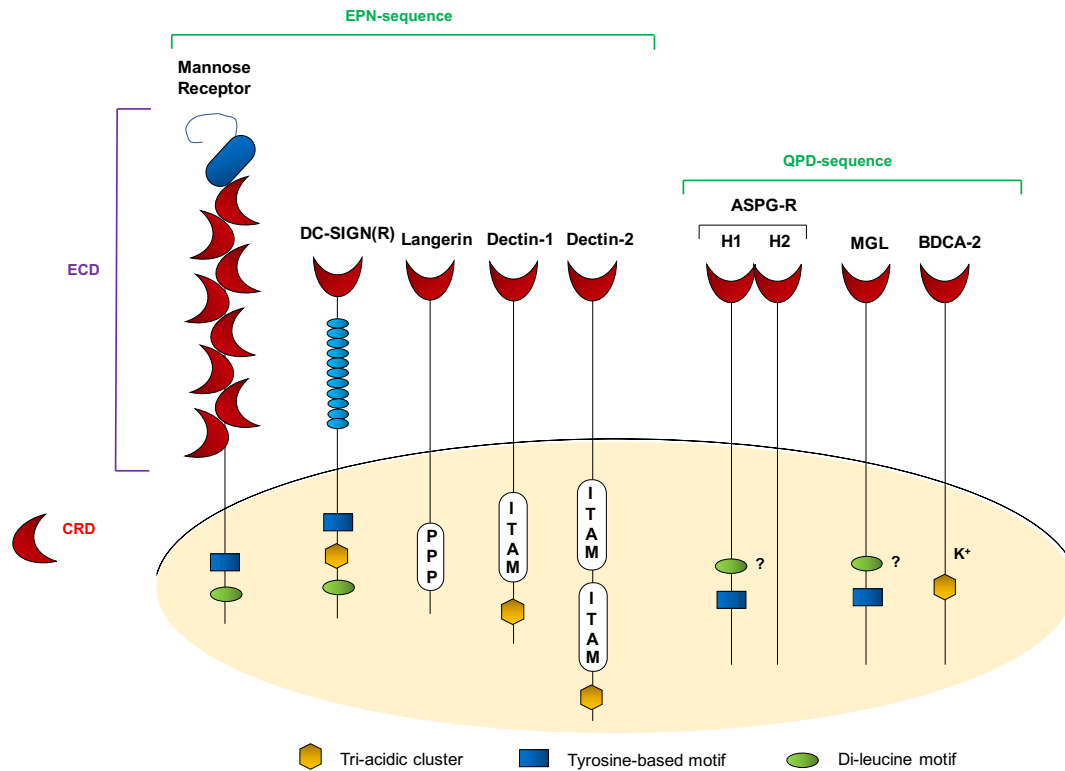


Figure 1.6 Internalization and signaling motifs in human C-type lectin and C-type lectin-like molecules. These motifs are involved in clathrin-mediated endocytosis and/or the subsequent targeting of the cargo antigen. These motifs include the tri-acidic cluster, a tyrosine-based internalization motif, and a di-leucine motif. Only a partial di-leucine motif is present within the cytoplasmic region of MGL. The C-type lectins Dectin-1 and Dectin-2 contain a partial ITAM (immunoreceptor tyrosine-based activation motif) and ITAM-containing signaling molecules such as Fc receptor γ (FcR γ) respectively. Langerin possesses a proline-rich stretch while BDCA-2 a positively charged lysine residue.

In this Figure, the most extensively studied lectins are reported; for clarity, receptors are shown as single molecules, whereas, on the cell membrane, these receptors might be expressed as oligomers. Picture modified from *Trends in Immunology*, 2008.¹³

Although within each group of C-type lectins there is a common mechanism of binding to a monosaccharide residue in a primary binding site, diversity in binding of oligosaccharide and glycoconjugate ligands is achieved; indeed, the presence of extended and secondary binding sites, that are unique to individual lectin, and lectin multimerization adds an additional layer of specificity on carbohydrate-lectin binding.

For instance, mannose-type lectins as DC-SIGN, E-selectin and the macrophage receptor Mincle show quite different oligosaccharide binding profiles despite all of them are classified as mannose specific lectins ; in particular, DC-SIGN is able to interact with

Le^x structures while E-selectin and Mincle accommodate, in secondary binding site, non-sugar substituents as sulfate groups and hydrophobic acyl chains respectively (Figure 1.7).¹⁴

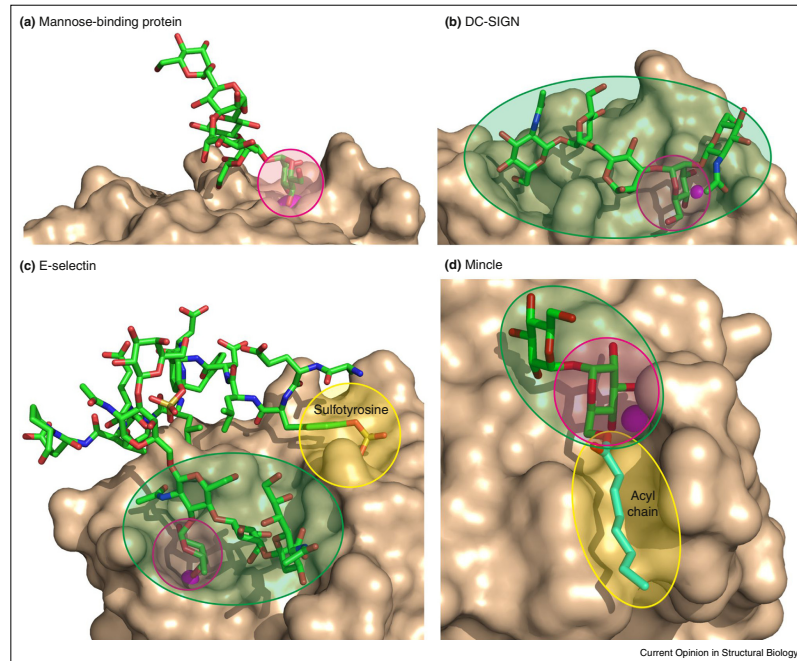


Figure 1.7 Binding specificity of CRDs toward oligosaccharides: primary binding sites are shown in magenta while extended oligosaccharide- and accessory-binding sites are in green and yellow respectively. Picture taken from *Current opinion in structural biology*, 2014.¹⁵

1.2.1 Mannose-type lectins (EPN-sequence)

1.2.1.1 DC-SIGN and DC-SIGNR

DC-SIGN and L-SIGN (also called DC-SIGNR) are type II trans-membrane proteins organized into tetramers that share 77% amino acid sequence identity;¹⁵ both DC-SIGN and DC-SIGNR are composed of a short cytoplasmic tail, which is responsible for signaling and internalization, a transmembrane region, a neck domain, which consists of eight repeat regions of 23 amino acids, and a carbohydrate recognition domain that bind ligands bearing mannose and related sugars through the CRDs.

The CRDs of DC-SIGN and DC-SIGNR specifically bind Man₉GlcNAc₂ oligosaccharide 130- and 17-fold respectively more tightly than the single mannose, and the affinity for a glycopeptide bearings two such oligosaccharides is increased by a further factor of 5- to 25-fold. Both DC-SIGN and DC-SIGNR interact with glucose and GlcNAc more weakly than they interact with mannose; in addition, DC-SIGN has higher affinity for L-fucose than for mannose whereas DC-SIGNR has higher affinity for mannose than for

L-fucose.¹⁶

DC-SIGN/DC-SIGNR has been shown to mediate interactions between dendritic cells and T-cells by binding ICAM-3, an intercellular adhesion molecule.¹⁷ Further studies have highlighted the role of DC-SIGN and DC-SIGNR in viral infection; both lectins can bind to the glycans of envelope proteins of HIV, cytomegalovirus (CMV), DENV, WNV, Severe acute respiratory syndrome coronavirus (SARS-CoV), HCV, Ebola virus and MARV facilitating viral entry.¹⁸

1.2.1.2 Langerin

Langerin is a type II transmembrane C-type lectin selectively expressed in Langerhans cells as a trimeric protein and is localized in Birbeck granules (BGs), organelles present in the cytoplasm of Langerhans cells.¹⁹ Langerin is rapidly endocytosed from the cell surface and binds microorganisms carrying mannose-type residues. It is a C-type lectin that recognizes mannose, fucose and N-acetylglucosamine structures and thus Langerhan cells respond to several pathogens as HIV-1,¹⁹ *Mycobacterium leprae*²⁰ and *Candida Albicans*^{21,22} despite the consequence of pathogen recognition by langerin is for most pathogens unknown.²³

Recent data suggest that Langerin is capable of directly capturing HIV-1 and sequentially degrading it in BGs to promote T cells-mediated elimination of HIV-1 infection²⁴

1.2.1.3 Dectin-1 and Dectin-2

Dectin-1 and dectin-2 are type II transmembrane proteins of the C-type lectin family, mainly expressed on dendritic cells and macrophages, with a monomeric recognition domain (CRD) in their extracellular region. Dectin-1 recognizes β -glucans with its CRD and transduces signal through its immune receptor tyrosine-based activation motif (ITAM)-like in the cytoplasmic domain;²⁵ On the other hand, Dectin-2 recognizes α -mannans and transduces its signal through association with the ITAM-containing Fc receptor γ chain (FcR γ).²⁶

Recently, it was reported that Dectin-1 takes an important role in the protection against *Pneumocystis carinii* by inducing cytokines and reactive oxygen species (ROS) to protect hosts from fungal infection, whereas both Dectin-1 and Dectin-2 play important role in defense against pathogenic fungi as *C. albicans* by preferentially inducing T(h)17 cell differentiation.²⁷

1.2.1.4 Mannose-binding lectin (MBL)

Mannose-binding lectin (MBL), one of the most intensively studied lectins, is a member of the collectin family, a subgroup of C-type lectins. The native functional form of MBL is a hexamer; however, although MBL can form several different oligomers, dimers and trimers do not show biological activity, and at least a tetramer is required to activate the complement cascade.²⁸ MBL shows selective and calcium dependent binding to terminal D-mannose, L-fucose and N-acetyl-D-glucosamine;^{29,30} this binding promiscuity permits the protein to interact with a wide selection of viruses, bacteria, yeasts, fungi and protozoa decorated with such sugars.

MBL is a major component of the innate immune system; indeed, it has been suggested that MBL plays an important role in the first hours/days of any primary immune response to a sugar decorated pathogen³¹ providing the host with a first line of defense before the adaptive immune system becomes operative. Moreover, a recent report has indicated that MBL can bind to apoptotic cells and initiate their uptake by macrophages.³²

1.2.2 Galactose-type lectin (QPD-sequence)

1.2.2.1 Macrophage Galactose Lectin (MGL)

Galactose-type lectins, of which only macrophage galactose-type lectin (MGL) is found within the immune system, have been less studied than the mannose-type lectins.

MGL is exclusively expressed as a homo-oligomer on myeloid antigen presenting cells (APCs), such as dendritic cells (DCs) and macrophages. Its recognition profile is still under debate and has led to some controversy; indeed, early studies with purified human MGL from transfectants suggested a rather broad specificity including binding to galactose, GalNAc, and fucose containing glycans.³³ By contrast, later studies with recombinant MGL suggested a more restricted specificity limited to GalNAc only.³⁴

Further experiments have confirmed that MGL displays an exclusive specificity for terminal α - and β -linked GalNAc residues which are revealed on the tumor-associated mucin MUC1 and CD45 on effector T cells. These findings implicate MGL in the discrimination between healthy and tumor tissue and homeostatic control of adaptive immunity.⁵

1.3 Carbohydrate lead for drug development

Carbohydrates are ubiquitous and important biomolecules since they form the structural framework of cells and tissues.

Carbohydrates are presents, mainly linked to proteins or lipids, on cell surface of nearly every cell ranging from bacteria to mammalian cells; their interactions with C-type lectins play crucial roles in multiple biological processes including immunity, homeostasis, cellular communication, cell migration and the regulation of serum glycoprotein levels.³⁵ In addition, the glycosylation pattern of a cell is a code of cellular physiology, thus changes in glycosylation are often a hallmark of disease state.³⁶

The set of all these biological phenomena related to carbohydrate-lectin interactions, make carbohydrates an attractive supply of novel therapeutics in drugs discovery.

Unfortunately, natural carbohydrate structures often do not make good therapeutics due to a variety of reasons like their tendency to be degraded by digestive, plasma and cellular glycosidases, and their usually low binding affinity for C-type lectins.

Indeed, the K_D values are generally ranging between 1-0.1 mM,³⁷ although there are exceptions: for example, the *Griffonia simplicifolia* lectin GS-IV has been reported to bind the Lewis B antigen with a K_D value of 24 μ M,³⁸ the anti-Salmonella O-antigen monoclonal antibody Se155-4 binds the trisaccharide $\text{Abe}\alpha 1,3(\text{Gal}\beta 1,2)\text{Man}\alpha\text{OMe}$ with a K_D value of 15 μ M,³⁹ etc.

In general, the weakness observed in carbohydrate-lectin interactions can be related to different causes as: competition between bulky solvent and the ligand to form hydrogen bonds network with binding site, lack of hydrophobic groups in sugar which are often dominant in high-affinity interactions, loss of entropy into the binding pocket that make interactions thermodynamically unfavorable, etc.⁴⁰

Chemical modification and multivalent presentation of carbohydrate scaffolds are the most common approaches adopted to strengthen carbohydrate-lectin binding.

1.3.1 Glycomimetics

Over the years, many research groups have designed and synthesized artificial compounds that are mimetics of carbohydrates associated with important signaling and recognition events but possess improved properties with regard to stability, specificity, affinity and synthetic availability.⁴¹

1. Introduction

The most common approaches adopted to design glycomimetics that mimic the active conformation and function of carbohydrate ligands consist to (Figure 1.8):

- 1) Keep the original glycosidic scaffold, retaining the conformational properties, while removing or replacing unnecessary functional groups. In general, not all the functional groups of a carbohydrate ligand are essential for the interaction with the lectin and replacing hydrophilic groups with hydrophobic ones increase the binding affinity if there is a complementary hydrophobic site in the receptor; moreover, hydrophobic mimetics are less solvated from the water and therefore, once they interact with the receptor, the energy penalty for desolvation is reduced compared to their natural compounds. Regarding the stability, it may be improved by changing the O-linked to C-linked (or S-linked) saccharide, or to O-linked carbocycles.
- 2) Abandon the glycosidic scaffold entirely obtaining non-carbohydrate framework with complete new functional groups while the same orientation in the space of parent structure is maintained.

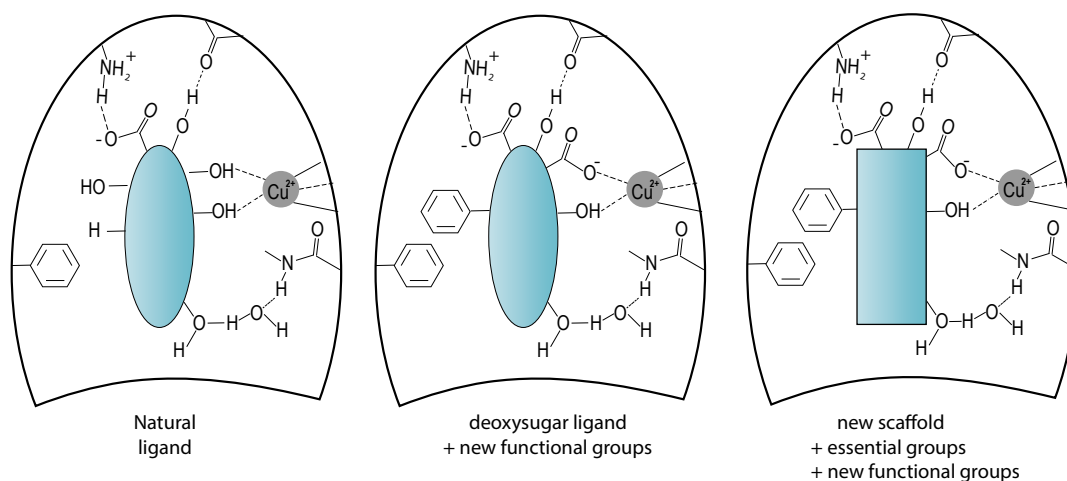


Figure 1.8 Comparison of interaction networks in CRD. *On the left* the interaction between the natural carbohydrate and the protein receptor is reported; in the other diagrams, the natural compound is replaced by mimetic obtained exchanging unnecessary hydroxylic groups with additional functional groups (*in the middle*) or by mimetic made with a non-glycosidic scaffold (*on the right*). Picture modified from *Angew. Chem. Int. Ed.* **1999**.⁴¹

In the last decades, a great effort has been done from several research groups to develop glycomimetics, above all for DC-SIGN targeting; this mannose-binding C-type lectin can promote the dissemination of a number of viruses (e.g. HIV-1, hepatitis C virus, human cytomegalovirus, Dengue virus and Ebola virus)⁴¹ and

participate in suppressing immune response to some pathogens (e.g. *Mycobacterium tuberculosis* and *Helicobacter pylori*),⁴² thus, blocking DC-SIGN function could have many therapeutic benefits.

The main carbohydrate ligand recognized by DC-SIGN is high-mannose glycan ($(Man)_9(GlcNac)_2$), a branched oligosaccharide presented in multiple copies by several pathogen glycoproteins and specifically by the pg120 envelope protein of HIV. DC-SIGN can also recognize branched fucosylated structures bearing terminal galactose residue, such as the Lewis antigens.⁴³

On the base of the high-mannose glycan structure, Bernardi's team⁴⁴ has designed smaller glycomimetic molecules containing conformationally locked cyclohexanediol and spacer arm terminated with azido or amino functionality (Figure 1.9).

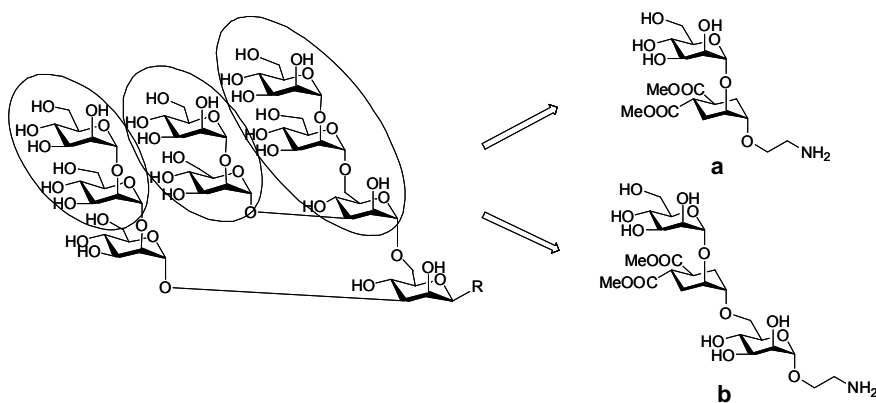


Figure 1.9 Glycomimetics **a** and **b** based on the high-mannose oligosaccharide. Picture taken from *Mini Rev. Med. Chem.* 2012.⁴⁵

The mimetic **a** showed interaction with DC-SIGN and inhibition of Ebola virus entry by DC-SIGN with IC_{50} three times lower compared to the natural $Man\alpha(1,2)Man$ (D2 arm of high-mannose);⁴⁶ on the other side, the pseudo-trisaccharide **b**, mimicking the linear $Man\alpha(1,2)Man\alpha(1,6)Man$ of the D3 arm of high-mannose, inhibits DC-SIGN binding to mannosylated BSA with an IC_{50} values of 130 μM (by SPR).⁴⁷

Although glycomimetics **a** and **b** have shown higher affinity for DC-SIGN compared to their respective natural scaffolds, the binding of these monovalent ligands with DC-SIGN is too weak to represent effective inhibitors for DC-SIGN-mediated infections and their therapeutic potential is limited; appropriate levels of affinity have been obtained when the ligands were presented in a multimeric form.^{48,49}

1. Introduction

Kiessling and coworkers⁵⁰ have developed a solid phase strategy to prepare a library of hundred and diversified non-carbohydrate mannose mimetics that vary at three positions ([Figure 1.10](#)); the approach consists to use shikimic acid as building block and introduce different amino acid and dithiol linkers.⁵¹ Among all the synthesized mimetics, only one compound (**c**) has been selected as promising inhibitor for DC-SIGN which has shown to be 3.5-fold more potent than the natural inhibitor (N-acetylmannosamine). Moreover, a better inhibition property of this glycomimetic has been achieved through the preparation of a multivalent polymer: the polymer bearings 29 copies of the non-carbohydrate inhibitor is 1000-fold more potent than the monovalent inhibitor.⁵²

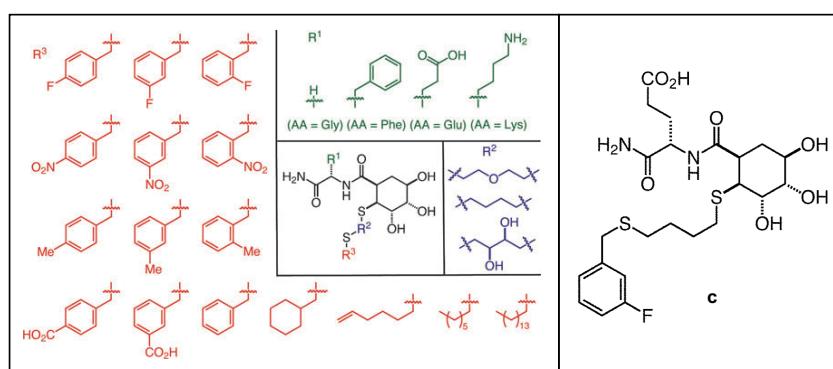


Figure 1.10 Features of the glycomimetic library targeting DC-SIGN and the most potent non-carbohydrate inhibitor (**c**) identified from library screen. Picture taken from *Chem. Commun.*, 2010.⁵¹

More recently, Anderluh and co-workers⁵³ have designed a series of D-mannose-based DC-SIGN antagonists bearing different aryl moieties on glycerol or 1,3-diaminopropan-2-ol linker attached to D-mannose in the α configuration ([Figure 1.11](#)).

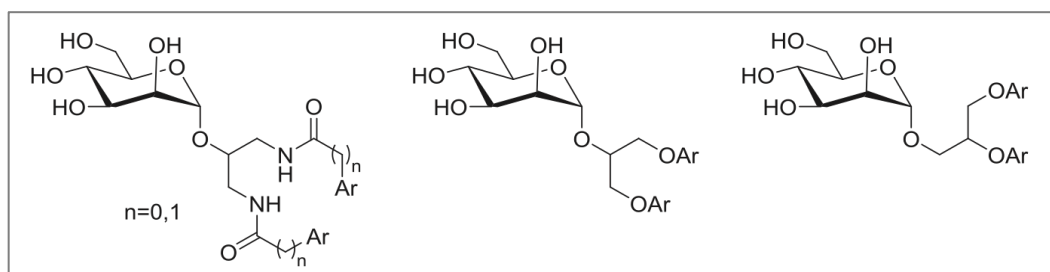
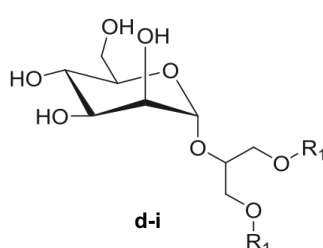
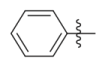
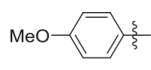
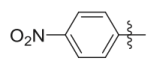
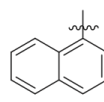
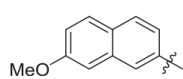
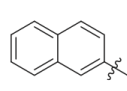


Figure 1.11 Potential D-mannose-based DC-SIGN antagonists bearing aromatic moieties designed to target the hydrophobic groove of DC-SIGN. Picture taken from *J. Med. Chem.*, 2014.⁵⁴

1. Introduction

Screening this library of mimetics in competition assays with HIV-1 gp120 for binding to DC-SIGN, the 1-naphthyl-based compound (**g**) and the 7-methoxy-2-naphthyl-based compound (**h**) have shown the most potent ability to inhibit the binding of HIV-1 gp 120 with IC₅₀ of 40 and 50 μM respectively (Figure 1.12).



R ₁	Compd	^a DC-SIGN IC ₅₀ [mM]
	d	2.41 ± 0.15
	e	5.15 ± 1.72
	f	>0.5
	g	0.04 ± 0.03
	h	0.05 ± 0.01
	i	7.16 ± 0.73
—		

^a IC₅₀ of compounds in the DC-SIGN extracellular domain assay.

Figure 1.12 Picture modified from *J. Med. Chem.*, 2014.⁵⁴

1.3.2 Multivalence

Lectins usually display poor affinities for their monovalent ligands, thus multivalence is largely invoked to improve affinity and selectivity *in vivo*.

Indeed, cell surface normally is covered by a dense and complex coat of carbohydrates, by glycoproteins or glycolipids, fixed in a lipid bilayer (Figure 1.13); the high local concentration of each epitope leads to a multiple ligand presentation that requires a multivalent binding with C-type lectins.¹² On the other side, lectins often oligomerize into homodimers, homotrimers and high-order oligomers, which increase their avidity for multivalent ligands.

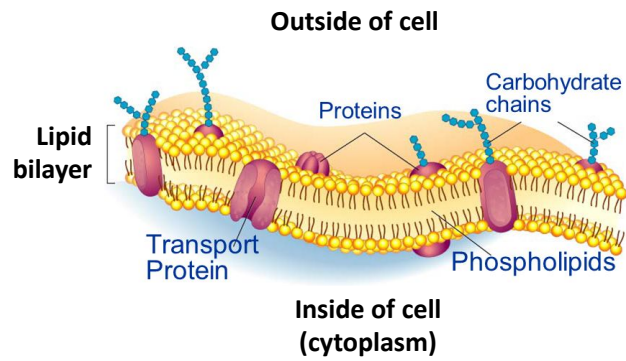


Figure 1.13 Structure of the cell membrane.

In general, the interactions between a multi-glycosylated system and an oligomeric lectin can occur through different mechanisms¹² ([Figure 1.14](#)):

- 1) *Chelate binding*: a series of simultaneous interactions between n receptors of lectin and m copies of ligand of the multi-glycosylated structure.
- 2) *Subside binding*: when lectin interacts with binding partner, a second binding pocket with different affinity and specificity can associate with other sites of the ligand.
- 3) *Receptor clustering*: a phenomenon related to monovalent lectins or ligands anchored to the cell membrane. In presence of a multivalent binding partner, receptors can diffuse through the dynamic lipid bilayer and become clustered by the multivalent ligand.
- 4) *Statistical re-association*: in high density system, the presence of close ligands admits that the dissociation of a single ligand-receptor complex is quickly replaced by another binding event.

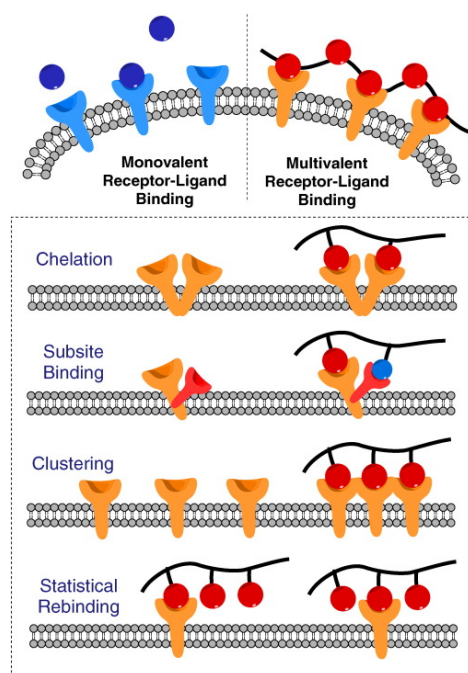


Figure 1.14 Mechanisms of interaction between multivalent ligands and multivalent receptors. Picture taken from *J. Control. Release*, 2015.⁵⁴

Since multivalent carbohydrate-lectin interactions play a decisive role in biological systems for recognition, adhesion, and signal processes, the design and the synthesis of multivalent glycosylated architectures was largely explored in the past decades to improve the targeting of carbohydrate lectin receptors (CLRs).⁵⁵

To design a structure of multivalent ligands, it is important to not only take into account affinity of each ligand to the targeted lectin but also several topologic elements that are crucial in the binding event such as: valence number, nature and length of the spacer arm, geometry of the central core scaffold, etc.^{12,56}

A wide range of multivalent ligand architectures with different size, shape and physical properties have been developed. The most versatile methods for synthesizing multivalent ligands involve the incorporation of carbohydrate ligands to synthetic or natural scaffolds like proteins, synthetic polymer, dendrimers, clusters, solid supports, nanoparticles, etc. (Figure 1.15). For our purposes, we are going to focus our attention only on two types of multivalent systems: protein conjugates and dendrimers/dendrons.

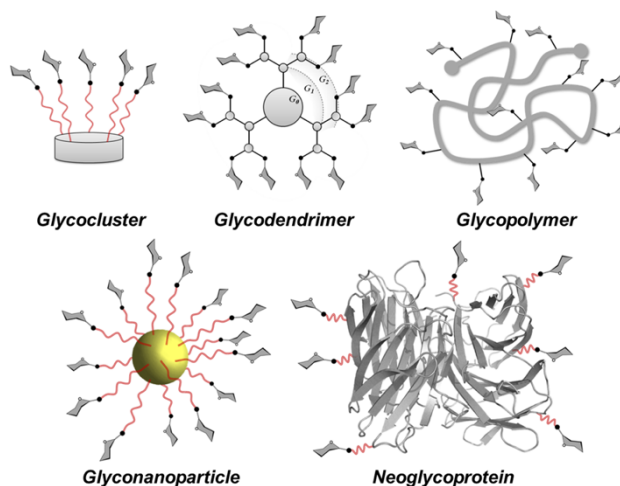


Figure 1.15 Different types of multivalent glycoconjugates. Picture taken from *Chem. Rev.*, 2014.¹²

1.3.2.1 Protein conjugates

Over the years, a large number of synthetic strategies have been adopted to prepare protein conjugates.

The extremely widespread approach consists in a semisynthetic routes that involve incorporation of ligands on well-characterized and readily available carrier proteins such as streptavidin, bovine serum albumin (BSA), Ovalbumin (OVA), human serum albumin (HAS), etc. (Figure 1.16).

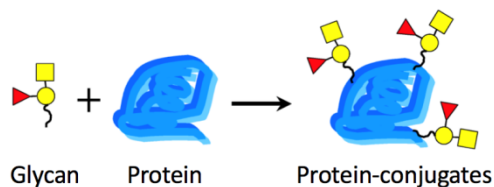


Figure 1.16 Overview of protein-conjugates assembly.

The ligand attachment on the carrier protein is performed by a first activation of ligand with an unnatural and reactive linkage, followed by a second reaction with natural amino acid residues as lysine, cysteine, threonine or serine. N-hydroxysuccinimide⁵⁷- and azide-based⁵⁸ activation are the most common adopted ways to incorporate ligands on protein scaffolds.

In the last decades, an alternative approach that allows to utilize a wide range of chemical handles, coupling patterns and orthogonal conditions has been developed.⁵⁹ It consists to introduce activated ligands on unnatural amino acids (UAAs) previously prepared; among

the natural amino acids, the tyrosine is generally modified due to its phenolic hydroxyl group that possess unique reactivity.

1.3.2.2 Dendrimers and dendrons

Dendrimers are highly branched molecules that consist of three regularly structured regions (Figure 1.17):

- 1) a core or focal point
- 2) layers of branching repeated units, where each layer is called *generation* and typically results from one stage of growth
- 3) end functional groups on the peripheral layer

A dendron represents a small structural component of the dendrimer; in particular, highly branched molecules are called dendrons when they involve to a maximum of three generations (three layers).⁶⁰

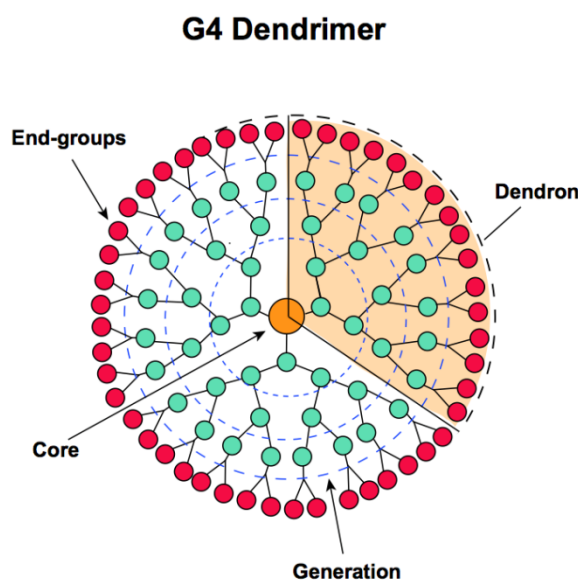


Figure 1.17 Different structural components of the dendrimer.

Dendrimers are fairly homogeneous and their architectural features are defined by the choice of the scaffold and the methods used for their synthesis. For example, Polyamidoamine (PAMAM) dendrimers of generation 0 have diameters of 1.5 nm and valences of four, each increase of generation increases the diameter by 0.7 to 1.6 nm while also doubling the maximum valency. Thus, as the size of the dendrimer increases, so does the ligand density.⁶¹

In general, the synthesis of these complex architectures involves repetitive stepwise

growth and deprotection/activation protocols with careful purification procedures between each generation. Several chemistries have been employed for the synthesis of glycodendrimers as amide, ester, ether bond formation, etc.; recently, copper(I)-catalyzed alkyne-azide cycloaddition (CuAAC) became the most widespread approach for the synthesis of glycodendrimers.^{62,63}

1.4 Carbohydrate microarrays technology in carbohydrate-lectin binding assays

Carbohydrate microarrays consist to a solid surface on which a large number of structurally distinct carbohydrates, derived from either natural or synthetic sources, are immobilized in an orderly manner at specific locations called *spots*; a microarray can contain up to thousands of spots.

Since their advent,⁶⁴ carbohydrate microarrays have shown to be a suitable tool for the elucidation of interactions of different carbohydrate structures with a wide variety of biological targets including antibodies, proteins, viruses and cells. Particularly, plants and human lectins are among the most extensive studied proteins due to their important biological roles.⁶⁵

The most important advantages of carbohydrate arrays technology over conventional approaches, such as enzyme-linked lectin assay (ELISA), surface plasmon resonance (SPR) or isothermal titration calorimetry, are related to the ability to screen several thousand binding events on a single slide and the tiny amounts of both analyte and ligand required for one experiment.

Additionally, since carbohydrates immobilized on a solid surface are displayed in a multivalent manner, by mimicking cellular membrane, they interact strongly with biomolecules that generally have low binding affinities to monovalent carbohydrates in solution phase. As a results, carbohydrate microarrays offer highly sensitive and rapid analysis of carbohydrate-mediated binding events.⁶⁶

1. Introduction

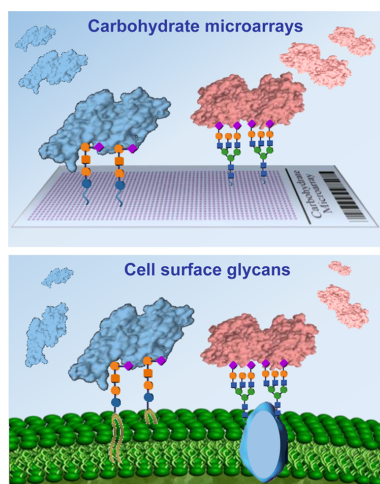


Figure 1.18 Carbohydrates immobilized on a microarray (above) are displayed in a multivalent manner like cell surface carbohydrates (bottom). Picture taken from *Chem. Res.*, 2017.⁶⁷

Over the years, several lectins have been screened on microarrays against a large collection of carbohydrate ligands to determine if a protein recognizes carbohydrates, identify natural ligands, and develop probes/inhibitors to modulate the activity of lectins.

Shin and coworkers have used carbohydrate microarrays containing diversified glycans (mono-, di-, oligo- and polysaccharides) to analyze binding properties of several plant⁶⁸ and mammalian lectins⁶⁹

Feizi and her team have broadly explored the binding properties of large collections of oligosaccharides against Siglec family⁷⁰, novel proteins as *malectin*⁷¹, murine SIGN-R1, SIGN-R3, Langerin,⁷² etc.

In addition, Wong⁷³ has developed a quantitative method to determine surface dissociations constant in carbohydrate-lectin binding events.

Beyond that, further lectins' screening on diversified types of glycan array libraries have been performed, by several research groups worldwide, to provide extensive lectin binding specificity data that are available on Website of the Consortium for Functional Glycomics (www.functionalglycomics.org).

In addition, over the years, microarrays-based technology has been adopted to detect pathogens, to analyze carbohydrate-content on cell membranes and rapidly assess substrate specificities of carbohydrates-processing enzymes. More recently, microarrays have been also employed as synthetic tool for the on-chip preparation of novel ligands (Figure 1.18).^{68,74}

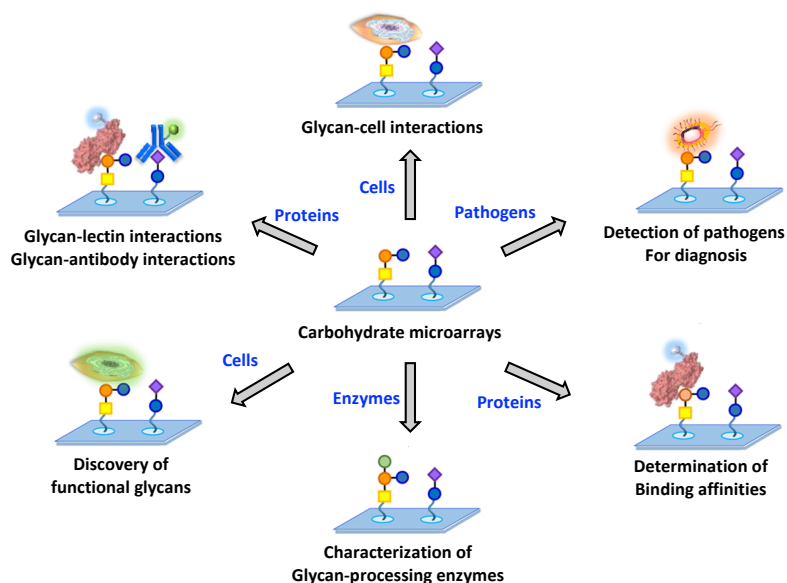


Figure 1.18 Carbohydrate microarrays application. Picture modified from *Chem. Res.*, 2017.⁶⁸

1.4.1 Fabrication of carbohydrate microarrays

Generally, the most commonly employed solid support for the microarray fabrication is the glass microscope slide that has low cost, allows easy manipulation and is compatible with optical detection system. Alternatively, gold, microtiter plates, aluminum, 3D gel beads and nitrocellulose membranes have also been employed as solid material.⁷⁵

Carbohydrates required for immobilization on microarrays are usually either functionalized with a reactive spacer or in free reducing form, in according to the type of activated solid surface and immobilization method adopted.

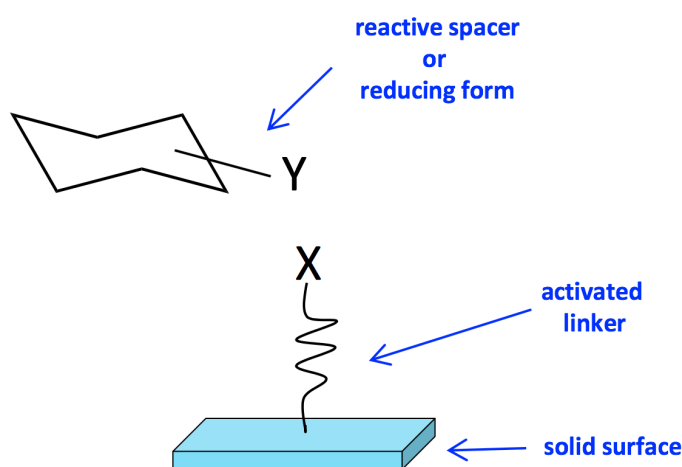


Figure 1.19 Schematic illustration of carbohydrate microarrays

In general, the immobilization strategies could be divided in two main classes: **covalent attachment** and **physical adsorption**.⁷⁶

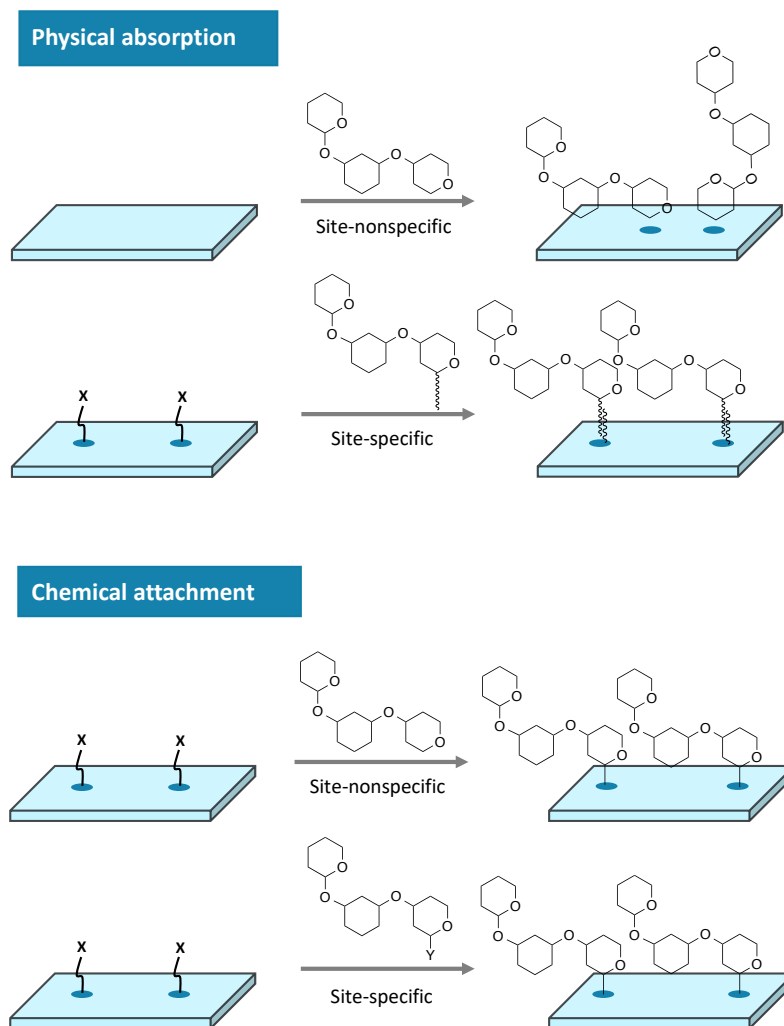


Figure 1.20 Immobilization strategy for construction of carbohydrate microarrays. **(a)** Noncovalent, site-nonspecific attachment of carbohydrate on the surface, **(b)** noncovalent, site-specific attachment of carbohydrate on the surface, **(c)** covalent, site-nonspecific attachment of carbohydrate on the surface, and **(d)** covalent, site-specific attachment of carbohydrate on the surface. Picture modified from *Chem. Soc. Rev.*, 2013.⁶⁷

The *chemical attachment* consists to immobilize carbohydrates onto a properly functionalized solid support through a chemical reaction; the coupling reaction on the activated surface should be fast, specific and high yielding.

The carbohydrate used for this approach can be in free reducing form or modified with a spacer suitable to react with the functionalized surface without interfering with other groups presents on the carbohydrates.

The functional groups of spacers usually include maleimides,⁷⁷ amine,⁷⁸ thiols,⁷⁹

cyclopentadienes⁸⁰ and alkynes⁸¹ that react with complementary activated surfaces; on the other hand, unmodified carbohydrates are able to covalently conjugate to surfaces coated by aryltrifluoromethyldiazirine,⁸² aminoxy⁸³ and hydrazide^{84,85} activated groups.

The *Physical absorption method* consists to immobilize polysaccharides, on surfaces like polystyrene or nitrocellulose coated glass slides, through ionic interactions, hydrogen bonding and hydrophobic interactions. The main advantage of this type of carbohydrate immobilization is that ligands have the ability to move and rearrange as clusters for optimal protein binding without overpass the spots area.

Although the non-covalent attachment has proven to maintain the carbohydrates' antigenic properties against a panel of specific biomolecules, this method led a random orientation of the ligands on the surface and is limited to only oligosaccharide large enough for tight adsorption on the surface (typically 3-2000 KDa); in contrast, this attachment is enable to retain low-mass carbohydrates under washing.⁷⁷

This issue can be overcome by conjugation of small oligosaccharides to a carrier molecule as lipid, protein, polyacrylamide chain or biotin; by adopting this solution, Feizi and co-workers⁸⁶ have conjugated differently sized carbohydrates to lipids in order to generate neoglycolipids with a strong retention on nitrocellulose array.

1.4.2 Detection methods

A variety of methods to detect carbohydrate-proteins binding events or check enzymatic/chemical reaction taking place on carbohydrate microarrays have been largely explored including fluorescence method,⁸⁷ SPR (Surface Plasmon Resonance),⁸⁸ detection of radioactivity,^{89,90,91} electrochemoluminescence,⁹² semiconductor-based electric signal readout,⁹³ mass spectroscopy,⁹⁴ etc. Among the detection methods developed, fluorescence imaging is the most versatile and sensitive approach.

There are many variants of fluorescent detection methods, some examples include the *direct fluorescent labelling* of proteins or the use of *fluorophore-labeled secondary reagents* that bind directly the proteins or that bind tags (e.g. biotin, His tag) attached on the proteins.

Although fluorescent is the most widespread detection method, it presents some limitations; first, fluorescently labelling reactions performed on the lectin can alter activity and selectivity of binding.⁹⁵ Second, the fluorophore-labeled secondary reagents

are not available for many proteins and, in some cases, they can give carbohydrate-binding properties of their own.⁶⁷

A further disadvantage of the fluorescent detection is related to its impossibility to reveal the formation by-products and to calculate the degree of conversion when chemical or enzymatic reactions are performed on the immobilized substrates.

To overcome these issues, advanced array platforms that admit mass surface detection have been recently developed;^{95,96} this approach allows a more detailed quantitative analysis of binding constants together to an *in situ* analysis of substrate-spot composition after performing substrate modification. Moreover, the total absence of labelled probe, fluorescent marker or radiolabel, gives to mass detection a great experimental flexibility. On the other hand, mass spectrometry analysis shows a less sensitivity compared to other detection methods and therefore it requires a higher amount of sample immobilized on the surface.

As emerged, it does not exist the best technique to carry out microarrays detection since each of them presents own limitations; the selection of the detection strategy and thus the array manufacturers is strictly related to the type of assays to perform on the immobilized carbohydrates.

1.4.3 Carbohydrates' presentation and effect of the epitope density on microarray-based binding events

Carbohydrates immobilized on microarrays surface are displayed in multiple copies that strongly interact with oligomeric lectins through a cluster effect; to achieve a multivalent complex, the spacing and the orientation of ligands must match the spacing and the orientation of the binding sites of lectin. In addition, the linker used to immobilize the ligands on the surface should be long enough to separate the ligands from the solid support and to allow the ligands adopting appropriate topology to interact with lectins.⁹⁷ Therefore, features of carbohydrate presentation and density have a great influence on carbohydrate-lectin binding events.⁹⁸

For a given lectin, the optimal ligand presentation is not easily predictable, and the spacing as well as the orientation of the same ligand can be modulated by modifying the type of solid surface, the type of linker, and ligand's concentration used.

A common manner to modulate spacing and orientation of carbohydrate on the surface is to print multivalent glycoconjugates as neoglycoproteins/neoglycopeptides⁹⁹ or glycodendrimers¹⁰⁰ instead than monovalent carbohydrates.

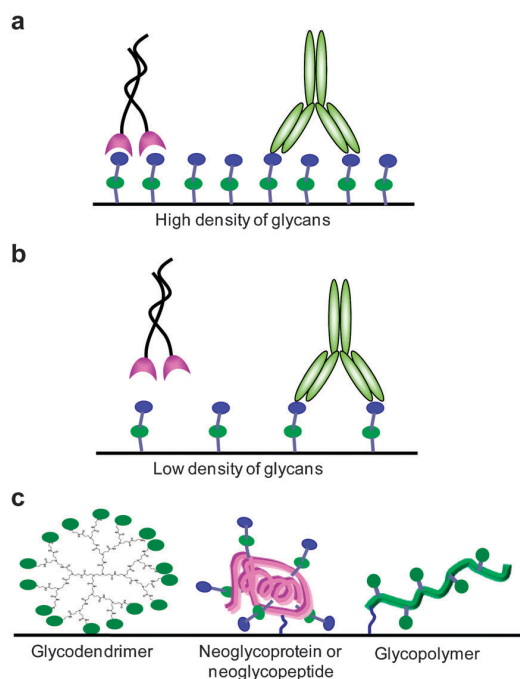


Figure 1.21 Carbohydrates immobilized on microarray surface. **(a)** A lectin with short spacing between binding sites interact strongly to high density surface. **(b)** A lectin with a short spacing between binding sites can weakly bind to the low density surface. **(c)** Carbohydrate presentation on surface can be modulate by immobilization of multivalent conjugates. Picture taken from *Chem. Soc. Rev.* 2013.⁶⁷

Several research groups have explored the effect of carbohydrates presentation and density on carbohydrate-lectin binding events.

For instance, Gildersleeve's group¹⁰¹ have immobilized, on an epoxide-coated glass slide, several BSA-based neoglycoproteins with variations in carbohydrate structures and density; by performing binding assays with either lectins or monoclonal antibodies, it was observed a strong preference for the high-density forms while no binding was detected for some low density forms. In this same work, Gildersleeve has also proven that, the selectivity of a protein for a particular carbohydrate generally deteriorates at high density; indeed, the *Vicia villosa lectin B₄* have bound many different GalNAc-containing sugars at high ligand densities but bound selectively to far less conjugates at low densities.

More recently, Bertozzi and coworkers¹⁰² have performed a qualitative evaluation of lectin binding to mucin-like glycoconjugates by modulating ligands density and molecular composition. Despite the capacity of all the four lectins to cross-link low valency glycoconjugates, only *Soybean agglutinin (SBA)* has shown a strenghten in the carbohydrate-lectin binding by increasing the carbohydrate density; this phenomenon can

possibly be attributed to steric interferences between lectin molecules bound to proximal ligands on the array surface.

In general, there are at least two mechanisms that provide density-dependent carbohydrate binding of lectins: ¹⁰³

- 1) *Internal diffusion*: in this mechanism, a lectin “binds and jumps” from carbohydrate to carbohydrate epitope along the scaffold; the affinity of lectin increases by increasing the number of carbohydrate epitopes and reducing the distance between two epitopes. (Figure 1.22-A, B)
- 2) *Face-to-face*: this mechanism is exclusively related to lectins that possess multiple CRDs in a common direction that can simultaneously bind to multiple copies of a carbohydrate epitope; in this case, they affinity enhancement is large for a high-density surface. (Figure 1.22-C)

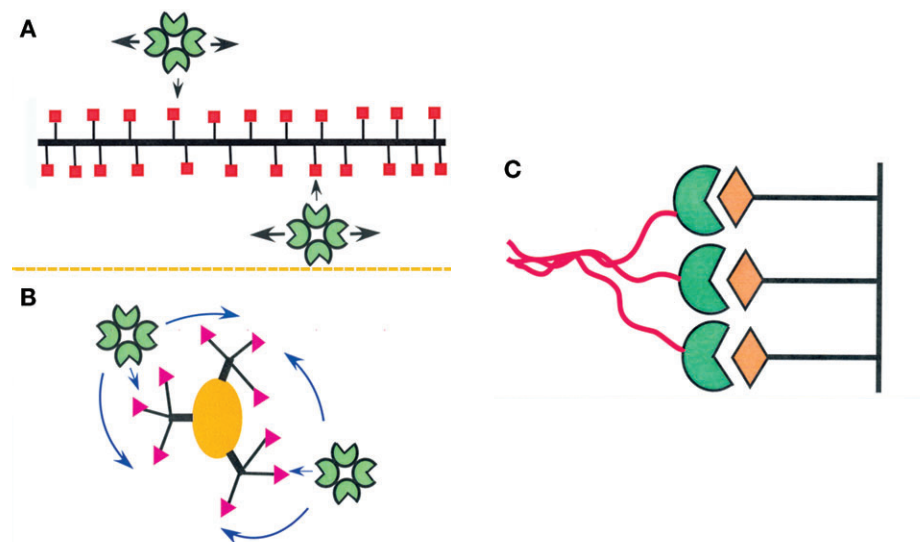


Figure 1.22 Schematic representation of lectin binding to (a) linear glycoprotein (b) globular glycoprotein via the *internal diffusion mechanism*. In (c) an example is given of the ‘face to face’ lectin-glycan binding mechanism. Picture taken from *Glycobiology*, 2009.¹⁰⁴

Ligand surface density is an important parameter, but usually not easily controlled in microarray applications, especially in the study of multivalent interactions.^{102,103} Thus, the need to perform extended and reliable microarray studies of multivalent systems leads to develop proper density quantification methods.

The present literature, shows only few examples for surface quantification methods. One of the first attempts to quantify carbohydrates immobilization on microarray surfaces

was made by Wong and co-workers: by attaching an amine-pentyl mannoseglycoside onto activated N-hydroxysuccinimide (NHS)-glass slides, at varying concentrations and performing binding assays with fluorescent labeled Concanavalin A, Wong 's team has quantified the relative amounts of immobilized sample and the maximum loading capacity.¹⁰⁴

Additionally, using a radiometric read-out format our research group⁹² could determine the structure-dependent variations in surface density at constant spotting concentration.

1.5 Further carbohydrate microarrays applications

1.5.1 Assessment of enzymes specificity

Glycosidases and glycosyltransferases have become routine tools for the preparation of large sized carbohydrates due by their high selectivity for substrates and linkages.

Extensive studies about glycoenzymes specificity could be quickly performed by using microarray technology to confirm known specificities or identify new reactivities and thereby extending their synthetic utilities.⁷⁷

Different examples of enzymatic reaction on carbohydrate microarrays have been described; for instance, Seibel and co-workers¹⁰⁵ have carried out on-chip identification of new acceptor specificities for Glycosyltransferases R, from *Streptococcus oralis*, by using fluorescently-labeled lectins to evaluate the success of the reaction.

Mrksich's team¹⁰⁶ has performed glycosylation reactions on an immobilized N-acetyl-D-glucosamine with β -1,4-galactosyltransferase to evaluate the importance of ligand density in the enzyme glycosylation; the reaction has been monitored by adopting radiolabelled UDP-[¹⁴C]galactose.

Park *et al*^{88b} have screened β -1,4-galactosyltransferase on a small library of carbohydrates immobilized on an epoxy-coated glass slide evaluating the degree of conversion by performing binding assays with fluorescently-labeled lectins; moreover, in the same work, on-chip studies of enzymatic glycosylation rates on the N-acetyl-D-glucosamine acceptor have been also performed.

The β -1,4-galactosyltransferase has been also tested from Flitsch's team¹⁰⁷ against a panel of immobilized mono and disaccharides on gold platform and from Beloqui *et al*^{95c} on synthetic N-glycans attached on hydrophobic-ITO surface; in both the

two cases, the enzyme activity and selectivity has been tested in a label-free manner by using MALDI-TOF analysis.

Our group¹⁰⁸ have screened α -1,3- and α -1,6-fucosyltransferases against a panel of synthetic N-glycans immobilized on NHS-activated glass slide; binding assays with fluorescently-labeled lectins have been adopted to evaluate the success of enzymatic reaction.

Many other enzymes have been tested on carbohydrate microarrays to achieve detailed information regarding activity and specificity; for the purpose, several types of array manufacturers and detection methods have been developed.

1.5.2 Carbohydrate microarrays as synthetic tool for the preparation of novel ligands

Over the years, many biological relevant oligosaccharides, as well as their relative mimetic and multivalent forms, have been synthesized to perform more detailed biological studies with the purpose to better understand their role in carbohydrate-based binding events.

Although carbohydrates synthesis has been significantly improved in term of rapidity and throughput allowing the preparation of varied oligosaccharides, the synthesis of any individual carbohydrate is still challenging; in fact, selective protection/deprotection reactions and tedious purification steps are often required.

An important advancement to carbohydrates preparation was achieved with the solid-phase synthesis and in particular with the automated solid-phase synthesis, developed from Seeberger and co-workers, that completely remove the long chromatography-based purification procedures.¹⁰⁹

Despite the solid-phase approach presents major improvements in time and yield compared with manual synthesis of oligosaccharides, this method usually requires the use of huge excess of synthetically complex building blocks. Moreover, when the automated or the manual synthesis are used to prepare a large number of oligosaccharides, the size of library is usually limited by the amounts of building block that has to be prepared for the construction of the library; this limitation could be removed if the synthesis of the oligosaccharides library and the screening with biological targets could both be performed *on-chip*.

The **on-chip synthesis** has the advantage to perform a simultaneous preparation of several ligands in a time- and material-saving manner; the microarray approach admits to use very small amounts of reagents and to replace tedious purification processes, usually adopted to remove un-reacted reagents or byproducts, by simple washing steps. Building up a library of hundred or thousand ligands *on-chip* usually requires microgram amounts of each scaffold and submilligram amounts of each further reagent. In addition, microarray-based method offers a platform to screen the novel synthesized ligands against biological targets.

On the other hand, it is important to take into account that reactions carry out at solid-liquid interphase are slower than ones performed in solution and therefore more time or more cycles of reaction are generally required to run the reaction to completion. The absence of purification steps to remove possible by-products can lead to products mixtures in the final spots; the presence of impurities in the analyzed spots can affect the biological read-out. In addition, all the ligands synthesized on microarray cannot be immediately used in additional biological assays like NMR, ELISA, etc.

One of the first attempts to synthesize novel saccharides by microarrays-based technology was carried out by Mrksich's team;¹¹⁰ they have synthesized 21 disaccharides by on-chip chemical synthesis on a self-assembled monolayer (SAM) gold surface by detecting the conversion of every single step of reaction through SAMDI-TOF MS. These novel synthesized saccharides have been then used for β -1,4-galactosyltransferase's activity assays.

An extended library of thousand sialoside mimetics has been prepared by Paulson and co-workers¹¹¹ by performing CuAAC with a set of azides on alkyne-sialoside scaffolds immobilized onto an NHS-activated surface; after establishing the effectiveness of on-chip reaction by fluorescent spectroscopy, binding assays with Siglec-7 and Siglec-10 have been carried out to identify novel high affinity ligands. The most interesting results have been achieved regarding the Siglec-7 and thus the most promising Siglec-7 ligands have been resynthesized in solution and coupled to PEGylated lipids, for liposomes preparation, to perform cell binding studies.

By combining chemical and enzymatic reactions, Flitsch and coworkers;^{112,113} have developed an on-chip strategy for the preparation of glyco-peptides. The established method consists to first perform repeated cycles of amino acid coupling on SAM-gold surface to prepare several peptides with different length and aminoacid composition, and

then carry out enzymatic elongation to introduce galactosamine moieties on serine or threonine residues. MALDI-TOF MS has been used to monitor all the performed reactions.

In addition, they have¹¹⁴ developed an on-chip enzymatic synthesis of sialo-oligosaccharides by employing trans-sialidase from *Trypanosoma cruzi* (*TcTS*) as enzyme and, consequently, the sialo-derivatives were screened against Chinese Hamster Ovary cells expressing full-length murine sialoadhesin.

Our group⁷⁵ have performed up to three sequential enzymatic elongations with α -1,6-fucosyltransferases, β -1,4-galactosyltransferase and α -2,6-sialyltransferase for the *on-chip spotwise* preparation of a N-glycans library.

On the base of these encouraging attempts of on-chip synthesis of oligosaccharides performed over the years, carbohydrate microarrays aim to be a time- and material-saving tool to quickly synthesize an extended panel of novel diversified ligands, natural or mimetic, with the main purpose to explore their binding properties against a large number of biomolecules.

References

1. A. J. MacPherson Gordon, *Explor. Immunol. Concepts Evidence*, Wiley-VCH Verlag GmbH Co. KGaA, 2012
2. Essential of Glycobiology, 3rd edition, *Cold Spring Harbor Laboratory Press*, 2015-2017.
2. F. Bacon, *Primer to Immune Response*, 2014, 3–20. <http://dx.doi.org/10.1016/B978-0-12-385245-8.00001-7>
3. J. Hütter, B. Lepenies. *Carbohydrate-based vaccines (methods and protocols)*, Bernd Lepenies Editor, *Humana Press*. **2015**, ISBN 978-1-4939-2873-6
4. S. J. Van Vliet, J. J. García-Vallejo and Y. Van Kooyk, *Immunol. Cell Biol.*, 2008, **86**, 580–587.
5. A. Rubartelli, M. T. Lotze, *Trends Immunol.*, 2007, **28**, 429-436.
6. T. Daoling, R. Kang, C. B. Coyne, H. J. Zeh and M. T. Lotze, *Immunol. Rev.*, 2012, **249**, 158–175.
7. D. L. Rosin and M. D. Okusa, *J. Am. Soc. Nephrol.*, 2011, **22**, 416–425.
8. M. L. Kapsenberg, *Nat. Rev. Immunol.*, 2003, **3**, 984–993.
9. N. Sharon and H. Lis, *Glycobiology*, 2004, **14**, 53–62.
10. S. T. Iobst, M. R. Wormald, W. I. Weis, R. A. Dwek and K. Drickamer, *J. Biol. Chem.*, 1994, **269**, 15505–15511.
11. S. Cecioni, A. Imberty and S. Vidal, *Chem. Rev.*, 2015, **115**, 525–561.
12. M. E. Taylor, K. Drickamer. *Introduction to Glycobiology*. *Oxford University Press, Oxford, UK*, **2003**.
13. S. J. van Vliet, E. Saeland and Y. van Kooyk, *Trends Immunol.*, 2008, **29**, 83–90.
14. M. E. Taylor and K. Drickamer, *Curr. Opin. Struct. Biol.*, 2014, **28**, 14–22.
15. E. J. Soilleux, R. Barten and J. Trowsdale, *J. Immunol.*, 2000, **165**, 2937–2942.

16. D. A. Mitchell, A. J. Fadden and K. Drickamer, *J. Biol. Chem.*, 2001, **276**, 28939–28945.
17. E. J. Soilleux, *Clin. Sci.*, 2003, **104**, 437–446.
18. Y. Liu, J. Liu, X. Pang, T. Liu, Z. Ning and G. Cheng, *Molecules*, 2015, **20**, 2272–2295.
19. L. De Witte, A. Nabatov, M. Pion, D. Fluitsma, M. A. W. P. De Jong, T. De Gruijl, V. Piguet, Y. Van Kooyk and T. B. H. Geijtenbeek, *Nat. Med.*, 2007, **13**, 367–371.
20. R. E. Hunger, P. A. Sieling, M. T. Ochoa, M. Sugaya, A. E. Burdick, T. H. Rea *et al*, *J Clin Invest*, 2004, **113**, 701–708.
21. M. A. de Jong, L. E. Vriend, B. Theelen, M. E. Taylor, D. Fluitsma, T. Boekhout *et al*, *Mol Immunol*, 2010, **47**, 1216–1225.
22. H. Tateno, K. Ohnishi, R. Yabe, N. Hayatsu, T. Sato, M. Takeya *et al*, *J Biol Chem* 2010, **285**, 6390–6400.
23. M. Van Der Vlist, T. Geijtenbeek, *Immunology and Cell Biology*, 2010, **88(4)**, 410-415.
24. **(a)** J. Valladeau, O. Ravel, C. Dezutter-Dambuyant, K. Moore, M. Kleijmeer, Y. Liu, V. Duvert-Frances, C. Vincent, D. Schmitt, J. Davoust, C. Caux, S. Lebecque and S. Saeland, *Immunity*, 2000, **12**, 71–81. **(b)** S. G. Turville, P. U. Cameron, A. Handley, G. Lin, S. Pöhlmann, R. W. Doms, A. L. Cunningham, *Nat. Immunol.*, 2002, **3**, 975–983. **(c)** O. Schwartz, *Nat. Med.*, 2007, **13**, 245–246.
25. P. R. Taylor, S. V. Tsoni, J. A. Willment, K. M. Dennehy, M. Rosas, H. Findon, K. Haynes, C. Steele, M. Botto, S. Gordon and G. D. Brown, *Nat. Immunol.*, 2007, **8**, 31–38.
26. S. Saijo, S. Ikeda, K. Yamabe, S. Kakuta, H. Ishigame, A. Akitsu, *et al*, *Immunity*, 2010, **32**, 681–691.
27. S. Saijo and Y. Iwakura, *Int. Immunol.*, 2011, **23**, 467–472.

- 28 S. Sheriff, C. Y. Chang and R. A. B. Ezekowitz, *Nat. Struct. Biol.*, 1994, **1**, 789–794.
29. W. I. Weis, K. Drickamer and W. A. Hendrickson, *Nature*, 1992, **360**, 127–134.
30. K. Drickamer, *Nature*, 1992, **360**, 183–186.
- 31 W. K. Eddie, I. Kazue, T. R. A. Ezekowitz, L. M. Stuart, W. K. E. Ip, K. Takahashi, R. A. Ezekowitz and R. Alan, *Immunol. Rev.*, 2009, **230**, 9–21
32. C. A. Ogden, A. deCathelineau, P. R. Hoffmann, D. Bratton, B. Ghebrehiwet, V. A. Fadok and P. M. Henson, *J. Exp. Med.*, 2001, **194**, 781–796.
33. N. Suzuki, K. Yamamoto, S. Toyoshima, T. Osawa, T. Irimura, *J. Immunol.*, 1996, **156**, 128–135.
34. S. Iida, K. Yamamoto and T. Irimura, *J. Biol. Chem.*, 1999, **274**, 10697–10705.
35. (a) P. Sears, C.-H. Wong, *Cell. Mol. Life Sci.*, 1998, **54**, 223-252. (b) H. Lis, N. Sharon, *Eur. J. Biochem.* 1993, **218**, 1–27. (c) A. Varki, *Glycobiology*, 1993, **3**, 97–130.
36. (a) E. Meezan, , H. C. Wu, P. H. Black, P. W. Robbins, *Biochemistry*, 1969, **8**, 2518–2524. (b) G. A. Turner, *Clin. Chim. Acta*, 1992, **208**, 149–171. (c) J. S. Axford, *Biochim. Biophys. Acta*, 1999, **1455**, 219–229. (d) A. Mackiewicz, K. Mackiewicz, 1995, *Glycoconj. J.* **12**, 241–247.
37. R. T. Lee, Y. Lee, *Glycoconjugate Journal*, 2000, **17**, 543-551.
38. R. U. Lemieux, *Acc. Chem. Res.* 1996, **29**, 373–380.
39. A. Schon, E. Freire, *Biochemistry* 1989, **28**, 5019–5024.
40. P. Sears and C.-H. Wong, *Angew. Chemie - Int. Ed.*, 1999, **38**, 2300–2324.
41. (a) T. B. H. Geijtenbeek *et al*, *Cell*, 2000, **100**, 587-597. (b) Y. van Kooyk, T. B. H. Geijtenbeek, *Nat. Rev. Immunol.* 2003, **3**, 697- 709. (c) C. P. Alvarez, F. Lasala, J. Carrillo, *et al*, *J. Virol.*, 2002, **76**, 6841-6844. (d) B. Tassaneeritthep, *et all*, *J. Exp. Med.*, 2003, **197**, 823-829. (e) L. Wu, V. N. KewalRamani, *Nat. ReV. Immunol.*, 2006, **6**, 859-868.

42. (a) T. B. H. Geijtenbeek, S. J. van Vliet, E. A. Koppel, M. Sanchez-Hernandez, C. Vandenbroucke-Grauls, B. Appelmelk, Y. van Kooyk, *Y. J. Exp. Med.*, 2003, **197**, 7-17. (b) L. Tailleux, *et al*, *Exp. Med.*, 2003, **197**, 121-127. (c) M. P. Bergman, *et al*, *Exp. Med.* 2004, **200**, 979- 990.
43. (a) H. Feinberg, R. Castelli, K. Drickamer, P. H. Seeberger, W. I. Weis, *J. Biol. Chem.*, 2007, **282**, 4202-4209. (b) Y. Guo, H. Feinberg, E. Conroy, D. A. Mitchell, R. Alvarez, O. Blixt, M. E. Taylor, W. I. Weis, K. Drickamer, *Nat. Struct. Mol. Biol.*, 2004, **11**, 591– 598. (c) H. Feinberg, D. A. Mitchell, K. Drickamer, W. I. Weis, *Science*, 2001, **294**, 2163-2166.
44. J. J. Reina, S. Sattin, D. Invernizzi, S. Mari, L. Martínez-Prats, G. Tabarani, F. Fieschi, R. Delgado, P. M. Nieto, J. Rojo, A. Bernardi, *ChemMedChem*, 2007, **2**, 1030–1036.
45. J. J. Reina and A. Bernardi, *Mini Rev. Med. Chem.*, 2012, **12**, 1434–1442.
46. S. Mari, H. Posteri, G. Marcou, D. Potenza, F. Micheli, F. J. Cañada, J. Jimenez-Barbero, A. Bernardi, *European J. Org. Chem.*, 2004, 5119–5125.
47. S. Mari, I. Sánchez-Medina, P. Mereghetti, L. Belvisi, J. Jiménez-Barbero, A. Bernardi, *Carbohydr. Res.*, 2007, **342**, 1859–1868.
48. S. Sattin, A. Daghett, M. Thépaut, A. Berzi, M. A. Sánchez-Navarro, G. Tabarani, J. Rojo, F. Fieschi, M. Clerici and A. Bernardi, *ACS Chem. Biol.*, 2010, **5**, 301–312.
49. J. Luczkowiak, S. Sattin, I. Sutkevičiute, J. J. Reina, M. Sánchez-Navarro, M. Thépaut, L. Martínez-Prats, A. Daghetti, F. Fieschi, R. Delgado, A. Bernardi and J. Rojo, *Bioconjug. Chem.*, 2011, **22**, 1354–1365.
50. K. C. A. Garber, K. Wangkanont, E. E. Carlson, L. L. Kiessling, *Chem. Commun.*, 2010, **46**, 6747–6749.
51. M. C. Schuster, D. A. Mann, T. J. Buchholz, K. M. Johnson, W. D. Thomas, L. L. Kiessling, *Org. Lett.*, 2003, **5**, 1407–1410.
52. M. Kanai, K. H. Mortell and L. L. Kiessling, *J. Am. Chem. Soc.*, 1997, **119**, 9931–9932.

53. T. Tomašić, D. Hajšek, U. Švajger, J. Luzar, N. Obermajer, I. Petit-Haertlein, F. Fieschi and M. Anderluh, *Eur. J. Med. Chem.*, 2014, **75**, 308–326.
54. J. Li, F. Yu, Y. Chen and D. Oupický, *J. Control. Release*, 2015, **219**, 369–382.
55. C. Fasting, C. A. Schalley, M. Weber, O. Seitz, S. Hecht, B. Kokschi, J. Dervede, C. Graf, E. W. Knapp and R. Haag, *Angew. Chemie - Int. Ed.*, 2012, **51**, 10472–10498.
56. (a) O. C. Grant, H. M. K. Smith, *et al*, *Glycobiology*, 2014, **24**, 17–25. (b) D. M. Lewallen, D. Siler and S. S. Iyer, *ChemBioChem*, 2009, **10**, 1486–1489. (c) V. Padler-Karavani, X. Song, H. Yu, N. Hurtado-Ziola, *et al*, *J. Biol. Chem.*, 2012, **287**, 22593–22608. (d) T. Pochechueva, F. Jacob, D. R. Goldstein, *et al*, *Glycoconj. J.*, 2011, **28**, 507–517.
57. S. Kalkhof, A. Sinz, *Anal. Bioanal. Chem.*, 2008, **392**, 305–312.
58. Q. Wang, *et al*, *J. Am. Chem. Soc.*, 2003, **125**, 3192–3193
59. (a) K. L. Seim, A. C. Obermeyer, M. B. Francis, *J. Am. Chem. Soc.*, 2011, **133**, 16970–16976. (b) T. L. Schlick, Z. Ding, E. W. Kovacs, M. B. Francis, *J. Am. Chem. Soc.*, 2005, **127**, 3718–3723. (c) J. M. McFarland, N. S. Joshi, M. B. Francis, *J. Am. Chem. Soc.*, 2008, **130**, 7639–7644. (d) S. D. Tilley, M. B. Francis, *J. Am. Chem. Soc.*, 2006, **128**, 1080–1081.
60. C. C. Lee, J. A. MacKay, J. M. J. Fréchet and F. C. Szoka, *Nat. Biotechnol.*, 2005, **23**, 1517–1526.
61. L. L. Kiessling, J. E. Gestwicki and L. E. Strong, *Angew. Chemie - Int. Ed.*, 2006, **45**, 2348–2368.
62. A. Carlmark, C. Hawker, A. Hult and M. Malkoch, *Chem. Soc. Rev.*, 2009, **38**, 352–362.
63. M. Sowinska and Z. Urbanczyk-Lipkowska, *New J. Chem.*, 2014, **38**, 2168–2203.

64. (a) S., Park, I. Shin, *Angew. Chem., Int. Ed.*, 2002, **41**, 3180–3182. (b) S. Fukui, T. Feizi, C. Galustian, A. M. Lawson, W. Chai, *Nat. Biotechnol.*, 2002, **20**, 1011–1017. (c) B. T. Houseman, M. Mrksich, *Chem. Biol.*, 2002, **9**, 443–454. (d) W. G. T. Willats, S. E. Rasmussen, T. Kristensen, J. D. Mikkelsen, J. P. Knox, *Proteomics*. 2002, **2**, 1666–1671. (e) F. Fazio, M. C. Bryan, O. Blixt, J. C. Paulson, V.-H. Wong, *J. Am. Chem. Soc.* 2002, **124**, 14397–14402.
65. Y. Chevolut, *Carbohydrate Microarray, Methods and Protocol*, 2012. ISBN 978-1-61779-373-8
66. S. Park, J. C. Gildersleeve, O. Blixt and I. Shin, *Chem. Soc. Rev.*, 2013, **42**, 4259–4506.
67. J. Y. Hyun, J. Pai and I. Shin, *Acc. Chem. Res.*, 2017, **50**, 1069–1078.
68. S. Park, M. R. Lee and I. Shin, *Bioconjug. Chem.*, 2009, **20**, 155–162.
69. J. Pai, J. Y. Hyun, J. Jeong, S. Loh, E. H. Cho, Y. S. Kang, I. Shin, *Chem. Sci.* 2016, **7**, 2084–2093.
70. M. A. Campanero-Rhodes, R. A. Childs, M. Kiso, S. Komba, C. Le Narvor, J. Warren, D. Otto, P. R. Crocker and T. Feizi, *Biochem. Biophys. Res. Commun.*, 2006, **344**, 1141–1146.
71. T. Schallus, V. Jaekch, K. Fehér, A. S. Palma, Y. Liu, J. C. Simpson, M. Mackeen, G. Stier, T. J. Gibson, T. Feizi, T. Pieler, C. Muhle-Goll, *Mol. Biol. Cell Vol.*, 2008, **19**, 3404–3414.
72. C. Galustian, C. G. Park, W. Chai, M. Kiso, S. A. Bruening, Y.- S. Kang, R. M. Steinman and T. Feizi, *Int. Immunol.*, 2004, **16**, 853–866.
73. P. H. Liang, S. K. Wang, C. H. Wong, *J Am Chem Soc*, 2007, **129**, 11177–11184.
74. S. Serna, J. Etxebarria, N. Ruiz, M. Martin-Lomas and N. C. Reichardt, *Chem. A Eur. J.*, 2010, **16**, 13163–13175.
75. C.-H. Liang and C.-Y. Wu, *Expert Rev. Proteomics*, 2009, **6**, 631–645.
76. N. Laurent, J. Voglmeir and S. L. Flitsch, *Chem. Commun.*, 2008, **37**, 4400–4412.

77. S. Park, M. R. Lee and I. Shin, *Nat. Protoc.*, 2007, **2**, 2747–2758.
78. (a) V. I. Dyukova, E. I. Dementieva, D. A. Zubtsov, O. E. Galanina, N. V. Bovin, A. Y. Rubina. *Anal. Biochem.* 2005, **347(1)**, 94–105. (b) O. Blixt, S. Head, T. Mondala, *et al*, *Proc. Natl Acad. Sci. USA*, 2004, **101(49)**, 17033–17038. (c) M. D. Disney, P. H. Seeberger, *Chem. Biol.* 2004, **11(12)**, 1701–1707. (d) J. L. de Paz, C. Noti, P. H. Seeberger, *J. Am. Chem. Soc.*, 2006, **128(9)**, 2766–2767. (e) N. V. Shilova, O. E. Galanina, A. Y. Rubina *et al*, *Glycoconj. J.* 2008, **25(1)**, 11–14.
79. (a) E. W. Adams, D. M. Ratner, H. R. Bokesch, J. B. McMahon. B. R. O’Keefe, P. H. Seeberger, *Chem. Biol.*, 2004, **11(6)**, 875–881. (b) D. M. Ratner, E. W. Adams, M. D. Disney, P. H. Seeberger, *ChemBioChem*, 2004, **5(10)**, 1375–1383. (c) M. A. Brun, M. D. Disney, P. H. Seeberger. *ChemBioChem*, **7(3)**, 421–424.
80. B. T. Houseman, M. Mrksich, *Chem. Biol.*, 2002, **9(4)**, 443–454.
81. (a) X.-L. Sun, C. L. Stabler, C. S. Cazalis and E. L. Chaikof, *Bioconjugate Chem.*, 2006, **17(1)**, 52–57. (b) M. C. Bryan, F. Fazio, H.-K. Lee, C.-Y. Huang, A. Chang, M. D. Best, D. A. Calarese, O. Blixt, J. C. Paulson, D. Burton, I. A. Wilson and C.-H. Wong, *J. Am. Chem. Soc.*, 2004, **126**, 8640–8641.
82. S. Angeloni, J. L. Ridet, N. Kusy, *et al*, *Glycobiology*, 2005, **15(1)**, 31–41.
83. (a) X. Zhou, J. Zhou. *Biosens. Bioelectron.* 2006, **21(8)**, 1451–1458. (b) S. Park, M. R. Lee, I. Shin. *Bioconjug. Chem.* 2009, **20(1)**, 155–162.
84. M. R. Lee, I. Shin *Org. Lett.* 2005, **7(19)**, 4269–4272.
85. Z. L. Zhi, A. K. Powell, J. E. Turnbull. *Anal. Chem.* 2006, **78(14)**, 4786–4793.
86. Fukui S, Feizi T, Galustian C, Lawson AM, Chai W. *Nat. Biotechnol.* 2002, **20(10)**, 1011–1017.
87. (a) S. Park, I. Shin, *Angew. Chem. Int. Ed. Engl.*, 2002, **41(17)**, 3180–3182. (b) S. Park S, Shin, *Org. Lett.*, 2007, **9(9)**, 1675–1678.

88. (a) E. A. Smith, W. D. Thomas, L. L. Kiessling, R. M. Corn. *J. Am. Chem. Soc.*, 2003, **125**(20), 6140–6148. (b) A. R. de Boer, C. H. Hokke, A. M. Deelder, M. Wuhrer. *Glycoconj. J.*, 2008, **25**(1), 75–84. (c) R. Karamanska, J. Clarke, O. Blixt *et al*, *Glycoconj. J.*, 2008, **25**(1), 69–74.
89. M. Shipp, R. Nadella, H. Gao, V. Farkas, H. Sigrüst and A. Faik, *Glycoconj. J.*, 2008, **25**, 49–58.
90. H. L. Pedersen, J. U. Fangel, B. McCleary, C. Ruzanski, M. G. Rydahl, M. C. Ralet, V. Farkas, L. Von Schantz, S. E. Marcus, M. C. F. Andersen,
91. S. Serna, C. H. Hokke, M. Weissenborn, S. Flitsch, M. Martin-Lomas, N. C. Reichardt, *ChemBioChem*, 2013, **14**, 862–869.
92. E. Han, L. Ding, S. Jin and H. Ju, *Biosens. Bioelectron.*, 2011, **26**, 2500–2505.
93. J. Baader, H. Klapproth, S. Bednar, T. Brandstetter, J. Rühle, M. Lehmann and I. Freund, *Biosens. Bioelectron.*, 2011, **26**, 1839–1846.
94. (a) B. T. Houseman and M. Mrksich, *Chem. Biol.*, 2002, **9**, 443–454. (b) J. Su, M. Mrksich, *Angew. Chem. Int. Ed. Engl.*, 2002, **41**, 4715–4718. (c) A. Beloqui, *et al*, *Angew. Chemie - Int. Ed.*, 2013, **52**, 7477–7481.
95. Y. Fei, Y. S. Sun, Y. Li, K. Lau, H. Yu, H. A. Chokhawala, S. Huang, J. P. Landry, X. Chen and X. Zhu, *Mol. Biosyst.*, 2011, **7**, 3343–3352.
96. (a) N. Laurent, J. Voglmeir, *et al*, *ChemBioChem*, 2008, **9**, 883–887. (b) Z. L. Zhi, N. Laurent, A. K. Powell, R. Karamanska, *et al*, *ChemBioChem*, 2008, **9**, 1568–1575.
97. D. M. Lewallen, D. Siler and S. S. Iyer, *ChemBioChem*, 2009, **10**, 1486–1489.
98. J. C. Paulson, O. Blixt and B. E. Collins, *Nat. Chem. Biol.*, 2006, **2**, 238–248.
99. (a) J. C. Manimala, T. A. Roach, Z. Li and J. C. Gildersleeve, *Angew. Chem., Int. Ed.*, 2006, **45**, 3607–3610. (b) J. C. Manimala, *et. al*, *ChemBioChem*, 2005, **6**, 2229–2241. (c) E. W. Adams, J. Ueberfeld, D. M. Ratner, B. R. O’Keefe, D. R. Walt and P. H. Seeberger, *Angew. Chem., Int. Ed.*, 2003, **42**, 5317–5320. (d) A. Walz, S. Odenbreit, J. Mahdavi, T. Boren and S. Ruhl, *Glycobiology*, 2005, **15**, 700–708 (e) H. Tateno, *et al*, *Glycobiology*, 2008, **18**, 789–798.

100. (a) T. Fukuda, S. Onogi and Y. Miura, *Thin Solid Films*, 2009, **518**, 880–888. (b) H. M. Branderhorst, R. Ruijtenbeek, R. M. J. Liskamp and R. J. Pieters, *ChemBioChem*, 2008, **9**, 1836–1844. 133 (c) P. N. Parera, H. M. Branderhorst, R. Kooij, *et al*, *ChemBioChem*, 2010, **11**, 1896–1904.
101. O. Oyelaran, Q. Li, D. Farnsworth and J. C. Gildersleeve, *J. Proteome Res.*, 2009, **8**, 3529–3538.
102. K. Godula and C. R. Bertozzi, *J. Am. Chem. Soc.*, 2012, **134**, 15732–15742.
103. T. K. Dam and C. Fred Brewer, *Glycobiology*, 2009, **20**, 270–279.
104. P. H. Liang, S. K. Wang and C. H. Wong, *J. Am. Chem. Soc.*, 2007, **129**, 11177–11184.
105. J. Seibel, H. Hellmuth, B. Hofer, A. M. Kicinska and B. Schmalbruch, *ChemBioChem*, 2006, **7**, 310–320.
106. B. T. Houseman and M. Mrksich, *Angew. Chem., Int. Ed.*, 1999, **38**, 782–785.
107. Z.-l. Zhi, N. Laurent, *et. al.*, *ChemBioChem*, 2008, **9**, 1568–1575.
108. S. Serna, S. Yan, M. Martin-Lomas, I. B. H. Wilson and N. C. Reichardt, *J. Am. Chem. Soc.*, 2011, **133**, 16495–16502.
109. O. J. Plante, E. R. Palmacci and P. H. Seeberger, *Science (80-.)*, 2001, **23**, 1523–1527.
110. L. Ban, M. Mrksich, *Angew. Chem.*, 2008, **120**, 3444–3447.
111. C. D. Rillahan, E. Schwartz, C. Rademacher, R. McBride, J. Rangarajan, V. V. Fokin and J. C. Paulson, *ACS Chem. Biol.*, 2013, **8**, 1417–1422.
112. N. Laurent, J. Voglmeir, A. Wright, J. Blackburn, N. T. Pham, S. C. C. Wong, S. J. Gaskell and S. L. Flitsch, *ChemBioChem*, 2008, **9**, 883–887.
113. N. Laurent, R. Haddoub, J. Voglmeir, S. C. C. Wong, S. J. Gaskell, S. L. Flitsch, *ChemBioChem.*, 2008, **9**, 2592–2596.
114. R. Šardžik, R. Sharma, S. Kaloo, J. Voglmeir, P. R. Crocker and S. L. Flitsch, *Chem. Commun.*, 2011, **47**, 5425–5427.

2. Objectives

2. Objectives

The thesis project here presented is part of a **Marie Skłodowska Curie European Training Network**, named IMMUNOSHAPE, that brings together 14 leading European partners involved in the development of glycan-based immunotherapeutics for the treatment of cancer, autoimmune diseases and allergy. Being carbohydrate-lectin interactions on the base of the immune response, the targeting of specific C-type lectins represents a powerful strategy to modulate the immune response.

Although C-type lectins preferentially bind to specific natural carbohydrates, their binding are quite weak; chemical modification and/or multiple copies presentation of ligands are often required to strengthen carbohydrate-lectin binding.

Our main role in the European training network was the development of a versatile microarray surface to use for the synthesis and the biological evaluation of new generations of glycomimetics and multivalent constructs in a time- and material-saved manner.

To achieve this main purpose, the first part of this thesis has been addressed on the following partial objectives:

1. Development of NHS-activated hydrophobic ITO-surface that allows to perform MALDI-TOF analysis and Fluorescent detection with high-quality data (**Chapter 3**).
2. Optimization of on-chip chemical and enzymatic reactions with respect to the surface stability and experimental reproducibility (**Chapter 3** and **Chapter 4**).
3. Elaboration of a mass-based method to relatively quantify ligands' density on the surface (**Chapter 4**),
4. Performing a quick and parallel lectin's binding study on a large collection of different ligands (**Chapter 3** and **Chapter 4**).
5. Making a cross-comparison among carbohydrate-lectin binding assays performed on different array formats and binding conditions (**Chapter 4**).

The use of microarray technology to synthesize and then evaluate the binding assays of novel constructs allowed to explore how the nature of epitope and its presentation can affect the carbohydrate-lectin binding. With this strategy it was possible to quickly select,

2. Objectives

among a large collection of ligands, the most promising binders for a targeted lectin that would be then scaled up synthetically to perform further biological evaluation.

In the second part of this thesis (**Chapter 5**), the microarray technology has been abandoned for synthesizing OVA-based glycoconjugates to test in immunological assays. The scope of this work consisted to develop novel glycoconjugates able to induce a pronounced immune responses via internalization in dendritic cells and the subsequent T cell activation.

With this aim, the second part of this work has been addressed on the following partial objectives:

1. Development of a general protocol for the synthesis of properly functionalized sugars used to decorate OVA-surface by well-established conjugation method.
2. In *vitro* tests to estimate the immunological implication of our new constructs.

The preliminary results achieved with OVA-based glycoconjugates here synthesized would represents an interesting starting point for future improvement in DCs targeting.

3. On-chip chemo-enzymatic synthesis of N-glycan mimetics

3. On-chip chemo-enzymatic synthesis of a N-glycan mimetics library

N-glycans are a class of complex oligosaccharides with a common pentasaccharidic core, $\text{Man}\alpha 1-6(\text{Man}\alpha 1-3)\text{Man}\beta 1-4\text{GlcNAc}\beta 1-4\text{GlcNAc}\beta 1$, that are covalently attached to glycoproteins at asparagine residues, within the Asn-X-Ser/Thr consensus sequence; they are ubiquitously present on cells and tissues and show a large degree of heterogeneity due to variations in the number of antennae, terminal residues and core modifications.^{116,117}

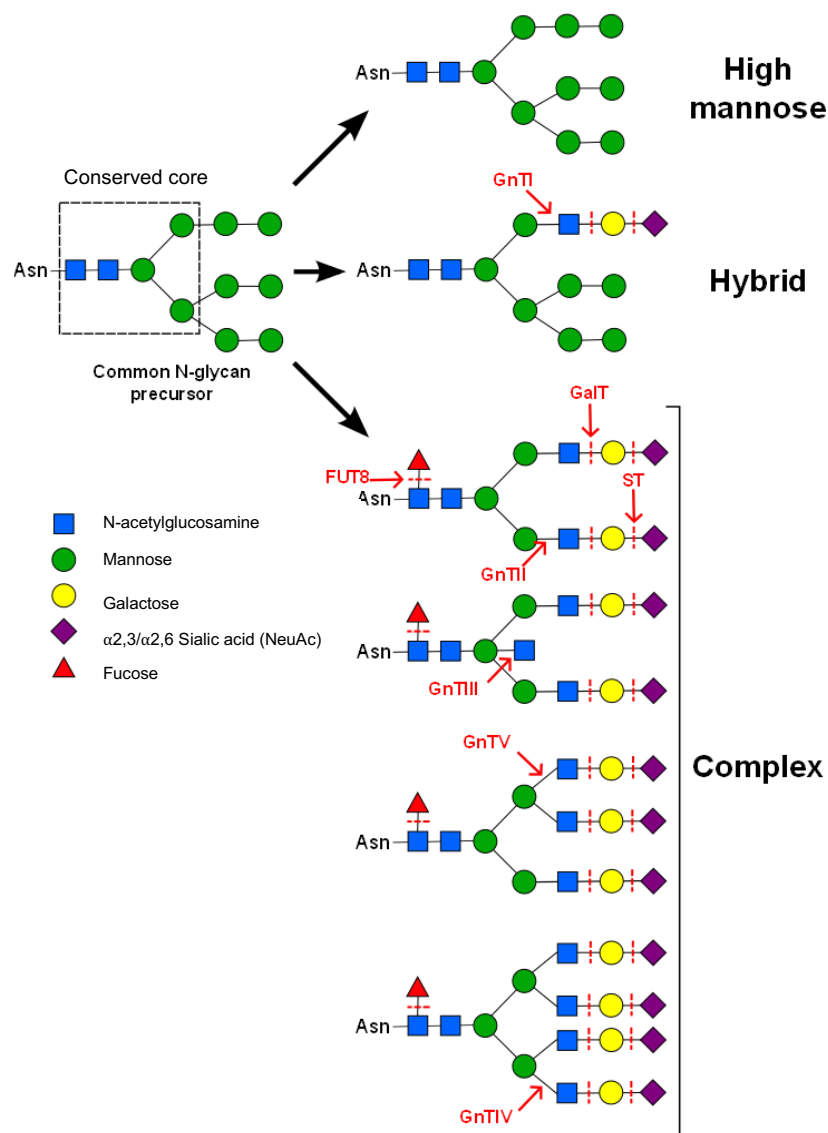


Figure 3.1 Typical structure of the common Man 9-precursor of N-glycans contained in eukaryotes and the three classes of existing N-linked glycans. Dashed bars depict the elongation of the pentasaccharide core with complex antennae, generating a wide panel of N-glycans.

Abbreviations: GnT: N-acetylglucosaminyltransferase, FUT8: fucosyltransferase, ST: sialyltransferase, GalT: galactosyltransferase.¹¹⁸

N-glycans are involved in many biological events occurring in human body including cell–cell communication and signal transduction;¹¹⁹ since they are located on the outermost layer of the cell, N-glycans are the first molecules to be encountered and recognized by other cells, antibodies, invading viruses, and bacteria.

Moreover, modification on N-glycan structures affect protein folding and stability, and have the ability to interfere with carbohydrate–carbohydrate, carbohydrate–protein, and glycoprotein–glycoprotein interactions; therefore glycosylation patterns can serve as markers for certain disease states including cancer metastasis, development, and differentiation.¹²⁰

In this thesis we mainly focused on the use of N-glycans as lead structures for the preparation of mimetics with improved affinity for a specific class of proteins: C-type lectin receptors CLR_s.

Some natural carbohydrates play an important role in therapeutic applications, these include the Heparin¹²¹ used as anticoagulant in heart disease and the acarbose¹²² which allows to control blood glucose levels. Nevertheless, natural carbohydrates are rarely employed in the development of new therapeutics because of their low stability toward endogenous degradative enzymes, generally low affinity interactions with biological target when presented in monovalent form, and the complexity to scale up their synthesis for therapeutics applications.

To limit the synthetic efforts, one approach for targeting lectins is generally based on the synthesis of non-natural mono- to trisaccharidic mimetics, with improved pharmacokinetic profile and potentially higher binding affinity.⁴¹

With the aim to produce a library of mimetic scaffolds in a time- and material-saved manner, we have developed a rapid and versatile protocol for the *on-chip* chemo-enzymatic synthesis of N-glycan mimetics. The synthetic strategy consisted in 1. immobilizing, twenty different N-glycan structures (**G1-G20**) on a NHS-activated hydrophobic ITO-glass slide, 2. performing enzymatic elongation with azido-N-acetyl-D-galactosamine, and 3. coupling of the azide-glycans (**G1.1-G1.17**) with twenty-nine alkynes (**a1-a29**) by Copper(I)-Catalyzed Alkyne Azide Cycloaddition (CuAAC) to prepare close to 500 different triazoles as N-glycan mimetics ([Figure 3.2](#)). Finally the collection of N-glycomimetics have been screened with a number of plant and human C-type lectins to identify novel leads for lectin targeted therapy.

Both the enzymatic elongation and the cycloaddition are known to be highly selective for

substrates and linkages, in such a way that they can be performed without adopting protection/deprotection steps and with formation of a limited number of by-products. Moreover, both reactions are compatible with media which does not affect the stability of the hydrophobic surface.

In addition, the NHS-activated hydrophobic surface we employed in our strategy allows the analysis of surface reactions by MALDI-TOF MS analysis, and at the same time, the detection of carbohydrate protein binding events by fluorescence.^{95c}

Since we introduced azido-galactosamine residues into the N-glycan structures, after triazole formation, we expected binding primarily to occur with galactosamine-binding lectins like *Wisteria floribunda Agglutinin (WFA)* and the *Macrophage Galactose Lectin (MGL)*. But as we were dealing with N-glycans which can interact with lectins via a number of different binding modes, we also conceived the screening of other non-galactose/galactosamine binding lectins to evaluate the effect of local modifications on the terminal sugars on the binding event.

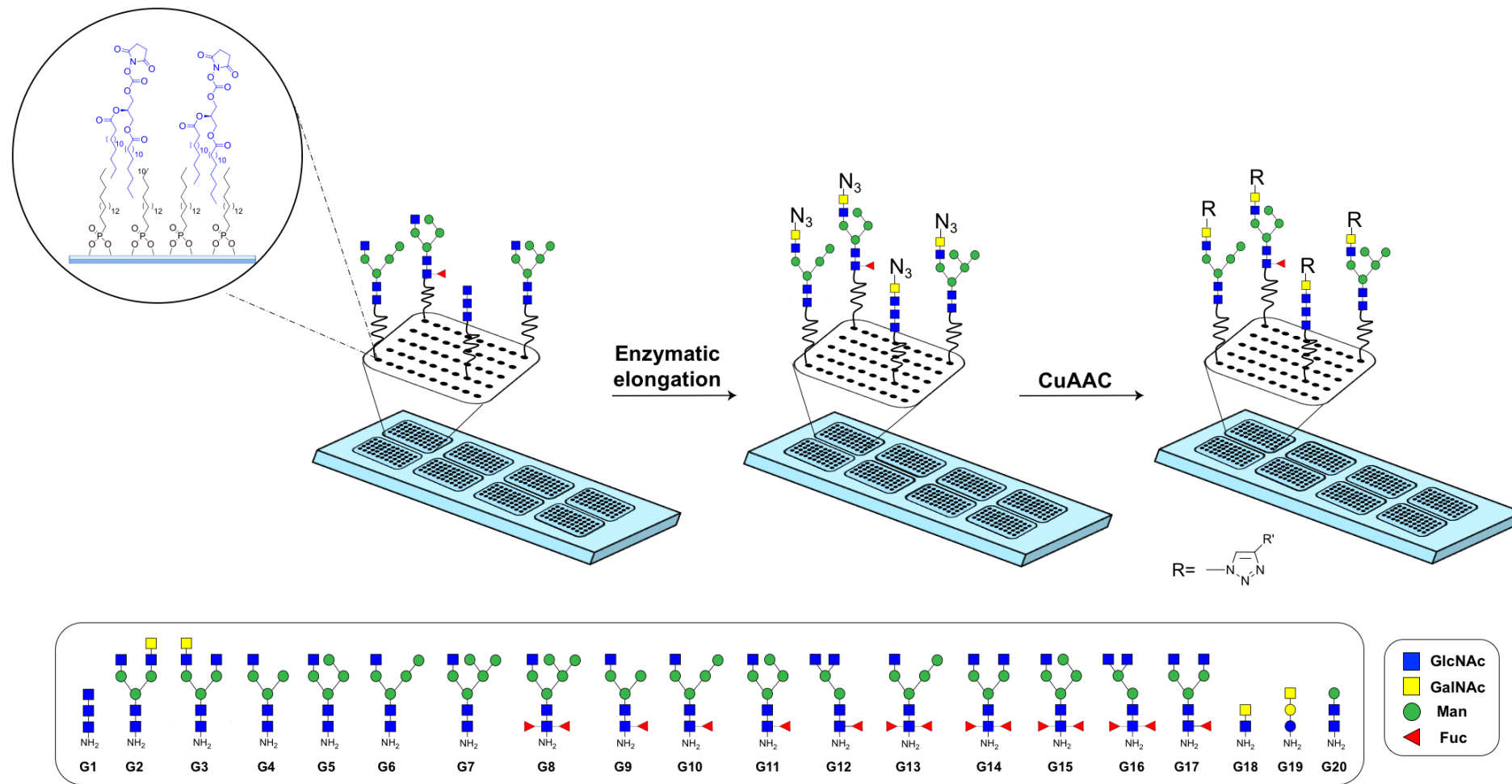


Figure 3.2 General strategy for on-chip chemo-enzymatic synthesis of N-glycan mimetics.

3.1 Development of NHS-activated hydrophobic ITO (Indium-Tin Oxide)-coated glass slide

The activated surface used to immobilize different scaffolds and perform on-chip reactions and/or lectin-binding assays is the N-Hydroxy-succinimide-activated ITO-coated glass slide (Figure 3.3).

This surface was prepared by 1. functionalizing commercially available Indium-Tin Oxide-coated glass slides with a alkylphosphonate monolayer and 2. no-covalent attachment of a hydrophilic bidentate linker with an NHS activated headgroup; this linker reacts with primary amines to form amide bonds.

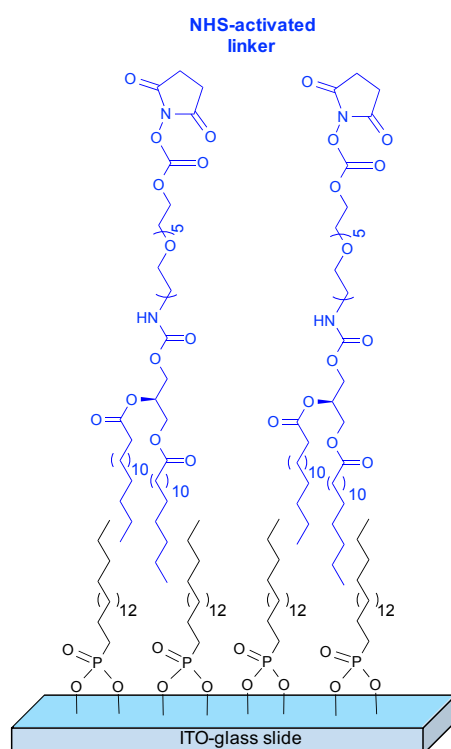


Figure 3.3 An NHS-activated bidentate linker is stabilized on ITO-surface through hydrophobic interactions.

A similar surface, using a silane monolayer instead, had been developed previously in our laboratory (Beloqui *et al*, *Angew. Chemie – Int. Ed.* **2013**)^{95c} to prepare a glycan arrays with dual read-out functionality by mass spectrometry and fluorescence detection.

In this thesis work, we propose an optimization of the previous platform by adopting phosphonate-based monolayer; compared to its silane analogue, this type of monolayer is less susceptible to self-condensation reaction and which in the case of phosphonates occur only under high-temperature dehydrating conditions.¹²³

Moreover, while in the previous work, two NHS-activated bidentate linkers of different length (**1** and **2**) had been used (Figure 3.4), here we have employed only the longer linker **2** which seems to improve the accessibility of enzymes and other reagents to the solid-supported ligands.

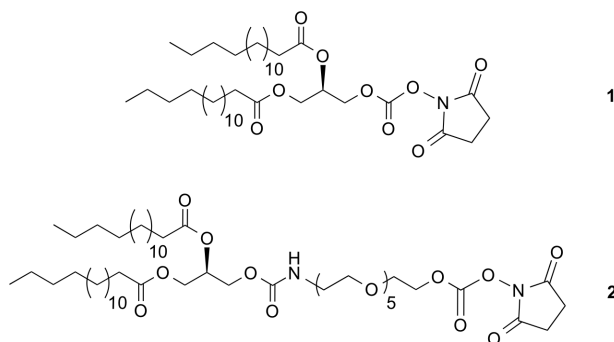


Figure 3.4 NHS-activated bidentate linkers (**1**) and (**2**).

3.1.1 ITO-glass slide modification with phosphonate-based hydrophobic monolayer

Starting from commercial ITO-glass slides, the functionalization with octadecylphosphonic acid (ODPA) to form a hydrophobic monolayer was performed by adopting the T-BAG (Tethering by Aggregation and Growth) process.¹²⁴ (Figure 3.5)

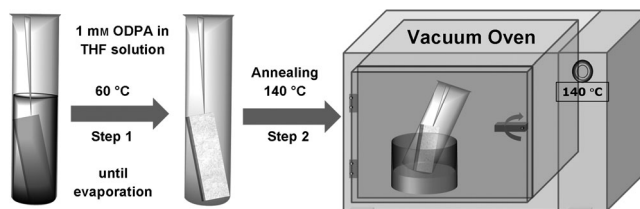


Figure 3.5 Schematic representation of T-BAG process. Picture taken from *Angew. Chem. Int. Ed.*, 2014.¹²⁵

The T-BAG process consists to clean the slide in piranha solution (7:1:1 solution of water, NH_3 , H_2O_2), functionalize it by incubation with a solution of octadecylphosphonic acid (ODPA) in THF and then performing a thermally annealing at 140°C to induce heterocondensation.

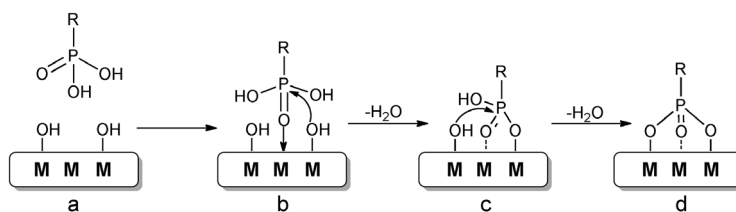


Figure 3.6 Mechanism of phosphonic acid attachment to Lewis acid metal oxides like Indium-tin Oxide. **(a)** initial conditions, **(b)** coordination of the phosphoryl oxygen to a Lewis acidic site on the surface followed by heterocondensation with the now more electrophilic phosphorus, **(c)** additional heterocondensation, and **(d)** final tridentate binding state.¹²⁶

3.1.2 NHS-activation of hydrophobic ITO surface with linker 1 and linker 2

In the beginning, for the preparation of the final activated hydrophobic sandwich structure, the alkylphosphonate functionalized surface was modified with both the NHS-activated bidentate linkers (**1**, **2**) as previously described.^{95c}

After the immobilization of several N-glycan structures on the NHS-activated surfaces, binding assays with *Wheat Germ Agglutinin* have been performed to evaluate their respective fluorescent data quality ([Figure 3.7](#)).

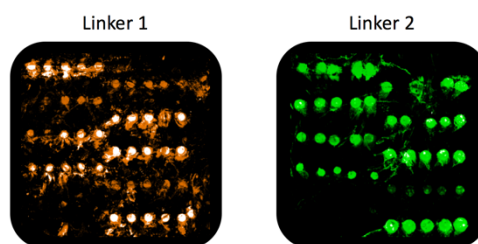


Figure 3.7 Fluorescent image of N-glycan array, with linkers **1** and **2**, after incubation with *WGA-Alexafluor647*.

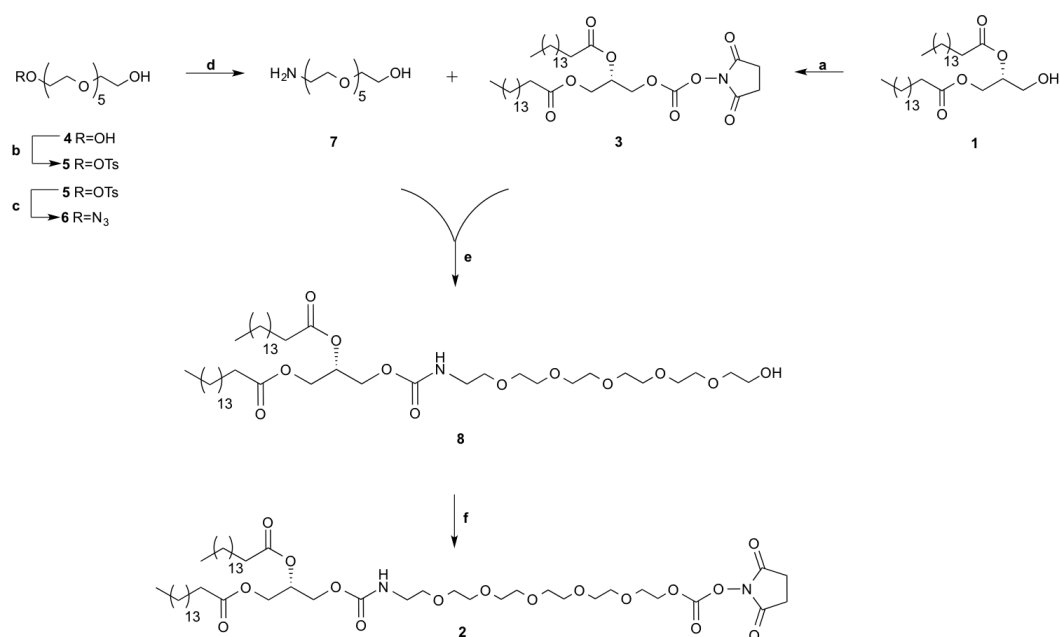
Although both linkers differ from each other only in the presence of a hexaethylene glycol chain, these preliminary assays show that surface activation with linker **2** offers a better, but improvable, fluorescent data quality in terms of background signal and spot morphology compared to surface functionalized with linker **1**. ([Figure 3.7](#)).

In fact, as described in previous works, polyethylene glycol (PEG) tags, at different chain lengths, have well-known protein-repelling properties giving as a result arrays with exceptionally low background.¹²⁷ Moreover, PEG chains are ideal spacers for attaching ligands to a surface at a tuned distance, which helps to improve receptor as well as enzyme accessibility of substrates.¹²⁸

Indeed, when Belouqui *et. al*^{95c} have used the two NHS-activated surface types (**1**, **2**) to

perform enzymatic elongation on immobilized substrates, a substantial difference in term of reactivity has been observed between the two surfaces; in particular, while fucosyltransferases as AtFutA and AgFUT6 have shown almost quantitative conversions for substrates immobilized on surface **2**, a maximum of 50% of conversion has been achieved from surface **1**.

Both linkers were synthesized in our laboratory according to previous procedures^{95c} with the exception of final activation **step f** (Scheme 3.1), for which the yield was improved significantly.



Scheme 3.1: (a) TsOCl, Ag₂O, LiI, DCM, 0°C, 30 min, 52%; (b) NaN₃, DMF, 50°C, overnight, 90%; (c) ET₃SiH, Pd/C 10%, MeOH, r.t., 5 min, 70%; (d) DSC, TEA, DCM, 0°C-r.t., O/N, 90%; (e) DIPEA, DCM, r.t., 1h, 80%; (f) DSC, DMAP, dioxane/acetone, 3h, r.t, quantitative.

3.1.3 Optimized procedure to NHS-activation of hydrophobic ITO surface with linker 2

Our first attempts to coat the hydrophobic slide with the bidentate NHS activated carbamate linker were carried by immersing the slide in a solution of linker **2** overnight. Unfortunately surface coating by immersion followed by washing and drying steps led to an inhomogeneous functionalization of the surface as seen by high fluorescence background and large variability in the spot to spot morphology (Figure 3.7)

We were able to improve the linker coating procedure by dispensing a solution of linker **2** by vibrational vaporization (*IMAGEPrep*®) which resulted in a highly homogeneous functionalization of the hydrophobic ITO slide.

In [Figure 3.8](#), two fluorescent read-outs of printed slides activated with NHS-linker **2** by using immersion coating (*on the right*) and vibrational vaporization (*on the left*) are compared side by side. These fluorescent images have been achieved by 1. printing 5 different N-glycans (in 20 spot replicates) on the two NHS-activated slides, and 2. incubating the immobilized substrates with *WGA-Alexafluor647*.

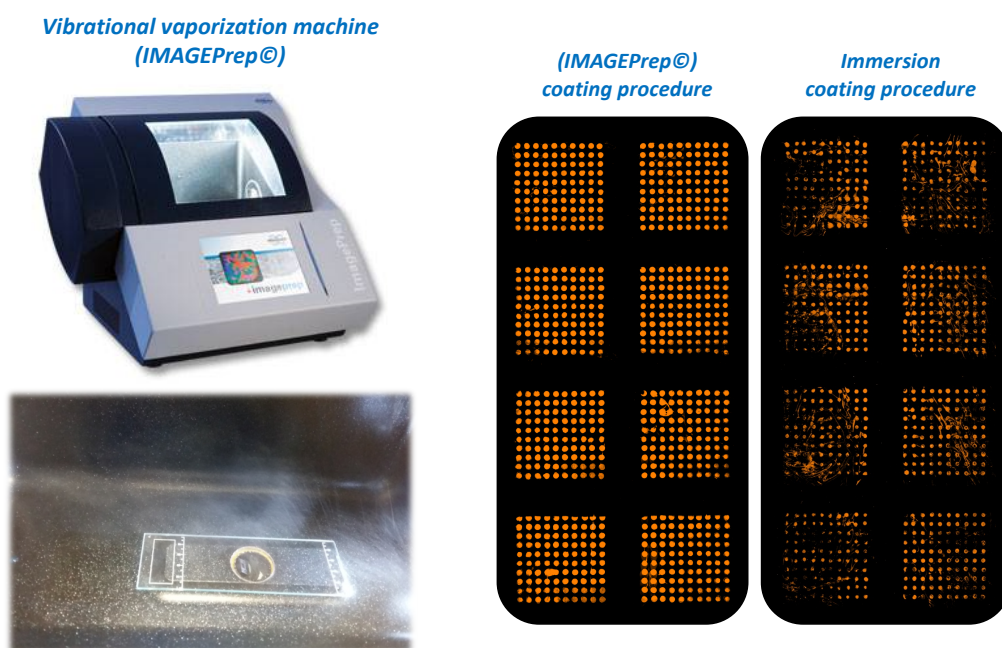


Figure 3.8 Fluorescent read-outs obtained from ITO-glass slide activated with NHS-linker by manual incubation and by vibrational vaporization using Bruker *IMAGEPrep*® nebulizer.

3.1.4 Surface characterization by contact angle measurement

The hydrophobicity of a particular surface is defined by its contact angle. The contact angle (Θ) is measured by placing a droplet of water on the surface and measuring the angle between the substrate surface and the tangent at the point of contact between the droplet surface and the substrate surface ([Figure 3.9](#)). The resulting tangent-surface plane angle is dependent on the surface energy of the substrate and the surface tension of the liquid used (assuming that the gas phase remains constant).

For complete surface wetting, the contact angle will approach zero while for partial wetting, the resulting contact angle adopts values between 0 and 180 degrees

(Figure 3.9a). The contact angle is usually measured to evaluate the hydrophobicity degree of novel developed slide to properly set the printing buffer.

The contact angle was measured for each modification step performed on the commercial ITO-surface to enrich the NHS-activated slide; starting from a commercial ITO-slide with contact angle value of $\Theta = 67^\circ$, the hydrophobicity of the surface was reduced during the piranha solution washing step ($\Theta = 27^\circ$) to be dramatically increased after incubation with ODPAs ($\Theta = 113^\circ$). The incubation step with NHS-activated linker **2** and subsequent washing cycles lead to a hydrophobic surface with contact angle value of $\Theta = 84^\circ$ (Figure 3.9b).

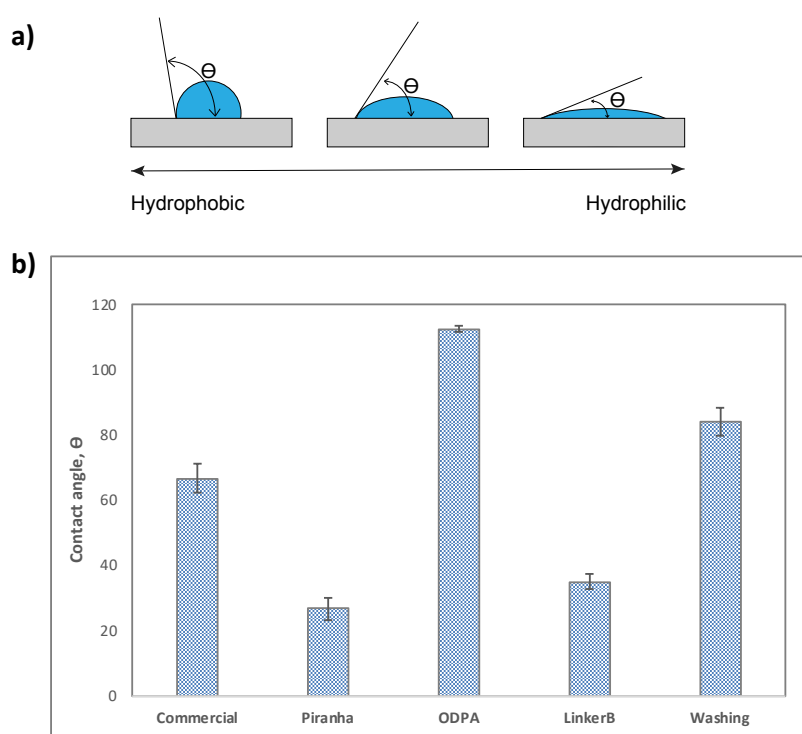


Figure 3.9 (a) Scheme showing drop profile of water spotted onto surfaces of varying degrees of hydrophobicity where Θ is the contact angle. **(b)** Comparison of contact angle values measured after each modification step performed to prepare NHS-activated hydrophobic ITO-surface.

3.2 N-glycans immobilization on NHS-activated ITO surface

An NHS activated carboxylate linker had been chosen for the covalent attachment of an existing library of N-glycans aminopentylglycosides by amide bond formation; this is a high yielding reaction that results in a stable bond which we and others have been employed in the past for the immobilization of glycans and proteins in the preparation of N-glycan and lectin arrays.¹²⁹

3. On-chip chemo-enzymatic synthesis of N-glycan mimetics

From our glycan library of nearly printable 140 structures, we have chosen 20 N-glycans (**G1-G20**) with terminal GlcNAc residues as acceptors for the enzymatic elongation reactions; the glycans showed a large variety in antennae structure (hybrid, complex) terminal residues and core modifications. N-glycans with three or more terminal GlcNAc residues have not been included among the selected structures because of the poor reactivity showed in preliminary enzymatic assays.

Among the selected 20 N-glycans, compounds **G18**, **G19** and **G20** were included as negative controls for the enzymatic elongations and positive internal controls for fluorescent binding assays.

We designed a microarray around 20 N-glycans (**G1-G20**) that were spotted in 8 subarrays in replicates of 4 spots per glycan each subarray. The average spot diameters varied between 321 to 392 μm for different glycans, with a distance between spots of 409 μm in both, x and y axes ([Figure 3.10](#)).

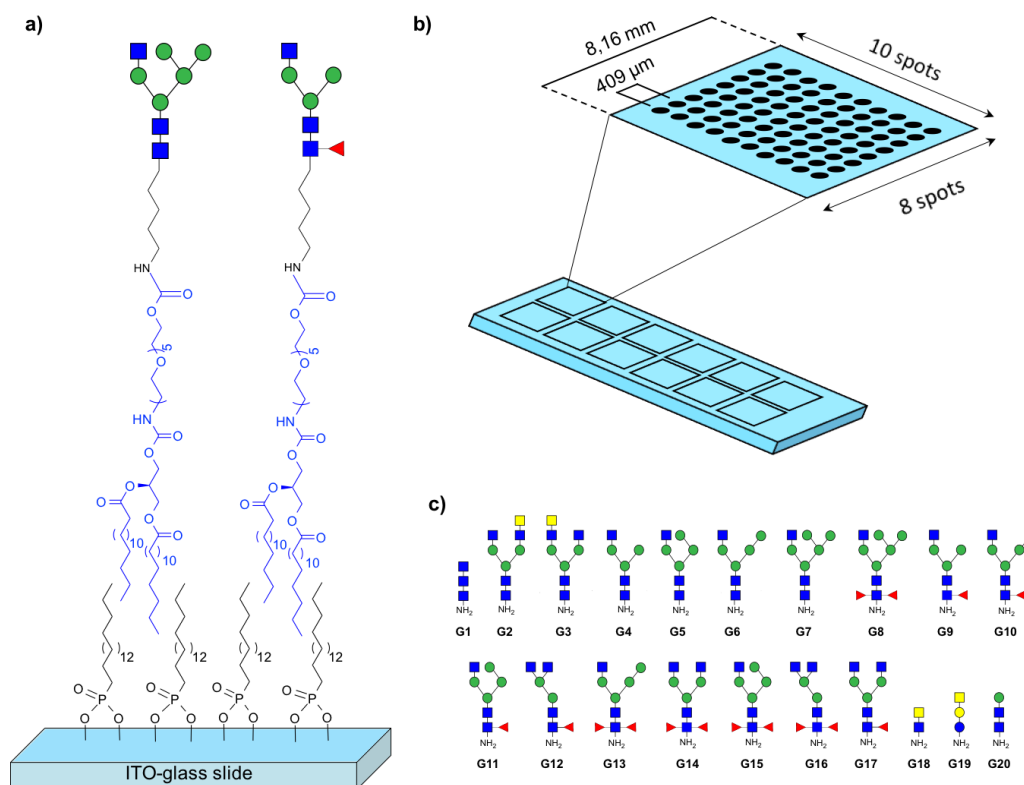


Figure 3.10 (a) Schematization of N-glycans immobilized on NHS-activated ITO-surface through amide bond; (b) Design of glycan microarray format used for preparation of glycomimetics library; (c) N-glycan structures selected for the purpose (**G1-G20**).

3. On-chip chemo-enzymatic synthesis of N-glycan mimetics

Stock solutions (50 μ M in phosphate buffer 300mM, pH 8.7) of synthetic pentyl-amino linked N-glycans (**G1** to **G20**) were prepared in a 384 multi-well source plate; up to 50 drops of each N-glycan solution were printed, onto the NHS-activated hydrophobic-ITO slide, with a *Sciension non-contact printer* and left to react overnight.

For an efficient immobilization of the glycans on the surface, the rapid evaporation of the tiny droplets has to be avoided e.g by performing the spotting and incubation process under controlled humidity (90%) and low temperature (18°C).

Individual spot analysis by MALDI-TOF MS proved to be a rapid method to evaluate successful immobilization.

Unless to use an internal standard, it is not possible to calculate the concentration of each immobilized glycans; on the other hand, we could estimate the glycan amount contained in each tiny printed spot.

Taking into account that we printed 50 drops of 50 μ M glycan solution in each spot and each drop had an average volume of 230 pL (11.5 nL/spot), the final amount of each glycan used for one printed spot was about 0.58 pmol/spot. This printing concentration allowed to immobilize a sufficient amount of sample to acquire MALDI-TOF spectra with high signal to noise ratio.

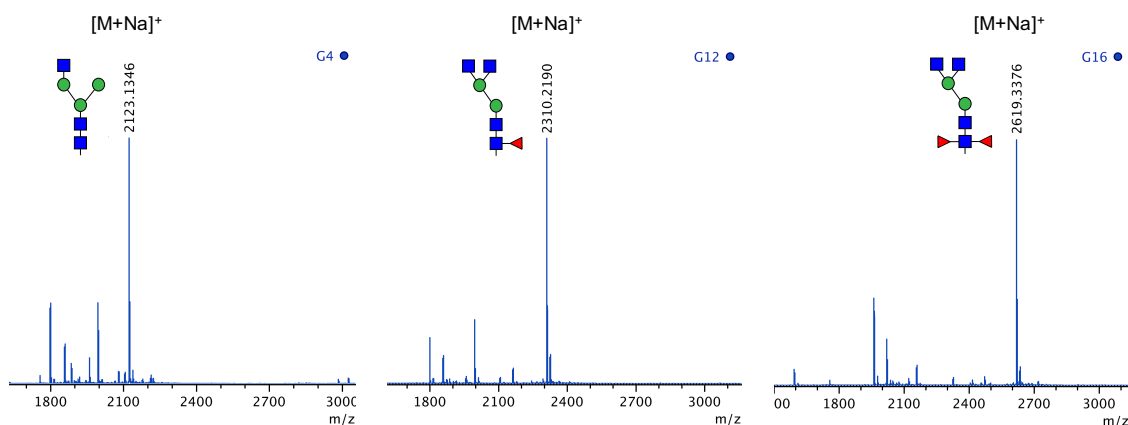


Figure 3.11 Example of MALDI-TOF spectra recorded after N-glycans immobilization.

The microarray printing procedure and in particular the number of droplets employed in printing the arrays described above was developed considering the different sensitivity of the two analytic techniques employed on this surface: fluorescence and MALDI-TOF spectroscopy.

Fluorescence detection is a very sensitive technique, that requires low amounts of immobilized glycans and a highly homogenous surface to reduce background fluorescence and improve spot morphology. In contrast, the detection by MALDI-TOF

MS requires printing the glycans at high concentrations and in a large number of drops. As a result, all the conditions for surface preparation and glycan immobilization were a compromise to allow the efficient detection by both methodologies.

3.3 On-chip enzymatic elongation with azido-N-acetyl-D-galactosamine and double mutant of β -1,4-galactosyltransferase I (C342T_Y289L)

The first step for on-chip synthesis of N-glycan mimetics library was to introduce GalNAz residues on terminal GlcNAc structures (**G1-G17**) using a double mutant of β -1,4-galactosyltransferase I (C342T&Y289L).

3.3.1 Double mutant of β -1,4-galactosyltransferase I (C342T_Y289L) and activity assays

β 1,4-Galactosyltransferase I (Gal-T1) is an enzyme that transfers a galactose moiety from an UDP-Gal donor to GlcNAc residues, with a β -1,4-stereoselectivity. In addition, Gal-T1 can transfer GalNAc from UDP-GalNAc to GlcNAc, but with only 0.1% of the activity seen for the galactose transfer.¹³⁰

To explain this low GalNAc-transferase activity, Qasba and coworkers¹³¹ analyzed the crystal structure of the *Gal-T1 · LactAlbumin (LA)* complex with UDP-GalNAc at 2.1-Å resolution ([Figure 3.12](#)). The crystal structure revealed that UDP-GalNAc binding to Gal-T1 was similar to the binding of UDP-Gal to Gal-T1, except for an additional hydrogen bond bridging the N-acetyl group of GalNAc moiety with the Tyr-289 side chain hydroxyl group ([Figure 3.12a](#)). This hydrogen bond would hinder the required displacement of the GalNAc moiety during the disaccharide linkage formation. Therefore, based on this observation, it was hypothesized that lack of space is responsible for the poor GalNAc-T activity.

Finally, Qasba et al observed that the elimination of this additional hydrogen bond by mutating Tyr-289 residue to Leucine enhanced the GalNAc-transferase activity ([Figure 3.12b](#)); an additional mutation regarding Cys342 in Threonine was also needed to improve the stability of mutated protein.

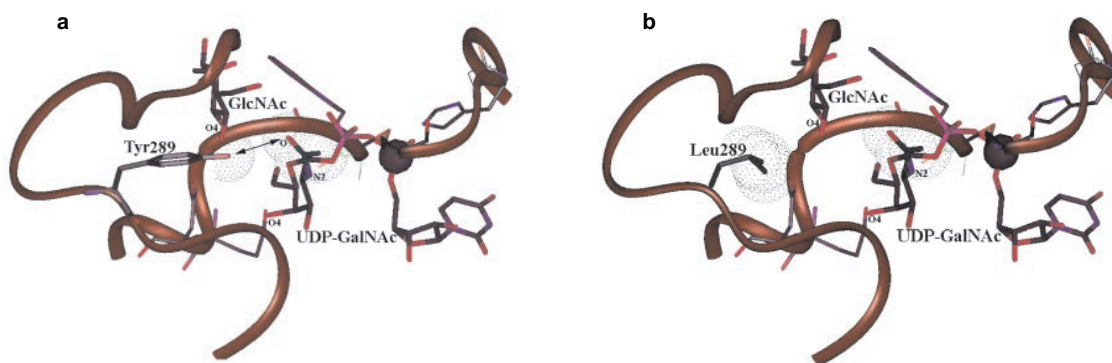


Figure 3.12 (a) Modeling of the GlcNAc in its binding site on the *Gal-T1-LA·UDP-GalNAc·Mn²⁺* crystal structure. (b) Based on the hypothesis that more space is needed between the N-acetyl group of UDP-GalNAc and Tyr-289 residue to facilitate the reaction, the substitution of Tyr-289 by Leucine is modeled. Picture taken from *J.Biol.Chem.*, 2002, **277**, 20833-20839.¹³¹

Ramakrishnan and coworkers have demonstrated that double mutant β -1,4-galactosyltransferase (DM-GalT1) is able to catalyze the transfer not only of natural sugars like GalNAc or Gal but also unnatural moieties like azido-N-acetyl-D-galactosamine and 2keto-galactose.¹³²

According to this activity studies, our purpose was to use the double mutant of β -1,4galactosyltransferase I (DM-GalT1) to transfer GalNAz from the unnatural donor UDP-GalNAz to terminal GlcNAc portions of diversified substrates. The expression of the DM-GalT1 was performed in our laboratory by following a procedure reported in literature;¹³³ few changes to the original protocol were needed to improve the expression yields.

To evaluate GalNAz-transferase activity of DM-GalT1, parallel affinity trials were performed in solution by using 1-*p*-nitrophenyl N-acetyl-D-glucosamine (**11**) as acceptor and UDP-GalNAz (**9**) and UDP-GalNAc (**10**) as donor (Figure 3.13).

The use of compound (**11**) allowed the UV-detection (298 nm) of the final products (**12a,12b**), as well as the starting material (**11**), necessary for quantification of enzymatic conversion.

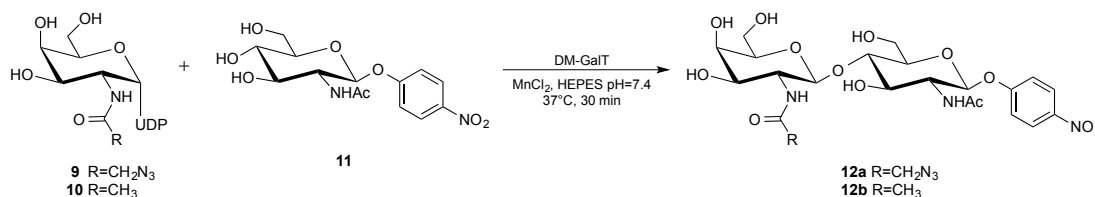


Figure 3.13

3. On-chip chemo-enzymatic synthesis of N-glycan mimetics

The reactions were performed by mixing UDP-derivatives and acceptor (**11**) at a ratio of 1:1 (33 nmol) in a buffer solution of HEPES (50 mM, pH=7.4), containing 1.15 mg/mL of enzyme and MnCl₂ (10 mM). The reactions were shaken at 37°C for 30 minutes, stopped by ten-fold dilution with AcCN and injected in UPLC/MS (HILIC column). The UV detection wavelength was set at 298 nm to measure the peak areas corresponding to starting material (**11**, Rt 0.99) and products (**12a** Rt 1.47, **12b** Rt 1.39).

In [Figure 3.14](#), the chromatograms obtained at 298 nm are reported: blue and green peaks represent starting material (**11**) and final products (**12a**, **12b**) respectively.

As emerged from the activity assays, the DM-GalT1 was able to catalyse the formation of a β -1,4 glycosidic bond with the natural donor UDP-GalNAc (**10**) as well as its azide-derivative (**9**) with comparable activities, 38% and 42% of conversion respectively.

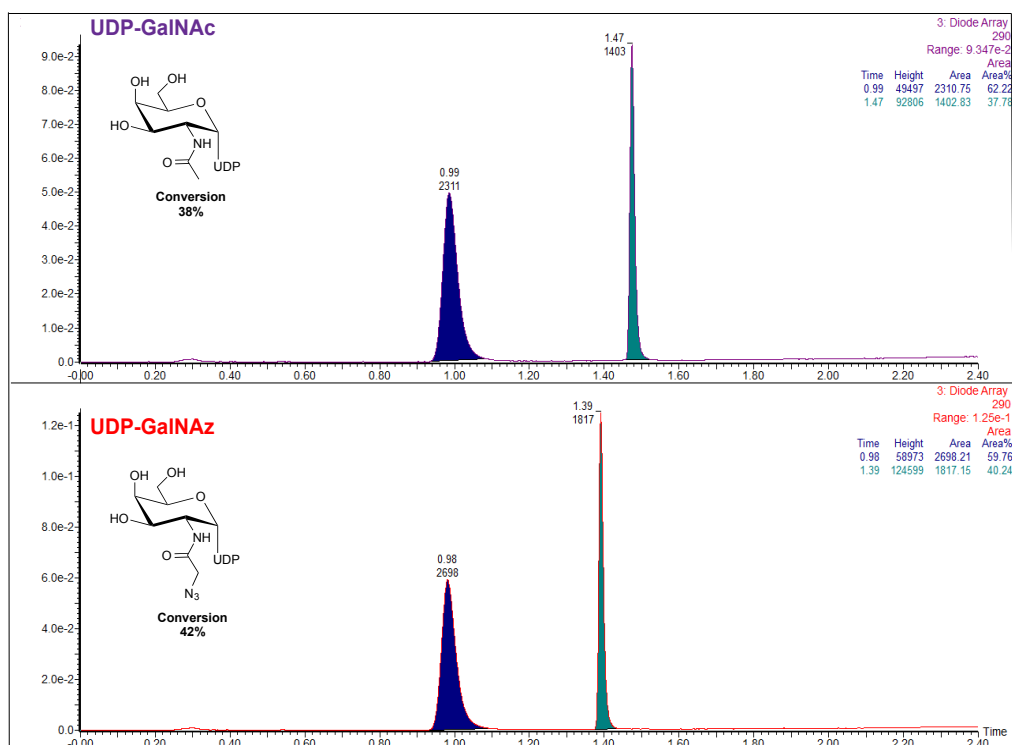


Figure 3.14 Chromatogram spectra detected at 298 nm of enzymatic solution regarding UDP-GalNAc (*above*) and UDP-GalNAz (*below*).

3.3.2 Optimization of on-chip enzymatic protocol with DM-GalT1 and UDP-azido-N-acetyl-D-galactosamine

The enzymatic elongation on array was performed by physically dividing the slide with the help of silicone gaskets into several subarrays that to which we individually applied the enzyme solution; after incubation, the slide was washed to remove all the impurities

from the surface.

A crucial point of this process was to achieve high conversion for all the printed N-glycans, by avoiding enzyme precipitation during incubation, and to develop an effective cleaning procedure that, at the same time, did not affect the stability of the surface. As the non-covalent attachment via hydrophobic interactions was needed for analyzing slides by MALDI-TOF MS, special care had to be taken by avoiding the use of high percentages of organic solvents or detergents which would immediately remove the compound from the slide.

➤ Selection of slide module for enzymatic incubation

To avoid excessive enzyme precipitation we carefully chose the gasket used to delineate the subarrays on the slides into individual wells. Enzymatic elongations with DM-GalT1 were performed on two printed slides, covered with **(a)** a *16-well proplate® Module/6x7mm* and **(b)** a *hybridization gasket from Agilent (8 microarrays/slide format)* (Figure 3.15).

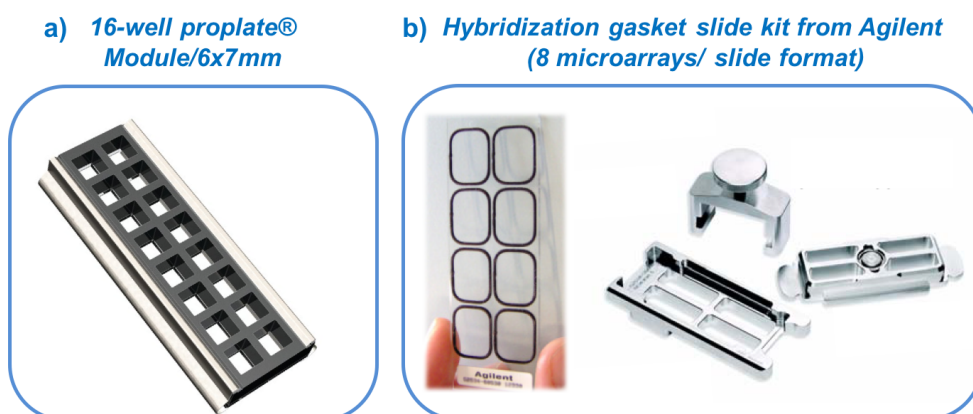


Figure 3.15 Slide modules used to perform preliminary on-chip enzymatic elongation assays.

While enzyme precipitation was observed with gasket **(a)** with consequent lower conversion ratios (detected by MALDI-TOF MS analysis), the enzymatic solution remained transparent when gasket **(b)** was employed and thus overall higher conversions were obtained.

➤ Selection of washing solution to remove enzymatic impurities from surface

Next, a washing buffer composition had to be developed that would efficiently remove the excess reagents after on-chip enzymatic reactions but leave the immobilized glycans untouched.

Preliminary assays were performed by testing different washing solutions on a NHS-quenched ITO slide that was previously incubated overnight with an enzymatic solution of DM-GalT1 at 37°C.

After washing the subarrays with different washing solutions (Figure 3.16), individual wells were incubated with fluorescently labeled *Wheat Germ Agglutinin* (WGA) in duplicates.

Since there were no substrates immobilized on the slide and the DMGalT1 is an unglycosylated protein, the fluorescent read-outs of these assays gave information about unspecific surface-lectin interactions and the effectiveness of the different washing solutions to remove impurities from surface after enzymatic reaction.

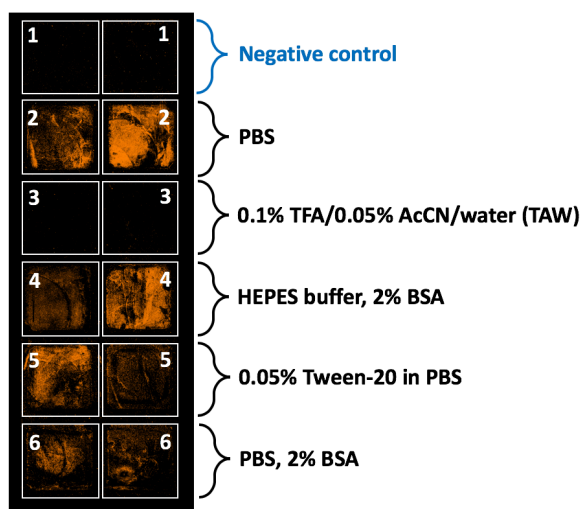


Figure 3.16 All the subarrays were incubated with enzymatic solution, except of **sub-array 1**, and each of them was washed with proper washing solutions. Incubation with WGA-Alexafluor647 has been performed to check the effectiveness of each washing solution.

From Figure 3.16 it was concluded that, among the different washing solutions tested, the TAW solution (**subarrays 3**) led the most efficient cleaning of the surface from enzymatic impurities, obtaining the consequent reduction of background signals in fluorescence assays. On the other hand, in the case of the other mixtures, significant background signals were found by fluorescent read-outs as a consequence of ineffective washing methods.

Since in the previous experiment, TAW solution had shown to be the best candidate for washing the slide after enzymatic elongation with DM-GalT1, a similar assay was repeated on a glycan-printed slide to evaluate the compatibility of TAW-washing with

3. On-chip chemo-enzymatic synthesis of N-glycan mimetics

glycan immobilization stability. The high-quality of the data achieved from this experiment, both in MALDI-TOF detection and fluorescent read-out with WGA-Alexafluor647, confirmed the effectiveness of TAW solution to remove enzymatic impurities without leading to substantial losing of immobilized material from the surface. As a result, TAW-solution proved to satisfy all the requirements to be used in the washing of glycan-immobilized surfaces after performing enzymatic elongation with DM-GalT1.

➤ Selection of reaction conditions to achieve high conversions

To achieve high conversion for all the N-glycan substrates immobilized on the surface, the effect of a number of reaction parameters such as UDP-donor concentration, buffer or reaction time on conversion were systematically explored and accordingly adjusted. Preliminary conditions were tested only on two N-glycan structures **G4** and **G12** and employing UDP-GalNAc, instead of the expensive UDP-GalNAz to save precious material.

Substrate	[donor]	buffer	time	Conversion
G4	1mM	HEPES, pH 7.4	2h	12%
	1mM	Tris-Cl, pH 8.5	2h	18%
	1mM	HEPES, pH 7.4	O/N	74%
	1mM	Tris-Cl, pH 8.5	O/N	73%
	2mM	HEPES, pH 7.4	O/N	86%
	2mM	Tris-Cl, pH 8.5	O/N	66%
	1mM+1mM	HEPES, pH 7.4	2 cycles	87%
G12	1mM	HEPES, pH 7.4	2h	G12(2)=1.7% G12(1)=7.6%
	1mM	Tris-Cl, pH 8.5	2h	G12(2)=5.3% G12(1)=15%
	1mM	HEPES, pH 7.4	O/N	G12(2)=69% G12(1)=0.9%
	1mM	Tris-Cl, pH 8.5	O/N	G12(2)=68% G12(1)=8.1%
	2mM	HEPES, pH 7.4	O/N	G12(2)=72% G12(1)=12%
	2mM	Tris-Cl, pH 8.5	O/N	G12(2)=80% G12(1)=8.9%
	1mM+1mM	HEPES, pH 7.4	2 cycles	G12(2)=70% G12(1)=10%

Table 3.1 On-chip enzymatic elongation assays on N-glycans **G4** and **G12** at different reaction conditions with their respective conversions quantified by MALDI-TOF analysis (G12(2)= bi-glycosylated product, G12(1)= mono-glycosylated product). The conditions that gave the best results in terms of conversion and MALDI-TOF data quality are highlighted in yellow.

Our results summarized in [Table 3.1](#) suggested that an incubation period of 10 hours was needed to achieve conversions of around 70% (G4= 73%; G12(2)=68%) while only a slight improvement in conversion was observed when the donor concentration was increased from 1 mM to 2 mM. Although conversion rates for reactions performed in Tris- buffer were similar or slightly higher than for HEPES, HEPES buffer was chosen since Tris-Cl led to precipitation after overnight incubation.

The best conversions (highlighted in yellow in [Table 3.1](#)) based on assessment by MALDI-TOF MS were achieved by: 1. Performing repeated and short cycles of reaction (2 cycles, 8 hours each), instead of one long cycle, 2. using solution containing DM-GalT1 (0.5 mg/mL), UDP-GalNAc (1mM), HEPES 100 mM pH=7.4, MnCl₂ (10 mM), BSA (0.2%), alkaline phosphatase1U/μL (0.5 μL), and 3. adopting gasket model **(b)**.

Employing these conditions all N-glycans on our array (**G1-G17**) could be extended with UDP-GalNAz to the azido-derivatives (**G1.1-G17.1**) with conversion up to 90% ([Figure 3.17](#)); although quantitative conversion was not achieved in any of the cases, conversions are satisfactory for solid-phase reactions and using the non-natural donor UDP-GalNAz.

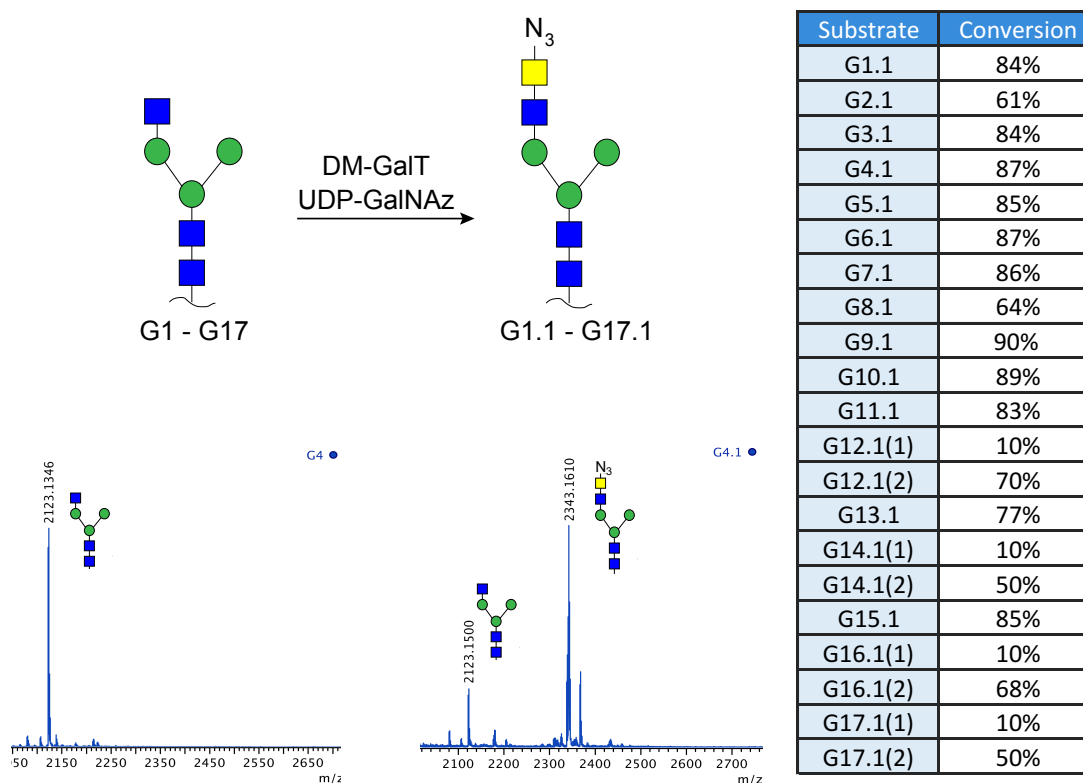


Figure 3.17 (a) Enzymatic elongation with UDP-GalNAz on the immobilized N-glycans (G1-G17); (b) table with conversions of reaction; (c) example of MALDI-TOF spectra before and after elongation with UDP-GalNAz. (Gx.1(2)= bis-glycosylated product, Gx.1(1)= mono-glycosylated product).

➤ Optimization of analysis of spot compositions by MALDI-TOF MS

In all experiments, 2,5-Dihydroxybenzoic acid (DHB) was used as a matrix for MALDI-TOF analysis of arrays. For the azide-derivatives (G1.1-G17.1), we added 0.01 mM of *sodium citrate* to improve the signal by the formation of a single sodium adduct.

The reason to improve the signal is related by in-source fragmentation of instable azide-containing compounds that is usually observed with the formation of peaks $[M-N_2+H]^+$, $[M-N_2+Na]^+$ and $[M-N_2+K]^+$, in agreement with the loss of a nitrogen molecule, next to their respective parent ions $[M+H]^+$, $[M+Na]^+$ and $[M+K]^+$.

The presence of Na^+ ions, introduced by sodium citrate, leads to an enrichment of $[M+Na]^+$ and $[M-N_2+Na]^+$ peaks with a consequent intensity reduction of non-sodiated mass peaks.

Figure 3.18, compares MALDI-TOF spectra of azide-glycan G4.1 obtained with (green) and without sodium citrate (blue) in the matrix solution.

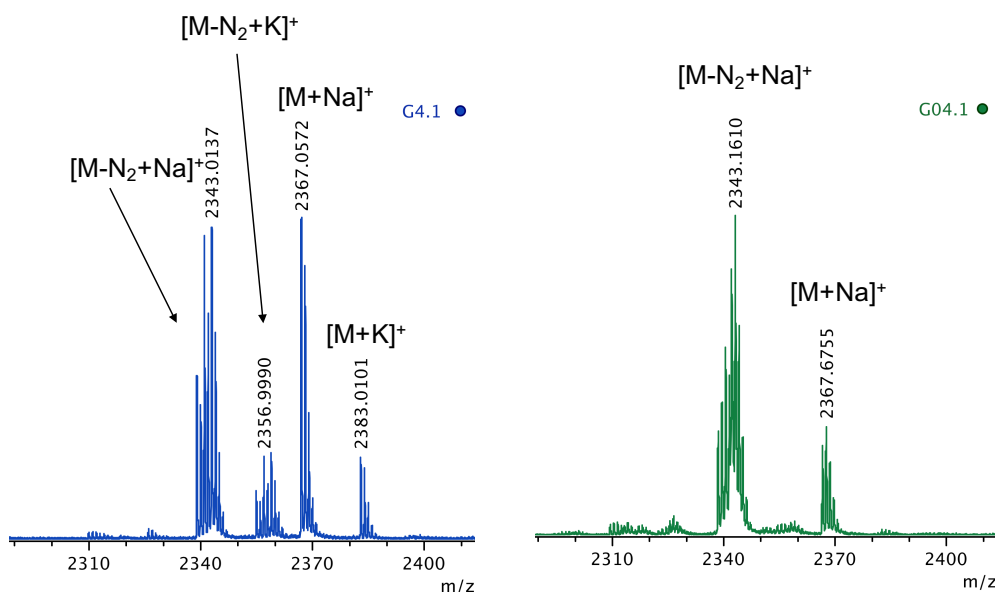


Figure 3.18 MS spectra of the azide-glycan **G4.1** was acquired by using DHB matrix only (*blue*) and DHB matrix containing Na citrate (*green*).

3.3.3 On-chip enzymatic elongations with UDP-GalNAc and UDP-Gal

To evaluate the effect of local non-natural modifications on Gal/GalNAc residues on the binding affinity of N-glycans with C-type lectin receptors, we also prepared the natural galactose and GalNAc homologues as reference materials.

N-Acetyl-D-galactosamine- (**G1.2-G17.2**) and D-galactose-derivatives (**G1.3-G17.3**), were prepared by on-chip glycosylation with UDP-GalNAc and UDP-Gal respectively; the double mutant galactosyltransferase DM-GalT1 was employed for the synthesis of GalNAc derivatives while a commercial β -1,4-galactosyltransferase from bovine milk (EC 2.4.1.22)¹³¹ was used for the preparation of terminal galactosides.

After enzymatic elongation of all the N-glycan substrates with UDP-GalNAc and UDP-Gal, their corresponding glycan-derivatives (**G1.2-G17.2**) and (**G1.3-G17.3**) were obtained with reaction conversions up to 89% and 87% respectively (Figure 3.19).

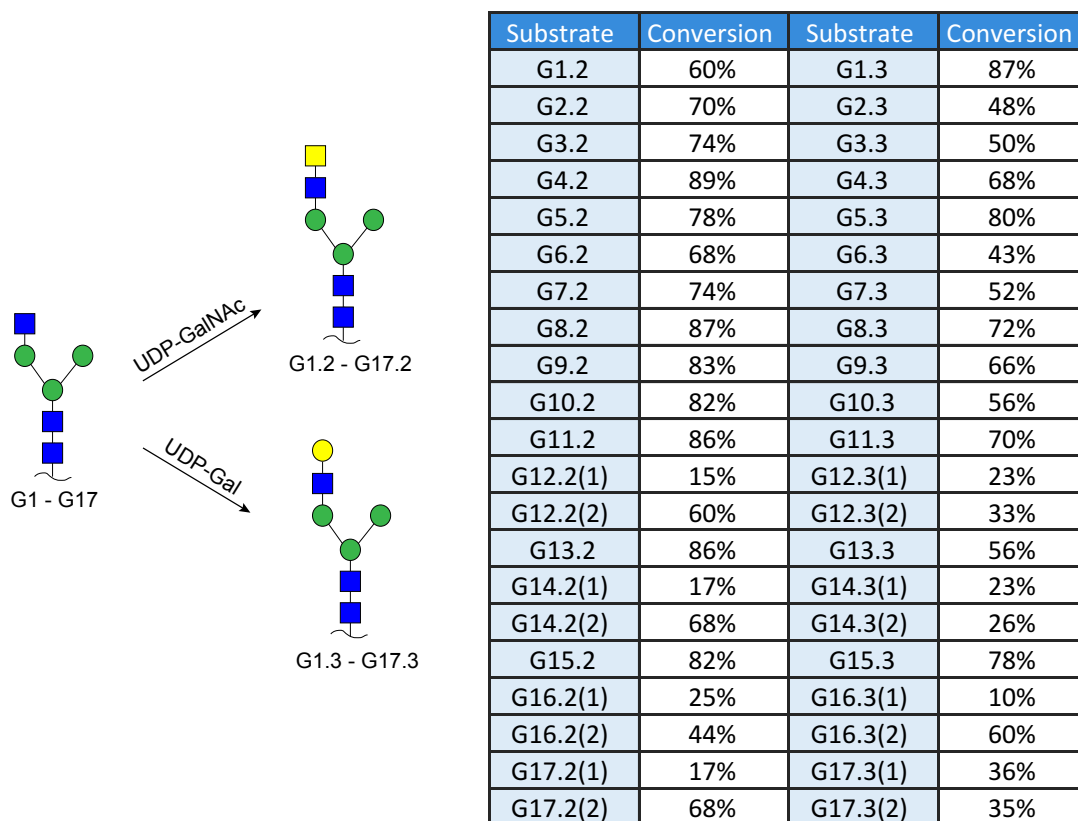


Figure 3.19 The enzymatic elongation scheme with UDP-GalNAc and UDP-Gal on the immobilized N-glycans (**G1-G17**) and a table with their corresponding reaction conversions are reported. (Gx.y(2)= bi-glycosylated product, Gx.y(1)= mono-glycosylated product).

3.4 On-chip Copper(I)-catalyzed Alkyne Azide Cycloaddition (CuAAC) on immobilized azide-N-glycan derivatives

The N-glycan mimetics library was prepared by on-chip Copper(I)-Catalyzed Alkyne Azide Cycloaddition (CuAAC) of the azide-glycans (**G1.1-G17.1**) with a collection of structurally varied alkynes.

The CuAAC, a typical click chemistry reaction, is an orthogonal 1,3-dipolar cycloaddition reaction between an azide and a terminal alkyne that allows triazole formation in the presence of a large number of unprotected functionalities. Moreover, the use of copper(I) salts as catalyst allows the regioselective and efficient preparation of 1,4-disubstituted 1,2,3-triazoles at room temperature, in very short reaction times and tolerating a variety of solvents including aqueous media.¹³⁴

3. On-chip chemo-enzymatic synthesis of N-glycan mimetics

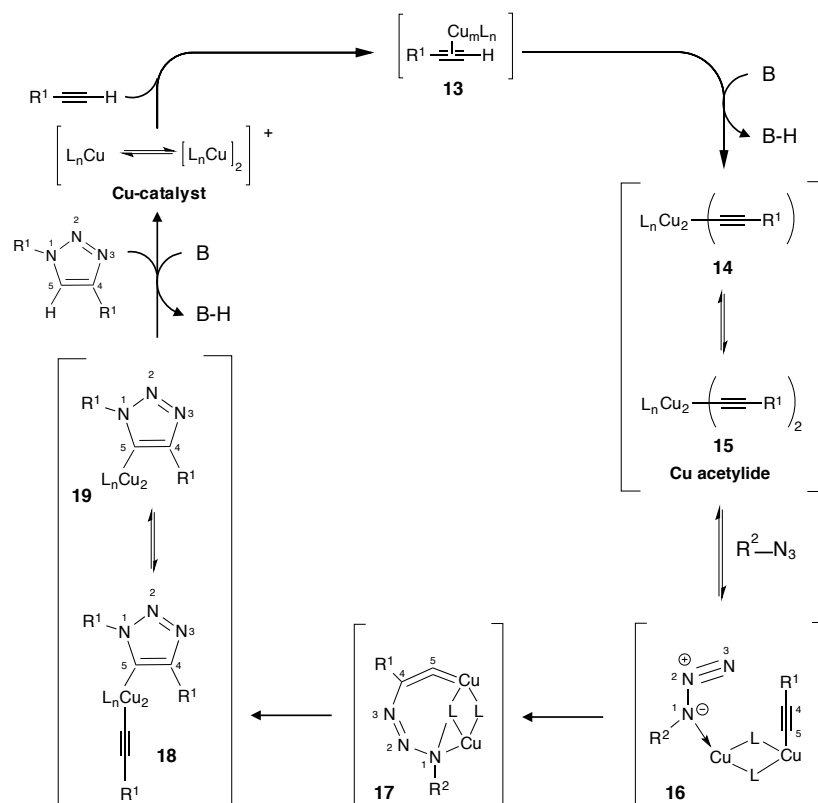


Figure 3.20 Proposed outline of species involved in the stepwise catalytic cycle. Picture modified from *Eur. J. Org. Chem.* **2006**.¹³⁵

Compared to other metal-catalyzed reactions, the use of Cu(I) presents the major advantages of being inexpensive and easy to handle. Indeed, most of the protocols involve the reduction of stable sources of Cu(II) with sodium salts (e.g. Na ascorbate) or the comproportionation of Cu(II)/Cu(0) species. In addition, both alkyne and azide functional groups present high stability under a variety of conditions and can be incorporated into a wide range of compounds by several methods.¹³⁶

All these features, combined with the potentially favorable physicochemical properties of the resulting triazoles, have propelled the Cu(I)-catalyzed cycloaddition to be one of the most popular and efficient reactions to rapidly create molecular diversity.

The copper(I)-catalyzed cycloaddition is often addressed to modification of proteins through formation of 1,4-disubstituted triazoles, excellent mimetics of the peptide bonds, that provide an increased peptide stability toward mammalian, bacterial and viral proteases.¹³⁷

The triazole group is often introduced on natural or therapeutic molecules to enhance their solubility and/or bioavailability, to attach fluorophore or to modify the drug structures. Moreover this type of reaction has been used to introduce ^{18}F label on several compounds

such as small organic molecules, carbohydrate, amino acid and nucleotide with high radiochemical yields.¹³⁸

In Glycoscience, the CuAAC is often adopted to bind sugars to biomolecules or synthetic macromolecules, modify sugars by creating diversified glycomimetics, prepare multivalent architectures as dendrons and dendrimers, etc.¹³⁹

Although the Cu(I)-catalyzed cycloaddition has been extensively used for many diverse applications involving numerous azide- and alkyne-type substrates, few examples of *on-chip* CuAAC have been reported in literature.

First attempts of *on-chip* Cu(I)-catalyzed cycloaddition reaction were performed by Paulson and co-workers for the preparation of a sialoside library. These attempts were achieved by coupling a set of azides on alkyne-sialoside compounds immobilized onto commercial NHS-activated surface (Schott-Nexterion slide-H). To assess on chip conversion, the authors coupled unreacted alkynes with a fluorescent azide in a second step. After this second click reaction, absent or low-intensity fluorescent signals was interpreted as a high reaction yield during initial cycloaddition.

With this strategy, Paulson and co-workers prepared a large sialoside library reaching near-quantitative conversion for all the azide-alkyne couples involved and therefore proving the high versatility and effectiveness of this reaction-type on solid platform.

In contrast to Paulson's approach, in our case the azides were immobilized on the surface instead of alkynes and the spot compositions were analyzed by *in situ* MALDI-TOF MS to achieve more detailed information about reaction conversions and number/types of species present in analyzed spots.

3.4.1 Optimization of on-chip CuAAC

Preliminary reaction conditions were optimized on the small azide-disaccharide **G21.1** by using first alkyne **a1**. Afterwards, the assays were extended to include a small collection of further 28 terminal alkynes ([Figure 3.21](#)) which have been selected among a large collection of commercially available structures.

Since carbohydrate-lectin complex stability is related to a network of numerous weak interactions, we have chosen those alkynes functionalized with groups able to establish additional interactions or replace the already existing ones.

With this purpose, diversified alkynes functionalized with polar heads (amine-, alcohol-type), aromatic rings (with electron withdrawing or donating groups), hydrophobic chain,

3. On-chip chemo-enzymatic synthesis of N-glycan mimetics

etc. have been used for the preparation of the N-glycan mimetics library.

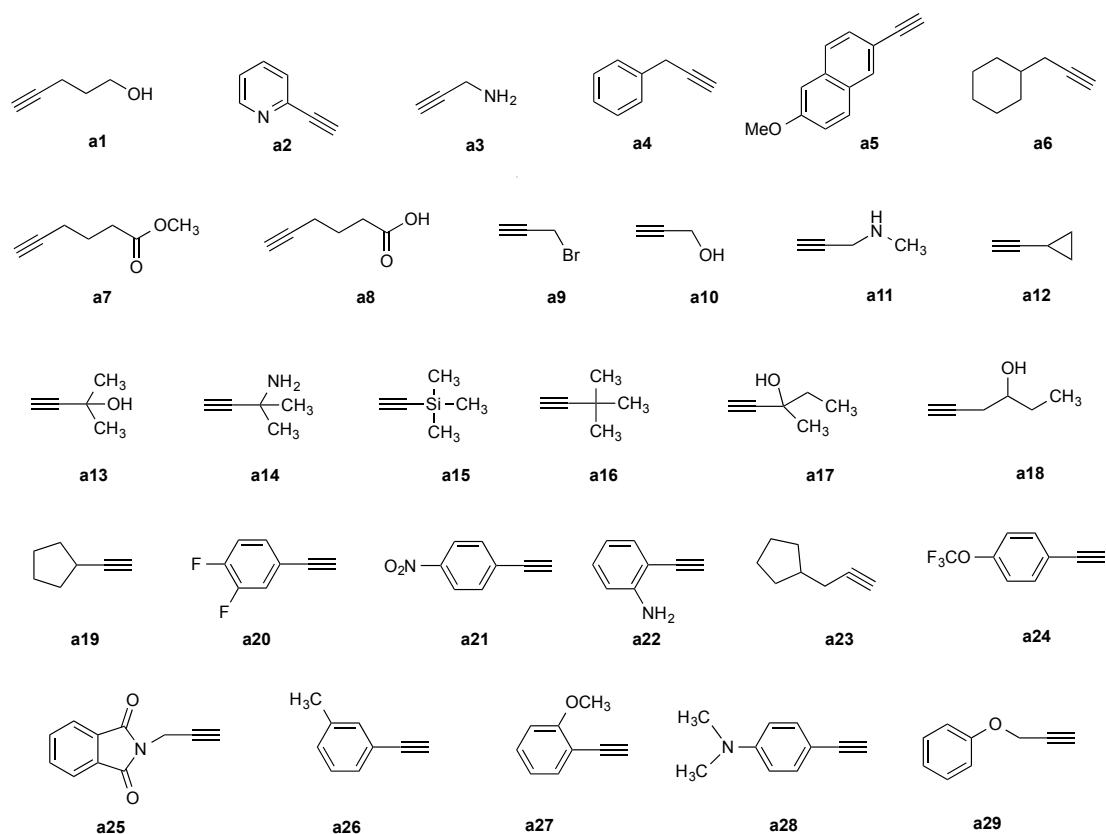
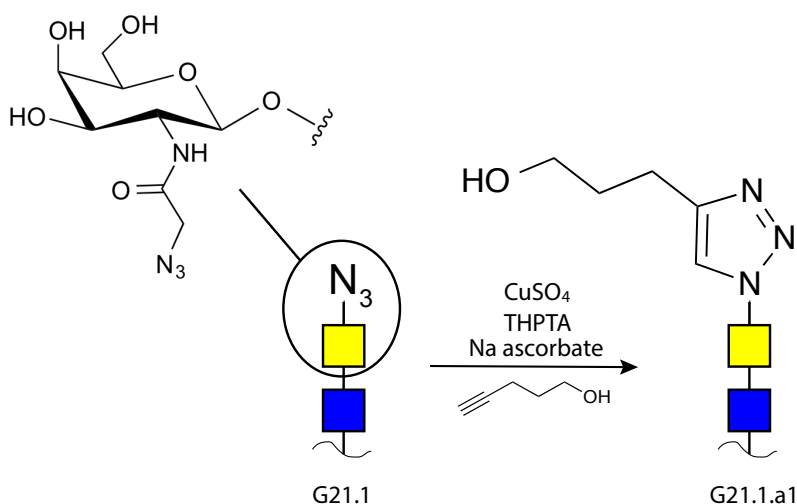


Figure 3.21 Structures of alkynes employed in the cycloaddition on immobilized azide-glycans.

The on-chip preliminary CuAAC was performed by physically dividing the slide into several subarrays with a silicon gasket. Each subarray, printed with 10 copies of **G21.1**, was individually coated with differently composed solution that contained: alkyne **a1** (4-pentyn-1-ol), CuSO_4 , sodium ascorbate, THPTA (tris-hydroxypropyltriazolylmethylamine) and DMSO (up to 1%) in aqueous solution.

THPTA is a water-soluble, very effective ligand for Cu(I)-catalyzed cycloaddition and serves a dual purpose: 1. acceleration of the CuAAC reaction by maintaining the Cu(I) oxidation state of copper sources and 2. protection of biomolecules from oxidative damage during the labeling reaction (in case of bioconjugation).^{140,141}



[CuSO ₄]	Na ascorbate	THPTA	time (min)	Conversion
1.15 μM	11.5 μM	5.1 μM	120	60%
11.5 μM	115 μM	51 μM	120	70%
57.5 μM	288 μM	575 μM	120	quantitative
57.5 μM	288 μM	575 μM	20	quantitative

Figure 3.22 Representation of Cu(I)-catalyzed cycloaddition on the azide-disaccharide **G21.1** with alkyne **a1** and table containing different reaction conditions and relative conversions. The conditions highlighted in green are the best in terms of conversion and time of reaction.

By using a large concentration of reagents, it was possible to achieve quantitative conversion for azide **G21.1** with alkyne **a1** in only 20 minutes ([Figure 3.22](#), highlighted in green).

Subsequently, these established conditions were adopted to perform the Cu(I)-catalyzed cycloaddition on the azide-disaccharide **G21.1** with all the 29 selected alkynes (**a1-a29**); the effectiveness of every single reaction was checked by MALDI-TOF MS analysis ([Table 3.2](#)).

3. On-chip chemo-enzymatic synthesis of N-glycan mimetics

alkyne	conversion	alkyne	conversion
a1	quantitative	a16	quantitative
a2	quantitative	a17	quantitative
a3	quantitative	a18	quantitative
a4	quantitative	a19	-
a5	quantitative	a20	20%
a6	quantitative	a21	-
a7	quantitative	a22	quantitative
a8	-	a23	quantitative
a9	-	a24	-
a10	quantitative	a25	quantitative
a11	quantitative	a26	quantitative
a12	quantitative	a27	90%
a13	quantitative	a28	quantitative
a14	quantitative	a29	quantitative
a15	-		

Table 3.2 Conversion achieved by performing CuAAC on azide-glycan **G21.1** with 29 alkynes (**a1-a29**).

The assays reported in [Table 3.2](#) showed cycloadditions performed on the same azide-substrate (**G21.1**) present a strong variability in conversion for different alkynes; moreover, by coupling the same alkyne on the azide-glycans (**G1.1-G17.1**), a further discrepancy in term of conversion have been observed.

In contrast to Paulson's experiments (C. D. Rillahan, *ACS Chem. Biol.*, 2013, **8**, 1417–1422), the on-chip Cu(I)-catalyzed cycloaddition performed in this thesis work seems to not go always to completion but reaction conversions have a large degree of alkyne-azide dependent variability.

Finally, to drive reactions towards completion, the use of a large reagents excess, extended reaction times and basic pH have been required; in addition, DMSO (from 1% to 10%) was employed to improve the solubility of the alkynes in aqueous media without affecting the surface stability.

Each single click reaction was quantified by MALDI-TOF analysis after removing click solution by washing the slide with water.

Even after optimization of reaction conditions we observed that for around 10 alkynes the cycloaddition did not take place or proceeded with yields below 20%; therefore, these alkynes were excluded from our synthetic strategy.

3. On-chip chemo-enzymatic synthesis of N-glycan mimetics

Figure 3.23 shows the range of conversion for those compounds which exhibited appreciable reactivity in the on-chip cycloaddition; these 19 alkynes were selected for the synthesis of a N-glycan mimetics library.

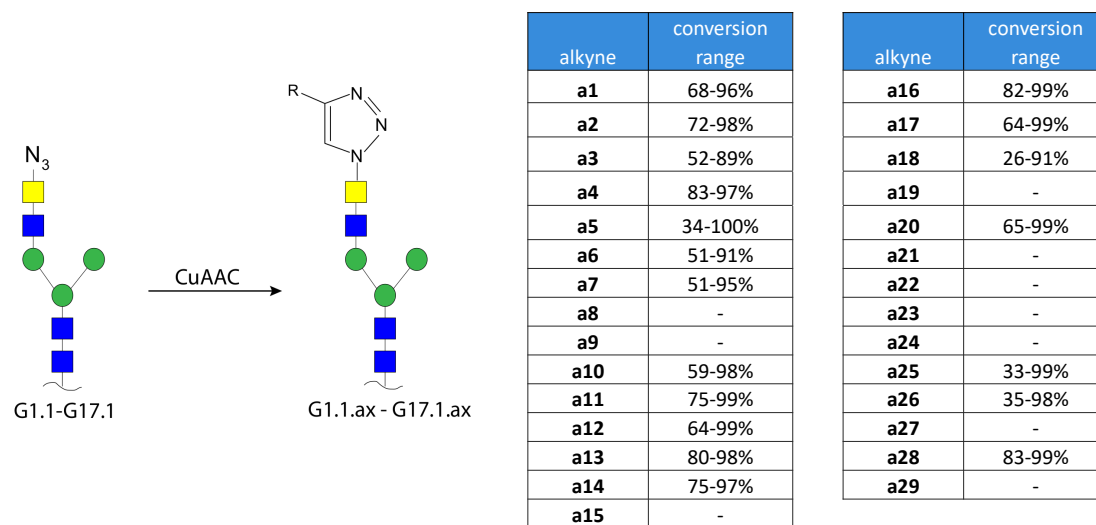


Figure 3.23 CuAAC performed on immobilized azide-glycans and table with conversion ranges achieved with 19 selected alkynes.

The *in situ* MS analysis, in contrast to the fluorescent detection used by Paulson and coworkers, allowed the analysis of spot compositions after each reaction step and, therefore, detect the formation of by-side products as in the case of alkynes **a21** and **a23** during their coupling with all azide N-glycans (**G1.1-G17.1**). Moreover, the MALDI-TOF MS analysis provides, within its limit of detection, a better method for detecting unreacted azides than employing a fluorophore that is even bulkier than the initial azide.

As alternative to the coating approach, we also tried to perform a *spotwise method* which consists in robotically spotting, on the top of immobilized substrate, nanodroplets of reactant solution and letting the reaction works in such small volume. This method of on-chip reaction has been already used in our lab⁷⁵ to perform enzymatic elongations with diverse enzymes including α -2,6-sialyltransferase, α -1,3-fucosyltransferase and β -1,4-galactosyltransferase for the preparation of a N-glycan library.

While in the published work the spotwise approach admitted to perform high yielding enzymatic modifications by using reduced amounts of precious glycosyltransferases, in our case the method was not successful; the main reason for failure was the large size of printed N-glycan spots on the surface.

Indeed, in Serna's work the printed spots have a diameter of 100-200 micrometers that

could be totally covered by 2-5nL of reactant solution; in this thesis work, for reasons previously discussed, the printed spots are usually characterized by a diameter of 240-306 micrometers that is difficult to completely cover with alkyne-containing nanodroplets.

In addition, even by spotting a large number of drops (100 drops, ~23 nL), after only 2 hours of reaction, all the spots were completely dry. As a result, after reaction incubation, the spot composition appeared heterogeneous and conversions were lower than the ones found with the same type of alkynes when *coating approach* was employed.

By using the optimized *coating procedure* with the selected nineteen alkynes (Figure 3.22) and azide N-glycans (**G1.1-G17.1**), **323 novel ligands** were synthesized.

These N-glycan mimetics together to glycan-derivatives synthesized by performing enzymatic elongation with UDP-GalNAz (**G1.1-G17.1**), UDP-GalNAc (**G1.2-G17.2**) and UDP-Gal (**G1.3-G17.3**) constitute a library with a total of **374 novel ligands** that were characterized by MALDI-TOF MS analysis and used in binding assays with several different lectins.

3.5 Microarray-based lectin-binding assays of N-glycan mimetics library

According to array designing that admit a maximum of 80 spots for each well together to the use of a *hybridization gasket from Agilent (8 microarrays/slide format)* to perform enzymatic elongation and the selection of 19 alkynes for the preparation of the library, a total of four ITO-slides have needed for the preparation of **374 ligands** to test against each selected C-type lectin.

Binding properties of novel ligands have been evaluated by incubation of each single sub-array with buffer solution containing fluorescently labeled lectin and subsequent analysis in fluorescence reader such as the ProScanArray (PerkinElmer, Waltham, MA).

The comparison of fluorescent intensities detected on different slides or different wells within the same slide can be challenging since reaction and washing cycles performed on the slide can introduce variation in the measurements difficult to control.

To overcome this issue, fluorescent signals were normalized to an internal standard.¹⁴² The *normalization method* consists in determining the signal intensity of one ligand, chosen as reference sample over the entire sub-array, and calculating the ratio of such intensity to an arbitrary value (e.g. 100). This ratio represents the *normalization factor (NF)* that is multiplied by all the signal intensities detected on the sub-array to give final

data that could be compared with other fluorescence data detected (and normalized) on other sub-arrays either on the same slide (intra-slide) or on different slides (inter-slide).

In order to make reliable the normalization process, the reference sample must satisfy two conditions: 1. its fluorescent signal intensity has to be quite strong to give low variability, 2. the sample reference has to be inert to all the processes that occur on the surface before performing the binding assays.

We employed **G18** (for WGA and MGL) and **G20** (for Langerin) as internal standards since they are not substrates for DM-GalT1 and GalT1 and they are also inert in click reaction. After choosing a standard value of 100 to calculate the normalization factor, the normalization was performed for all of our slides by using the same reference sample in all the sub-arrays.

3.5.1 Binding assays with *Wisteria Floribunda* Agglutinin (WFA)

First binding studies were carried out by screening the 374 ligands of N-glycan and mimetics library with fluorescently labeled *Wisteria Floribunda Agglutinin (WFA)*, a plant lectin which specifically binds to glycans presenting α - and- β *N*-Acetyl-D-galactosamine residues.¹⁴³ Preliminary screening assays by using WFA were necessary as proof of concept of the established protocol and to optimize the fluorescence binding assays; **G18** was chosen as internal reference to normalize the array intensities.

Figure 3.24, shows the Heat Map of WFA-Alexafluor647 screening towards the 374 novel synthesized ligands.

As expected, among the printed N-glycans (**G1-G20**), only those substrates with terminal GalNAc residues (**G2, G3, G18**) gave a strong binding (RFU \geq 100) with WFA.

The introduction of galactose residues (**G1.3-G17.3**) did not afford any difference in the binding compared to their respective parent N-glycan scaffolds (**G1-G17**). On the other hand, the GalNAz- (**G1.1-G17.1**) and the GalNAc-derivatives (**G1.2-G17.2**) showed a general increase in binding strength.

By coupling reaction with alkynes, it is interesting to observe that the binding strength of each azide-N-glycan structure (**G1.1-G17.1**) can dramatically change according with the nature of the alkyne employed in the cycloaddition reaction. For instance, the GalNAz derivative **G8.1** that had RFU=131, when it was coupled with 2-ethynyl pyridine (**a2**) to afford compound **G8.1.a2**, its RFU was 48. On the contrary, if azido-derivative **G8.1** was coupled with 5-hexyn-3-ol (**a18**) to obtain compound **G8.1.a18**, its RFU was 283. Thus, it is remarkable to note how the azide N-glycan scaffold **G8.1** can become a weak or a strong binder by only changing the type of alkynes used in the copper(I)-catalyzed cycloaddition.

In [Figure 3.25](#), the structures of the strongest binders (RFU $>$ 200) for *Wisteria Floribunda Agglutinin* (WFA) are shown. The 7 ligands are based on 5 different glycan scaffolds and 4 different alkynes. Notably, scaffold **G11** shows strong binding to WFA when presenting 3 different triazoles formed from alkynes **a12**, **a18** and **a6**, respectively. The triazole based on the cycloaddition of 5-hexyn-3-ol (**a18**) also provides strong binding for scaffolds **G8**, **G11** and **G12**. Likewise, the triazole based on cyclopropylacetylene (**a12**) provides excellent binding to WFA when presented either on scaffold **G1** or **G11**. Scaffold **G4** is structurally quite similar to **G11** or **G8** which carry one or two additional mannose residues, but only the presentation of the triazole based on *tert*butylalkyne **a16** results in a strong binding above the threshold of 200 RFU.

3. On-chip chemo-enzymatic synthesis of N-glycan mimetics

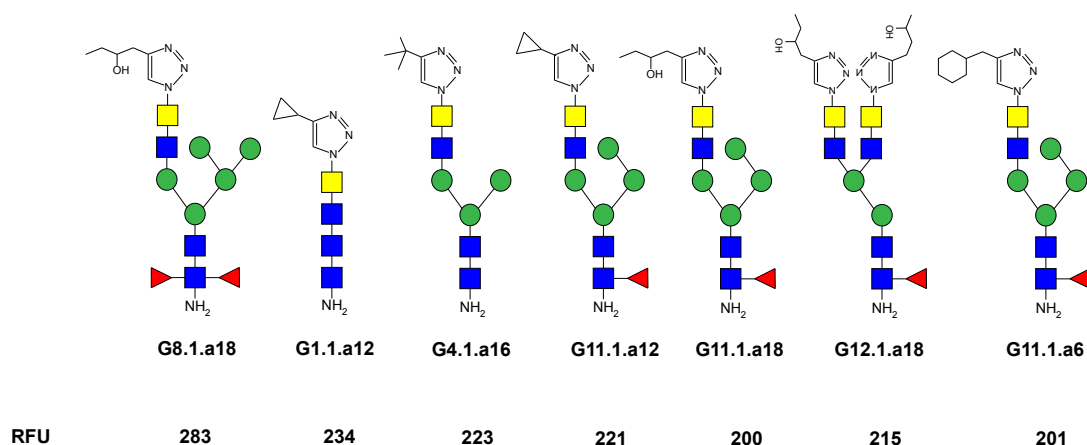


Figure 3.25 N-glycan mimetic structures showing the highest affinity for *Wisteria Floribunda Agglutinin*.

Since the on-chip reactions performed to prepare the N-glycan mimetics library did not lead to quantitative conversions, the spots analyzed in binding assays always presented a mixture of products, which was analyzed by MALDI-TOF MS.

As the enzymatic glycosylation with GalNAz was the lowest-yielding reaction, the main by-products of the analyzed spots were starting N-glycans (**G1-G17**) which showed a general low or absent binding with the WFA. Consequently, we assume by-products on the spots only contribute to the dilution of the target glycomimetic concentration on the surface but without significantly altering the binding event.

3.5.2 Binding assays with Macrophage Galactose Lectin ECD (extracellular domain)

Recombinant *Macrophage galactose lectin ECD* (*MGL ECD*) is a human lectin that shows a narrow specificity for binding to terminal GalNAc-residues.³⁵

Macrophage Galactose Lectin ECD was screened with our 374 ligands and **G18** was chosen as internal reference to normalize the array intensities.

Figure 3.26, shows the Heat Map of MGL-Alexafluor555 screening towards the 374 novel on-chip synthesized ligands.

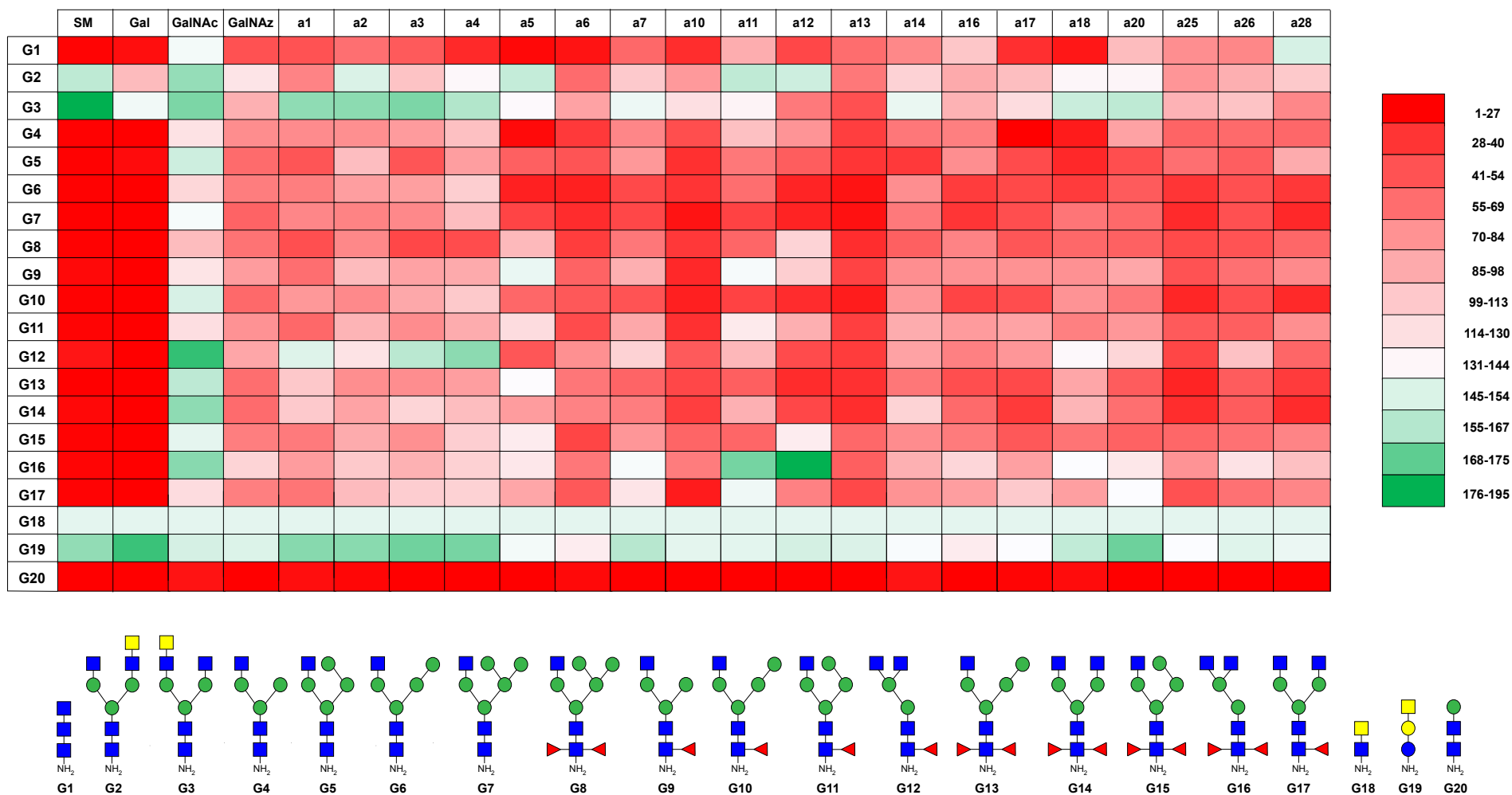


Figure 3.26 Heat map of the normalized relative fluorescence unit (RFU) relate to the binding of the 374 ligands with MGL-Alexafluor555

As anticipated, among the printed N-glycans (**G1-G20**), only those structures with terminal GalNAc residues (**G2, G3, G18, G19**) showed strong interaction with *MGL ECD* (RFU \geq 100).

After glycosylation with GalNAc, derivatives (**G1.2-G17-2**) showed a general significant increase ($72 < \text{RFU} < 174$) in binding compared to the corresponding parent N-glycans (**G1-G17**). On the other hand, the glycosylation with Galactose or GalNAz residues gave a general weak binding compared to the GalNAc glycosylation.

By coupling the 19 alkynes with the azide N-glycans (**G1.1-G17.1**), any binding improvement was generally observed compared to respective azido substrates. The azido-glycan **16.1** derivatized with triazole based on cyclopropylacetylene (**a12**) was one of the few exceptions that showed a pretty high value of relative fluorescence unit RFU=194. From these results emerge how *MGL ECD* is strictly selective for own galactosamine epitope and every small modification performed on this monosaccharidic moiety can weaken the lectin binding.

The structures of the best ligands (RFU $>$ 137) for *MGL ECD* are reported in [Figure 3.27](#); this lectin showed a narrow specificity for *N*-acetyl-*D*-galactosamine epitope, as reported by Irimura and co-workers,³⁵ with a particular preference for bi-antennary derivatives. Our results showed that any modification performed on the GalNAc epitope, even the simple substitution of GalNAc moiety with GalNAz, provided a general and dramatic weaken of the binding.

On the bases of the experiments here reported and the known high selective of the first binding pocket of MGL, the future development of MGL inhibitors could be rather addressed on the modification of sugar moieties interacting with extended or secondary binding sites of the lectin.

As discussed for WFA, the impurities present in the spots only contributed to dilute ligand concentration on the surface without interfering in the binding events.

3. On-chip chemo-enzymatic synthesis of N-glycan mimetics

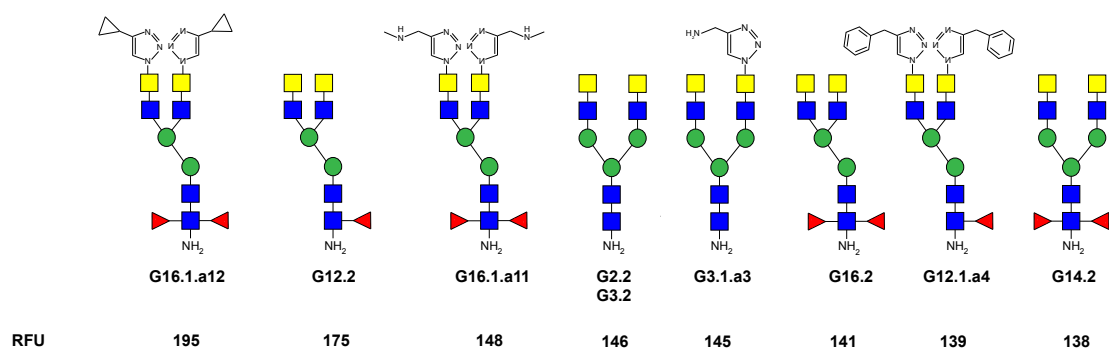


Figure 3.27 N-glycan mimetic structures showing the highest affinity for *Macrophage Galactose Lectin ECD*.

3.5.3 Binding assays with Langerin ECD (extracellular domain)

Langerin is a type II transmembrane C-type lectin showing selectivity for mannose-, fucose- and N-acetylglucosamine-containing carbohydrates³² but also β -glucans¹⁴⁴ and sulfated carbohydrates.¹⁴⁵ Based on the primary glycan binding specificity of Langerin, we chose the N-glycan **G20** with a terminal mannose as internal standard to normalize the fluorescence data. [Figure 3.28](#), shows the Heat map for *Langerin-Cy3* screening toward the 374 mimetics and N-glycans library.

3. On-chip chemo-enzymatic synthesis of N-glycan mimetics

By screening the *Langerin ECD-Cy3* on the N-glycans (**G1-G20**), a selective binding (RFU ≤ 100) was observed for those structures containing mannose-terminal epitopes. In addition, modifying glycan structures by glycosylation and/or triazole formation, the binding of Langerin became weaker than the respective parental N-glycans.

Nevertheless, some exceptions were observed in the case of N-glycan mimetics functionalized with aromatic alkynes, such as **a5**, **a20**, **a25**, **a26** and **a28** which have shown strong fluorescent signals (RFU > 100).

The structures of the best ligands (RFU > 200) for *Langerin ECD* are reported in [Figure 3.29](#); although these structures are based on different glycan scaffolds, all of them are characterized by aromatic triazoles based on the cycloaddition reaction of 3,4-difluorophenylacetylene (**a20**), 3-ethynyltoluene (**a25**), and 2-ethynyl-2-methoxybenzene (**a26**).

In this binding screening, we observed how binding properties of certain lectins could be perturbed by proper modification of cores that apparently are not involved in the first binding pocket; indeed, a binding of a mannose-type lectin as *Langerin ECD* was affected by local modifications performed on the azido-N-Acetyl-D-galactosamine core and, in particular, a strengthened binding has been achieved when glycans were functionalized with aromatic-based triazoles. With these results in our hands, we can furnish a further proof regarding the role of secondary and extended binding pockets of lectins to indirectly interfere with lectin binding affinity.

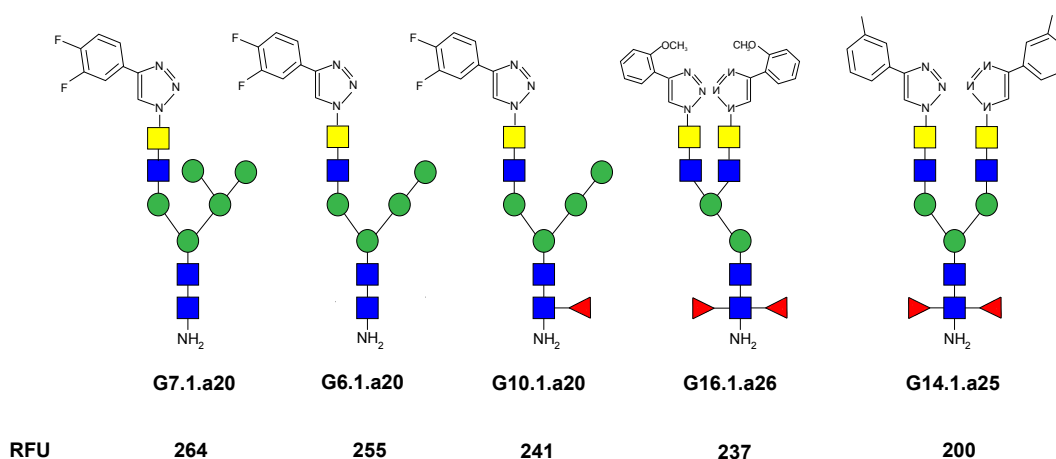


Figure 3.29 N-glycan mimetic structures showing the highest affinity for *Langerin ECD*.

Unlike *WFA* and *MGL ECD*, *Langerin ECD* showed a moderate binding for almost all the immobilized N-glycans (**G1-G20**). As results, the presence of impurities in analyzed spots, due mainly to incomplete enzymatic elongations, can affect the *Langerin ECD* screening.

It is important to take into account that the microarray-based technology is a *qualitative* analytical method that allows to perform quick and preliminary carbohydrate-lectin binding study and select the most promising binders among a large collection of ligands. Complete lectin binding studies are achieved by upscaling the selected ligands in solution and re-analyzing their pure form by microarray and other proper analytical techniques.

3.6 Conclusion

In this chapter, we developed an NHS-activated hydrophobic ITO-glass slide optimized to perform MALDI-TOF analysis of immobilized substrates and fluorescence detection of binding events.

Although this array format presents glycans hydrophobically attached on the surface through a NHS-linker, this type of immobilization proved to be enough stable to perform either enzymatic or chemical functionalization, followed by proper washing steps, without losing ligand-linked material.

With this powerful surface in our hand, we established an on-chip chemo-enzymatic protocol for the preparation of the first library of N-glycan mimetics for improved carbohydrate lectin recognition targeting. In particular, the synthetic strategy adopted included high yielding reactions as enzymatic elongations with UDP-azido-N-acetyl-D-galactosamine and a later Cu(I)-catalyzed cycloaddition with several types of alkynes.

As mentioned, one of the limitations of on-chip reactions was related to the impossibility to purify the final product from starting substrate and by-side products; about this, the use of MALDI-TOF MS detection gave the advantage of quantifying the conversion of each on-chip reaction and verifying the formation of by-products or intermediates.

In our specific assays, MALDI-TOF analysis contributed to exclude ten alkynes from the synthetic protocol because of their low conversions during CuAAC (lower than 20%) or the formation of by-side products (as in the case of alkyne **a21** and **a23**). By including only the high-yielding 19 alkynes tested, we achieved a higher degree of purity in analyzed spots and, therefore, high reliable binding data.

Finally, with the developed on-chip synthetic strategy, a total of **374 novel ligands** were prepared in high-yielding conversions. Afterwards, they were characterized by MALDI-TOF analysis and screened with three types of fluorescently labeled lectins: *Wisteria Floribunda Agglutinin (WFA)*, *Recombinant Macrophage Galactose Lectin ECD (MGL)* and *Langerin ECD*.

The WFA was used to perform proof of concept studies to optimize the fluorescent binding assays and improve the reproducibility; from WFA screening we observed that the binding strength for a glycan scaffold can be dramatically affected to the nature of triazole formed by coupling reaction. Indeed, for the same scaffold (e.g. **G8.1**) strong (**G8.1.a18**) or weak (**G8.1.a2**) binders can be achieved in according to the type of alkyne used in coupling reaction. For this lectin, very strong binders with RFU>200 have been identified.

Unlike WFA, Macrophage galactose lectin has showed a narrow specificity for terminal GalNAc glycans with particular preference for bi-antennary derivatives; any modification performed on the GalNAc epitope, even by replacing GalNAc with GalNAz or Gal, provided a general and dramatic weaken of the binding. These results suggest that the modification of terminal GalNAc epitope on N-glycans structures could not be the correct approach to design MGL inhibitors; rather mimetics prepared by modification of carbohydrate moieties involved in secondary or extended binding sites of lectin could be a valid alternative.

The proof that for certain lectins the modification of cores different by epitope can affect the binding is given by the Langerin; indeed, even if the Langerin is a mannose-type binding lectin, we have observed that properly modifying the terminal GalNAc residue of a glycan scaffold, Langerin binding strenghten could be achieved. In particular, by functionalizing some glycan scaffolds with aromatic-based triazoles (e.g. **a5**, **a20**, **a25**, **a26** and **a28**), it was possible to determine strong binders for Langerin ECD with RFU>200.

In summary, the microarray-based assays performed in this thesis chapter suggested how carbohydrate-lectin binding can be modulated by direct modification on the binding epitope or on adjacent sites of N-glycan structures. Moreover, by these screenings we were able to identify the best binders for the three type of lectins.

The microarray-based technology is a *qualitative* analytical technique that gave preliminary information about binding properties of novel synthesized ligands and

allowed to select the strongest binders for the examined lectins. In order to have more detailed study, the selected ligands should be synthesized in solution in higher scale to be then analyzed either by microarray or by *in vitro* experiment.

As we mentioned in the introduction chapter, carbohydrate-lectin binding could be easily affected by a lot of parameters which include structure and nature of the ligand/protein as well as experimental conditions like concentration, temperature, etc. Therefore, the combination of different techniques and thus diverse micro-environments of analysis could provide a wide overview regarding the examined carbohydrate-lectin binding.

For these reasons, in future perspective, the strongest ligands found for the three examined lectins will be synthesized in solution in a proper scale to allow to perform further binding studies; in the meantime, the **374 novel ligands** could be screened with further C-type lectins to achieve more detailed information about their binding properties and rather find among them strong binders for further C-type lectins.

References

116. N. Lannoo and E. J. M. Van Damme, *Plant Sci.*, 2015, **239**, 67–83.
117. H. J. Gabius, S. André, J. Jiménez-Barbero, A. Romero and D. Solís, *Trends Biochem. Sci.*, 2011, **36**, 298–313.
118. S. Donadio-Andréi, C. Iss, N. El Maï. V. Calabro, C. Ronin, *Carbohydrate Chemistry*, 2012, 38, 94-123
119. **(a)** A. Varki, *et. al.*, *Glycobiology* 1993, **3**, 97 – 130. **(b)** R. A. Dwek, *et. al.*, *Biochem.Soc. Trans.* 1995; **23**, 1 – 25. **(c)** E. Saxon, C. R. Bertozzi CR, *Annu. Rev. Cell. Dev. Biol.*, 2001, **17**, 1–23. **(d)** N. Taniguchi, E. Miyoshi, J. Gu, K. Honke, A. Matsumoto, *Curr. Opin. Struct. Biol.*, 2006, **16**, 561 – 566.
120. J. W. Dennis, M. Granovsky, C. E. Warren, *Bioessays* 1999; **21**: 412 – 421.
121. R. J. Linhardt, *J. Med. Chem.*, 2003, **46**, 2551–2564.
122. M. Artavia, M. Blanco, S. Rene, A. Enciso, F. Ramos, B. Van Doorslaer, D. Fumagalli, S. Niemeyer, J. Francisco and M. Robert, 2014, **359**, 1–36.
123. P. H. Mutin, G. Guerrero and A. Vioux, *J. Mater. Chem.*, 2005, **15**, 3761–3768.
124. A. Vega, P. Thissen and Y. J. Chabal, *Langmuir*, 2012, **28**, 8046–8051.
125. S. P. Pujari, L. Scheres, A. T. M. Marcelis and H. Zuilhof, *Angew. Chemie - Int. Ed.*, 2014, **53**, 6322–6356.
126. P. J. Hotchkiss, S. C. Jones, S. A. Paniagua, A. Sharma, B. Kippelen, N. R. Armstrong and S. R. Marder, *Acc. Chem. Res.*, 2012, **45**, 337–346.
127. J. Etxebarria, S. Serna, A. Beloqui, M. Martin-Lomas and N. C. Reichardt, *Chem. - A Eur. J.*, 2013, **19**, 4776–4785.
128. C. J. Gray, M. J. Weissenborn, C. E. Eyers and S. L. Flitsch, *Chem. Soc. Rev.*, 2013, **42**, 6378–6405.
129. S. Serna, J. Etxebarria, N. Ruiz, M. Martin-Lomas and N. C. Reichardt, *Chem. - A Eur. J.*, 2010, **16**, 13163–13175.
130. K. Y. Do, S. I. Do, R. D. Cummings, *The J. of Biol. Chem.*, 1995, **270(31)**, 18447–18451.
131. B. Ramakrishnan and P. K. Qasba, *J. Biol. Chem.*, 2002, **277**, 20833–20839.

132. P. K. Qasba, E. Boeggeman and B. Ramakrishnan, *Biotechnol. Prog.*, 2008, **24**, 520–526.
133. E. E. Boeggeman, B. Ramakrishnan and P. K. Qasba, *Protein Expr. Purif.*, 2003, **30**, 219–229.
134. (a) V. V. Rostovtsev, L. G. Green, V. V. Fokin, K. B. Sharpless, *Angew. Chem. Int. Ed.*, 2002, **114**, 2708-2711. (b) C. W. Tornøe, C. Christensen, M. Meldal, *J. Org. Chem.*, **2002**, **67**, 3057-3064. (c) L. Zhang, X. Chen, P. Xue, H. H. Y. Sun, I. D. Williams, K. B. Sharpless, V. V. Fokin, G. Jia, *J. Am. Chem. Soc.*, 2005, **127**, 15998-15999. (d) L. K. Rasmussen, B. C. Boren, V. V. Fokin, *Org. Lett.*, 2007, **9**, 5337-5339. (e) B. C. Boren, S. Narayan, L. K. Rasmussen, L. Shang, H. Zhao, Z. Lin, G. Jia, V. V. Fokin, *J. Am. Chem. Soc.* 2008, **130**, 8923-8930. (f) M. C. Meldal, W. Tornøe, *Chem. Rev.*, 2008, **108**, 2952-3015.
135. V. D. Bock, H. Hiemstra and J. H. Van Maarseveen, *European J. Org. Chem.*, 2006, 51–68.
136. F. Amblard, J. H. Cho and R. F. Schinazi, *Chem. Rev.*, 2009, **109**, 4207–4220.
137. (a) K. Oh, Z. Guan, *Chem. Comm.*, 2006, **29**, 3069-3071. (b) W. S. Horne, M. K. Yadav, C. D. Stout, M. R. Ghadiri, *J. Am. Soc.* 2004, **126**, 15366-15367. (c) C. W. Tornøe, S. J. Sanderson, J. C. Mottram, G. H. Coombs, M. Meldal, *J. Comb. Chem.*, 2004, **6**, 312-324.
138. U. Sirion, H. J. Kim, J. H. Lee, J. W. Seo, B. S. Lee, *et al*, *Tetrahedron Lett.*, 2007, **48**, 3953-3957.
139. (a) M. Melai, C. W. Tornøe, *Chem. Rev.*, **2008**, **108**, 2952-3015. (b) V. O. Rodionoc, V. I. Presolski, D. D. Diaz, V. V. Fokin, M. G. Finn, *J. Am. Chem Soc.*, 2007, **129**, 12705-12712. (c) J. E. Hein, V. V. Fokin, *Chem. Soc. Rev.*, 2010, **39**, 1302-1312. (d) P. L. Golas, K. Matyjaszewski, *Chem. Soc. Rev.*, 2010, **39**, 1338-1354. (e) V. Aragão-Leonati, V. L. Campo, A. S. Gomes, R. A. Field, I. Carvalho, *Tetrahedron*, 2010, **66**, 9475-9492.
140. S. I. Presolski, V. Hong, M. G. Finn, *Curr. Protoc. Chem. Biol.*, 2011, **3**, 153-162
141. V. Hong, S. I. Presolski, C. Ma and M. G. Finn, *Angew. Chemie - Int. Ed.*, 2009, **48**, 9879–9883.

142. C. T. Campbell, Y. Zhang, J. C. Gildersleeve, *Curr. Prot. Chem. Biol.*, 2010, **2**, 37-53.
143. T. Kurokawa, M. Tsuda and Y. Sugino, *J. Biol. Chem.*, 1976, **251**, 5686–5693.
144. M. A. de Jong, L. E. Vriend, B. Theelen, M. E. Taylor, D. Fluitsma, T. Boekhout, *et al*, *Mol Immunol*, 2010, **47**, 1216–1225.
145. H. Tateno, K. Ohnishi, R. Yabe, N. Hayatsu, T. Sato, M. Takeya, *et al*, *J Biol Chem*, 2010, **285**, 6390–6400.

**4. On-chip synthesis of multivalent constructs
to strengthen carbohydrate-lectin binding**

4. On-chip synthesis of multivalent constructs to strengthen carbohydrate-lectin binding

One of the main purposes of IMMUNOSHAPE ETN network was the development of a series of glycomimetic structures that, presented on multivalent scaffolds, showed strengthened binding for targeted C-type lectins compared to their relative natural and/or monovalent form.

In a recently published work (Medve *et al*, *Chem. A Eur. J.* **2018**),¹⁴⁶ Anna Bernardi's team had developed the synthesis of a glycomimetics library that, in collaboration with our groups, had been screened against C-type lectins as *Dectin-2*, *DC-SIGN/R* and *Langerin*.

In particular, a collection of fucose- and mannose-based glycomimetics bearing azido-ethyl functionalization had been synthesized and coupled with a commercially available BCN-cyclooctyne (*N*-[(1*R*,8*S*,9*S*)-Bicyclo[6.1.0]non-4-yn-9-ylmethoxycarbonyl]-1,8-diamino-3,6-dioxaoctane) via SPAAC.

These BCN-conjugates, bearing an amine arm, had been immobilized on commercially NHS-functionalized glass slide (Nexterion® SlideH- Schott AG) to perform binding assays with targeted lectins.

On the base of binding properties shown from the glycomimetics library,¹⁴⁶ some structures have been selected for the preparation of dendron-based multivalent scaffolds with aim to further strengthen their binding toward selected C-type lectins.

With this aim, a completely new class of activated Cyclooctyne-dendrons based on bis-MPA (2,2-bismethylpropionic acid) skeleton,¹⁴⁷ at different valences (**d1-3**), have been synthesized ([Figure 4.1](#)) in Dr. Javier Rojo's laboratory (CSIC, Seville) from his PhD student Antonio Di Maio.

The general idea was to couple the azidoethyl glycomimetics on activated Cyclooctyne-dendrons (**d1-3**) through *strain promoted alkyne azido cycloaddition* (SPAAC) and then immobilize the novel-synthesized glycodendrons on commercially NHS-functionalized glass slide (Nexterion® SlideH- Schott AG) to perform binding assays.

4. On-chip synthesis of multivalent constructs to strengthen carbohydrate-lectin binding

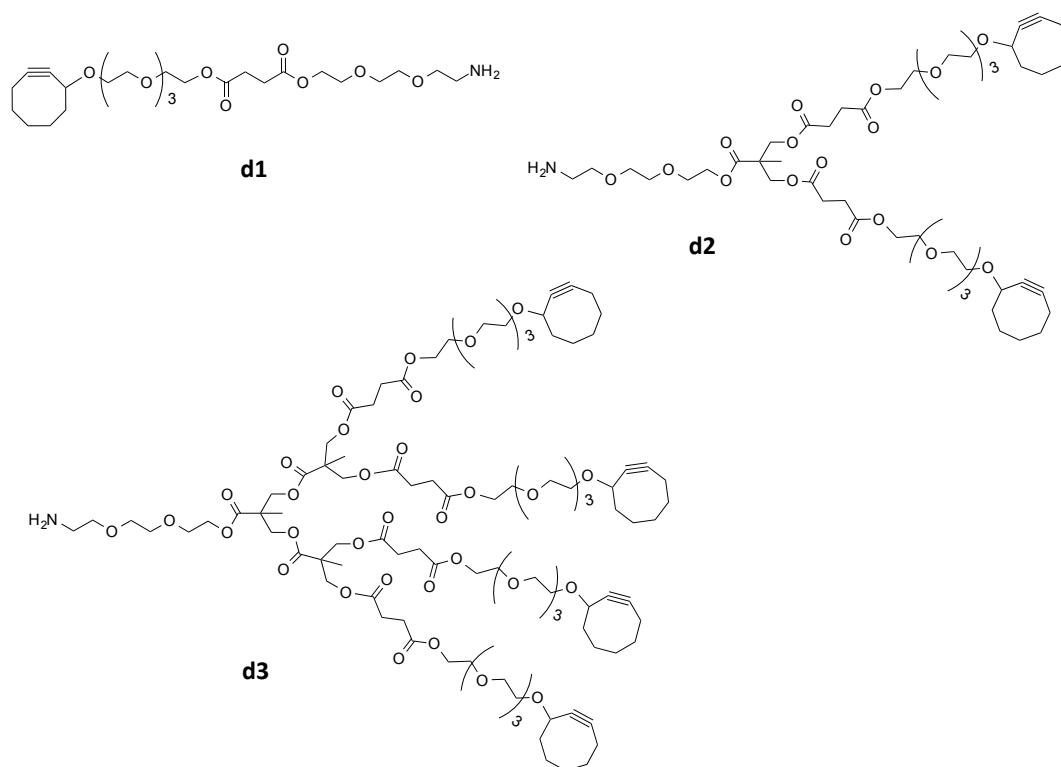


Figure 4.1 Synthetic cyclooctyne-dendrons (d1-3).

Free-catalyst *strain promoted alkyne azide cycloaddition* (SPAAC) consists in a reaction between a strained cyclooctyne and an azide ligand. This strategy was developed in 2004 by Bertozzi and co-workers¹⁴⁸ as coupling method in covalent modifications of living systems.

It is important to note that, in contrast to metal-catalyzed cycloaddition that lead a regioselective coupling product, the SPAAC affords in a regioisomers mixture (1,4- and 1,5-regioisomer); therefore, when new ligands are synthesized by using this type of reaction, their binding properties are related to the coexistence of two regioisomers.

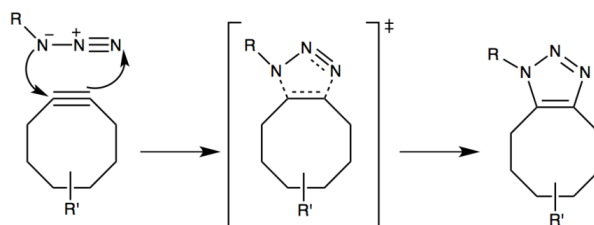


Figure 4.2 Strain-promoted alkyne azide cycloaddition (SPAAC) mechanism.

In preliminary experiments for the metal-free cycloaddition optimization, simple azidoethyl carbohydrates (**z1-4**) have been used instead of azidoethyl glycomimetics with the aim to save precious material ([Figure 4.3](#)).

4. On-chip synthesis of multivalent constructs to strengthen carbohydrate-lectin binding

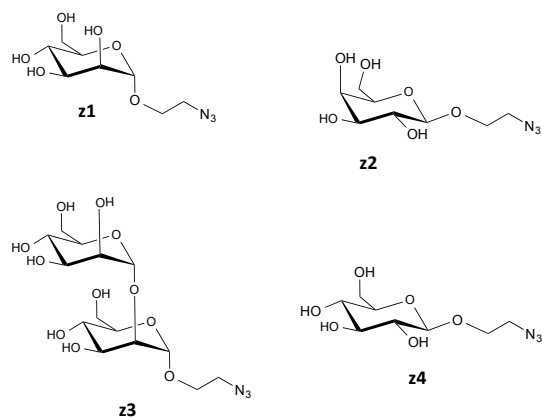


Figure 4.3 Azidoethyl carbohydrates (**z1-4**) synthesized in Dr. Javier Rojo's group.

From the first attempts with the azides **z1-4**, incomplete conversions and partial hydrolysis of the bis-MPA skeleton of dendrons (**d1-3**)¹⁴⁹ have been achieved. Since the optimization of the synthetic protocol needed to use large excess of azides and prolonged time of reaction, the solution-phase approach was replaced from the *on-chip synthesis*.

For this purpose, a NHS-activated hydrophobic ITO glass slides (presented in **chapter 3**) have been used to immobilize the cyclooctyne dendrons (**d1-3**), through their amine core, at slightly basic pH; afterwards, *spot-wise* functionalization with azidoethyl carbohydrates (**z1-4**) was performed through *strain promoted alkyne azido cycloaddition* (SPAAC). After proving the completion of the on-chip reaction by MALDI-TOF analysis, binding assays with fluorescently labeled plant (*ConA*, *WFA*, *PSA*, *PA-I*) and human lectins (*DC-SIGN*, *DC-SIGNR*, *Langerin*, and *Dectin-2*) were performed.

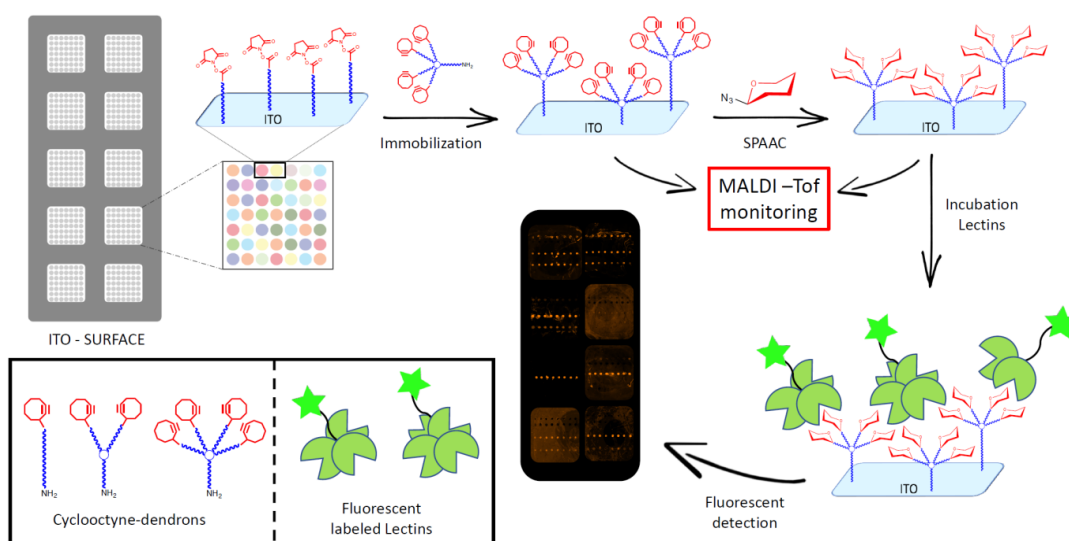


Figure 4.4 General Strategy for on-chip synthesis of glycodendrons and consequent binding assays with fluorescently labeled lectins.

4. On-chip synthesis of multivalent constructs to strengthen carbohydrate-lectin binding

4.1 Cyclooctyne dendrons immobilization on NHS-activated hydrophobic ITO glass slide

The immobilization of cyclooctyne dendrons (**d1-3**) on NHS-activated hydrophobic ITO glass slide can be performed by physically dividing the slide in subarrays by a silicon gasket and incubating each subarray with one cyclooctyne dendron solution. The reaction was left 2h at room temperature and MALDI-TOF analysis was performed to check cyclooctyne immobilization (MALDI spectra are reported in **Appendix**).

4.1.1 Surface density quantification of Cyclooctyne-dendrons by MALDI-TOF detection

In addition to evaluate the reaction conversions by MALDI-TOF analysis, the developed NHS-activated hydrophobic ITO glass slide admits to quantify the relative surface density of immobilized cyclooctyne-dendrons using the unreacted NHS-activated linker mass peak (m/z 1040) as internal standard.

The possibility of relatively quantifying ligand surface density on the surface is an important advantage since this parameter dramatically affects carbohydrate-lectin binding.

With this aim, Mono-, Di- and Tetra-valent cyclooctyne-dendrons (**d1-3**) were coupled with NHS-activated ITO slides at five different concentrations, ranging from 5 to 30 μ M, and MALDI-TOF MS analysis have been performed to calculate the dendron/linker ratio at each coating concentration.

Figure 4.5 shows MALDI-TOF spectrum detected after incubation of NHS-activated surface with Mono-cyclooctyne dendron (**d1**) solution (*picture above*) and the graphs dendron/linker ratio against coating concentration drew for the three dendrons (*picture below*). The spectra detected for all the dendrons at different coating concentrations are reported in **Appendix**.

4. On-chip synthesis of multivalent constructs to strengthen carbohydrate-lectin binding

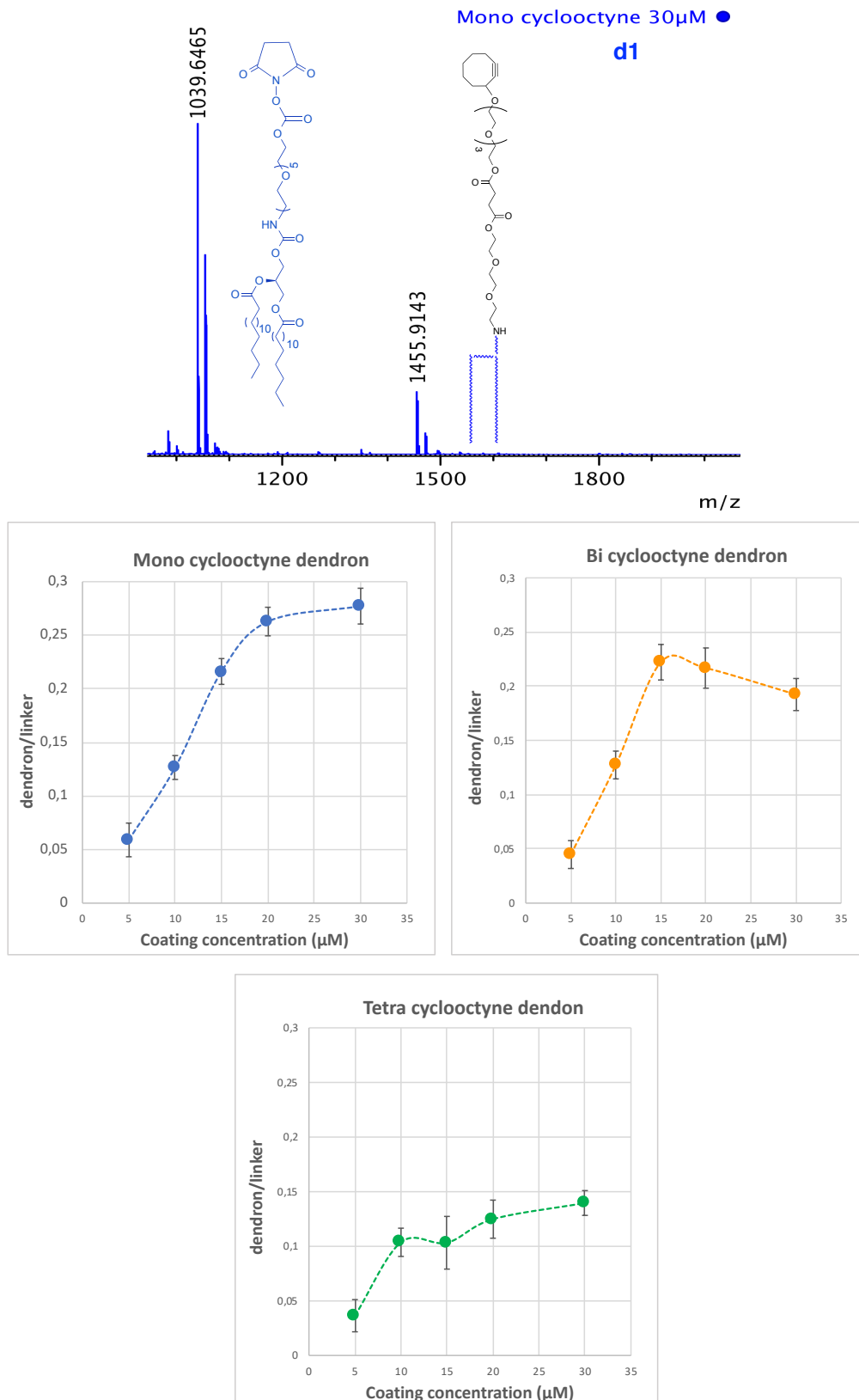


Figure 4.5 (a) MALDI-TOF spectrum showing immobilized Mono-cyclooctyne (**d1**) mass peak (m/z 1456) vs unreacted NHS-linker mass peak (m/z 1040). **(b)** Graphics of the dendron/linker ratio against coating concentration.

4. On-chip synthesis of multivalent constructs to strengthen carbohydrate-lectin binding

The variation observed in dendron/linker ratio, from one dendron structure to the others, was likely due to the structure-dependent response rate ionization of the constructs and to spatial requirements during immobilization. As a result, it was not possible to compare the degree of immobilization between different dendrons; on the contrary, density at maximum loading could be determined for each dendron.

Thus, while surface saturation occurred at 20 μM coating concentration for our Monovalent dendron **d1** (Figure 4.5), for our Bivalent dendron **d2** and Tetravalent dendron **d3**, saturation was reached at 15 μM and 10 μM respectively, highlighting the growing spatial requirements for larger constructs.

4.1.2 Preliminary glycodendrons binding assays with Concanavalin A (Con A)

Since we had developed an array format that offers two types of detection methods (fluorescence and mass analysis) with different sensitivities, the concentration selected for the assays had to provide high-quality data in both of the analytical techniques.

We had already observed, in the previous section, that high-quality mass spectra could be obtained by employing coating concentrations ranging from 5 to 30 μM . Thus, we wanted to check if fluorescence quality data could be also obtained within this range of concentrations.

With this aim, we functionalized the NHS-activated slide with Mono-, Bi- and Tetra-valent dendrons at concentrations of 5 μM , 10 μM and 15 μM in separate subarrays. Afterwards, azidoethyl carbohydrates (**z1-4**) were coupled on the cyclooctyne arrays (**d1-3**) to provide novel synthesized glycodendrons which were incubated with fluorescently labeled Concanavalin A (Con A) for 1h and the slides scanned after washing off unbound lectin (Figure 4.5).

Concanavalin A is member of the legume lectin family and it binds specifically to $\alpha\text{-D-mannosyl}$ and $\alpha\text{-D-glucosyl}$ groups.¹⁵⁰ According to its binding properties, ConA showed binding only for mono- or polyvalent forms of the disaccharide $\alpha\text{Man1,2Man}$ (**z3**) and $\alpha\text{-Man}$ (**z1**). In particular, while strong binding was observed for disaccharide $\alpha\text{Man1,2Man}$ (**z3**) at all the valences and concentrations tested, $\alpha\text{-Man}$ (**z1**) bound Con A only when it was in a Tetra-valent form; the absence of signal for its Mono (**d1.z1**) and Bi-valent dendrons (**d2.z1**) could be associated to the low-density form of the ligand on the surface. For both of the two ligands (**z1**, **z3**), a strengthened binding is achieved by increasing the number of copies in all the employed concentrations (Figure 4.5a).

4. On-chip synthesis of multivalent constructs to strengthen carbohydrate-lectin binding

In [Figure 4.5](#) fluorescence intensities and images obtained by performing binding assays on glycodendrons at different densities are reported; increasing dendron coating concentration led to stronger binding, irregular spot morphology and high signal intensity background. Indeed, a 22% reduction of signal/noise related to the Tetra-valent cyclooctyne (**d3**) was achieved passing from coating concentration of 5 μM to 15 μM . Therefore, although the experiment performed at a dendrons coating concentration of 5 μM showed less fluorescence signal intensities than the ones achieved at higher concentrations, it represented the best assay in terms of background signal and spot morphology.

On the base of these results, the coating concentration of 5 μM has been selected for all the three Cyclooctyne-dendrons to perform the on-chip synthesis of glycodendrons and their binding evaluation against several C-type lectins.

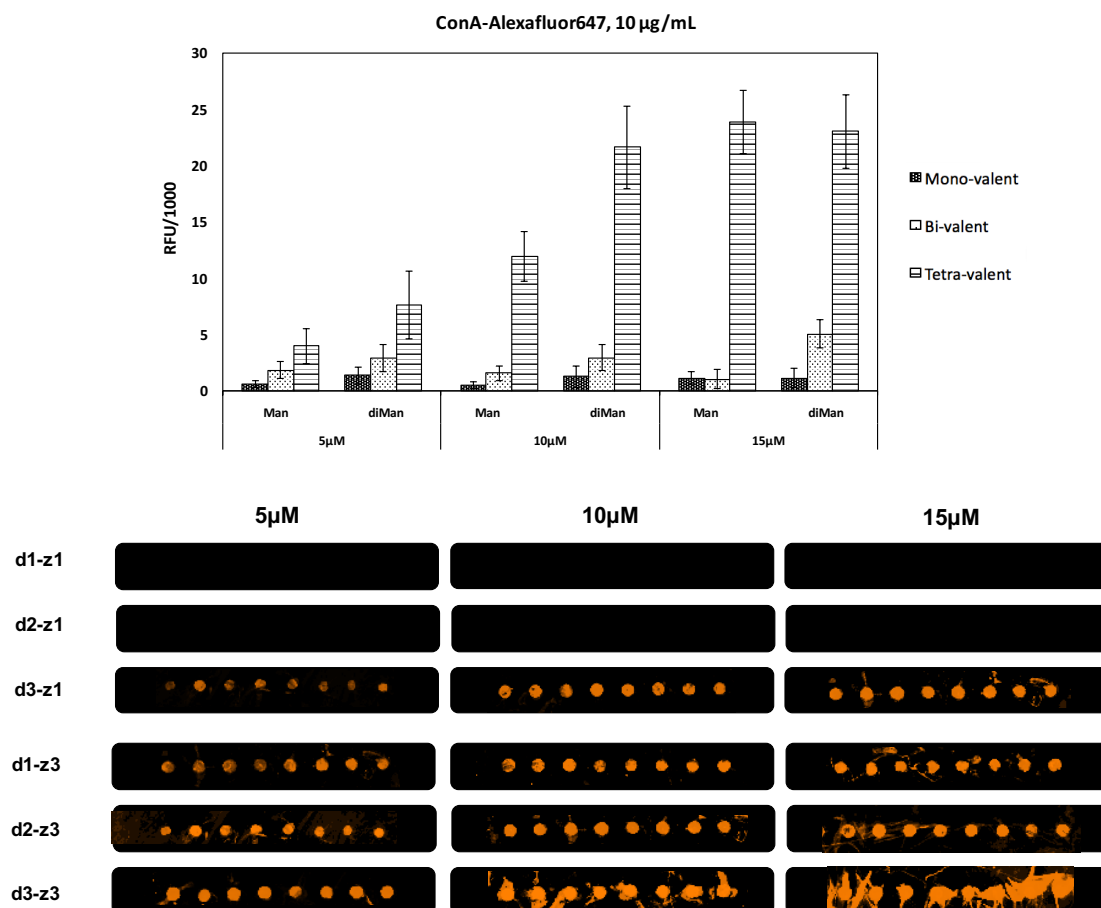


Figure 4.5 (a) Fluorescence quantification of Concanavalin A binding to Man (**z1**) and $\alpha\text{Man}1,2\text{Man}$ -based (**z3**) glycodendrons. **(b)** Fluorescence image of the neo-glycodendron arrays after incubation with *Con A* (10 $\mu\text{g}/\text{mL}$).

4.2 On-chip synthesis of glycodendrons

The glycodendrons have been prepared by automatically spotting the azidoethyl carbohydrates (**z1-4**) on the freshly generate surface of cyclooctynes (**d1-3**) and leaving the reaction occurs in nanodroplets.

The main challenge of *spotwise* cycloaddition is to achieve near-quantitative conversions within the short life-time of the azidoethyl carbohydrate droplets on the surface; in fact, in spotwise coupling, the reaction has to happen before that reagent droplets dry completely by evaporation.

Low temperatures and high humidity percentages in air were the first parameters set up in order to increase the time of life of nanodroplets; but the use of large excess of reagents and small percentage (10%) of a high-boiling solvent like DMSO were also required to get near-quantitative conversions and make the protocol highly reproducible.

Indeed, performing the spotwise reaction in an atmosphere of 70% humidity at 19°C for 2 hours followed by overnight desiccation in oven, almost complete conversion (>95%) has been achieved for all dendron-azido-linked carbohydrate pairs within the limit of detection of the analytical method. Moreover, in contrast to cycloaddition reactions performed in solution, no hydrolysis of ester skeleton of dendrons has been observed.

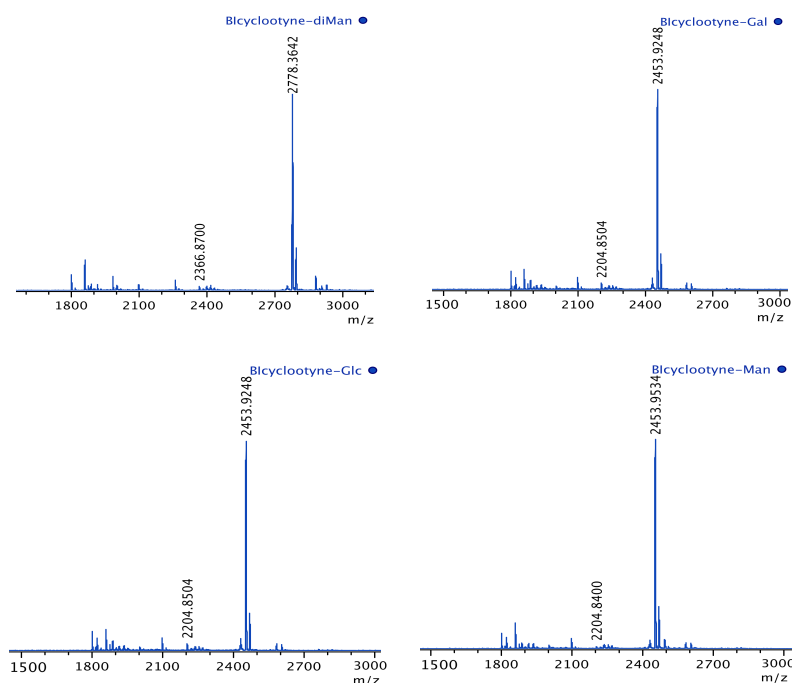


Figure 4.6 MALDI-TOF MS spectra detected after on-chip SPAAC on Bi-cyclooctyne surface (**d2**). The rest of the MALDI-TOF MS spectra are reported in **Appendix**.

The array of glycodendrons was built by choosing a 6x2 microarray format with twelve identical subarrays. Each subarray was designed to fit 32 spots with 8 spots per row and

4. On-chip synthesis of multivalent constructs to strengthen carbohydrate-lectin binding

4 spots per column. Each azide was printed in eight replicates, what resulted in one ligand per row of each subarray. The average spot diameters varied from 240 to 306 μm , with a distance between spots of 408 μm in both x and y axes (Figure 4.7).

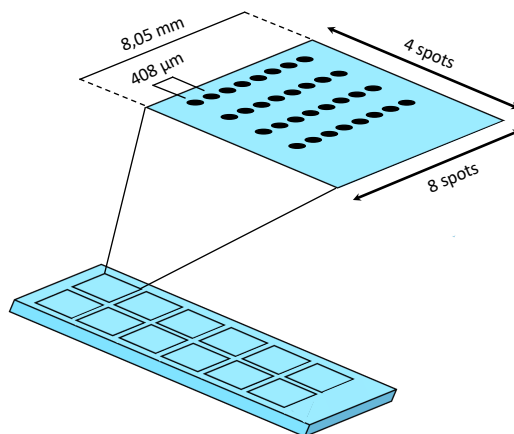


Figure 4.7 The design of the microarray format used for preparation of glycodendrons by using azides **z1-4**.

4.3 Binding assays with fluorescently labeled lectins

With the aim to evaluate the effect of ligand presentation in carbohydrate-lectin binding assays and at the meantime test the versatility of developed protocol, several plant and human lectins with different sugar-specificity were selected. These include *Pisum Sativum* (PSA), *Wisteria floribunda* (WFA), *Pseudomonas Aeruginosa I* (PA-I), *DC-SIGN ECD*, *DC-SIGNR ECD*, *Langerin ECD* and *Dectin-2 ECD*.

Plant lectins as *Wisteria Floribunda* and *Pseudomonas Aeruginosa I* usually show binding preference for galactose or galactosamine epitopes, while *Pisum Sativum* specifically recognizes mannose moiety.¹⁵¹

Regarding the human C-type lectins here employed, all of them are *ECD* (*extracellular domain*)-type and have binding preference mainly for mannose terminal sugars and, in particular, for $\alpha\text{Man}1,2\text{Man}$ moiety. Moreover, both *DC-SIGN* and *Langerin* recognize also fucose residue while *DC-SIGN* is the only one to present a feeble specificity also for glucose epitope.^{144,152}

The on-chip binding assay performed by screening *Pisum Sativum* with glycodendrons showed lectin binding preference for the disaccharide $\alpha\text{Man}1,2\text{Man}$ (**z3**) at all the three valences with an increasing of the intensities given by the multivalent and presentation effect. However, no binding was observed in any case of the mannose-based dendrons

4. On-chip synthesis of multivalent constructs to strengthen carbohydrate-lectin binding

(**z1**), due to the low-density form of the ligand. For galactose- or glucose-based glycodendrons, no binding was observed. (Figure 4.8).

As expected, galactose-binding lectins as *WFA* and *PA-I* gave specific binding for galactose moiety **z2** and a strong multivalent effect emerged from these assays. On the other side, Mannose- (**z1**), α Man1,2Man- (**z3**) and glucose- (**z4**) derivatives were not recognized by these two lectins (Figure 4.8).

Human C-type lectins as *Langerin ECD*, *Dectin-2 ECD* and *DC-SIGNR ECD* showed a preference for α Man1,2Man epitope (**z3**) at all the valences tested, observing the binding strengthened when increasing dendron valency. For none of the mannose-functionalized dendrons (**d1.z1**, **d2.z1**, **d3.z1**) was observed any binding with these human lectins, due to the low-density form of the ligand and the low binding specificity of these lectins for this sugar epitope (Figure 4.8).

4. On-chip synthesis of multivalent constructs to strengthen carbohydrate-lectin binding

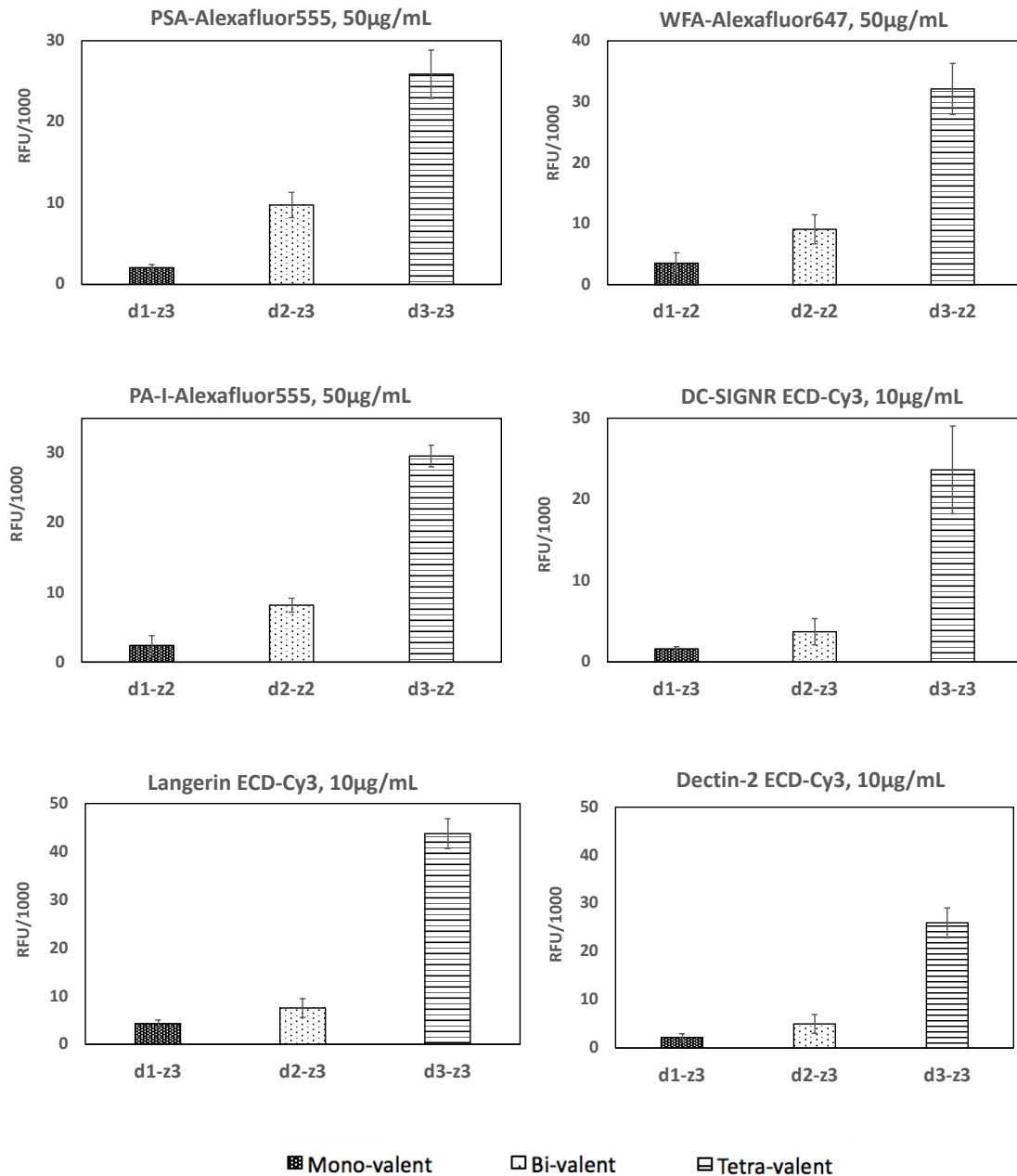


Figure 4.8 Overview of fluorescence quantification of plant and human lectins binding to glycodendrons.

DC-SIGN ECD showed a similar binding strength for dimannose-(z3), mannose-(z1) and glucose- (z4) based dendrons when they are presented in mono- and bi-valent form (Figure 4.9). However, by increasing dendron valence from two to four, a binding strength was achieved exclusively for α Man1,2Man (z3) epitope.

The *non-multivalent effect* showed from the weaker *DC-SIGN ECD*'s binders (z1 and z4) is a proof that increasing the number of ligand copies not necessarily leads to binding strength.

4. On-chip synthesis of multivalent constructs to strengthen carbohydrate-lectin binding

Carbohydrate-lectin binding is not only affected by the nature and the number of ligand/lectin involved but also by their relative spatial arrangement (presentation); indeed, if multivalent presented ligand and multimeric lectin do not possess proper geometric features to match each other leading simultaneous and multivalent interactions, no binding strengthen can be achieved.

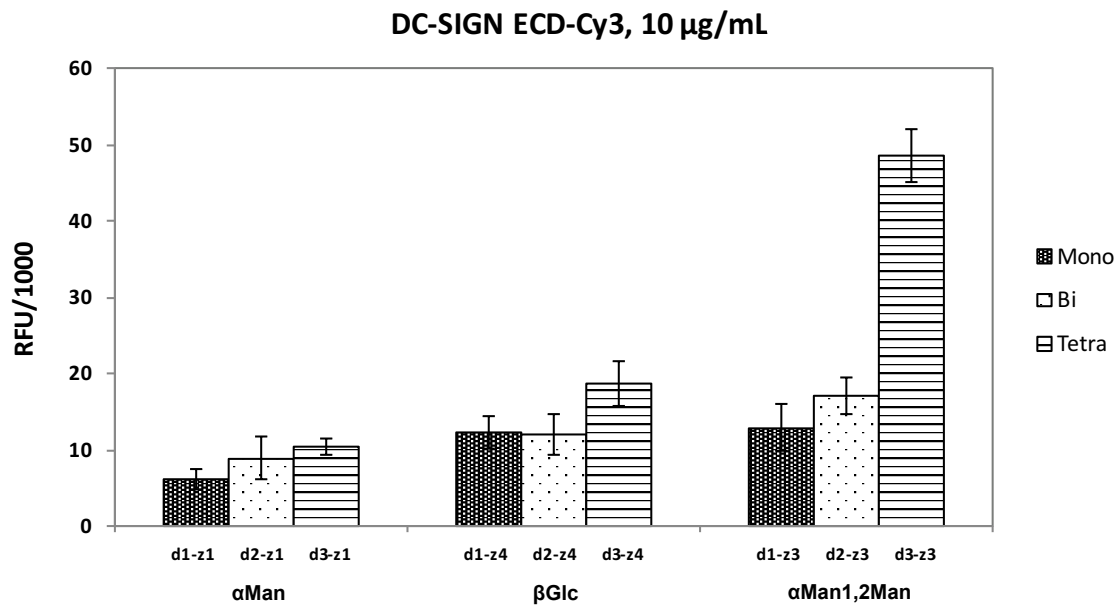


Figure 4.9 Fluorescence quantification of *DC-SIGN ECD* binding to glycodendrons.

4. On-chip synthesis of multivalent constructs to strengthen carbohydrate-lectin binding

4.4 On-Chip synthesis of glycomimetic dendrons and role of ligand presentation in carbohydrate-lectin strength

By using the above developed protocol, we aimed to prepare a collection of glycomimetics dendrons by coupling, on the cyclooctyne surfaces (**d1-3**), a selected collection of azidoethyl glycomimetics (Figure 4.10).

Once prepared, the binding properties of novel glycomimetic dendrons were screened with fluorescently labeled plant lectins as *Concanavalin A*, *Auleria Aurantia Lectin*, and human lectin including *DC-SIGN*, *DC-SIGNR*, *Langerin*, *Dectin2* and *Mannose Binding Lectin*.

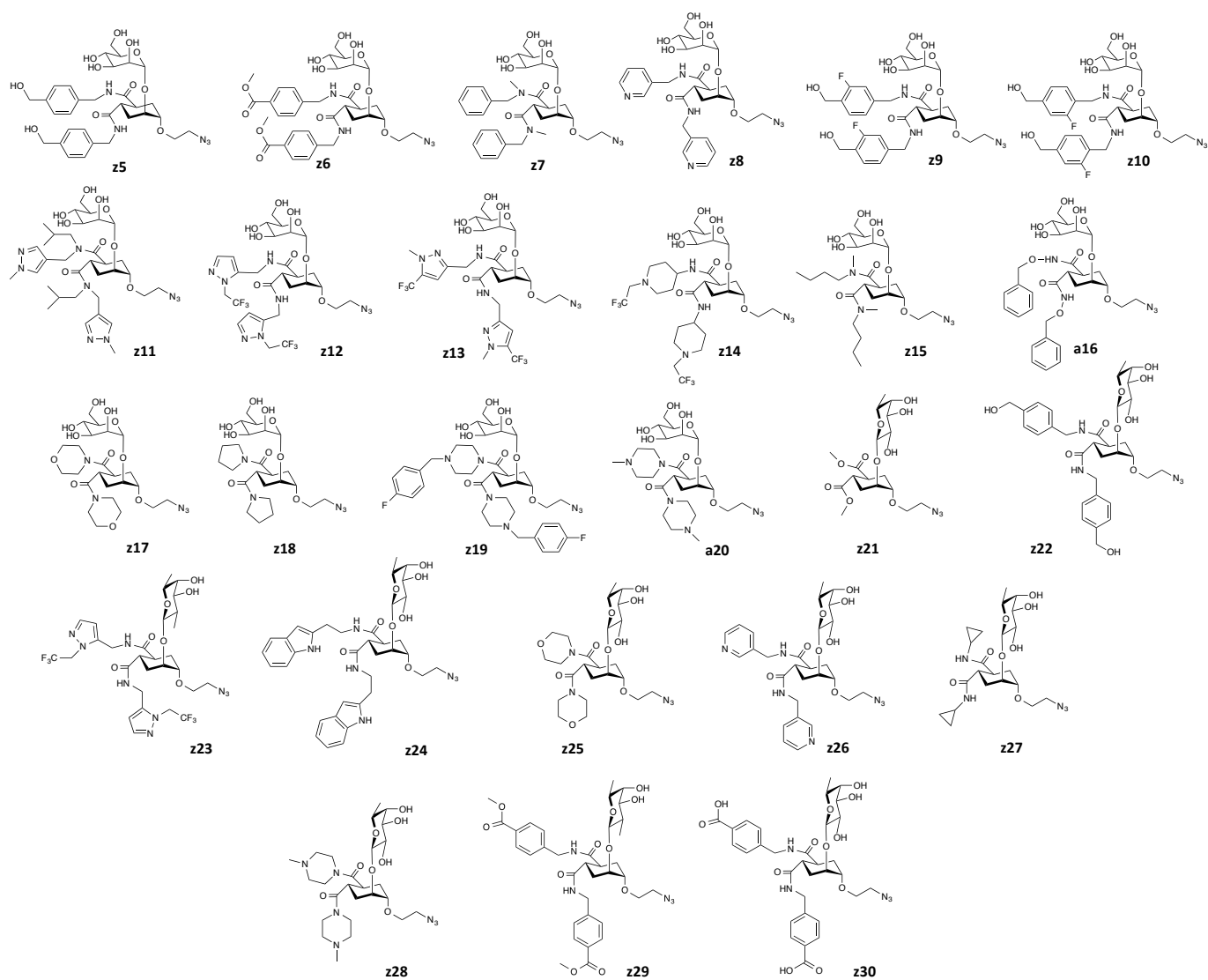


Figure 4.10 Azidoethyl glycomimetics synthesized by Dr. Laura Medve in Prof. Anna Bernardi's laboratory (University of Milan, Italy).

4.4.1 On-chip synthesis of glycomimetic dendrons

By adopting the procedure described in **section 4.2**, almost complete conversion (>93%) was achieved for all dendron-azido-linked glycomimetic pairs, as measured by MALDI-TOF MS.

For our purpose, we built an array of twenty-seven azidoethyl-carbohydrates (**z3** and **z5-30**) by choosing an 8x1 microarray format with twelve identical subarrays. Each subarray was designed to fit 135 spots with 20 spots per row and 7 spots per column. Each azide was printed in five replicates, what resulted in four mimetics per row of each subarray. The average spot diameters varied from 230 to 326 μm , with a distance between spots of 408 μm in both x and y axes (**Figure 4.11**).

The $\alpha\text{Man1,2Man}$ -azide (**z3**) was printed together to our azidoethyl-glycomimetics to be used as internal control in the on-chip SPAAC protocol as well as in the fluorescence binding assays.

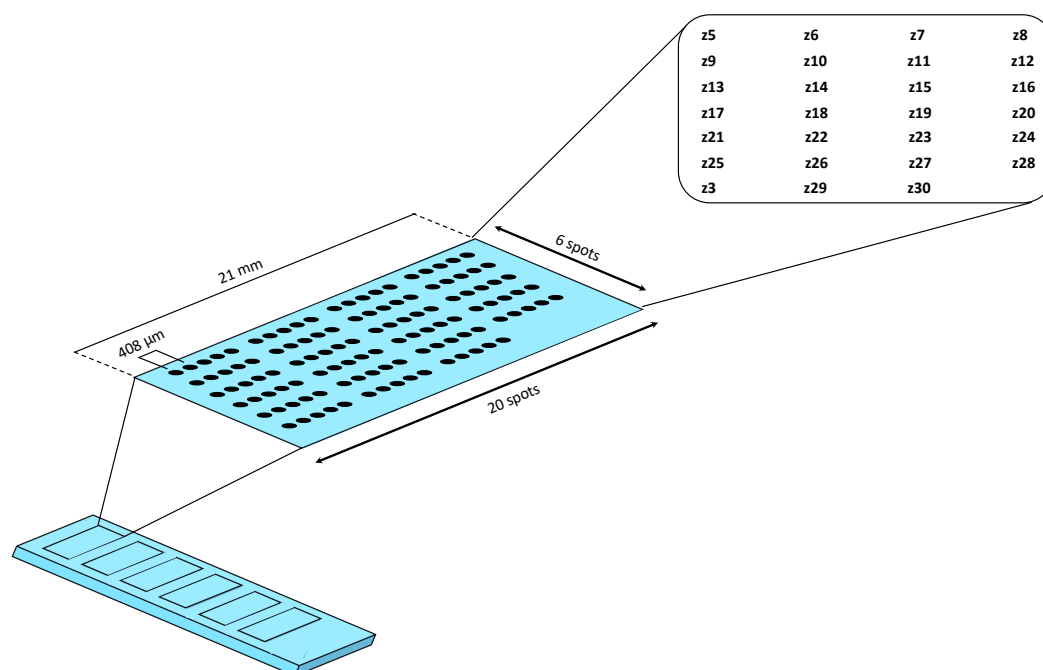


Figure 4.11 Design of the microarray format used for the preparation of glycodendrons by using azides (**z3**, **z5-z30**).

4.4.2 Glycomimetics dendrons binding assays with plant and human lectins

➤ Plant lectins

Since the glycomimetics library reported in Figure 4.10 consists to fucose- and mannose-based glycomimetics, first binding assays have been performed with Concanavalin A (ConA) and Aleuria Aurantia Lectin (AAL) that bind α -D-mannosyl and α -1,6- or α -1,3-linked fucose¹⁵³ respectively.

Concanavalin A was found to recognize most of the Mono-valent mannose-based glycomimetics (**d1.z5** to **d1.z20**) and many of them seemed to interact more efficiently than α Man1,2Man (**z3**) itself. Among them, the strongest interaction with this lectin was achieved by two regioisomers, **z9** and **z10**. On the other hand, no binding was observed for fucose-based mimetics (from **d1.z21** to **d1.z30**).

Increasing the ligand valency from Mono- to Bi-valent presentation did not change array, quite similar binding profile and signal intensities were achieved. By contrast, when the glycomimetics were presented on the Tetra-valent array (**d3**), a general enhancement of fluorescence signals was observed, except for mimetics **z14**, **z16** and **z19**. This general signal increasing was due to a higher number of ligand copies and a different ligand presentation on the arrays. Moreover, on the Tetra-valent surface **d3**, *ConA* showed binding affinity for a higher number of mimetics than on the Mono- and Bi-valent arrays and α Man1,2Man-based Tetra-form (**d3.z3**) bound this lectin as efficiently as mimetic derivatives (Figure 4.12 above).

On the contrary, AAL recognized most of the fucose-based derivatives (from **z21** to **z30**) while mannose-based dendrons did not interact with this lectin.

From Mono-valent to Bi-valent arrays, no significant differences were observed in terms of signal intensity. However, once the number of ligand copies was increased from two to four, a general strengthen of fucose-type ligand-binding was achieved. The mimetic **z26** is the only exception of this behavior since it showed a weak binding at all the *n*-valent presentations (Figure 4.12 below).

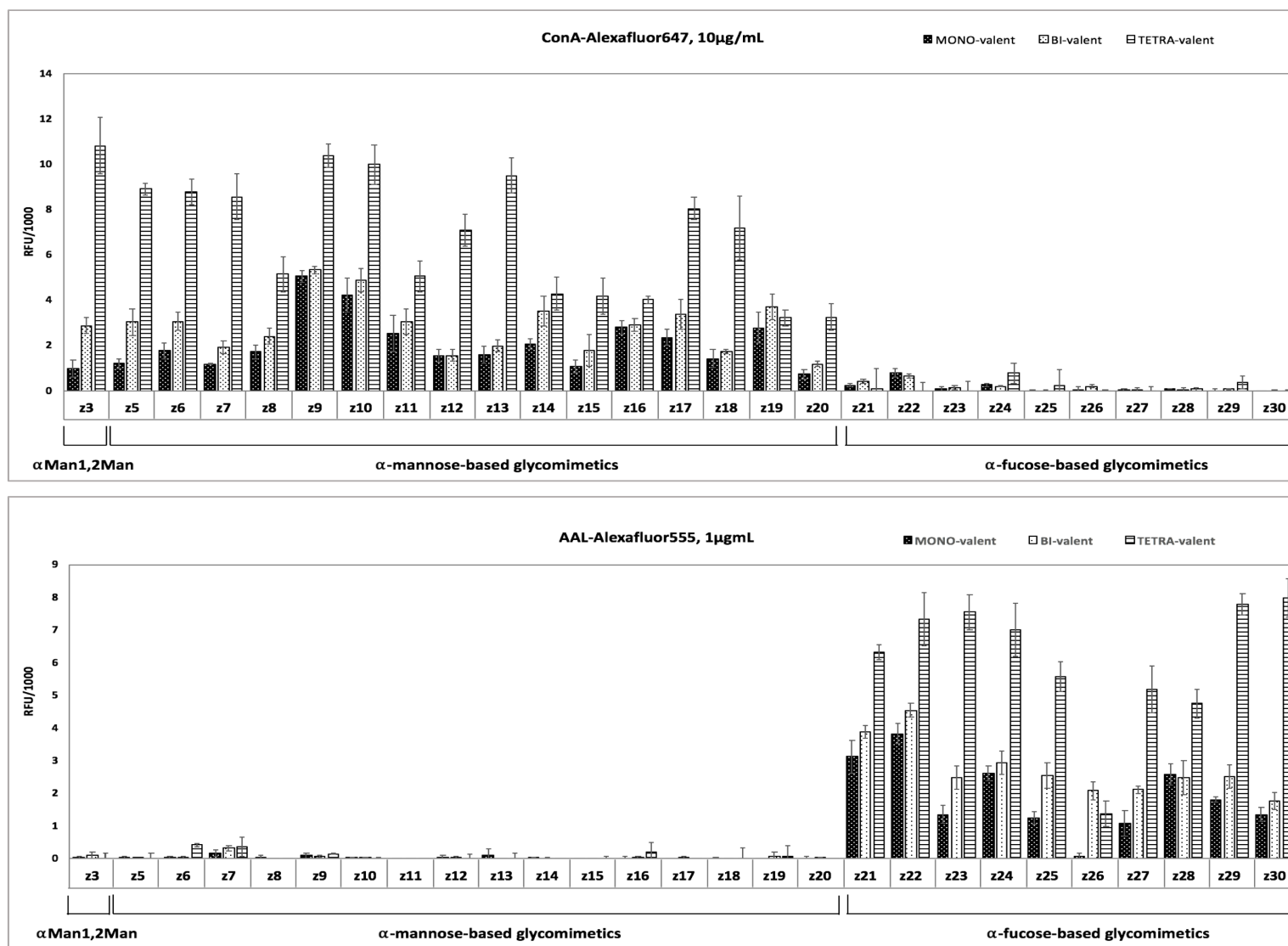


Figure 4.12 Fluorescence quantification of *ConcanavalinA* (above) and *Aleuria Aurantia Lectin* (below) binding to glycomimetic-dendrons.

➤ **Langerin ECD**

After screening *Langerin ECD* on Mono and Bi-valent mimetic arrays, a quite similar profile was observed: most of the mannose-based dendrons were bounded, with diverse strength, except for **z18**- and **z20**-derivatives. Among fucose-based substrates, only **z21**, **z22** and **z23** showed a significant binding. The strongest ligands detected on mono- and bi-valent surfaces were **z19** and **z22** (Figure 4.13).

At higher ligand valences (on surface **d3**), a general strengthen of lectin binding was achieved for most of the mimetics. In addition, mimetics as **z18**, **z25**, **z26**, **z29** and **z30** were recognized by *Langerin* only when presented in Tetra-valent presentation, while fluorescence signals for **z20** and **z28** were absent at all the valences tested. It is interesting to note that mimetics **z20** and **z28** were mannose- and fucose-based scaffolds respectively, characterized by a common amide-substituent, 1-methylpiperazide.

About the control α Man1,2Man (**z3**), its Mono- and Bi-valent forms interacted less efficiently with *Langerin* than most of our mimetics, while its Tetra-valent derivative bound the lectin as efficiently as the Tetra-valent mimetics.

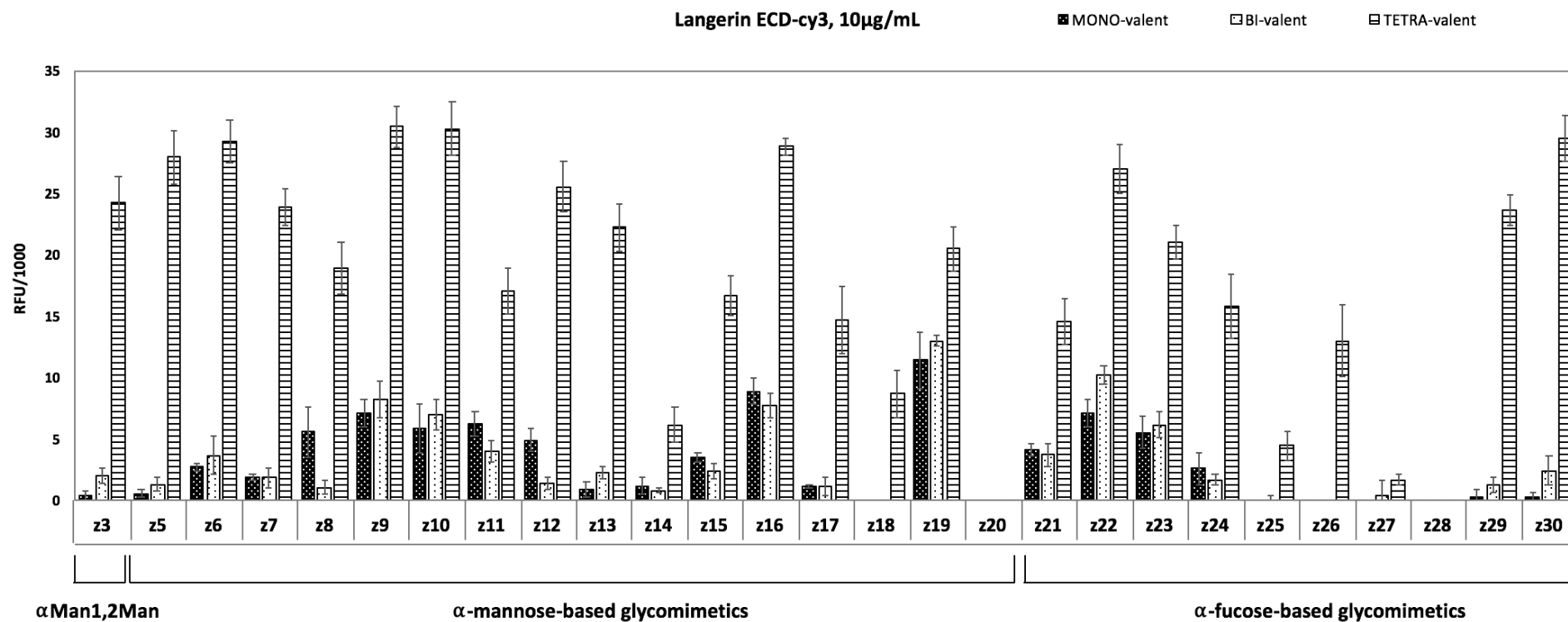


Figure 4.13 Fluorescence quantification of *Langerin ECD* binding to glycomimetic-dendrons.

➤ **Dectin-2 ECD**

In line with its binding specificity (**section 1.2.1.3**), *Dectin-2 ECD* did not show significant binding for fucose-based mimetics in any of the three dendron surfaces ([Figure 4.14](#)).

Of the mannose-based mimetics, only few substrates showed significant binding on Mono- and Bi-valent arrays (**z8**, **z9**, **z10** and **z17**). If the valency was further increased to tetrameric presentation (on surface **d3**), a strong enhancement of binding was only achieved for mimetics **z5**, **z6** and **z9**.

Although α Man1,2Man (**z3**) weakly bound Dectin-2 on Mono- and Bi-valent surfaces, its Tetra-valent form was the best ligand for this lectin.

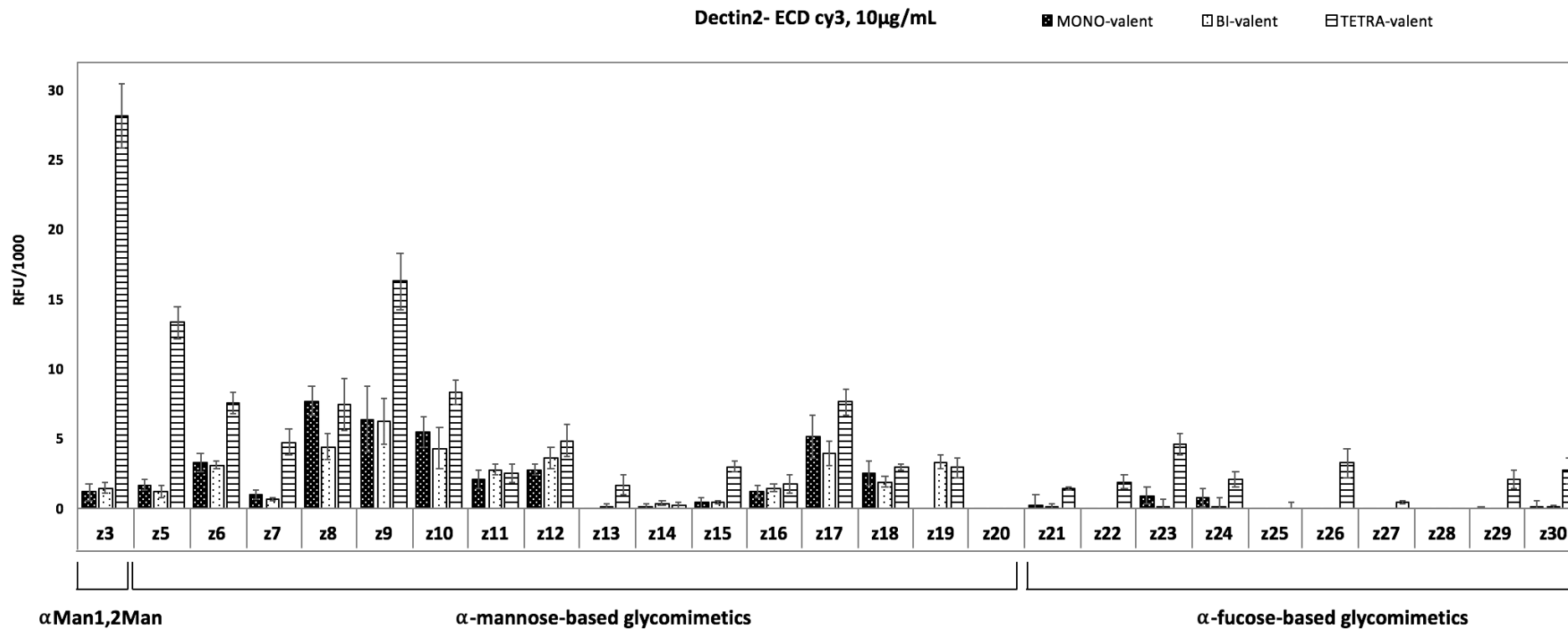


Figure 4.14 Fluorescence quantification of *Dectin-2 ECD* binding to glycomimetic-dendrons.

➤ **Human Mannose Binding Lectin (hMBL)**

On Mono- and Bi-valent array, *hMBL* presented high affinity for only few mannose-based mimetics (**z8** and **z19**). By increasing the number of ligand copies until four, novel interactions showed up and a strong enhancement in the binding was detected for **z5**, **z9**, **z17** and **z3** itself (Figure 4.15).

hMBL did not recognize fucose-based mimetics in any of the three dendron surfaces, as it was expected by its binding specificity described in **section 1.2.1.4**

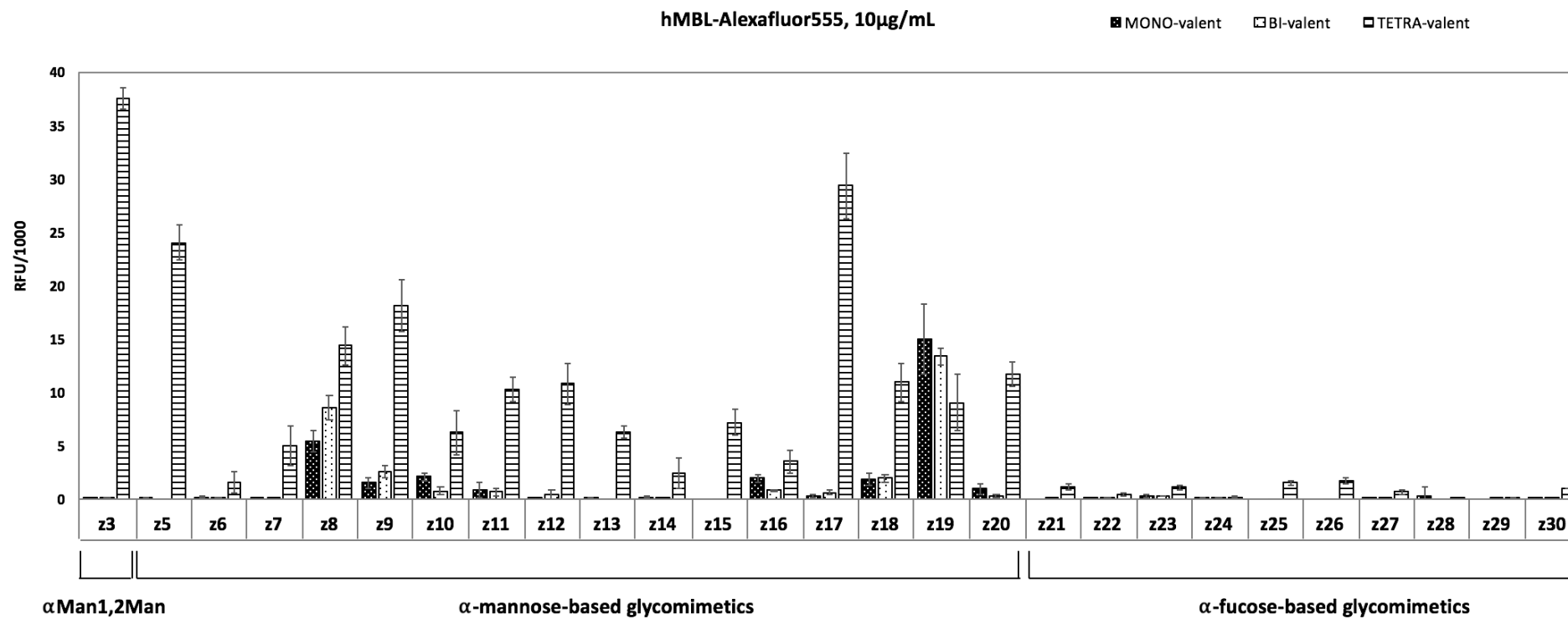


Figure 4.15 Fluorescence quantification of *human Mannose Binding Lectin* binding to glycomimetic-dendrons.

➤ DC-SIGN ECD

DC-SIGN ECD showed more binding preference for mannose-based mimetics than for fucose-based ligands: almost all mannose-type mimetics on Mono- and Bi-valent arrays showed a significant binding except for **z20**, while only fucose-derivatives **z21**, **z22**, **z23** and **z24** gave significant signal intensities.

Regarding Tetra-valent surface, a substantial binding improvement was observed for mannose-dendrons **z5**, **z6**, **z7** and fucose-dendrons **z23**, **z27**, **z29** and **z30**; some of these ligands shared similar aromatic-based amide substituents ([Figure 4.16](#)).

Although a binding enhancement was achieved for the control α Man1,2Man (**z3**) from Mono- to Tetra-valent form, DC-SIGN ECD showed binding preferences for mimetics dendrons instead of natural epitope (**z3**) on all *n*-valent arrays.

4. On-chip synthesis of dendritic system to strenghten carbohydrate-lectin binding

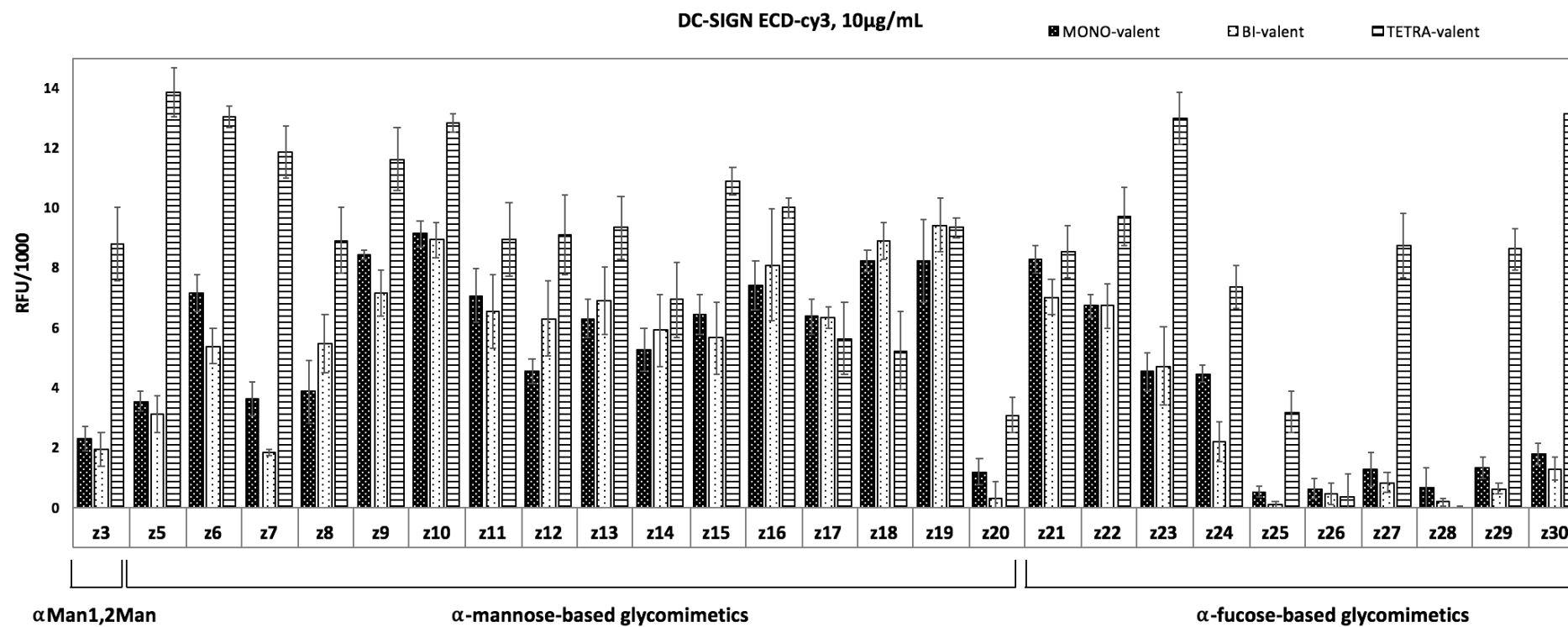


Figure 4.16 Fluorescence quantification of *DC-SIGN ECD* binding to glycomimetic-dendrons.

4.5 Comparison of glycomimetic binding to tetrameric *DC-SIGN* on different array formats

For the on-chip preparation of glycomimetics dendrons we used NHS-activated hydrophobic ITO glass slides due to the advantage to perform on-chip MALDI-TOF analysis to optimize reaction conversions and calculate dendrons density. On the contrary, Anna Bernardi and coworkers have adopted for their studies the commercial NHS-functionalized glass slide (Nexterion® SlideH- Schott AG).¹⁴⁶

Comparing the published data achieved from the monovalent BCN-glycomimetics with the binding results obtained on the monovalent surface **d1** (section 4.4.2) differences in binding profiles were observed (Figure 4.18).

For instance, in our assays *DC-SIGN ECD* showed a robust binding towards most mannose-based mimetics (**assay1**), while on the published data (**assay2**) this lectin strongly recognized only some mannose-derivatives, such as **z5**, **z6**, **z9** and **z10**. On the other hand, in Bernardi's work, only weak or no binding was found towards fucose-based mimetics (from **z21** to **z30**), while on our array *DC-SIGN* showed significant binding for fucose-based mimetics as **z21**, **z22**, **z23** and **z24**.

Although, the binding profiles for the two array formats differed considerably, glycomimetics **z9** and **z10** were among the strongest ligands in both cases.

The differences observed for *DC-SIGN ECD* in the binding trends of the two compared assays might be explained by the different ligand presentation on the two microarray surfaces used. The Schott Nexterion slide is coated with polyacrylamide-ethylenglycol hydrogel with activated headgroups for covalent ligand immobilization located all throughout the 3D mesh; on the other hand, our hydrophilic non-covalent sandwich array is perhaps a true 2D surface with possible some flexibility for lateral ligand movement through the non-covalent immobilization via hydrophobic interactions. In addition, in both formats, different printed concentrations and binding conditions were adopted (Figure 4.17).

4. On-chip synthesis of dendritic system to strengthen carbohydrate-lectin binding

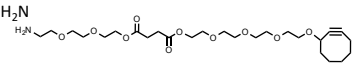
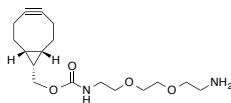
assay1	assay2
<ul style="list-style-type: none">❖ NHS-Hydrophobic glass slide❖ Mono-valent cyclooctyne d1 <div style="text-align: center;"><p>The structure shows a cyclooctyne ring (an eight-membered ring with one triple bond) attached to a long poly(ethylene glycol) (PEG) chain. The PEG chain consists of several repeating -CH2-CH2-O- units, ending in a primary amine group (-NH2).</p></div> <ul style="list-style-type: none">❖ Printed concentration: 5 μM❖ Lectins' incubation conditions: 10 μg/mL, 4°C, 2h	<ul style="list-style-type: none">❖ Nexterion® SlideH- Schott AG❖ Commercial cyclooctyne (BCN) <div style="text-align: center;"><p>The structure shows a cyclooctyne ring with a double bond in the ring. It is substituted with a methoxy group (-OCH3) and a primary amine group (-NH2) attached via a PEG chain (-CH2-CH2-O-CH2-CH2-O-CH2-CH2-O-CH2-CH2-NH2).</p></div> <ul style="list-style-type: none">❖ Printed concentration: 50 μM❖ Lectins' incubation conditions: 50μg/mL, 4°C, O/N

Figure 4.17 Comparison of conditions employed in the 2 binding assays with *DC-SIGN ECD*. **assay1**: binding experiment reported in **section 4.2.2**; **assay2**: binding experiment reported in Bernardi's literature.¹⁴⁶

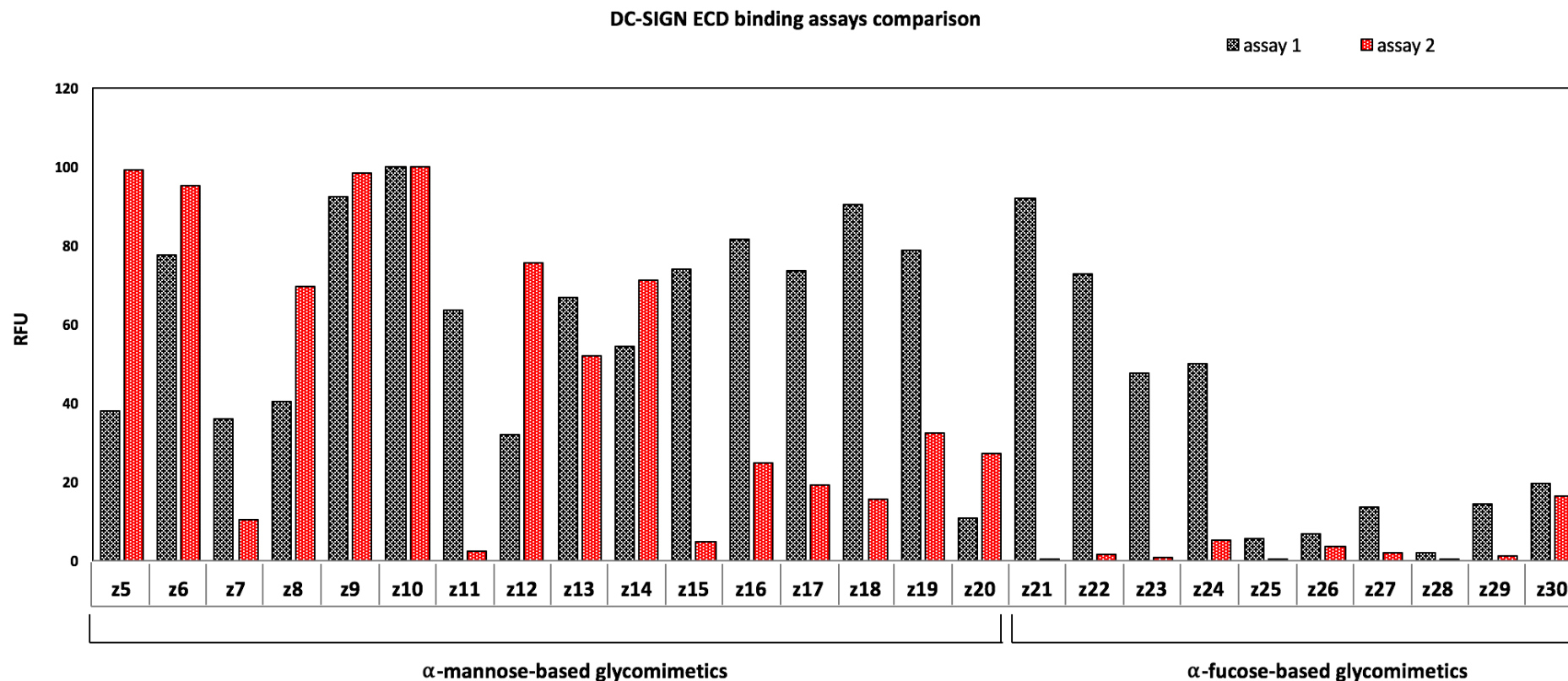


Figure 4.18 This graphic shows: **1.** Fluorescence quantification of *DC-SIGN ECD* binding to glycomimetics Mono-valent dendrons (*assay1*, in black); **2.** Fluorescence quantification of *DC-SIGN ECD* binding to BCN-glycomimetics conjugates (*assay2*, red). To report the two different experiments on the same graphic, mimetic **z10** was employed to normalize fluorescence intensities. An arbitrary value of 100 was chosen to calculate the normalization factor.

4. On-chip synthesis of dendritic system to strengthen carbohydrate-lectin binding

As mentioned above ([Figure 4.17](#)), these two types of array formats were characterized by a different ligand immobilization and density, which in turn affect ligand flexibility and accessibility that consequently will determine the carbohydrate-lectin binding mode. Thus, we cannot assume that different carbohydrate arrays with similar glycan structures give analogous results.

In the literature, there are only a few examples where binding profiles towards the same carbohydrate binding proteins have been compared for different microarray formats.

An interesting study was performed in 2012 by Karavani and co-workers¹⁵⁴ which immobilized a library of sialosides via two different linkers and on two different surfaces to perform a screening with several GBPs (Glycan Binding Proteins). From this work emerged that binding profiles towards the same receptors differed significantly for the two arrays highlighting the influence of ligand presentation and array architecture on the assay results.

Similar results were achieved few years later, when the cross-comparison was extended to six microarray laboratories (including ours) which tested a wide diversity of N-glycan structures against 5 plant lectins on different array platforms.¹⁵⁵

To be able to identify more easily the effect of individual surface parameters on the binding event, we compared the published results (**assay2**) with an additional binding experiment (**assay3**) performed on the hydrophobic ITO array by using the same BCN-linker, concentration and binding conditions adopted in published work for Schott Nexterion array. ([Figure 4.19](#)).

For this assay, the glycomimetics (**z5-z30**) were coupled to the BCN-linker in solution¹⁴⁶ and then immobilized onto a NHS-hydrophobic ITO glass slide at 50 μ M of concentration. After immobilization step, the binding assay with *DC-SIGN ECD-cy3* (50 μ g/mL) was performed overnight at 4°C in according to the published procedure.

4. On-chip synthesis of dendritic system to strengthen carbohydrate-lectin binding

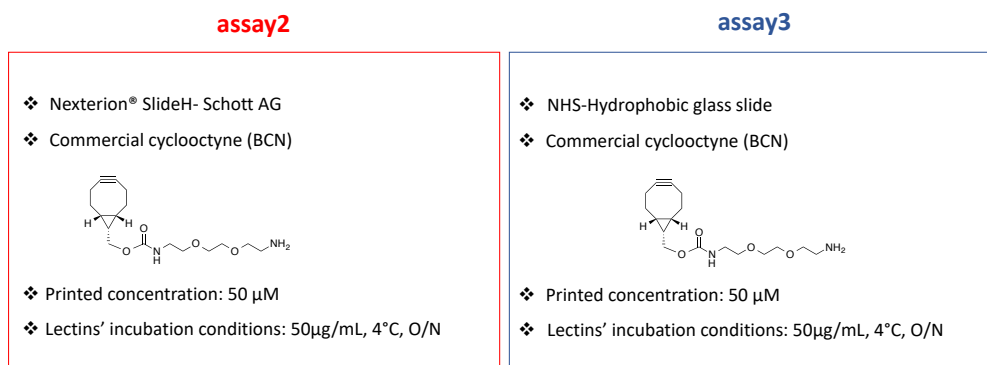


Figure 4.19 Conditions used in the compared binding assays with *DC-SIGN ECD*. **assay2**: binding experiment reported in Bernardi's work; **assay3**: binding experiment performed in **section 4.5**.

Even after the homogenisation of printing and incubation conditions for the two array formats we observed significant differences between the binding profiles of tetrameric DC-SIGN ECD highlighting the impact of ligand presentation on the carbohydrate-protein binding events (Figure 4.20).

With the exception of few ligands as **z10**, **z12**, **z13**, **z14** and **z17** which have shown a quite similar binding strength on both the two arrays, the general binding trends were still different and novel strong binders showed up with the new assay. Indeed, the fucose-based mimetics **z29** and **z30** as well as the mannose-mimetics **z7** and **z16** showed a strong binding with *DC-SIGN ECD* on the hydrophobic array while no binding had been reported for the Schott Nexterion slide based assay¹⁴⁶ (Figure 4.20). On the contrary, strong binders on Schott nexterion platform as **z6** and **z8** lost a part of their binding strength on hydrophobic array.

It is interesting to note that, in this new binding study, the glycomimetics **z9** and **z10** were among the strongest ligands for *DC-SIGN* as it was achieved in previous experiments.

The discrepancy among the binding results achieved from the diverse array formats does not question the role of microarray in carbohydrate-lectin binding studies. On the contrary, this dissertation only wants to emphasize the importance of all the different parameters that affect lectin recognition on microarray and make difficult a direct comparison between binding assays performed on diverse array formats.

Therefore, each microarray should be analyzed and interpreted with respect to the collection of ligands on each array and the information obtained should be combined with additional experiments, on array and/or in vitro, to perform complementary interpretations for glycan-binding protein specificity.

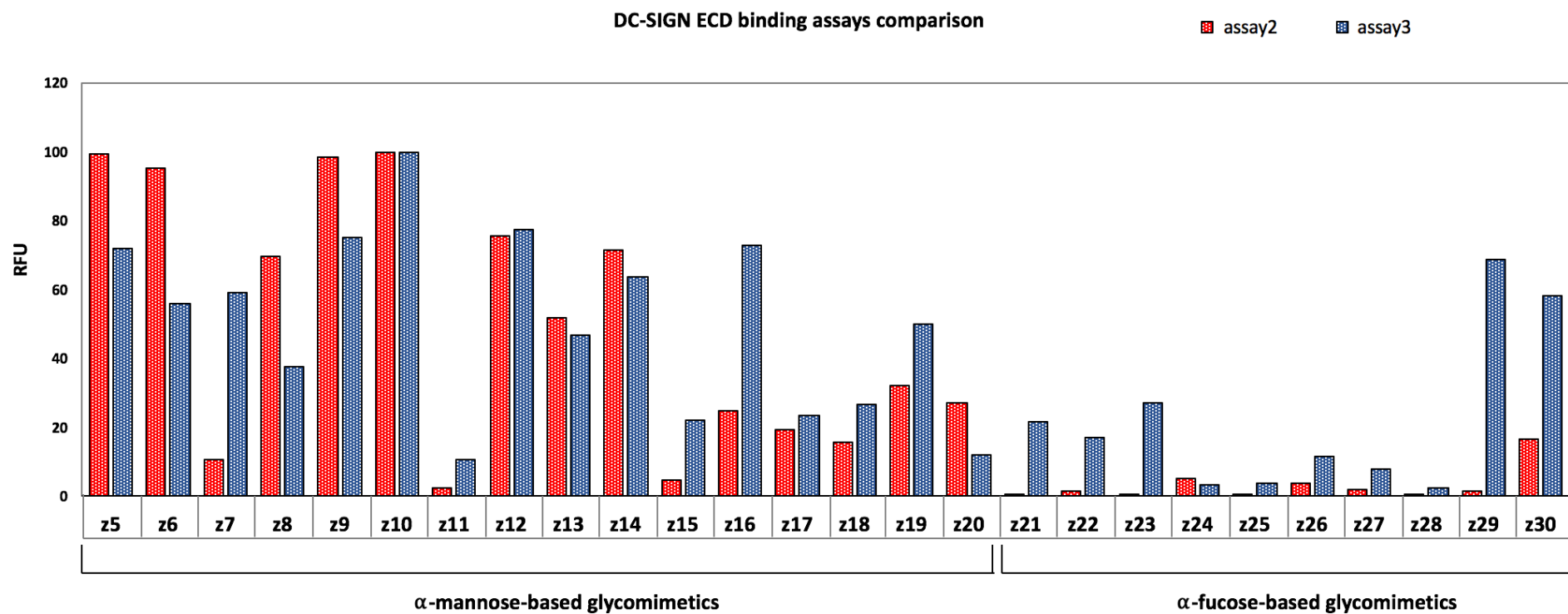


Figure 4.20 Comparison between fluorescence quantification of DC-SIGN ECD binding to glycomimetic-dendrons performed in *assay2* (in red) and fluorescence quantification of DC-SIGN ECD binding performed to glycomimetic-dendrons in *assay3* (in blue). To report the two different profiles on the same graphic, mimetic **z10** was employed to normalized fluorescence intensities. An arbitrary value of 100 was chosen to calculate the normalization factor.

4.6 Conclusion

In this thesis chapter we developed a versatile and reproducible on-chip procedure for the synthesis of glycodendrons, by metal-free cycloaddition, and their binding evaluation toward diverse C-type lectins.

This further application of the NHS-activated hydrophobic ITO slide proved the versatility of this surface as synthetic and analytical tool in drug development.

Performing *in situ* MALDI-TOF detection on the hydrophobic surface is an important advantage that allowed us to determine the conversion for each on-chip reaction as well as to quantify the relative amounts of immobilized dendrons on the surface. The quantification of ligand density on the surface by mass analysis was an important feature of the developed array format, since this parameter plays an important role in the carbohydrate-lectin recognition.

By using diverse cyclooctyne dendrons (**d1-3**), it was possible to vary the number of ligand copies and their presentation on the surface and evaluate how these parameters can affect carbohydrate-lectin binding.

In general, we observed that increasing the number of ligands copies do not necessarily lead to a strengthened binding; on the contrary, in some cases the high-valent form present a similar or a slight worse binding to the low-valent constructs. For instance, the mono- or bi-valent form of glycomimetic **z19** showed for *hMBL* a slight stronger binding than the related tetra-valent dendron.

A further important feature arose from these studies regard the effect of multivalent presentation in the modulation of lectin binding preferences; indeed, passing from mono-valent to tetra-valent array, a different binding profile was generally observed. For example, the fucose-based mimetic **z30** is one of the weakest ligands for *Langerin ECD* when presented as mono- or bi-valent dendron while, when it was coupled on the tetra-valent surface became one of the strongest binders.

The azidoethyl-glycomimetics (**z5-z30**) tested in this thesis chapter have been already screened on Schott Nexterion array against C-type lectins.¹⁴⁶ With the aim to assess the effect of ligand presentation on surface-based carbohydrate-lectin binding, we performed a cross comparison among the published data and binding assays performed on our hydrophobic surface.

The cross comparison of DC-SIGN ECD binding assays proved how parameters like ligand presentation, density and binding conditions can dramatically affect lectin

4. On-chip synthesis of dendritic system to strengthen carbohydrate-lectin binding

recognition. Indeed 3 different binding profiles have been achieved from the 3 diverse on-chip binding assays performed on the mono-valent form of glycomimetics.

An interesting exception was observed for the glycomimetics **z9**, **z10** which showed a strong and very similar binding profile for all the array formats and binding conditions adopted. This result suggests that these compounds can be promising inhibitors for DC-SIGN ECD since they preserve their binding properties in different presentation modes and binding environments.

In conclusion, in carbohydrate-based drug development is important to design the structures that better interact with the binding pocket of the targeted lectin but, in the meantime, spatial presentation and other topological features should be taken into account by performing more detailed studies. About this, carbohydrate microarrays represent a powerful and rapid tool to explore different ligand presentations and binding conditions.

Among the plenty microarray formats developed, it does not exist the best microarray platform since each of them possesses proper advantages and limitations. Therefore, each microarray-based assay should be analyzed and interpreted with respect to the collection of ligands and combined with additional experiments to collect complementary interpretations for glycan-binding protein specificity.

References

146. L. Medve, S. Achilli, S. Serna, F. Zuccotto, N. Varga, M. Thépaut, M. Civera, C. Vivès, F. Fieschi, N. Reichardt and A. Bernardi, *Chem. - A Eur. J.*, DOI:10.1002/chem.201802577.
147. E. Arce, P. M. Nieto, V. Díaz, R. García Castro, A. Bernad and J. Rojo, *Bioconjug. Chem.*, 2003, **14**, 817–823.
148. N. J. Agard, J. A. Prescher and C. R. Bertozzi, *J. Am. Chem. Soc.*, 2004, **126**, 15046–15047.
149. (a) N. Feliu, et al, *Biomaterials*, 2012, **33**, 1970–1981; (b) A. Carlmark, C. Hawker, A. Hult, and M. Malkoch, *Chem. Soc., Rev.* 2009, **38**, 352–362. (c) A. Carlmark, E. Malmström, and M. Malkoch, *Chem. Soc. Rev.*, 2013, **42**, 5858–5879
150. I. J. Goldstein and C. E. Hayes, *Adv. Carbohydr. Chem. Biochem.*, 1978, **35**, 127–340.
151. (a) A. Imberty, M. Wimmerova, E. P. Mitchell, N. Giboa-Garber, *Microbes and Infection*, 2004, **6(2)**, 221-228. (b) M. Sitohy, M. Doheim, H. Badr, *Food Chemistry*, **104(3)**, 971-979. (c) T. Kurokawa, M. Tsuda and Y. Sugino, *J. Biol. Chem.*, 1976, **251**, 5686–5693.
152. D. A. Mitchell, A. J. Fadden and K. Drickamer, *J. Biol. Chem.*, 2001, **276**, 28939–28945.
153. J. Olausson, L. Tibell, B. H. Jonsson and P. Pålsson, *Glycoconj. J.*, 2008, **25**, 753–762.
154. V. Padler-Karavani, X. Song, H. Yu, N. Hurtado-Ziola, S. Huang, S. Muthana, H. A. Chokhawala, J. Cheng, A. Verhagen, M. A. Langereis, R. Kleene, M. Schachner, R. J. De Groot, Y. Lasanajak, H. Matsuda, R. Schwab, X. Chen, D. F. Smith, R. D. Cummings and A. Varki, *J. Biol. Chem.*, 2012, **287**, 22593–22608.
155. L. Wang, R. D. Cummings, D. F. Smith, M. Huflejt, C. T. Campbell, J. C. Gildersleeve, et al, *Glycobiology*, 2014, **24 (6)**, 507-517.

**5. Synthesis of phosphorylcholine-containing
OVA-glycoproteins for dendritic cells
targeting**

5. Synthesis of phosphorylcholine-containing OVA-glycoproteins for dendritic cells targeting

5.1 Immunomodulation by Phosphorylcholine

Phosphorylcholine (PC) is an abundant component of eukaryotes where it is found as the polar head group of the phospholipids, phosphatidylcholine and sphingomyelin. However, in certain bacteria, fungi and lower invertebrates including filarial nematodes, PC has been found conjugated to carbohydrates.¹⁵⁶ Specifically, in filarial nematodes, PC has been found attached to both glycolipids¹⁵⁷ and glycoproteins.¹⁵⁸ Studies employing parasite PC-containing molecules indicate that it possesses a plethora of immunomodulatory activities which can be beneficial to both the parasite, in promoting its survival, and its host, in limiting pathology.¹⁵⁹

ES-62 (excretory-secretory, 62KDa), a PC-containing glycoprotein secreted by the rodent filarial nematode *Acanthocheilonema viteae* (long-lived parasite), provides a model system for studying the mechanisms of immune evasion induced by related PC-containing glycoproteins expressed by human filarial nematodes.

ES-62 exerts its immunomodulatory activities on a variety of immune cells such as B- cells, T-cells, dendritic cells and macrophages (Figure 5.1).

PC-antigens induce IL-10 cytokines production in B1 cells which negatively affect the levels of IgG2a-type antibodies (markers of Th2 lymphocytes) but favor IgG1-type expression (markers of Th1 lymphocytes). On the other side, the production of IL-10 by B-cells, together to the inhibition of key proliferative signaling pathways, suppress the up-regulation of co-stimulatory molecule expression on antigen presenting cells leading to a reduced T-cells activation.¹⁶⁰

Furthermore, the production of pro-inflammatory cytokines like TNF- α , IL-6, IL-12 is suppressed, whereas IL-4 production is favored indicating that the parasite molecule had polarized the re-call immune response in a Th-2 direction.¹⁶¹

More recently, the ability of ES-62 to induce immune responses via dendritic cells has been investigated.¹⁶² If the dendritic cells were pre-cultured with ES-62, there was an increase in the amount of IL-4 produced and a decrease in the amount of IFN- γ . Thus, ES-62 is apparently able to induce the maturation of dendritic cells with the capacity to

5. Synthesis of phosphorylcholine-containing OVA-glycoconjugates for DCs' targeting

induce Th-2 responses to unrelated antigens.¹⁶² Such a property will at the same time divert immune responses away from the Th-1 and hence pro-inflammatory phenotype.

The immunomodulation of ES-62 was found to be solely due to the phosphorylcholine moiety, as PC conjugated to albumin or even PC alone broadly reproduce the effects obtained with ES-62.¹⁶³

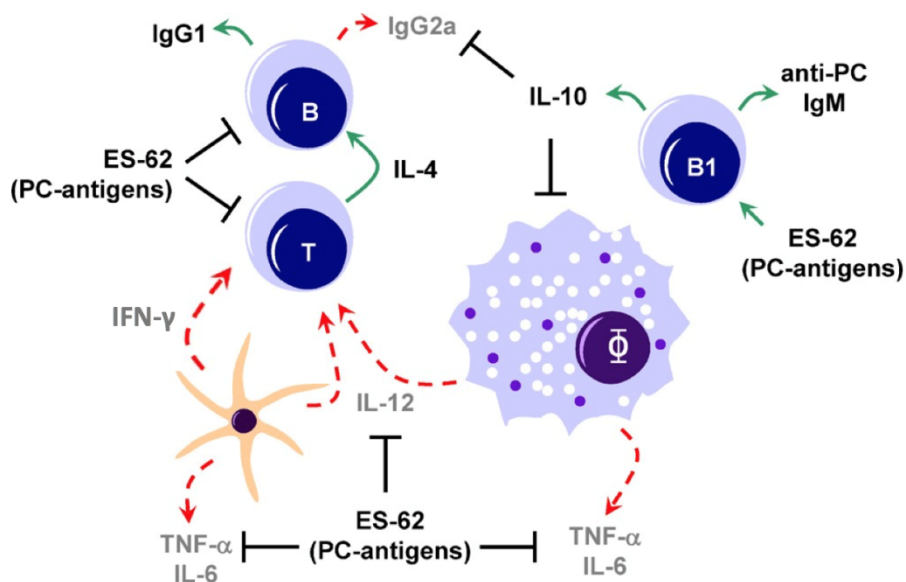


Figure 5.1 Immunomodulation by PC-antigens on the cellular level. **1.** ES-62 is able to induce the maturation of dendritic cells with the capacity to induce Th-2 responses to unrelated antigens and divert immune responses away from the Th-1; **2.** ES-62 induces the production of the anti-inflammatory cytokine IL-10 from B1 lymphocytes and this acts to suppress inflammation and polarize immune responses. Picture taken from *Molecular Immunology*, **2009**, *47*, 149-163.¹⁶¹

By secreting PC-containing molecules, adult filarial nematodes appear to modulate the immune response of the host to evade their recognition and elimination by the immune system.

The therapeutic use of PC might therefore hold opportunities for the treatment of autoimmune diseases; as PC apparently elicits a variety of immune responses including pro-inflammatory activities, more research is required before this intriguing molecule should be considered for use in therapy.

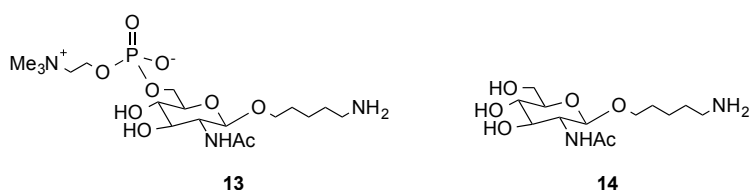
With the aim to evaluate if phosphorylcholine-based conjugates are suited for DCs targeting and subsequent T cells activation, we devised a strategy for the synthesis of PC-based sugars and their subsequent bioconjugation to Ovalbumin as a multivalent carrier protein. These OVA-based glycoproteins were tested in DC-T cells

5. Synthesis of phosphorylcholine-containing OVA-glycoconjugates for DCs' targeting

co-cultivation assays in collaboration with an Immunoshape partner laboratory in Hannover, Germany .

5.2 Synthesis of Phosphorylcholine (PC)-based sugars

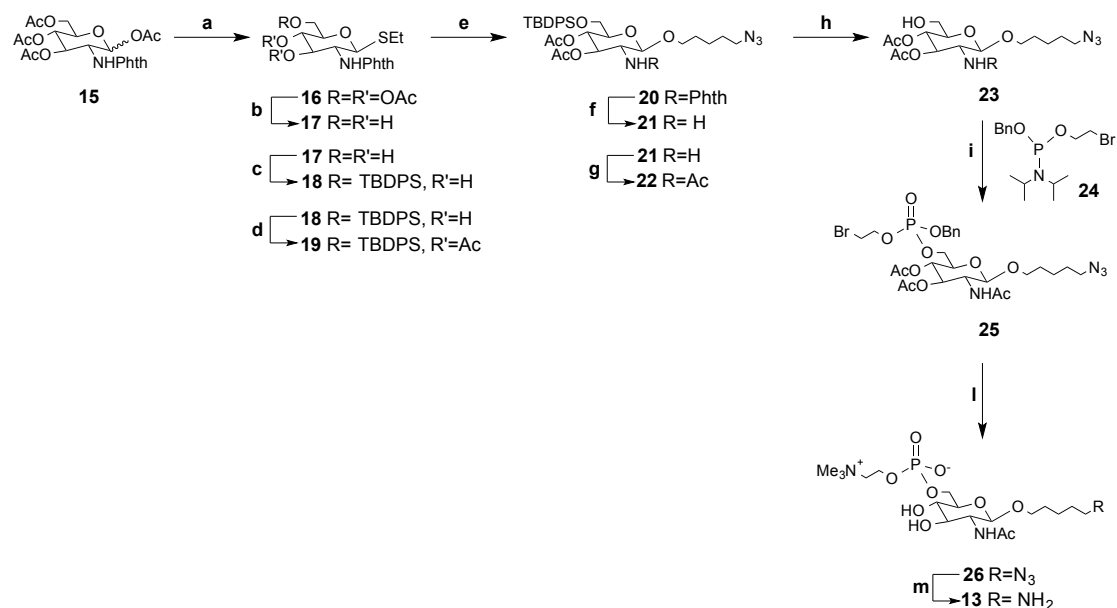
To set up a general protocol for the preparation of OVA-PC bioconjugates and their employment in DCs-T cells co-cultivation assays, preliminary attempts were directed towards a simple 6-O-PC-D-glucosamine moiety (**13**) instead of more complex structures as 6-O-PC-N-glycans. As a control the non-modified D-glucosamine derivative equipped with an anomeric azidopentyl linker (**14**) was employed.



The 6-O-PC-D-glucosamine (**13**) was prepared following the synthetic protocol developed first by Lafaye and co-workers¹⁶⁴ and later by Deming's team¹⁶⁵ ([Scheme 5.1](#)) while, the D-glucosamine substrate (**14**) was already available in our laboratory.¹²⁹

In [Scheme 5.1](#) is reported the synthetic strategy developed for the preparation of monosaccharide (**13**) but, starting from compound (**19**), this protocol could be easily adopted to synthesize more complex structures bearing terminal 6-O-PC-D-glucosamine.

5. Synthesis of phosphorylcholine-containing OVA-glycoconjugates for DCs' targeting



Scheme 5.1 (a) BrCH₂CH₂OH, -25°C-r.t., O/N, 46%; (b) DIPEA, TEA, -78°C-r.t., O/N; (c) DIPEA, BnOH, 0°C, 30 min, 84% two steps; (d) NaOMe, MeOH, 0°C-r.t., 1h; (e) TBDPSCl, imidazole, DMF, r.t., O/N, 92% two steps; (f) Ac₂O, pyridine, r.t., 1h, 92%; (g) NIS, TMSOTf, dry DCM, m.s., 0°C-r.t., 2h, 74%; (h) NH₂(CH₂)₂NH₂, *n*BuOH, microwave, 120°C, 30min; (i) Ac₂O, pyridine, r.t., 1h, 90% two steps; (l) TBAF, AcOH, THF, r.t.-60°C, 70%; (m) (i) *N,N*-diisopropyl-benzyl-2-bromoethylphosphoramidite (**24**), 4% tetrazole, dry AcCN, r.t., 2h; (ii) *t*BuOOH, 0°C-r.t., 1h, 94% two steps; (n) 20% NMe₃/water, 40°C, O/N; (o) H-cube/Pd, 1% TFA/MeOH, 50°C, 1mL/min, FullH₂, 30 min.

5.3 Synthesis of OVA-based bioconjugates

➤ Ovalbumin (OVA)

Ovalbumin exists physiologically as a tetramer¹⁶⁶ with four subunits of identical primary structure. Each subunit is composed by 385 amino acid residues, including 20 lysins, with a total molecular weight of 44.3 kDa.¹⁶⁷ Among the 20 lysins available for each subunit, only 10 residues are sterically available for bioconjugation with activated molecules (Figure 5.2).

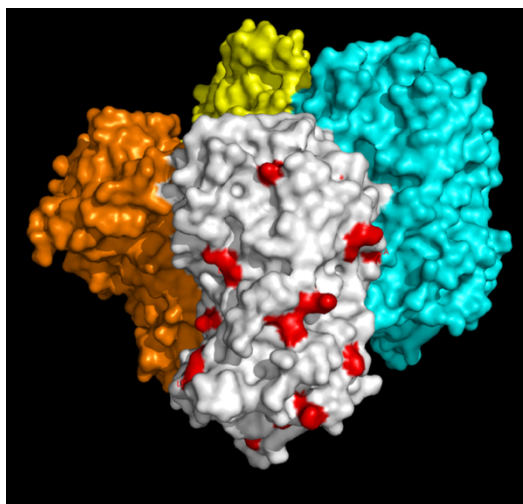
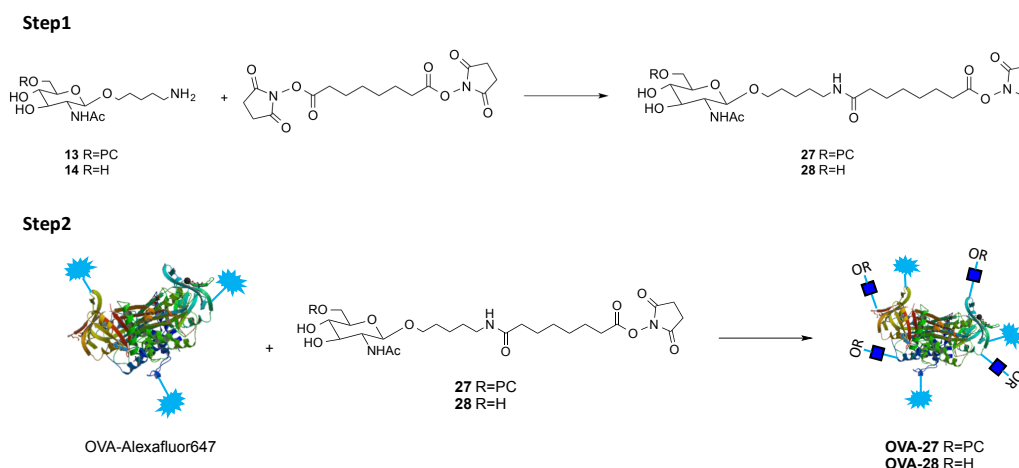


Figure 5.2 Ovalbumin tetrameric form: the four subunits are represented in four different colors. By focusing on one single subunit (*in white*), only 10 lysins (*in red*) are sterically available for cross-linking reaction with activated molecules. The picture was obtained by using *Pymol* software.

➤ OVA-based glycoconjugates synthesis

Ovalbumin (OVA) conjugates were generated by first activating carbohydrate-amino linkers (**13,14**) with disuccinimidyl suberate ester (DSS) (**27,28**) and then by crosslinking accessible OVA lysin residues in a second step.¹⁶⁸ Gel electrophoresis and MALDI-TOF mass spectrometry were carried out on the synthesized glycoconjugates **OVA-27** and **OVA-28** to determine the number of sugar covalently attached to the OVA.



Scheme 5.2 Synthetic strategy for preparation of NHS-activated 6-O-PC-D-glucosamine (**27**) and D-glucosamine (**28**) (*Step1*) with subsequent coupling reaction on fluorescently labeled Ovalbumin to enrich **OVA-27** and **OVA-28** (*Step2*).

5. Synthesis of phosphorylcholine-containing OVA-glycoconjugates for DCs' targeting

Different buffer solutions and reagents ratios were employed to maximize the number of sugar copies attached on the OVA-surface and, at the same time, to avoid the formation of cross-linked OVA (Table 5.1).

Sugar		DSS:sugar	sugar:OVA	buffer solution	sugar copies attached	OVA-OVA cross-linked
13	(a)	13:1	65:1	PBS, pH 7.8	5.7	YES
	(b)	5:1	70:1	NaHCO ₃ , pH 9.1	3.6	NO
	(c)	5:1	100:1	PBS, pH 7.8	5.2	NO
14	(d)	13:1	100:1	PBS, pH 7.8	5.0	YES
	(e)	13:1	100:1	NaHCO ₃ , pH 9.1	6.8	YES
	(f)	5:1	70:1	NaHCO ₃ , pH 9.1	5.0	NO
	(g)	5:1	100:1	PBS, pH 7.8	5.1	NO
	(h)	5:1	75:1	PBS, pH 7.8	3.1	NO

Table 5.1 Experimental conditions and relative conversion degrees for the synthesis of OVA-conjugates of sugars **13** and **14**.

A major challenge of the conjugation reactions (Scheme 5.2) was the removal of un-reacted DSS, after performing NHS-sugar activation, when large excess of this reagent was employed. In fact, if traces of DSS reagent were still present in the bioconjugation step, the formation of cross-linked OVA species, generated by coupling reaction between two or more distinct OVA molecules, could be observed. As a result, low-yielding and low-purity OVA-conjugates were achieved.

The formation of cross-linked OVA by-products at high molecular weight (MW>250 KDa) was detected by performing SDS-PAGE gel electrophoresis (Figure 5.3).

5. Synthesis of phosphorylcholine-containing OVA-glycoconjugates for DCs' targeting

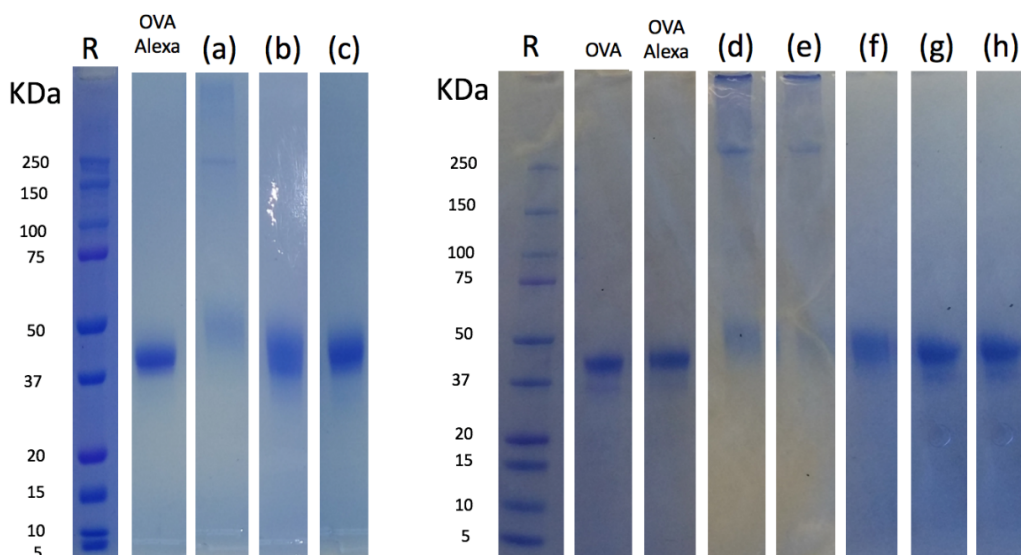


Figure 5.3 SDS-PAGE gel electrophoresis (10% acrylamide) stained with Coomassie Blue G-250; R= Prestained Protein Ladder-Broad molecular weight (5-250 KDa).

The use of a lower DSS:sugar ratio of 5:1 lead to an easy and complete removal of un-reacted DSS with subsequent high-yielding OVA-sugar conjugation (Table 5.1). Finally, with the optimized conditions, for both sugars **13** and **14** a maximum of 5 copies were attached on each Ovalbumin subunit.

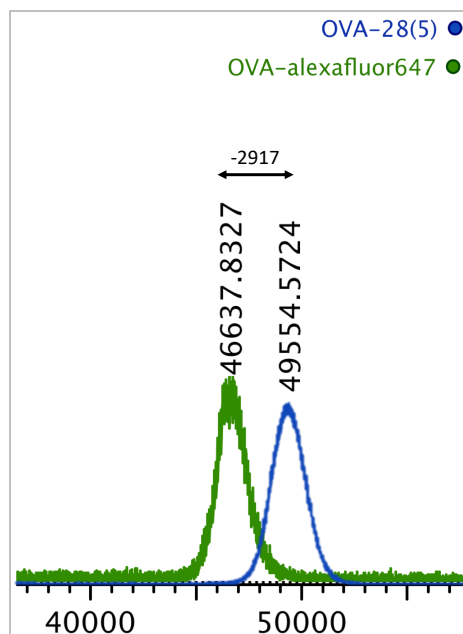


Figure 5.4 MALDI-TOF spectra of OVA-Alexafluor647 (in green) and OVA-28 with 5 copies of D-glucosamine attached on the OVA (in blue). The MALDI-TOF MS detected for all the synthesized OVA-glycoconjugates are reported in **Appendix**.

5.4 OVA-based glycoproteins in dendritic cells targeting

The uptake of the OVA-PC constructs and consecutive T-cell activation was evaluated on OT-II CD4⁺ T cells from transgenic mice which possess a T cell receptor specific for the model antigen protein ovalbumin (OVA) and recognize specifically the OVA₃₂₃₋₃₃₉ peptide when presented by MHC-II molecules of DCs.¹⁶⁹

To analyze the impact of PC-moieties and different glycan displays in DCs targeting through CLRs and further T cell activation, seven constructs were used in this study: **OVA-Alexafluor647** (positive control), **OVA-27(3)** (3 sugar copies), **OVA-28(3)** (3 sugar copies), **OVA-27(5)** (5 sugar copies), **OVA-28(5)** (5 sugar copies), **OVA-27(CL)** and **OVA-28(CL)** containing cross-linked OVA species. Both DCs uptake and T-cell activation assays were run on a flow cytometer.

5.4.1 Dendritic Cells uptake assays

The biological experiment report in this chapter was performed in Prof. Dr. Bernd Lepenies' laboratories, in University of Veterinary Medicine Hannover, under the supervision of his PhD student João Monteiro.

➤ DCs uptake assays on OVA-27(3) and OVA-28(3)

After 10 minutes of incubation, OVA alone was detected in about 33% of DCs while a slight increase was observed upon incubation with both conjugates **OVA-27(3)** (42%) and **OVA-28(3)** (45%). The presence of phosphorylcholine moiety on the OVA-based glycoconjugates did not entail any contribution in DCs' uptake process since the internalization values observed for constructs **OVA-27(3)** and **OVA-28(3)** were comparable (Figure 5.5).

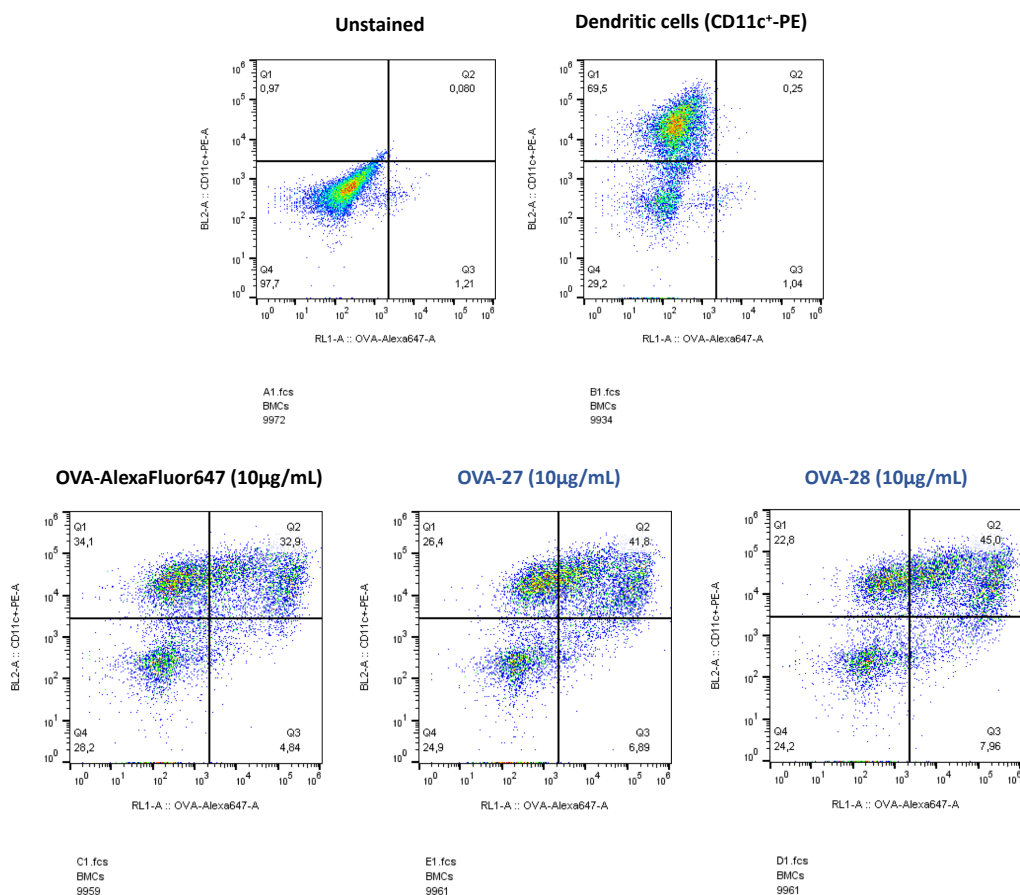


Figure 5.5 Uptake of OVA and glycoconjugates (bearing 3 sugar copies) analyzed by flow cytometry. Data are representative for three independent experiments.

➤ DCs uptake assays on OVA-27(5) and OVA-28(5)

In comparison with the assays reported above, the increase in the number of sugar copies on the OVA-surface did not provide better internalization properties. In fact, after 10 minutes of incubation, OVA alone was uptaken by a percentage of DCs (34%) comparable to what was detected for the constructs **OVA-27(5)** (36%) and **OVA-28 (5)** (41%).

Again, the presence of PC moiety on the OVA-based glycoconjugates did not entail any contribution in DCs' uptake (Figure 5.6).

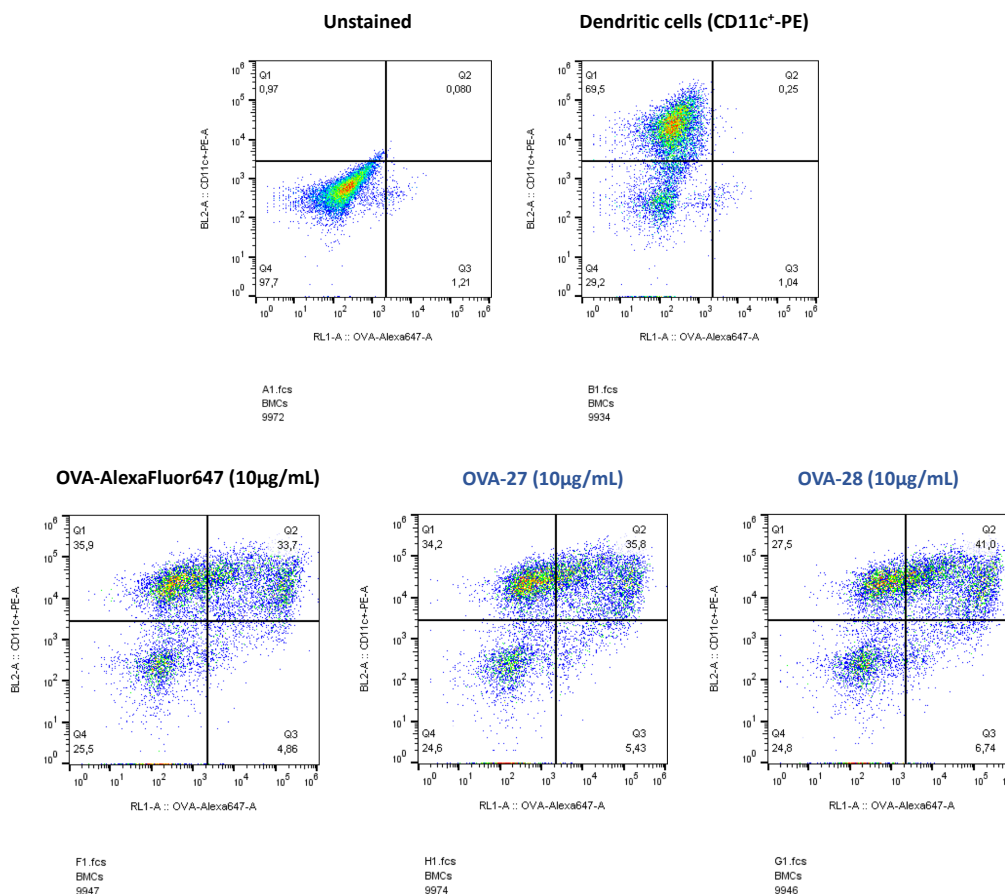


Figure 5.6 Uptake of OVA and glycoconjugates (bearing 5 sugar copies) analyzed by flow cytometry. Data are representative for three independent experiments.

➤ **DCs uptake assays on OVA-27(CL) and OVA-28(CL) containing cross-linked OVA-species**

In order to understand the possible role of cross-linked OVA species in the internalization process, **OVA-27(CL)** and **OVA-28(CL)** (batch **a** and **e** respectively, [Table 5.1](#)) containing high-molecular-weight constructs (>250KDa) were tested in DCs uptake assays.

After 10 minutes of incubation, OVA alone was detected in about 23% of DCs, while an increased internalization up to 62% were observed for glycoconjugates batches contained cross-linked OVA. Differences in DC uptaking between batch **a** (51%) and batch **e** (62%) could be related to different size distribution of cross-linked species, resulting in a size-dependent internalization process (Figure 5.7).

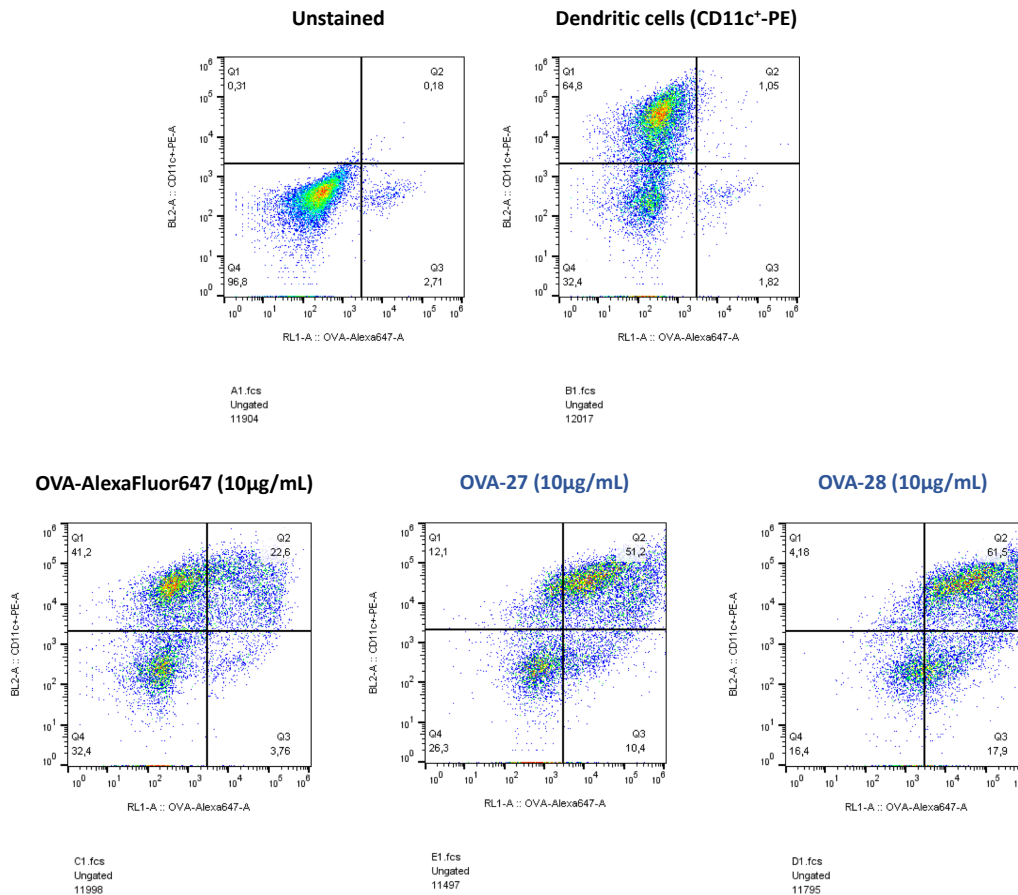


Figure 5.7 Uptake of OVA and glycoconjugate batches containing cross-linked OVA species analyzed by flow cytometry. Data are representative for three independent experiments.

5.4.2 In vitro stimulation and DCs/T cells co-culture

Upon internalization into DCs, antigens are processed and peptide fragments are presented on major histocompatibility complex (MHC) molecules to T cells. DCs may also shape T cell responses by inducing CD4⁺ T cell differentiation into Th1, Th2, or Th17 cells. To analyze whether the differential DC targeting capability of the OVA glycoconjugates also impacted subsequent T cell activation, a DCs/T cells co-cultivation assay was performed. To this end, CD11c⁺ splenic DCs were pulsed with OVA alone and OVA-based neoglycoconjugates (**OVA-27(3)**, **OVA-27(5)**, **OVA-28(3)**, **OVA-28(5)**) to be then incubated with purified CD4⁺ T cells from OT-II transgenic mice.

Incubation of T cells with the pulsed DCs took place for 72h. At time points 48h and 72h, supernatants were collected to stain the cells with anti-CD16/32 and fluorescently labeled monoclonal antibodies against CD69 and CD4. As a read-out, the expression of the early T cell activation marker (CD69⁺) was measured by flow cytometry.

5. Synthesis of phosphorylcholine-containing OVA-glycoconjugates for DCs' targeting

After 48h and 72h only a low number of cells expressed CD69 on their surface following stimulation with either the OVA alone or OVA-based glycoconjugates. No differences related to the PC-content or sugar density (3 or 5 copies) were observed.

In [Figure 5.8](#), a representative example of flow cytometry read-out about DCs/T cells co-cultivation of **OVA-27(5)** and **OVA-28(5)** is reported.

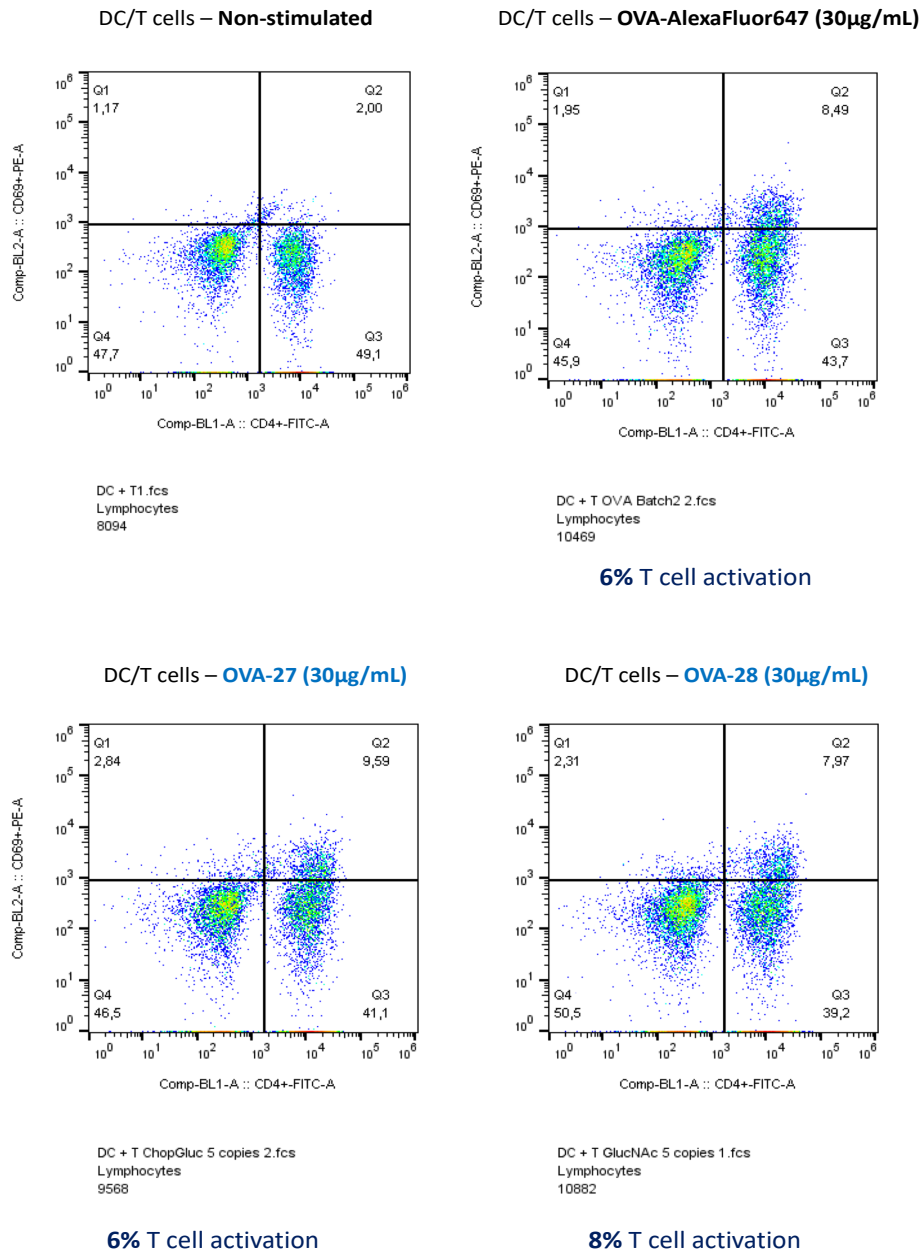


Figure 5.8 Labeled naïve OT-II CD4+ T cells stimulated with OVA alone and glycoconjugates **OVA-27(5)**, **OVA-28 (5)** stained for CD69 and CD4 and analyzed by flow cytometry.

5.4.3 Enzyme-Linked Immunosorbent Assay (ELISA)

Besides the evaluation of CD69 expression after 48h and 72h, the production of effector cytokines from activated T cells, namely, interferon gamma (IFN- γ) and interleukin-2 (IL-2) was measured by ELISA. IFN- γ is an effector cytokine mainly produced by Th1 cells¹⁷⁰ while IL-2 is produced by activated OT-II CD4⁺ T cells and triggers also T cell proliferation.¹⁷¹

In general, OVA-glycoconjugates led to higher IFN- γ production compared to OVA-alone (**Figure 5.9a**); a modest effect related to the PC-content was observed only for **OVA-27(3)** and **OVA-28(3)** in 48h DCs-T cells co-cultivation.

Regarding Interleukin-2 production (**Figure 5.9b**), a significant suppression of cytokine level was observed mainly for PC-containing construct **OVA-27(3)** after 72h of activation.

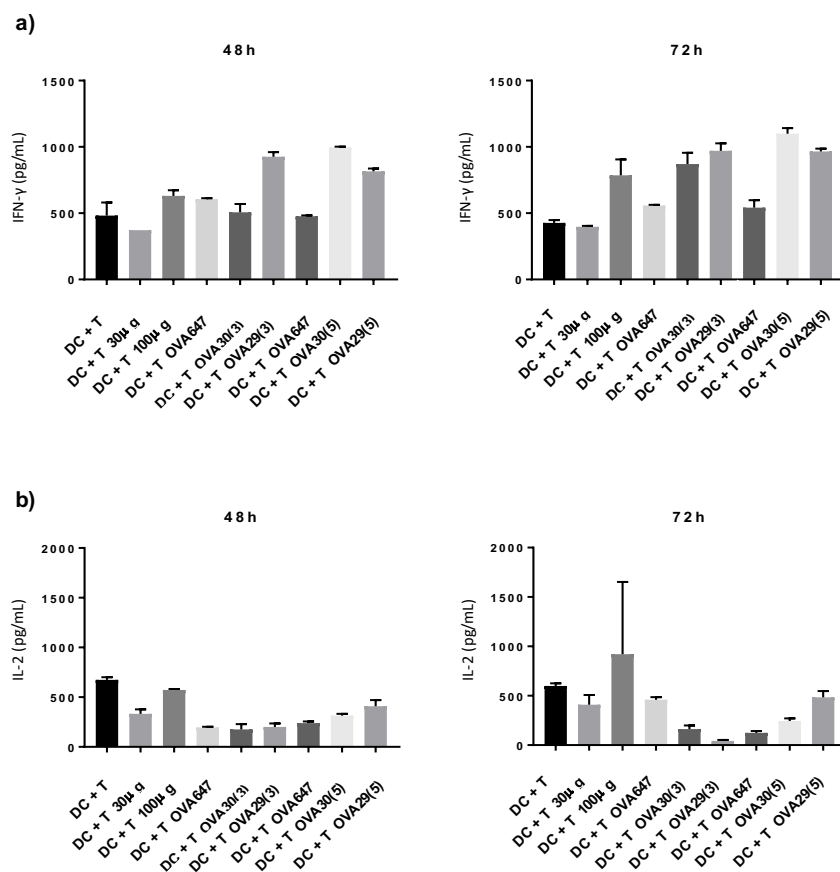


Figure 5.9 Cytokines production by OT-II CD4⁺ T cells in co-culture with CD11c⁺ DCs pulsed with OVA, OVA-27(3), OVA-27(5), OVA-28(3), OVA-28(5). (a) Interferon- γ (IFN- γ) production after 48 h and 72 h; (b) Interleukin-2 (IL-2) production after 48 h and 72 h.

5.5 Conclusion

In this work a general procedure for the synthesis of 6-O-PC-D-glucosamine (**13**) and more complex structures bearing terminal 6-O-PC-D-glucosamine were developed. By further optimization of well-established bio-conjugation protocol via NHS-activation,¹⁶⁸ OVA-based glycoproteins of 6-O-PC-D-glucosamine (**13**) and D-glucosamine (**14**), with different sugar content, were prepared and tested in DCs uptake and DCs-T cells co-cultivation assays.

Encompassing synthetic issues related to the formation of cross-linked OVA species, when large excess of activated reagent was used, a maximum of 5 sugar copies were attached on OVA-surface for both sugars (**13**) and (**14**).

As emerged from the biological assays, neither the presence of PC-moiety in glycoconjugates nor a high number of sugar copies on OVA-surface contributed to enhance internalization in DCs or to impact T cells activation.

Unremarkable results were also achieved in ELISA measurements of production of effector cytokines like INF- γ and IL-2. Although OVA-glycoconjugates led a general stimulation of INF- γ cytokines and suppression of IL-2 production, no significant differences related to PC-content were observed.

Although from the work carried out in this chapter arises that Phosphorylcholine (PC) moiety does not give any improvement to the sugar properties, it is still worth exploring the role of construct **OVA-27** in different immunological experiments and/or by using alternative cell models. Moreover, the synthesis of more complex PC-containing carbohydrates could contribute to largely explore the role of this functional groups in the immune system.

However, even though constructs **OVA-27** and **OVA-28** did not give very remarkable biological results, the experiments performed with the by-products **cross-linked OVA (OVA-27(CL) and OVA-28(CL))** were very interesting and could give important hints for future advances.

In fact, these big-size conjugates (>250KDa) showed a surprising more drastic DCs internalization than OVA alone compared to OVA-glycoconjugates. These results suggested how the size of constructs plays an important role in DCs uptake and that the bigger is the construct shape, the higher is the percentage of internalization in DCs.

5. Synthesis of phosphorylcholine-containing OVA-glycoconjugates for DCs' targeting

Perhaps, the unremarkable results achieved for **OVA-27** glycoconjugates could be given by the fact that only few copies of a small sugar are attached on a large carrier like Ovalbumin; therefore, the synthesized neoglycoproteins appear as multivalent constructs with a low-density presentation of ligands. As results the sugar copies are too far each other to provide multivalent interactions with receptors presented on dendritic cells and thus promote internalization.

On the base of these results, future improvement in DCs targeting could be achieved by increasing the size as well as the ligand density of the multivalent constructs; the synthesis of multivalent systems characterized to a proper carrier with attached several copies of PC-containing OVA-glycoconjugates can be a valuable starting point for future work.

References

156. W. Harnett and M. M. Harnett, *Immunol. Today*, 1999, **20**, 125–129.
157. M. Wuhrer, S. Rickhoff, R. D. Dennis, P. T. Soboslay, S. Baumeister and R. Geyer, *Biochem. J.*, 2000, **348**, 417–423.
158. K.M. Houston, W. Harnett, *Trends Glycosci. Glycotechnol.*, 1999, **11**, 43-52.
159. W. Harnett, I. B. McInnes and M. M. Harnett, *Immunol. Lett.*, 2004, **94**, 27–33.
160. W. Harnett, M. M. Harnett, *Trends Parasitol.*, 2006, **22**, 105–110.
161. J. Grabitzki and G. Lochnit, *Mol. Immunol.*, 2009, **47**, 149–163.
162. M. Whelan, M. M. Harnett, K. M. Houston, V. Patel, W. Harnett, K. P. Rigley, *J Immunol.*, 2000, **164**, 6453–60.
163. W. Harnett W, M. M. Harnett, *J Immunol*, 1993, **151**, 4829–4837.
164. S. Bay, V. Huteau, M. L. Zarantonelli, R. Pires, J. Ughetto-Monfrin, M. K. Taha, P. England, P. Lafaye, *J. of Med. Chem.*, 2004, **47**, 3916-3019.
165. I. Yakovlev, J. D. Timothy, *J. Am. Chem. Soc.*, 2015, **137**, 4078-4081.
166. P. E. Stein, A. G. W. Leslie, J. T. Finch and R. W. Carrell, *J. Mol. Biol.*, 1991, **221**, 941–959.
167. (a) L. McReynolds, et al, *Nature*, 1978, **273**, 723-728. (b) T. Tai, et al, *J. Biol. Chem.*, 1977, **252**, 6687-6694.
168. K. Brzezicka, U. Vogel, S. Serna, T. Johannssen, B. Lepenies and N. C. Reichardt, *ACS Chem. Biol.*, 2016, **11**, 2347–2356.
169. J. M. Robertson, P. E. Jensen, and B. D. Evavold, *J. Immunol.*, 2000, **164**, 4706-4712.
170. R. V. Luckheeram, R. Zhou, A. D. Verma, B. Xia, B. *Clinical and Developmental Immunology*. 2012, **2012**, ID 925135.
171. R. Spolski and W. J. Leonard, *Annu. Rev. Immunol.*, 2008, **26**, 57–79.

6. Experimental Part

6. Experimental part

General Methods

Chemicals were purchased from Sigma-Aldrich or Acros Organics and were used without further purification. Solvents employed were of HPLC quality. Nuclear Magnetic Resonance experiments were acquired on a Bruker 500 MHz spectrometer and chemical shifts (δ) are given in ppm relative to the residual signal of the solvent used (CDCl_3 7.26 ppm for $^1\text{H-NMR}$, 77.00 ppm for $^{13}\text{C-NMR}$). MALDI-ToF mass analysis were performed on an Ultraflextreme III time-of-flight mass spectrometer equipped with a pulsed Nd:YAG laser (355 nm) and controlled by FlexControl 3.3 and FlexImaging 2.1 softwares (Bruker Daltonics, Bremen, Germany). The acquisitions (total of 2000-3000) were carried out in positive reflector ion mode with pulse duration of 50 ns, laser fluence of 40 % and laser frequency of 500 Hz. Laser intensity was set marginally above the threshold of ionization to avoid fragmentation (less than 10 % for all the cases). All the peaks were detected as sodium adducts with high intensity signal (> 1000 U.A). The m/z range was chosen according to the mass of the sample. The acquired data was processed (baseline subtraction and normalized) using the Bruker software FlexAnalysis 3.3. MALDI-ToF/ToF analysis was performed in positive ionization mode with a LIFT cell voltage of 18.9 kV and a final acceleration voltage set at 29.3 kV. The parent mass ion was assigned manually (monoisotopic peak). The MS/MS spectra were acquired from 2000-3000 laser shots. High resolution mass measurements were carried out using the calibration standards of similar mass (Lamivudine m/z 230.0594, Leucine-enkephalin m/z 556.2766, des-Arg- Bradykinin m/z 904.4681, Angiotensin, m/z 1296.6853 and Glu-Fibrinopeptide B m/z 1570.6774) to achieve high mass accuracy. Contact angle measurements were performed at room temperature using DSA 100 contact angle meter (Krüss). Microarrays were printed employing a robotic piezoelectric SciFLEXARRAYER spotter S11 (Scienion, Berlin, Germany). Indium tin oxide (ITO) coated slides (75 mm x 25 mm) were obtained from Hudson Surface Technology, Inc. (Fort Lee, NJ). The slides have a nominal transmittance of >78 % and an ITO thickness of 130 nm. Modified surfaces were stored under vacuum conditions until its use. Plant lectins were purchased from Vector Laboratories and Sigma Aldrich while human lectins from institut de Biologie Structurale-Grenoble. All proteins were labeled with Alexafluor-647, Alexafluor-555 and Cy3 from Thermo Fisher Scientific according to the manufacturer's instructions. Enzymatic reactions and lectin incubations were performed

using the Hybridization gasket slide kit® from Agilent and 16-well Proplate module/6x7 mm from EMS ProSciTech. Fluorescence measurements were performed in an Agilent G265BA microarray scanner system (Agilent Technologies, Santa Clara, USA). Quantification was performed with ProScanArray® Express software (Perkin Elmer, Shelton, USA).

6.1 Preparation of NHS-activated hydrophobic ITO-coated glass slides

6.1.1 Modification of commercially available ITO-glass slides by phosphonate-based hydrophobic monolayer^{94,95}

The commercial ITO-coated glass slide (Type I, 1.1mm/25ea) was placed in a piranha solution (70 mL of water, 10 mL of NH₃, 10 mL of H₂O₂) at 70°C for 1 hour, washed with nanowater and dried with steam of air. Subsequently, it was incubated in 1mM solution of octadecylphosphonic acid (ODPA) in THF at room temperature for 3 hours and then left at 140°C for 20 hours. Finally, it was sonicated in methanol for 10 minutes, left in the same solvent for further 30 minutes without sonication, dried with steam of air and kept under high vacuum until use.

6.1.2 NHS-activation of hydrophobic ITO-glass slide

The hydrophobic ITO-slide, after previous washing in acetone, was placed in *vibrational vaporization machine (IMAGEPrep©)* where the NHS-activated linker **2** solution (15 mg/mL in 20mL CHCl₃:MeOH 1:1) was sprayed for 3 min; after that, the slide was dried under steam of air and the procedure was repeated one more time. Finally, the slide was sonicated in nanowater for 5 min and dried with steam of air.

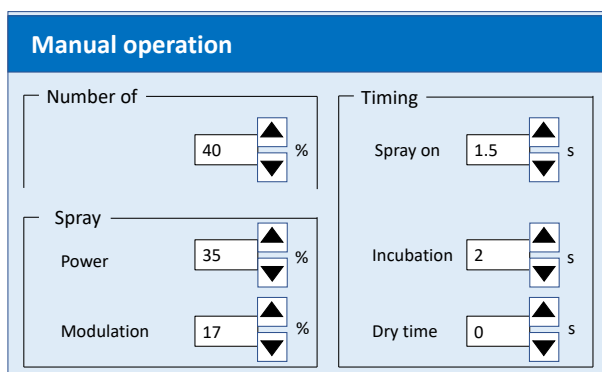
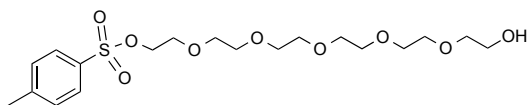


Figure 6.1 Set up conditions in *IMAGEPrep©* machine for the preparation of NHS-activated hydrophobic ITO glass slides.

6.2 Synthesis of NHS-activated linker (2)^{95c}

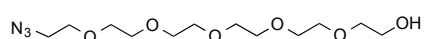
6.2.1 Preparation of *O*-(*p*-tolylsulfonyl)hexaethylene glycol (5)¹⁷²



To a cooled (0°C) solution of hexaethylene glycol (**4**) (2 g, 7.09 mmol) in CH₂Cl₂ (68 mL), silver oxide (1.5 eq, 2.46 g, 10.6 mmol), 4-toluenesulfonyl chloride (1.1 eq, 1.49 g, 7.80 mmol) and lithium iodide (0.2 eq, 190 mg, 1.42 mmol) were added; the solution was stirred at 0°C for 30 minutes. After this time, the reaction solution was filtered on a pad of celite by CH₂Cl₂ and concentrated under reduced pressure. The crude was purified by flash column chromatography (DCM:MeOH 100-98:2) to give the product as an oil (2.13 g, 69%).

¹H NMR (500 MHz, Chloroform-d) δ 7.76 (d, *J* = 8.0 Hz, 2H), 7.31 (d, *J* = 8.0 Hz, 2H), 4.12 (t, *J* = 4.8 Hz, 2H), 3.69 – 3.54 (m, 22H), 3.01 (bs, 1H), 2.41 (s, 3H).
¹³C NMR (126 MHz, Chloroform-d) δ 144.84, 133.02, 129.87, 128.00, 72.62, 72.57, 70.73, 70.61, 70.56, 70.53, 70.49, 70.49, 70.43, 70.36, 70.31, 70.19, 69.32, 68.69, 61.66, 21.67. HRMS (MALDI-TOF) *m/z* calculated for C₁₉H₃₂NaO₉S 459.1663, found 459.1693.

6.2.2 Preparation of azidoethyl hexaethylene glycol (6)¹⁷³



To a stirred solution of (**5**) (2.13 g, 4.89 mmol) in DMF (21 mL), sodium azide (4eq, 1.27 g, 19.5 mmol) was added; the solution was stirred overnight at 50°C. After that, the reaction solution was diluted with DCM and washed with a saturated solution of ammonium chloride and water; the crude was dried over Na₂SO₄, filtered and concentrated under reduced pressure. The product (1.33 g, 90%) was used for the next step without purification.

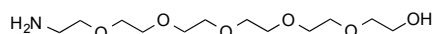
¹H NMR (500 MHz, Chloroform-d) δ 3.69 (t, *J* = 4.8 Hz, 2H), 3.66-3.61 (m, 20H), 3.58 (t, *J* = 4.8 Hz, 2H), 3.36 (t, *J* = 5.1 Hz, 2H), 2.91 (bs, 1H).

172. A. Bouzide, G. Sauve, *Org. Lett.*, 2002, **4**, 8781–8783.

173. H. A. Chokhawala et al, *ACS Chem. Biol.*, 2008, **3**(9), 567-576.

^{13}C NMR (126 MHz, Chloroform-*d*) δ 72.67, 70.71, 70.68, 70.66, 70.61, 70.57, 70.34, 70.08, 61.75, 50.74. HRMS (MALDI-TOF) m/z calculated for $\text{C}_{12}\text{H}_{25}\text{N}_3\text{NaO}_6$ 330.1640, found 330.1613.

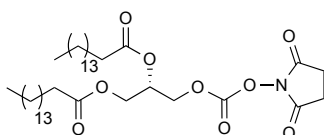
6.2.3 Preparation of aminoethyl hexaethylene glycol (**7**)¹⁷⁴



To a stirred mixture of **6** (1.33 g, 4.40 mmol) in dry CH_3OH (13 mL) and Pd/C (10% w/w, 133 mg), triethylsilane (10 eq, 7 mL, 44 mmol) was added dropwise under steam of Argon. The reaction was stirred at room temperature for 5 minutes. After this time, the reaction solution was filtered on a pad of celite by CH_2Cl_2 and concentrated under reduced pressure. The crude was purified by flash column chromatography (DCM: MeOH 80:20, 1% TEA) to give the product as an oil (757 mg, 61%).

^1H NMR (500 MHz, Chloroform-*d*) δ 3.72 (t, $J = 4.8$ Hz, 2H), 3.69 – 3.63 (m, 16H), 3.60 (t, $J = 4.8$ Hz, 2H), 3.54 (t, $J = 5.1$ Hz, 2H), 2.89 (t, $J = 5.1$ Hz, 2H). ^{13}C NMR (126 MHz, Chloroform-*d*) δ 73.00, 72.80, 70.96, 70.92, 70.87, 70.82, 70.67, 70.57, 70.24, 61.56, 41.65. HRMS (MALDI-TOF) m/z calculated for $\text{C}_{12}\text{H}_{27}\text{NO}_6\text{Na}$ 304.1735, found 304.1741.

6.2.4 Preparation of N-hydroxysuccinimidyl 1,2-dipalmitoyl-sn-glycerol (**3**)^{95c}



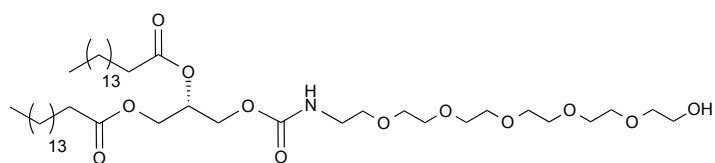
To a cooled (0°C) solution of 1,2-dipalmitoyl-*sn*-glycerol (500 mg, 1.03 mmol) in CH_2Cl_2 (300 mL), disuccinimidyl carbonate (DSC) (1.8 g, 7 mmol) and triethylamine (2.37 mL, 17 mmol) were added. The solution was stirred at room temperature for 16 hours. The organic layer was washed with water, dried over Na_2SO_4 , filtered and concentrated under reduced pressure. The crude was purified by flash column chromatography (Hexane:EtOAc 35:15) to give the compound **3** as a white solid (646 mg, 80%).

174. P. K. Mandal, J. S. McMurray, *J. Org. Chem.*, 2007, **72**, 6599–6601.

^1H NMR (500 MHz, Chloroform- d) δ 5.30 – 5.26 (m, 1H), 4.51 – 4.46 (dd, J = 12, 3.8 Hz, 2H), 4.44 – 4.39 (dd, J = 12, 5.8 Hz, 2H), 4.34 – 4.29 (dd, J = 12, 4.7 Hz, 2H), 4.18 – 4.12 (dd, J = 12, 5.8 Hz, 2H), 2.81 (s, 4H), 2.34-2.28 (m, 4H), 1.64 – 1.54 (m, 4H), 1.28-1.23 (m, 52H), 0.85 (t, J = 6.9 Hz, 6H).

^{13}C NMR (126 MHz, Chloroform- d) δ 173.18, 172.85, 168.49, 151.48, 68.69, 68.15, 61.50, 34.07, 34.03, 31.99, 29.77, 29.73, 29.70, 29.64, 29.55, 29.44, 29.34, 29.20, 29.18, 29.12, 25.52, 24.90, 24.82, 22.76, 14.18. HRMS (MALDI-TOF) m/z calculated for $\text{C}_{40}\text{H}_{71}\text{NO}_9\text{Na}$ 732.5025, found 732.5058.

6.2.4 Preparation of aminoethyl hexaethylene glycol 1,2- dipalmitoyl-*sn*-glycerol (8)

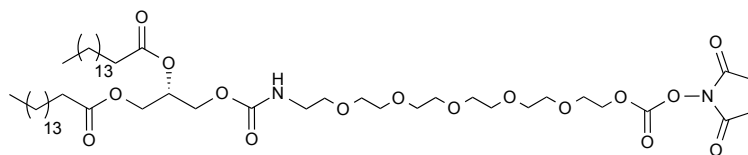


To a stirred solution of **3** (646 mg, 0.91 mmol) and **7** (307 mg, 1.1 mmol) in dry DCM (25 mL), DIPEA (196 μL , 1.1 mmol) was added dropwise under steam of Argon. The solution was stirred for 2 h at room temperature and then washed with a saturated solution of NH_4Cl . The crude was purified by flash chromatography (DCM:MeOH 99:1-98:2) to give the product as a white solid (637 mg, 80%).

^1H NMR (500 MHz, Chloroform- d) δ 5.25 – 5.23 (m, 1H), 4.32 – 4.12 (m, 4H), 3.75 – 3.70 (m, 2H), 3.69 – 3.60 (m, 18H), 3.56 – 3.54 (t, J = 5.4 Hz, 2H), 3.37 – 3.35 (m, J = 5.0 Hz, 2H), 2.33 – 2.28 (q, J = 7.6, 6.0 Hz, 4H), 1.66 – 1.54 (m, 4H), 1.31 – 1.25 (m, 48H), 0.89 – 0.86 (t, J = 6.9 Hz, 6H).

^{13}C NMR (126 MHz, Chloroform- d) δ 173.49, 173.07, 167.89, 72.81, 70.73, 70.69; 70.66, 70.61, 70.59, 70.34, 70.18, 69.39, 62.82, 62.37, 61.78, 41.10, 34.39, 34.22, 32.07, 30.51, 29.81, 29.78, 29.66, 29.50, 29.46, 29.43, 29.29, 29.25, 29.07, 25.04, 25.02, 23.13, 22.84, 14.23. HRMS (MALDI-TOF) m/z calculated for $\text{C}_{48}\text{H}_{93}\text{NNaO}_{12}$ 898.6594, found 898.6662.

6.2.6 Preparation of N-hydroxysuccinimidyl aminoethyl hexaethylene glycol 1,2-dipalmitoyl-sn-glycerol (**2**)¹⁷⁵



To a stirred solution of **8** (637 mg, 0.73 mmol) in dry dioxane (19.5 mL), disuccinimidyl carbonate (6 eq, 1.20 g, 4.68 mmol) and DMAP (6 eq, 570 mg, 4.4 mmol) in dry acetone (7.8 mL) were added under steam of Argon. The mixture was stirred at room temperature for 2 hours. After this time, the reaction solution was diluted with CH₂Cl₂, washed with water, dried over Na₂SO₄, filtered and concentrated under reduced pressure. The crude was dissolved in toluene and filtered; the filtrate was concentrated under reduced pressure to give the product as a white solid (quantitative yield, 748 mg).

¹H NMR (500 MHz, Chloroform-d) δ 5.45-5.43 (bs, 1H), 5.24 – 5.22 (m, 1H), 4.48 – 4.42 (m, 2H), 4.31 - 4.28 (dd, *J* = 12, 3.8 Hz, 2H), 4.25 - 4.22 (dd, *J* = 12, 4.5 Hz, 2H), 4.17 – 4.11 (m, 2H), 3.81 – 3.76 (m, 2H), 3.69 – 3.62 (m, 16H), 3.55 (t, *J* = 5.1 Hz, 2H), 3.37 – 3.34 (m, 2H), 2.83 (s, 4H), 2.34 – 2.28 (m, 4H), 1.31 – 1.25 (m, 52), 0.87 (d, *J* = 7.1 Hz, 6H).

¹³C NMR (126 MHz, Chloroform-d) δ 173.33, 172.92, 168.86, 155.99, 151.62, 70.77, 70.58, 70.50, 70.47, 70.45, 70.23, 69.91, 69.21, 68.30, 62.71, 62.20, 40.90, 34.20, 34.03, 31.90, 29.67, 29.64, 29.61, 29.54, 29.47, 29.40, 29.34, 29.28, 29.26, 29.10, 29.08, 25.42, 25.39, 24.85, 22.67, 14.10. HRMS (MALDI-TOF) *m/z* calculated for C₅₃H₉₆N₂NaO₁₆ 1039.6654, found 1039.6637.

6.3 On chip chemo-enzymatic synthesis of N-glycan mimetics

6.3.1 Immobilization of N-glycan structures (G1-G20) on the NHS-activated hydrophobic ITO-glass slide

Stock solution (50 μM in phosphate buffer 300 mM, pH 8.7) of synthetic C5-amino linked N-glycans (**G1** to **G20**)⁹⁸ were prepared in a 384 multi-well plate. By using *automated non-contact dispensing system of ultra-low volumes (sciFLEXARRAYER)*, 50 drops of

175. G. T. Hermanson, *Bioconjugate Tech.*, 2008, 936–960, ISBN 978-0-12-382239-0

each glycan solution were robotically printed, in a replicate of four spots, onto the NHS-activated hydrophobic-ITO slide and left to react overnight at 18°C under controlled humidity of 75%; After that, the slide was dried in oven at 40°C for 24 hours. Then, in order to quench the unreacted NHS-linker, the slide was placed 30 min in 50 mM ethanolamine solution (in 50 mM borate buffer pH 9.3) and dried under a steam of air. DHB matrix was spotted on the immobilized glycans and the effectiveness of the printing was checked by MALDI-TOF analysis; Mass spectra of immobilized substrates are reported in **Appendix**.

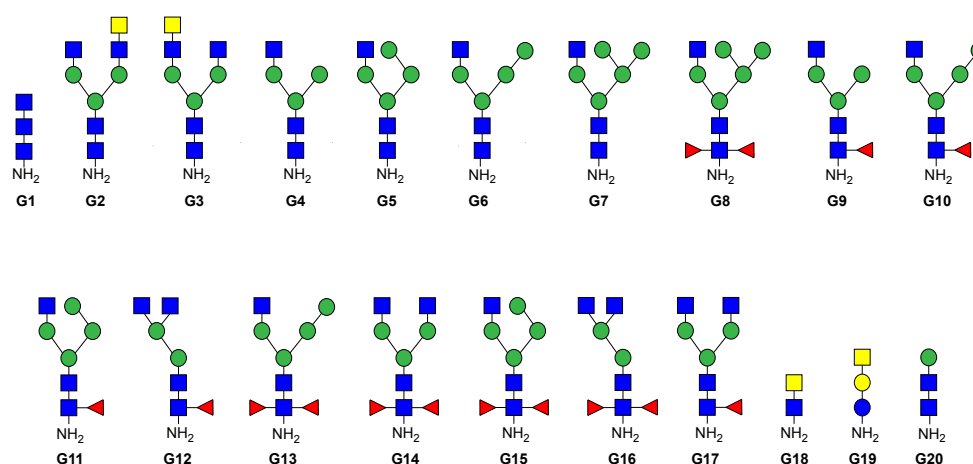


Figure 6.2 C5-amino linked N-glycan structures immobilized onto the NHS-activated ITO glass slide for the on-chip synthesis of glycomimetics library.

6.3.2 On-chip enzymatic elongations

A general on-chip enzymatic protocol has been adopted for the preparation of diversified N-glycan derivatives; DM-GalT1 together to UDP-GalNAz or GalNAc have been used for the preparation of (G1.1-G17.1) and (G.1.2-G17.2) respectively,^{176,177} while D-galactose derivatives (G1.3-G17.3) have been achieved by employing Sigma GalT-C3427 and UDP-Gal.¹⁷⁸

The enzymatic protocol consists to physically divide the slide in 8 subarrays by using *Hybridization gasket slide kit from Agilent (8 microarrays/slide format)* and incubate each subarray with 50 μ L of enzymatic solution containing: freshly prepared

176. B. Ramakrishnan, P. S. Shah and P. K. Qasba, *J. Biol. Chem.*, 2001, **276**, 37665–37671.

177. B. Ramakrishnan and P. K. Qasba, *J. Biol. Chem.*, 2002, **277**, 20833–20839.

178. P. K. Qasba, B. Ramakrishnan and E. Boeggeman, *Curr. Drug Targets*, 2008, **9**, 292–309.

HEPES 100 mM pH=7.4, 10 mM MnCl₂, 1mM UDP-donor, 0.5 mg/mL enzyme, 0.2% BSA, 0.5 μL alkaline phosphatase I U/μL.

The reaction was performed in 2 cycles of incubation at 37°C, 8 hours for each cycle; After each cycle of reaction, the slide was washed with aqueous solution containing 0.1%TFA and 0.05% AcCN. DHB matrix, containing 0.01 mM of sodium citrate, was spotted on the immobilized glycans and the conversion for each substrate was estimated by performing MALDI-TOF analysis ([Figure 3.17](#) and [Figure 3.19](#)). Mass spectra of neo-synthesized derivatives have been reported in **Appendix**.

6.3.2.1 Expression of double mutant of β1,4-galactosyltransferase I (C342T_Y289L) in *E.coli*¹³³

BL21 StarTM(DE3) *E. coli* cell line, containing the catalytic domain of double mutant of β-1,4-GalT gene, was seeded in Luria Bertani (LB) agar plates containing *kanamycin* (0.11 mg/mL) and incubated at 37°C overnight. A single colony was inoculated in 2mL of liquid LB containing 50 μg/mL of *kanamycin* and incubated, in appropriate incubation machine, overnight at 37°C (250 oscillation). The initial culture was diluted in 500 mL of liquid LB containing 50 μg/mL of *kanamycin* and bacterial growth was maintained at 37°C (250 oscillation) until cells reached the OD_{600nm} value of 0.6-0.7. At this point, protein expression was induced by the addition of 1mM of isopropyl β-D-1-thiogalactopyranoside (IPTG) and incubation at 37°C (250 oscillation) for further 4 hours.

After this time, the culture was collected in falcon tubes and centrifuged (4000 rpm, 4°C, 15 min) to collect the pellet; the latter was washed once with a solution containing Tris 50mM, NaCl 150 mM, pH=8.5 and then re-centrifuged. The pellet was then resuspended in 10 mL of lysis buffer (Tris 50 mM, NaCl 50 mM, 1% Triton x-100, 10 mM EDTA, PMSF 1mM, pH=8.5), sonicated by ultrasonicator (30 sec, 20 pulse, replaceable tip 3/4") and then centrifuged (4500 rpm, 4°C, 15 min); this process was performed for a total of three times followed by a last washing carried out in only water. The pellet was re-suspended in guanidine 5M until obtaining an absorbance (at 280 nm) around 1.9-2 and filtered in *CorningTM disposable vacuum filter* containing the folding buffer (Tris-HCl 50 mM pH=8.5, 10.56 mM NaCl, 0.44 mM KCl, 2.2 mM MgCl₂, 2.2 mM CaCl₂, 0.5M guanidineHCl, 8 mM cysteamine, 4 mM cystamine,

0.55M L-arginine). The volume of folding buffer used has to be 10 times the volume of guanidine solution used to dissolve the protein. The solution was storage 3 days at 4°C.

After the folding process, the solution was dialyzed by SnakeSkin™ dialysis tubing 10K MWCO against 2L of solution containing Tris-Cl 25 mM pH=6.5 and 150 mM NaCl at 4°C. The dialysis solution was refreshed twice every 3 hours and once after overnight at 4°C; the solution was then collected in falcon tubes and lyophilized. The enzyme was storage at 4°C until use.

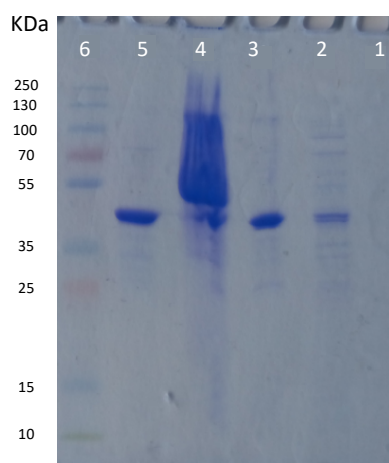


Figure 6.3 SDS-PAGE gel electrophoresis (10% acrylamide) stained with Coomassie Blue G-250; **(1)** Surnatant after IPTG induction **(2)** Surnatant of lysis buffer **(3)** Solution in guanidine **(4)** Pellet after lysis **(5)** After dialysis **(6)** Prestained Protein Ladder-Broad molecular weight (10-250 KDa).

6.3.3 Copper(I)-catalyzed Azide Alkyne Cycloaddition (CuAAC)⁸⁷

By using *16-well proplate® Module/6x7mm*, each array containing azido-N-glycans (**G1.1.-G17.1**) have been incubated with 100 µL of click solution containing: 0.058 mM CuSO₄, 0.29 mM THPTA, 0.58 mM alkyne in DMSO, bicarbonate buffer 300mM, pH=9 and 0.58 mM sodium ascorbate. After overnight incubation at RT, the slide was washed with water, dried with a steam of air and DHB matrix, containing 0.01 mM of sodium citrate, was spotted on each spot to quantify the reaction conversion by MALDI-TOF analysis. In [Table 6.1](#) all the conversions achieved by coupling the selected 19 alkynes on the immobilized azido-N-glycans (**G1.1.-G17.1**) have been described; Mass spectra of **232 novel glycomimetics** prepared after CuAAC have been reported in **Appendix**.

6. Experimental part

SM	a1	a2	a3	a4	a5	a6	a7	a10	a11	a12
G1.1	90%	92%	87%	83%	43%	51%	84%	59%	94%	81%
G2.1	93%	98%	89%	87%	64%	79%	84%	94%	99%	88%
G3.1	94%	88%	82%	96%	65%	90%	87%	96%	93%	98%
G4.1	85%	85%	89%	84%	74%	88%	73%	91%	91%	95%
G5.1	86%	90%	86%	96%	67%	87%	89%	98%	98%	64%
G6.1	88%	94%	76%	98%	49%	78%	91%	90%	95%	72%
G7.1	83%	96%	83%	89%	37%	78%	91%	93%	95%	99%
G8.1	84%	93%	84%	95%	55%	83%	89%	97%	92%	98%
G9.1	90%	87%	80%	97%	69%	81%	93%	97%	98%	97%
G10.1	83%	72%	78%	96%	45%	85%	87%	93%	94%	99%
G11.1	94%	88%	73%	94%	72%	82%	85%	98%	95%	66%
G12.1(1)	88%	93%	70%	93%	71%	87%	88%	75%	75%	84%
G12.1(2)	96%	95%	71%	98%	100%	93%	90%	88%	88%	97%
G13.1	81%	97%	61%	96%	62%	78%	73%	92%	92%	96%
G14.1(1)	68%	89%	72%	93%	58%	73%	89%	83%	91%	94%
G14.1(2)	75%	94%	80%	95%	68%	86%	95%	91%	83%	99%
G15.1	68%	72%	85%	94%	44%	70%	51%	96%	96%	98%
G16.1(1)	88%	94%	71%	84%	69%	81%	86%	94%	94%	97%
G16.1(2)	88%	96%	52%	96%	91%	91%	85%	84%	84%	98%
G17.1(1)	81%	86%	74%	96%	34%	64%	68%	97%	79%	93%
G17.1(2)	83%	93%	72%	91%	100%	85%	88%	96%	95%	96%

SM	a13	a14	a16	a17	a18	a20	a25	a26	a28
G1.1	98%	86%	82%	64%	65%	77%	95%	89%	88%
G2.1	98%	99%	99%	95%	48%	90%	67%	67%	99%
G3.1	96%	96%	87%	95%	61%	99%	66%	81%	98%
G4.1	91%	88%	98%	83%	78%	88%	87%	60%	98%
G5.1	96%	96%	99%	85%	33%	91%	92%	60%	98%
G6.1	96%	96%	94%	95%	26%	91%	92%	57%	89%
G7.1	94%	94%	96%	95%	58%	93%	91%	60%	97%
G8.1	92%	93%	96%	96%	79%	89%	85%	72%	98%
G9.1	97%	96%	98%	98%	69%	78%	94%	75%	98%
G10.1	94%	94%	97%	95%	61%	90%	94%	74%	96%
G11.1	98%	94%	89%	98%	91%	83%	94%	78%	91%
G12.1(1)	89%	76%	85%	98%	86%	86%	72%	60%	86%
G12.1(2)	95%	92%	95%	99%	89%	97%	98%	98%	99%
G13.1	93%	97%	85%	98%	65%	93%	95%	84%	97%
G14.1(1)	88%	84%	94%	96%	70%	84%	57%	80%	83%
G14.1(2)	92%	94%	94%	98%	71%	98%	94%	93%	94%
G15.1	80%	97%	96%	78%	63%	82%	33%	35%	94%
G16.1(1)	96%	75%	98%	77%	47%	80%	81%	72%	97%
G16.1(2)	96%	83%	97%	76%	66%	98%	97%	97%	87%
G17.1(1)	95%	96%	96%	94%	37%	65%	99%	48%	88%
G17.1(2)	95%	98%	99%	90%	69%	92%	95%	93%	97%

Table 6.1 CuAAC conversions calculated by MALDI-TOF analysis. (Gx.y(2) =bi-glycosylated product, Gx.y(1) =mono-glycosylated product).

6.4 On-chip binding assays of N-glycan mimetics library against fluorescently labeled lectins

The subarrays containing immobilized N-glycan mimetics have been incubated, by using *16-well proplate® Module/6x7mm*, with fluorescently labelled lectins (10 µg/mL) in binding buffer (Tris-HCl 100 mM, pH=7.5 with 2 mM CaCl₂, 2 mM MgCl₂, 0.2% BSA); The incubation has been left 1h in the dark at room temperature for WFA or 1h at 4°C for MGL and Langerin. Arrays were washed with water, dried and scanned with *Agilent G2565AA microarray scanner system* at 10 µm resolution.

Fluorescence images of glycomimetics arrays after incubation with fluorescently labelled lectins have been reported in **Appendix**.

6.5 Immobilization of Cyclooctyne-dendrons (d1-3) onto NHS-activated hydrophobic ITO-glass slide

The NHS-activated hydrophobic ITO-coated glass slide, prepared in according to the procedure described in the **Section 6.1**, was physically divided in subarrays by using *16-well proplate® Module/6x7mm* or *8-well proplate® Module/7x16mm* in **Section 4.1** and **4.4** respectively; each subarray was incubated with aqueous solution containing: 60 mM of phosphate buffer pH=7.8 and the desired cyclooctyne-dendron (**d1**, **d2** or **d3**). In **Section 4.13**, different concentrations of coating cyclooctyne-dendrons have been employed (5 µM, 10 µM, 20 µM, 30 µM) while, for all the other assays (**Section 4.2**, **Section 4.4.1**), a concentration of 5µM has been selected.

The reaction was left 2h at room temperature and washed with aqueous solution containing 0.1%TFA and 0.05% AcCN; after that, the unreacted NHS-surface was quenched with ethanolamine by 20 min incubation at room temperature.

Substrate	Theoretical m/z [M+Na] ⁺
NHS-linker	1049,3
d1	1456,5
d2	1954,2
d3	2951,7

Table 6.2. Theoretical ion [M+Na]⁺ mass peaks of NHS-linker and immobilized Cyclooctynes-dendrons (**d1-3**).

6.5.1 Surface characterization by contact angle (Θ)

After modifying the NHS-hydrophobic ITO-coated glass surface with cyclooctyne-dendrons, the contact angle was measured placing a droplet of water on the surface by *Drop Shape analyzer-DSA100*; by immobilization of cyclooctyne dendrons (**d1-3**) onto NHS-surface, no significant changes in term of surface hydrophobicity have been observed ($\Theta = 74^\circ$ - 84°).

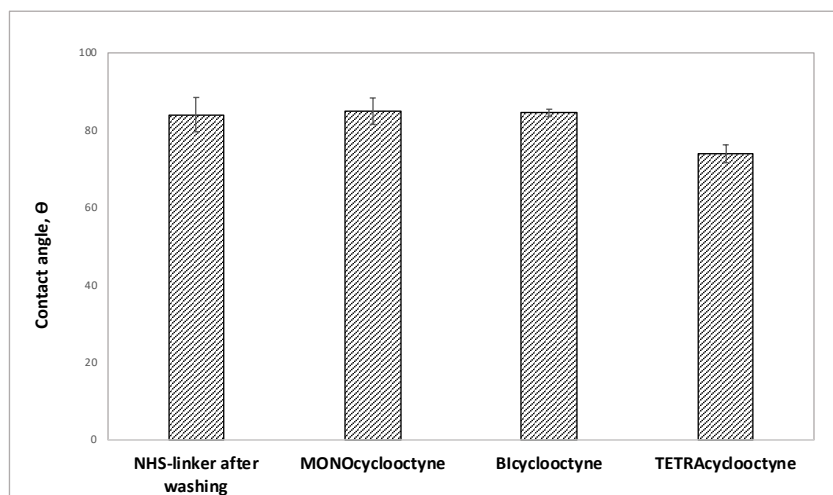


Figure 6.4 Comparison of contact angle values of hydrophobic ITO-glass surface before and after cyclooctynes immobilization.

6.6 On-chip SPAAC by using carbohydrate azides (**z1-4**)

The on-chip SPAAC was performed by robotic dispensing, via *automated non-contact dispensing system of ultra-low volumes (sciFLEXARRAYER)*, 5mM solution (10% DMSO in water) of azidoethyl glycosides (**z1-4**, 20 drops, 5.12 nL) on cyclooctyne surfaces (**d1-3**); for statistical studies, 8 copies for each carbohydrate azide were printed. The slide was placed 2h at 19°C under controlled humidity of 70% and then dried at 40°C for 16h; after that, it was washed with nanowater and dried under steam of air. DHB matrix, containing 0.01 mM of sodium citrate, was spotted on each spot to quantify reaction conversion by MALDI-TOF analysis. Almost complete conversion (>95%) has been achieved for all the employed azidoethyl glycosides (**z1-4**) on all the three cyclooctyne surfaces (**d1-3**). MALDI-TOF spectra have been reported in **Appendix**.

Substrate	Theoretical m/z [M+Na] ⁺	Percentage of conversion
d1.z1	1705,6	98%
d1.z2	1705,6	96%
d1.z3	1867,7	95%
d1.z4	1705,6	98%
d2.z1(1)	2203,3	1%
d2.z1(2)	2452,4	99%
d2.z2(1)	2203,3	2%
d2.z2(2)	2452,4	98%
d2.z3(1)	2365,7	3%
d2.z3(2)	2777,2	97%
d2.z4(1)	2203,3	2%
d2.z4(2)	2452,4	98%
d3.z1(1)	3200,8	nd
d3.z1(2)	3449,9	nd
d3.z1(3)	3699,0	5%
d3.z1(4)	3948,1	95%
d3.z2(1)	3200,8	nd
d3.z2(2)	3449,9	nd
d3.z2(3)	3699,0	4%
d3.z2(4)	3948,1	95%
d3.z3(1)	3362,9	nd
d3.z3(2)	3774,0	nd
d3.z3(3)	4185,2	3%
d3.z3(4)	4596,3	97%
d3.z4(1)	3200,8	nd
d3.z4(2)	3449,9	nd
d3.z4(3)	3699,0	3%
d3.z4(4)	3948,1	97%

Table 6.3 SPAAC conversion achieved on the three cyclooctyne-dendron surfaces (**d1-3**) with azidoethyl glycosides (**z1-4**). (dx.y(1) =mono-coupled product; dx.y(2) =bi- coupled product; dx.y(3) =tri- coupled product; dx.y(4) =tetra- coupled product; nd= not detected).

6.7 On-chip binding assays of glycodendrons with fluorescently labelled lectins (Section 4.2)

The subarrays containing glycodendrons have been incubated, by using *16-well proplate® Module/6x7mm*, with fluorescently labelled lectins in binding buffer (Tris-HCl 100 mM, pH=7.5 with 2 mM CaCl₂, 2 mM MgCl₂, 0.2% BSA); the incubation has been left 1h in the dark at room temperature for plant lectins as ConA, PSA, WFA or 1h at 4°C for human lectins as DC-SIGN, DC-SIGNR, Langerin and Dectin-2.

Arrays were washed with nanowater, dried and scanned with *Agilent G2565AA microarray scanner system* at 10 μm resolution.

6.8 On-chip SPAAC by using glycomimetics azides (z5-30)

For the preparation of glycomimetic dendrons, the same procedure reported in **Section 6.6** has been adopted with the only exception regarding the number of azides' copies printed on the surface; indeed, in this case, 5 copies of each azide have been spotted onto cyclooctyne surfaces.

Almost complete conversion (>95%) has been achieved for all the employed carbohydrate azides (**z5-30**) on all the three cyclooctyne surfaces (**d1-3**); MALDI-TOF spectra have been reported in **Appendix**.

Substrate	Theoretical m/z [M+Na] ⁺	Percentage of conversion	Substrate	Theoretical m/z [M+Na] ⁺	Percentage of conversion	Substrate	Theoretical m/z [M+Na] ⁺	Percentage of conversion
d1.z5	2129,8	99%	d2.z5(1)	2627,5	4%	d2.z18(1)	2495,5	2%
d1.z6	2185,8	99%	d2.z5(2)	3300,8	95%	d2.z18(2)	3036,7	93%
d1.z7	2097,8	99%	d2.z6(1)	2683,5	3%	d2.z19(1)	2741,6	1%
d1.z8	2071,8	98%	d2.z6(2)	3412,8	96%	d2.z19(2)	3528,9	98%
d1.z9	2165,8	99%	d2.z7(1)	2595,5	1%	d2.z20(1)	2553,5	1%
d1.z10	2165,8	99%	d2.z7(2)	3236,8	99%	d2.z20(2)	3152,9	99%
d1.z11	2189,9	100%	d2.z8(1)	2569,5	4%	d2.z21(1)	2401,4	1%
d1.z12	2213,8	99%	d2.z8(2)	3184,7	96%	d2.z21(2)	2848,6	99%
d1.z13	2213,8	99%	d2.z9(1)	2663,5	2%	d2.z22(1)	2611,5	1%
d1.z14	2219,8	99%	d2.z9(2)	3372,8	94%	d2.z22(2)	3268,8	96%
d1.z15	2029,8	98%	d2.z10(1)	2663,5	3%	d2.z23(1)	2695,5	1%
d1.z16	2101,8	99%	d2.z10(2)	3372,8	93%	d2.z23(2)	3436,7	99%
d1.z17	2029,8	96%	d2.z11(1)	2687,6	2%	d2.z24(1)	2657,5	nd
d1.z18	1997,8	99%	d2.z11(2)	3421,0	97%	d2.z24(2)	3360,9	100%
d1.z19	2243,9	100%	d2.z12(1)	2711,5	1%	d2.z25(1)	2511,5	1%
d1.z20	2055,8	99%	d2.z12(2)	3468,7	98%	d2.z25(2)	3068,7	98%
d1.z21	1903,7	98%	d2.z13(1)	2711,5	5%	d2.z26(1)	2553,5	1%
d1.z22	2113,8	99%	d2.z13(2)	3468,7	95%	d2.z26(2)	3152,7	99%
d1.z23	2197,8	98%	d2.z14(1)	2717,5	5%	d2.z27(1)	2451,4	1%
d1.z24	2159,8	98%	d2.z14(2)	3480,9	95%	d2.z27(2)	2948,5	99%
d1.z25	2013,8	94%	d2.z15(1)	2527,5	3%	d2.z28(1)	2537,5	nd
d1.z26	2055,8	99%	d2.z15(2)	3100,9	97%	d2.z28(2)	3120,9	98%
d1.z27	1953,7	99%	d2.z16(1)	2599,5	1%	d2.z29(1)	2667,5	nd
d1.z28	2039,8	100%	d2.z6(2)	3244,7	95%	d2.z29(2)	3380,8	99%
d1.z29	2169,8	100%	d2.z17(1)	2527,5	1%	d2.z30(1)	2639,5	8%
d1.z30	2141,8	98%	d2.z17(2)	3100,7	99%	d2.z30(2)	3324,7	92%

Table 6.4 SPAAC conversions achieved on the Mono- and Bi-valent cyclooctyne-dendrons surface (**d1-2**) with glycomimetic azides (**z5-30**).
(dx.y(1) =mono-coupled product; dx.y(2) =bi- coupled product)

Substrate	Theoretical m/z [M+Na] ⁺	Percentage of conversion	Substrate	Theoretical m/z [M+Na] ⁺	Percentage of conversion	Substrate	Theoretical m/z [M+Na] ⁺	Percentage of conversion
d3.z5(1)	3625	nd	d3.z14(1)	3715,03	nd	d3.z23(1)	3692,97	nd
d3.z5(2)	4298,3	nd	d3.z14(2)	4478,36	nd	d3.z23(2)	4434,24	nd
d3.z5(3)	4971,6	1%	d3.z14(3)	5241,69	nd	d3.z23(3)	5175,51	nd
d3.z5(4)	5644,9	98%	d3.z14(4)	6005,02	100%	d3.z23(4)	5916,78	100%
d3.z6(1)	3680,99	nd	d3.z15(1)	3525,04	nd	d3.z24(1)	3655,03	nd
d3.z6(2)	4410,28	1%	d3.z15(2)	4098,38	1%	d3.z24(2)	4358,36	1%
d3.z6(3)	5139,57	nd	d3.z15(3)	4671,72	nd	d3.z24(3)	5061,69	nd
d3.z6(4)	5868,86	98%	d3.z15(4)	5245,06	99%	d3.z24(4)	5765,02	99%
d3.z7(1)	3593,01	nd	d3.z16(1)	3596,96	nd	d3.z25(1)	3508,97	nd
d3.z7(2)	4234,32	1%	d3.z16(2)	4242,22	nd	d3.z25(2)	4066,24	1%
d3.z7(3)	4875,63	nd	d3.z16(3)	4887,48	nd	d3.z25(3)	4623,51	nd
d3.z7(4)	5516,94	99%	d3.z16(4)	5532,74	100%	d3.z25(4)	5180,78	99%
d3.z8(1)	3566,97	nd	d3.z17(1)	3524,96	nd	d3.z26(1)	3550,97	2%
d3.z8(2)	4182,24	1%	d3.z17(2)	4098,22	nd	d3.z26(2)	4150,24	nd
d3.z8(3)	4797,51	5%	d3.z17(3)	4671,48	nd	d3.z26(3)	4749,51	nd
d3.z8(4)	5412,78	94%	d3.z17(4)	5244,74	99%	d3.z26(4)	5348,78	98%
d3.z9(1)	3660,98	1%	d3.z18(1)	3492,97	nd	d3.z27(1)	3448,85	nd
d3.z9(2)	4370,26	nd	d3.z18(2)	4034,24	nd	d3.z27(2)	3946	nd
d3.z9(3)	5079,54	nd	d3.z18(3)	4575,51	2%	d3.z27(3)	4443,15	nd
d3.z9(4)	5788,82	99%	d3.z18(4)	5116,78	98%	d3.z27(4)	4940,3	100%
d3.z10(1)	3660,98	1%	d3.z19(1)	3739,07	nd	d3.z28(1)	3535,03	2%
d3.z10(2)	4370,26	1%	d3.z19(2)	4526,44	nd	d3.z28(2)	4118,36	nd
d3.z10(3)	5079,54	nd	d3.z19(3)	5313,81	nd	d3.z28(3)	4701,69	nd
d3.z10(4)	5788,82	98%	d3.z19(4)	6101,18	100%	d3.z28(4)	5285,02	100%
d3.z11(1)	3685,11	nd	d3.z20(1)	3551,03	nd	d3.z29(1)	3664,99	1%
d3.z11(2)	4418,52	nd	d3.z20(2)	4150,36	nd	d3.z29(2)	4378,28	2%
d3.z11(3)	5151,93	nd	d3.z20(3)	4749,69	nd	d3.z29(3)	5091,57	nd
d3.z11(4)	5885,34	100%	d3.z20(4)	5349,02	100%	d3.z29(4)	5804,86	97%
d3.z12(1)	3708,96	nd	d3.z21(1)	3398,89	1%	d3.z30(1)	3636,96	nd
d3.z12(2)	4466,22	nd	d3.z21(2)	3846,08	2%	d3.z30(2)	4322,22	nd
d3.z12(3)	5223,48	4%	d3.z21(3)	4293,27	nd	d3.z30(3)	5007,48	3%
d3.z12(4)	5980,74	96%	d3.z21(4)	4740,46	97%	d3.z30(4)	5692,74	97%
d3.z13(1)	3708,96	nd	d3.z22(1)	3609	nd			
d3.z13(2)	4466,22	1%	d3.z22(2)	4266,3	nd			
d3.z13(3)	5223,48	nd	d3.z22(3)	4923,6	nd			
d3.z13(4)	5980,74	99%	d3.z22(4)	5580,9	100%			

Table 6.5 SPAAC conversions achieved on the Tetracyclooctyne-dendrons surface (**3**) with glycomimetic azides (**z5-30**). (dx.y(1) =mono-coupled product; dx.y(2) =bi- coupled product; dx.y(3) =tri- coupled product; dx.y(4) =tetra- coupled product; nd = not detected)

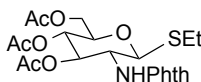
6.9 On-chip binding assays of glycomimetic dendrons with fluorescently labeled lectins (Section 4.4.2)

The subarrays containing dendrons have been incubated, by using *8-well proplate® Module/7x16mm*, with fluorescently labelled lectins in binding buffer (Tris-HCl 100mM, pH=7.5 with 2mM CaCl₂, 2mM MgCl₂, 0.2% BSA); the incubation has been left 1h in the dark at room temperature for AAL and ConA or overnight at 4°C for Langerin, Dectin-2, DC-SIGN and hMBL. Arrays were washed with nanowater, dried and scanned with *Agilent G2565AA microarray scanner system* at 10 μm resolution.

6.10 Preparation of OVA-based glycoconjugates

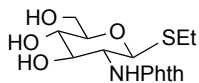
6.10.1 Synthesis of PC-containing glucopyranoside (13)

6.10.1.1 Synthesis of tioethyl 3,4,6-*O*-acetyl-2-phthalimido-β-D-glucopyranoside (16)

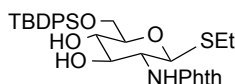


To a cooled (0°C) solution of **15** (559 mg, 1.25 mmol) in CH₂Cl₂ (3.8 mL), EtSOH (1.1 eq, 99 μL, 1.38 mmol) and BF₃OEt₂ (5eq, 0.78mL, 6.25 mmol) were added; the reaction was stirred overnight at room . After this time, the reaction solution was cooled (0°C) and quenched with saturated solution of NaHCO₃. The reaction mixture is further diluted with CH₂Cl₂, washed with a saturated solution of NaHCO₃ and Brine. The crude was purified by flash column chromatography (Hexane: EtOAc 5:1-1:1) to give the product as a white solid (420 mg, 70%).

¹H NMR (500 MHz, Chloroform-d) δ 7.88-7.84 (2H, m); 7.76 – 7.74 (2H, m); 5.85 – 5.81 (1H, dd, *J*= 10.3, 9.2 Hz, H-3); 5.50 – 5.48 (1H, d, *J*= 10.6 Hz, H-1); 5.20 – 5.16 (1H, dd, *J*= 10.2, 9.2 Hz H-4); 4.42 – 4.37 (1H, t, *J*= 10.5 Hz, H-4); 4.33 – 4.29 (1H, dd, *J*= 12.3, 4.9 Hz H-6a); 4.19 – 4.16 (1H, dd, *J*= 12.3, 2.3 Hz, H-6b); 3.99 – 3.88 (1H, m, H-5); 2.75 – 2.61 (2H, m, CH₂SEt), 2.11 (3H, s, CH₃OAc), 2.04 (3H, s, CH₃OAc), 1.86 (3H, s, CH₃OAc), 1.23 – 1.20 (3H, t, *J*= 7.4 Hz, CH₃SEt). ¹³C NMR (126 MHz, Chloroform-d) δ 170.88, 170.27, 169.64, 134.59, 131.76, 123.87, 81.35, 76.07, 71.70, 71.17, 69.03, 62.45, 53.82, 24.52, 20.93, 20.79, 20.61, 15.04. HRMS (MALDI-TOF) *m/z* calculated for C₂₂H₂₅NO₉SNa 502.1147, found 502.1097. [α]_D= +46.0 (CHCl₃).

6.10.1.2 Synthesis of tioethyl 2-phthalimido-6-tert-butylidiphenylsilyl-β-D-glucopyranoside (17)

To a cooled (0°C) solution of **16** (420 mg, 0.87 mmol) in MeOH (8.2 mL), NaOMe (0.3 eq, 14 mg, 0.26 mmol) was added. The reaction was stirred at room temperature for 1 hour. After that, *Amberlite H resin* was added until enrich pH=7 and the resulting mixture was filtrated on celite and concentrated under reduced pressure. The crude was used for the next step without purification step.

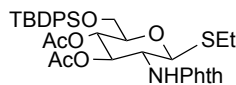
6.10.1.3 Synthesis of tioethyl 2-phthalimido-6-tert-butylidiphenylsilyl-β-D-glucopyranoside (18)

To a cooled (0°C) solution of **17** (420 mg, 0.87 mmol) and imidazole (2eq, 119 mg, 1.74 mmol) in DMF (5.9 mL), *tert*-butylidiphenylsilyl chloride (1.5 eq, 324 μL, 1.31 mmol) was added. The reaction was stirred overnight at room temperature. After that, the reaction was quenched with Et₂O, washed with HCl 1M solution and water. The crude was purified by flash column chromatography (Hexane:EtOAc

5:1-1:1) to give the product as a white solid (474 mg, 92%).

¹H NMR (500 MHz, Methanol-d₄) δ 7.92 – 7.78 (8H, m); 7.46 – 7.39 (6H, m); 5.34 (1H, d, *J*= 10.5 Hz, H-1); 4.32 – 4.28 (1H, dd, *J*= 10.5, 7.0 Hz, H-3); 4.12 – 4.04 (2H, m, H-2, H-6a); 3.97 – 3.93 (1H, dd, *J*= 5.0, 11.0 Hz, H-6b); 3.59 – 3.55 (2H, m, H-4, H-5); 2.77 – 2.60 (2H, m, CH₂SEt); 1.22 – 1.17 (3H, q, CH₃SEt); 1.08 (9H, s, CH₃tBu).
¹³C NMR (126 MHz, Methanol-d₄) δ 162.98, 162.74, 131.99, 131.89, 130.75, 130.67, 130.01, 129.86, 128.44, 128.19, 126.22, 126.19, 124.27, 120.20, 119.90, 80.71, 80.27, 72.46, 70.84, 63.87, 57.25, 28.34, 25.88, 21.48, 17.08. HRMS (MALDI-TOF) *m/z* calculated for C₃₂H₃₇NO₆SSiNa 614.2007, found 614.2016. [α]_D = -12.9 (CHCl₃).

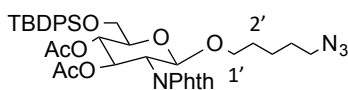
6.10.1.4 Synthesis of tioethyl 3,4-*O*-acetyl-2-phthalimido-6-*tert*-butyldiphenylsilyl- β -D-glucopyranoside (**19**)



To a solution of **18** (474 mg, 0.80 mmol) in Ac₂O (1.33 mL), pyridine (2.4 eq, 160 μ L, 1.92 mmol) was added. The reaction was stirred at room temperature for 1 hour. The reaction was diluted with EtOAc, washed with a saturated solution of NH₄Cl and water until pH=7. The product (497 mg, 92%) was used for the next step without purification step.

¹H NMR (500 MHz, Chloroform-d) δ 7.88 – 7.84 (2H, m, Phth); 7.75 – 7.68 (6H, m, Phth); 7.43 – 7.37 (6H, m, Ph); 5.85 – 5.81 (1H, dd, J = 10.3, 9.1 Hz, H-3); 5.48 – 5.46 (1H, d, J = 10.6 Hz, H-1); 5.25 – 5.21 (1H, m, H-4); 4.43 – 4.38 (1H, t, J = 10.4 Hz, H-2); 3.78 – 3.74 (3H, m, H-5, H-6); 2.78 – 2.61 (2H, m, CH₂SEt); 1.90 (3H, s, CH₃OAc); 1.86 (3H, s, CH₃OAc), 1.30 – 1.22 (4H, t, J = 7.5 Hz, CH₃SEt); 1.07 (9H, s, CH₃tBu). ¹³C NMR (126 MHz, Chloroform-d) δ 170.43, 169.46, 167.98, 167.40, 135.87, 135.77, 134.51, 134.36, 133.32, 133.22, 131.81, 131.37, 129.85, 127.84, 127.80, 123.82, 80.69, 79.02, 72.08, 69.27, 62.99, 53.95, 26.80, 24.00, 20.73, 20.67, 19.34, 15.16. HRMS (MALDI-TOF) m/z calculated for C₃₆H₄₁NO₈SSiNa 698.2218, found 698.2281. $[\alpha]_D^{25}$ = +60.5 (CHCl₃).

6.10.1.5 Synthesis of azidopentyl 3,4-*O*-acetyl-2-phthalimido-6-*tert*-butyldiphenylsilyl- β -D-glucopyranoside (**20**)

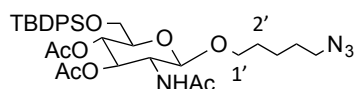


A mixture containing **19** (497 mg, 0.73 mmol), azidopentanol (1 eq, 94 mg, 0.73 mmol), NIS (1.5 eq, 246 mg, 1.1 mmol) and powdered 4 Å molecular sieves in dry CH₂Cl₂ (7.1 mL) was stirred at room temperature for 1 hour. After that, the reaction was cooled (0°C) and TfOH (0.3 eq, 19 μ L, 0.22 mmol) was added dropwise under steam of Argon. The reaction was left for 2 hours at room temperature, diluted with CH₂Cl₂ and filtered on a plug of celite. The solution was washed with a saturated solution of NH₄Cl and solid Na₂S₂O₄ was added until the organic phase become colorless. The crude was purified by

flash column chromatography (Hexane:EtOAc 5:1-4:2) to give the product as a white solid (401 mg, 74%).

^1H NMR (500 MHz, Chloroform- d) δ 7.82 – 7.74 (2H, m); 7.70 – 7.57 (6H, m); 7.40 – 7.26 (6H, m); 5.73 – 5.69 (1H, dd, J = 10.8, 9.0 Hz, H-3); 5.28 – 5.26 (1H, d, J = 8.4 Hz, H-1); 5.13 – 5.09 (1H, dd, J = 10.0, 9.0 Hz, H-4); 4.25 – 4.21 (1H, dd, J = 10.8, 8.4 Hz, H-2); 3.79 – 3.64 (4H, m, H-5, H-6a; H-6b, H-1'a); 3.39 – 3.36 (1H, m, H-1'b); 2.94 – 2.85 (2H, m, H-5'); 1.83 (3H, s, CH_3OAc); 1.78 (3H, s, CH_3OAc); 1.48 – 1.29 (4H, m, H-2'; H-4'); 1.13 – 1.10 (2H, m, H-3'); 0.99 (9H, s, CH_3tBu). ^{13}C NMR (126 MHz, Chloroform- d) δ 170.44, 169.45, 135.78, 135.66, 134.38, 133.36, 133.22, 131.49, 129.80, 127.79, 127.74, 123.81, 97.74, 74.78, 71.24, 69.50, 69.26, 62.97, 54.88, 51.17, 28.88, 28.39, 26.74, 23.18, 20.67, 20.59, 19.32. HRMS (MALDI-TOF) m/z calculated for $\text{C}_{39}\text{H}_{46}\text{N}_4\text{O}_9\text{SiNa}$ 765.2930, found 765.2940. $[\alpha]_D^{25}$ = +63.0 (CHCl_3).

6.10.1.6 Synthesis of azidopentyl 3,4-*O*-acetyl-2-*N*-acetyl-6-*tert*-butyldiphenylsilyl- β -D-glucopyranoside (22)

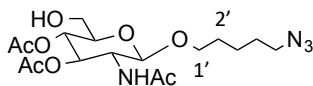


A solution of **20** (401 mg, 0.54 mmol) in *n*BuOH-Ethylendiamine (4:1, 15 mL) was heated at 120°C for 30 min in the microwave and then concentrated under reduced pressure by using EtOH/toluene mixture. After that, the crude was dissolved in 1 mL of Ac_2O and pyridine (2.4 eq, 160 μL , 1.3 mmol) was added. The reaction was stirred overnight at room temperature, diluted with EtOAc and washed with NH_4Cl and NaHCO_3 solutions. The crude was purified by flash column chromatography (Hexane: EtOAc 1:1) to give the product as a white solid (2 steps, 315 mg, 89%).

^1H NMR (500 MHz, Chloroform- d) δ 7.69 – 7.64 (5H, q); 7.42 – 7.35 (5H, m); 5.46 – 5.44 (1H, d, NH); 5.25 – 5.20 (1H, dd, J = 10.6, 9.3 Hz, H-3); 5.13 – 5.07 (1H, t, J = 9.6 Hz, H-4); 4.61 – 4.60 (1H, d, J = 8.3 Hz, H-1); 3.90 – 3.85 (2H, m, H-2, H-1'b); 3.76 – 3.70 (2H, m, H-6a; H-6b); 3.56 – 3.53 (1H, m, H-5); 3.50 – 3.46 (1H, m, H-1'a); 3.27 – 3.24 (2H, t, J = 6.8 Hz, H-5'); 2.02 (3H, s, CH_3); 1.95 (3H, s, CH_3OAc); 1.90 (3H, s, CH_3OAc); 1.64 – 1.57 (4H, m, H-2'; H-4'); 1.44 – 1.41 (2H, m, H-3'); 1.04 (9H, s, ^tBu). ^{13}C NMR (126 MHz, Chloroform- d) δ 166.06, 165.05, 164.26, 132.58, 132.47, 130.23, 130.18, 126.92, 125.01, 124.96, 99.44, 74.98, 73.25, 69.45, 63.71, 56.11, 52.92, 31.82, 31.39, 29.59, 26.49, 26.38, 24.02, 23.88, 22.47. HRMS

(MALDI-TOF) m/z calculated for $C_{33}H_{46}N_4O_8SiNa$ 677.2981, found 677.3008. $[\alpha]_D^{25} = +15.4$ ($CHCl_3$).

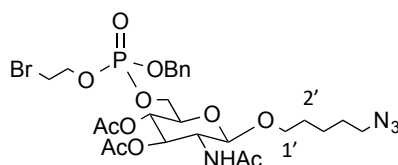
6.10.1.7 Synthesis of azidopentyl 3,4-*O*-acetyl-2-*N*-acetyl- β -D-glucopyranoside (**23**)



To a cooled ($0^\circ C$) solution of **22** (315 mg, 0.34 mmol) in dry THF (2.5 mL), TBAF (1.6 eq, 139 μL of 1M solution in THF) and AcOH (1.6 eq, 43 μL , 0.77 mmol) were added; the reaction was warmed until $60^\circ C$ and left overnight. After that, the solution was diluted with EtOAc, washed with NH_4Cl and water. The crude was purified by flash column chromatography (Hexane: EtOAc 1:2) to give the product as a white solid (140 mg, 70%).

1H NMR (500 MHz, Chloroform- d) δ 5.71 – 5.69 (1H, d, $J = 9.1$ Hz, NH); 5.10 – 5.06 (1H, dd, $J = 10.7$; 8.6 Hz, H-3); 4.55 – 4.53 (1H, d, $J = 8.4$ Hz, H-1); 4.50 – 4.46 (1H, dd, $J = 12.2$, 4.0 Hz, H-6a); 4.33 – 4.29 (1H, dd, $J = 12.2$, 2.1 Hz, H-6b); 3.89 – 3.83 (2H, m, H-2; H-1'a); 3.57 – 3.44 (3H, m, H-4, H-5, H-1'b); 3.30 – 3.23 (2H, t, H-5'); 2.12 (3H, s, CH_3); 2.11 (3H, s, CH_3OAc); 1.95 (3H, s, CH_3OAc); 1.65 – 1.54 (4H, m, H-2', H-4'); 1.45 – 1.36 (2H, m, H-3'). ^{13}C NMR (126 MHz, Chloroform- d) δ 172.04, 170.41, 101.17, 75.16, 74.18, 69.40, 68.97, 63.19, 54.44, 51.51, 29.83, 29.08, 28.66, 23.45, 23.30, 21.10, 21.03. HRMS (MALDI-TOF) m/z calculated for $C_{17}H_{28}N_4O_8Na$ 439.1804, found 439.1789.

6.10.1.8 Synthesis of *O*-((benzyloxy)(2-bromoethoxy)phosphoryl)-azidopentyl 3,4-*O*-acetyl-2-*N*-acetyl- β -D-glucopyranoside (**25**)

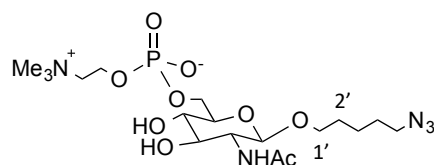


To a solution of **23** (140 mg, 0.48 mmol) in dry THF (2.8 mL), *N,N*-diisopropyl-benzyl-2-bromoethylphosphoramidite^{128,129} **24** (1.3 eq, 226 mg, 0.624 mmol) and 4% tetrazole in dry AcCN (3.7 mL) were added. After left the reaction stirring at room temperature for

2 hours, the mixture of reaction was cooled (0°C) and *t*-BuOOH (95 μ L) was added; the reaction was stirred 5 min at 0°C and 1 hour at room temperature. Subsequently, the *t*-BuOOH was quenched with saturated solution of Na₂SO₂O₄ and the mixture was further diluted with Et₂O and washed with 5% NaHCO₃. The crude was purified by flash column chromatography (Hexane: EtOAc 4:1) to give the product as a white solid (313 mg, 94%).

¹HNMR (500 MHz, Chloroform-*d*) δ 7.38 – 7.34 (5H, m); 5.68 – 5.64 (1H, t, NH); 5.36 – 5.32 (1H, m, H-3); 5.23 – 5.00 (2H, m, CH₂Bn); 4.70 – 4.64 (1H, d, *J*= 8.1 Hz, H-1); 4.49 – 4.36 (2H, m, H-4, H-6a); 4.30 – 4.10 (3H, m, H-6b; CH₂Br); 3.86 – 3.77 (2H, m, H-2, H-1'a); 3.71 – 3.64 (2H, t, H-5); 3.53 – 3.41 (2H, m, H-1'b, OCH₂); 3.39 – 3.34 (1H, t, *J*= 6.2 Hz, OCH₂OP); 3.27 – 3.21 (2H, t, *J*= 6.7 Hz, H-5'); 2.11 (3H, s, CH₃); 2.02 (3H, s, CH₃OAc); 1.95 (3H, s, CH₃OAc); 1.61 – 1.54 (4H, m, H-2', H-4'); 1.42 – 1.37 (2H, m, H-3'). ¹³C NMR (126 MHz, Chloroform-*d*) δ 171.35, 171.28, 170.79, 129.06, 128.94, 128.23, 100.75, 74.01, 73.99; 72.64, 72.38, 70.21, 69.53, 67.20, 62.31, 54.82, 51.45, 29.80, 29.43, 29.06, 28.61, 23.32, 21.11, 20.96, 20.85. HRMS (MALDI-TOF) *m/z* calculated for C₂₆H₃₈BrN₄O₁₁PNa 715.1354, found 715.1406. [α]_D = -11.7 (CHCl₃).

6.10.1.9 Synthesis of phosphatidylcholine azido-pentyl 2-N-acetyl- β -D-glucopyranoside (26)

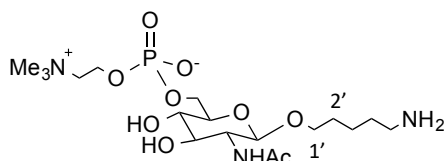


A solution of **25** (313 mg, 0.45 mmol) in 20% NMe₃/water (8.7 mL) was stirred overnight at 40°C. The solution was concentrated under reduced pressure and the crude was purified by flash column chromatography (DCM:MeOH 4:1) to give the product as a white solid (89 mg, 40%).

¹HNMR (500 MHz, Deuterium Oxide) δ 4.55 – 4.53 (1H, m, *J*= 8.1 Hz, H-1); 4.40 – 4.34 (2H, b, CH₂NMe₃); 3.99 – 3.87 (3H, m, H-3, H-1'a, H-6a); 3.82 – 3.78 (1H, dd, *J*= 12.9, 5.2 Hz, H-6b); 3.75 – 3.70 (2H, m, H-2, H-5); 3.68 – 3.64 (2H, m, OCH₂ OCH₂OP); 3.61 – 3.52 (1H, m, H-1'b) 3.56 – 3.53 (1H, t, H-4); 3.34 – 3.33 (2H, t, *J*= 6.9 Hz, H-5'); 3.21 (9H, s, CH₃NMe₃); 2.05 (3H, s, CH₃); 1.62 – 1.57 (4H, m, H-4', H-2'); 1.43 – 1.38

(2H, m, H-3'). ^{13}C NMR (126 MHz, Deuterium Oxide) δ 174.44, 101.05, 75.02, 74.33, 72.94, 70.24, 66.03, 60.44, 59.69, 56.69, 55.67, 54.01, 51.19, 27.62, 22.45, 22.09. HRMS (MALDI-TOF) m/z calculated for $\text{C}_{18}\text{H}_{36}\text{N}_5\text{O}_9\text{PH}$ 498.2328, found 498.2359. $[\alpha] = +1.8$ (DMSO).

6.10.1.10 Synthesis of phosphatidylcholine amino-pentyl 2-N-acetyl- β -D-glucopyranoside (13)



A solution of **26** (89 mg, 0.18 mmol) in 1% TFA/MeOH (11 mL) was passed through the hydrogenator *H-Cube* with a flow rate of 1 mL/min, at 50°C using full hydrogen conditions. The resulting mixture collected in 30 minutes was concentrated under reduced pressure and purified by graphite (water-water:MeOH 1:1) to give the product as a white solid with (84 mg, quantitative yield).

^1H NMR (500 MHz, Deuterium Oxide) δ 4.55 – 4.50 (1H, m, $J = 8.3$ Hz, H-1); 4.41 – 4.33 (2H, b, $\text{CH}_{2\text{NMe}_3}$); 4.01 – 3.86 (3H, m, H-3, H-1'a, H-6a); 3.82 – 3.78 (1H, dd, $J = 12.8, 5.2$ Hz, H-6b); 3.75 – 3.70 (2H, m, H-2, H-5); 3.67 – 3.60 (3H, m, $\text{OCH}_{2\text{OP}}$, H-1'b); 3.57 – 3.52 (1H, t, H-4); 3.21 (9H, s, $\text{CH}_{3\text{NMe}_3}$); 3.02 – 2.95 (2H, t, $J = 7.5$ Hz, H-5'); 2.04 (3H, s, CH_3); 1.70 – 1.58 (4H, m, H-4', H-2'); 1.43 – 1.37 (2H, m, H-3'). ^{13}C NMR (126 MHz, Deuterium Oxide) δ 174.46, 101.12, 75.03, 74.29, 72.89, 70.08, 65.99, 60.42, 59.69, 56.67, 55.67, 39.30, 28.04, 26.34, 22.08. HRMS (MALDI-TOF) m/z calculated for $\text{C}_{18}\text{H}_{18}\text{N}_3\text{O}_9\text{PH}$ 472.2423, found 472.2423. $[\alpha] = +2.88$ (DMSO).

6.10.2 Labelling of OVA (LPS free) with Alexafluor647

To 400 μL of OVA *LPS free* (10 mg/mL in NaHCO_3 100 mM, pH=9.1), 50 μL of Alexafluor647 (10 mg/mL in DMSO) purchased from *ThermoFisher* were added; the reaction was gently shaken 1h in the dark at room temperature. After that, the excess of Alexafluor647 has been removed by Amicon® Ultra-0.5mL Centrifugal filter 10KDa (3 cycles, 12000 rpm). The degree of labelling has been established by nanodrop measurement (DOL= 2.2).

6.10.3 Synthesis of OVA-29 (3)

Disuccinimidyl suberate (DSS) linker (3.9 mg, 10.6 μmol , 5 eq) was dissolved in 576 μL of DMSO and activated with 23 μL of triethylamine; to this mixture, a solution containing the compound **13** (1 mg, 2.12 μmol) in 436 μL of DMSO was added dropwise. The reaction was left stirring at room temperature for 2h. After this time, the product was extracted with 648 μL of NaHCO_3 (100 mM, pH 9.1), washed five times with chloroform (1,2 mL for each washing), and centrifuged at 3000 g to facilitate phase separation. Attachment of DSS linker to PC-glucosamine derivative **13** was confirmed by MALDI-TOF mass spectrometry.

The NHS-activated solution of **29** (70 eq) in NaHCO_3 was added to the 1.41 mg of OVA-Alexafluor647 and the reaction was left stirring overnight at RT. The sample was concentrated in a *Amicon® Ultra-0.5mL Centrifugal filter 10KDa* and dissolved in sterile PBS.

The above-described procedure, with proper adjusting related to the reagents molar ratio and buffer solutions ([Table 5.1](#)), has been adopted for the preparation of all the OVA-based glycoconjugates **OVA-29** and **OVA-30**.

6.11 Biological evaluation of OVA-based glycoconjugates

6.11.1 DCs cells uptake assays

Dendritic cells, after 9 days of differentiation on IMDM complete medium (10% FBS, 1% Pen/Strep, 1% L-Glu) + GM-CSF (10%), were seeded at a cell density of 2×10^4 cells/well into a 96-well plate in IMDM complete medium. After seeding, DCs were placed in an incubator (37 °C, 5% CO_2) for 30 min and after pulsed with 10 $\mu\text{g}/\text{mL}$ of each of the constructs per well: **OVA-Alexafluor647**, **OVA-29(3)**, **OVA-30(3)**, **OVA-29(5)**, **OVA-30 (5)**, **OVA-29(CL)** and **OVA-30(CL)**. After 10 min of incubation (37 °C, 5% CO_2), cells were carefully washed twice with cold PBS and subsequently stained with blocking antibody against CD16/32 (eBioscience, dilution 1:100) in 100 μL of FACS buffer (1x PBS, 2% FBS, 1mM EDTA) for 15 min at 4°C. After, monoclonal CD11c antibody (eBioscience, PE, 1:200) was used to stain DCs for 30 min at 4 °C in the dark. Cells were further washed two times with 200 μL of FACS buffer and finally suspended in 100 μL FACS buffer. Samples were analyzed using a *Attune NxT Flow Cytometer (ThermoFisher Scientific)*. Data were analyzed using *FlowJo Software (FlowJo, Ashland, OR, USA)*, where cells were first gated on live cells using the FSC/SSC

plot, then gated on single cells (FSC-H/FSC-A plot), followed by selection of CD11c⁺-PE cells population.

6.11.2 T-cells purification and DC-T cell co-cultivation

Dendritic cells, after 9 days of differentiation on IMDM complete medium (10% FBS, 1% Pen/Strep, 1% L-Glu) + GM-CSF (10%), were seeded at a cell density of 2×10^4 cells/well into a 96-well plate in IMDM complete medium. After seeding, DCs were placed in an incubator (37 °C, 5% CO₂) for 20 min and after stimulated with 30 µg/mL of each of the constructs per well: **OVA-Alexafluor647**, **OVA-29(3)**, **OVA-30 (3)**, **OVA-29(5)**, **OVA-30(5)**, **OVA-29(CL)** and **OVA-30(CL)**. Upon 2h of stimulation, purified T cells from OT-II mice were added to each well.

T cells from OT-II mice were isolated using a Pan T Cell Isolation Kit II (Miltenyi): non-targeted cells are magnetically labeled with a biotin-conjugated antibody cocktail (CD11b, CD11c, CD19, CD45R, CD49b, CD105, MHC-II and Ter-119) followed by an anti-biotin monoclonal antibodies conjugated to microbeads, thus resulting in the binding of these cells into the MACs column, while pure CD4⁺ T cells are collected in the flowthrough of the column.

Isolated T cells were centrifuged and suspended in IMDM complete medium and further seeded into the wells of the 96-well plate at a cell density of 1×10^5 cells/well. Incubation of T cells with the pulsed DCs took place for 72h. At time points 48h and 72h cells were stained for early T cell activation marker (CD69⁺). Moreover, T cell purity after MACs purification was also accessed by flow cytometry using an *Attune NxT Flow Cytometer* (*ThermoFisher Scientific*). Only isolated T cells that presented a purity $\geq 85\%$ of CD4⁺ and CD8⁺ T cells were used on the experiments. In addition, T cells unstimulated or stimulated with CD3/CD28 (5µg/ml) were used as a negative and positive control, respectively. Three independent experiments were done with technical triplicates each.

6.11.3 Detection of T cell activation markers by flow cytometry

The CD4⁺ T cells population was stained using a CD4-FITC monoclonal antibody (eBiosciences, 1:100) and early T cell activation marker using a monoclonal CD69-APC (eBiosciences, 1:200) antibody. After 48h and 72h of incubation, DCs and T cells were washed two times with FACs buffer and Fc receptors were blocked using anti-CD16/32 (eBioscience, dilution 1:100) in 100 µL of FACS buffer at 4 °C for 15 min. Subsequently,

cells were incubated with anti-CD4-FITC and anti-CD69 for 20 min at 4 °C in the dark. Cells were then centrifuged and washed 2 times with 200 µL of FACS buffer. Finally, cells were suspended in 100 µL of FACS buffer and analyzed by flow cytometer. Data were analyzed using *FlowJo Software (FlowJo, Ashland, OR, USA)*, where cells were first gated on live cells using the FSC/SSC plot, then gated on single cells (FSC-H/FSC-A plot), followed by selection of CD4⁺-FITC T cells population. In this population, CD69⁺-APC T cells were plotted.

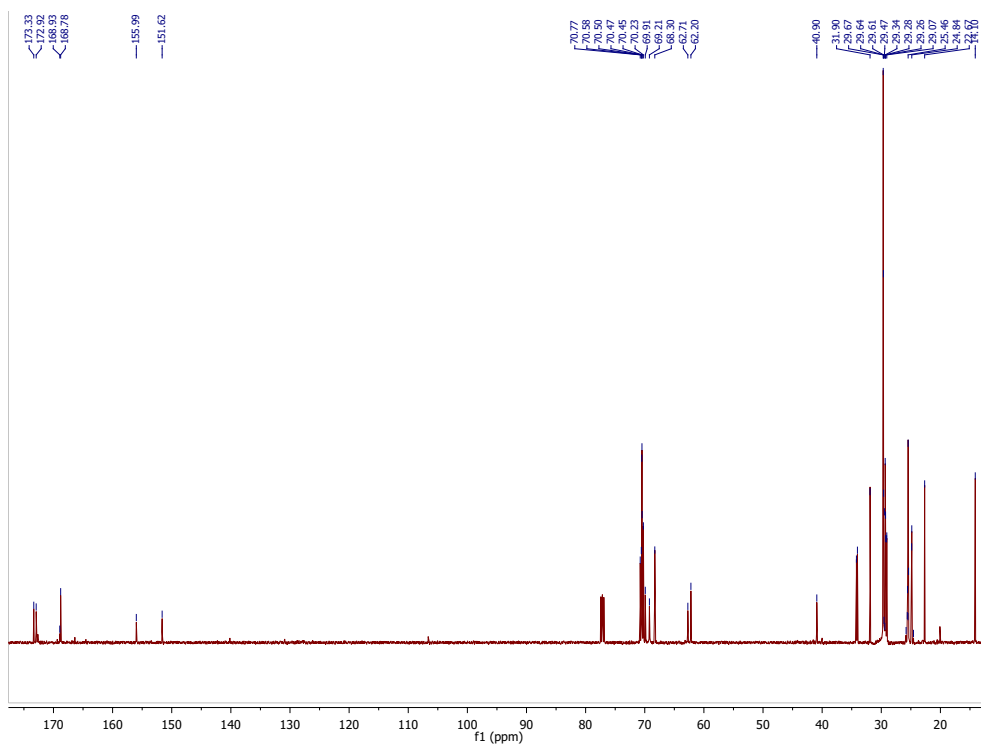
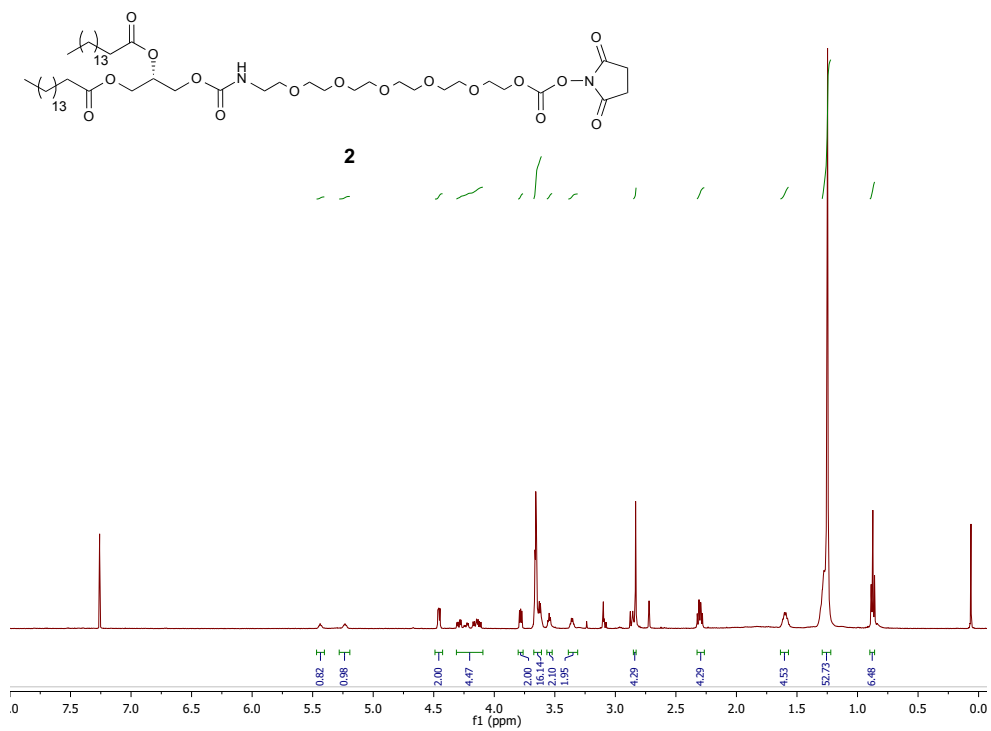
6.11.4 Enzyme-Linked Immunosorbend Assay (ELISA)

Supernatants collected after 48 and 72h of stimulation were analyzed for the cytokines IL-2 and IFN- γ according to the manufacturer's instructions (PeproTech). Plates were developed with a solution of ABTS (2,2'-azino-bis(3-ethylbenzothiazoline-6-sulphonic acid)). Absorbance was measured at 405 nm with a correction factor at 650 nm using a *Multiskan Go microplate spectrophotometer (ThermoFisher Scientific)*. Triplicates of each condition were performed.

7. Appendix

7. Appendix

7.1 N-hydroxysuccinimidyl aminoethyl hexaethylene glycol 1,2- dipalmitoyl-sn-glycerol (**2**):

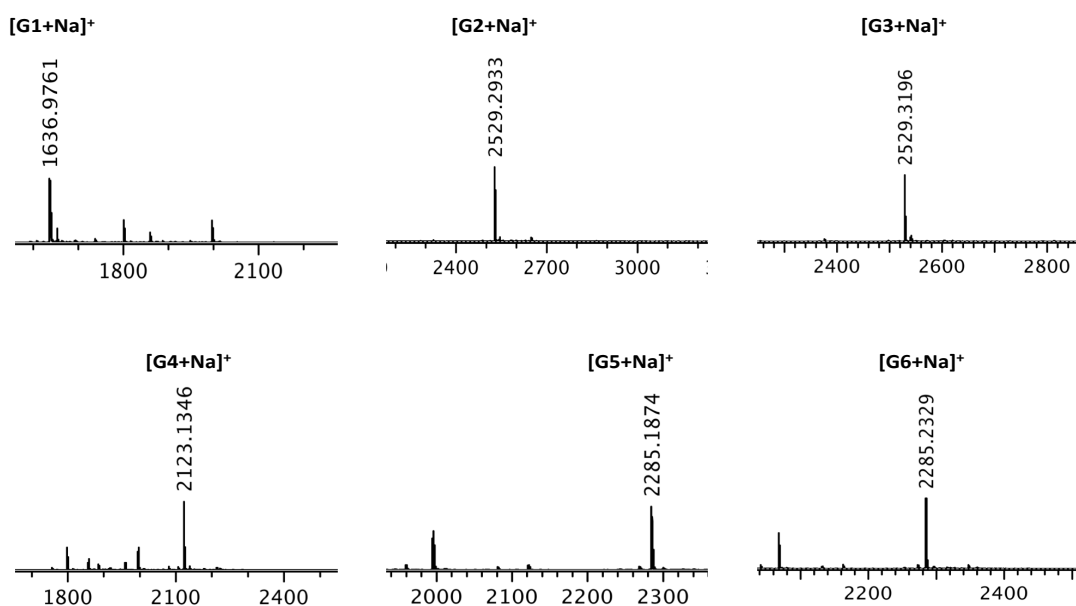


7.2 Immobilization of N-glycans on NHS-activated hydrophobic ITO-surface and on-chip enzyme assays

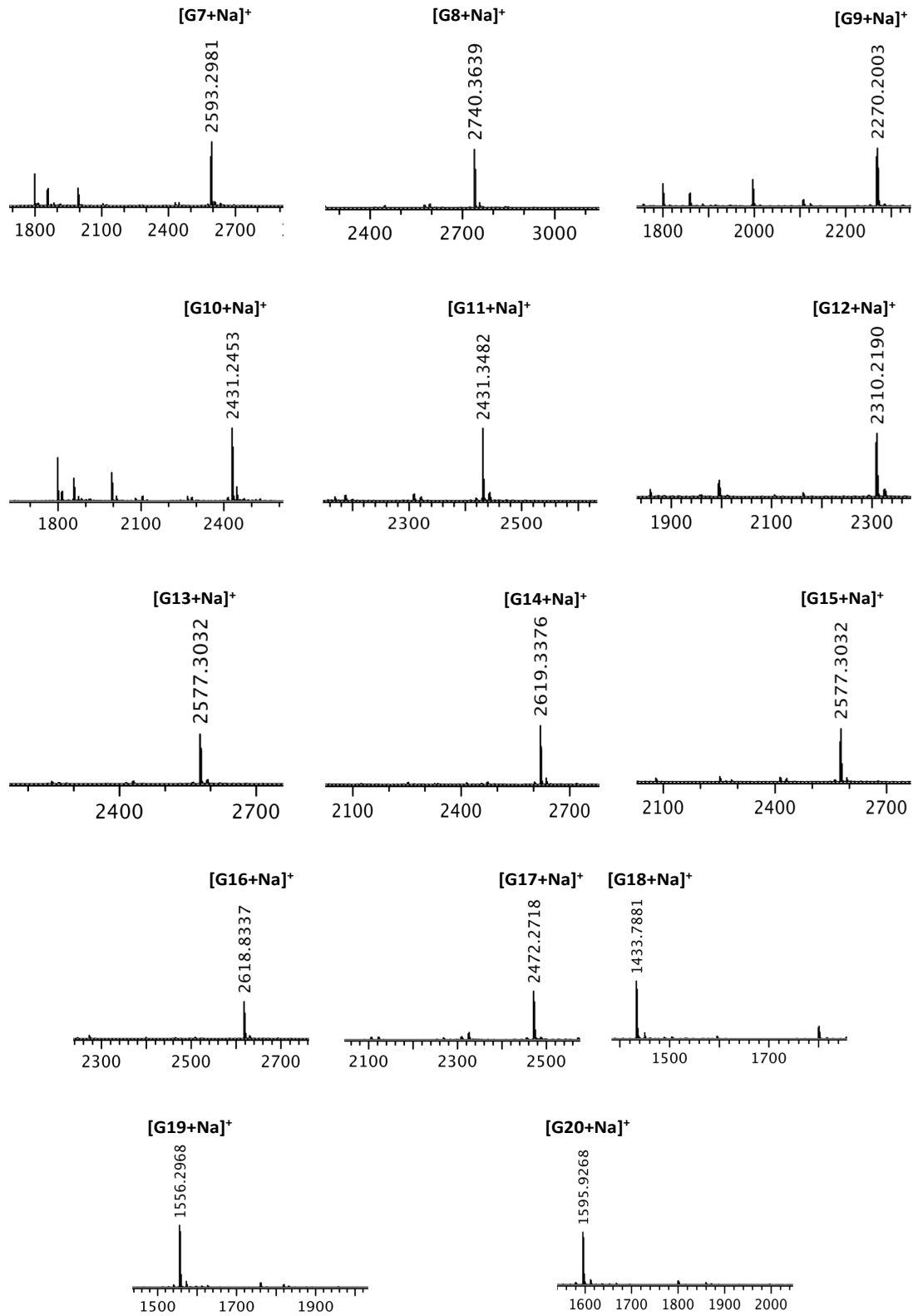
SM	Theoretical m/z [M+Na] ⁺	GalNAz	Theoretical m/z [M+Na] ⁺	Theoretical m/z [M+Na-N ₂] ⁺	GalNAc	Theoretical m/z [M+Na] ⁺	Gal	Theoretical m/z [M+Na] ⁺
G1	1637,0	G1.1	1882,0	1856,0	G1.2	1882,0	G1.3	1799,0
G2	2529,3	G2.1	2774,3	2748,3	G2.2	2774,3	G2.3	2691,4
G3	2529,3	G3.1	2774,3	2748,3	G3.2	2774,3	G3.3	2691,4
G4	2123,2	G4.1	2368,2	2342,2	G4.2	2368,2	G4.3	2285,2
G5	2285,2	G5.1	2530,2	2504,2	G5.2	2530,2	G5.3	2447,3
G6	2285,2	G6.1	2530,2	2504,2	G6.2	2530,2	G6.3	2447,3
G7	2593,3	G7.1	2838,3	2812,3	G7.2	2838,3	G7.3	2755,4
G8	2739,4	G8.1	2984,4	2958,4	G8.2	2984,4	G8.3	2901,4
G9	2269,2	G9.1	2514,2	2488,2	G9.2	2514,2	G9.3	2431,3
G10	2431,3	G10.1	2676,3	2650,3	G10.2	2676,3	G10.3	2593,3
G11	2431,3	G11.1	2676,3	2650,3	G11.2	2676,3	G11.3	2593,3
G12	2310,2	G12.1(1)	2555,2	2529,2	G12.2(1)	2555,2	G12.3(1)	2472,3
		G12.1(2)	2800,2	2774,2	G12.2(2)	2800,2	G12.3(2)	2634,3
G13	2577,3	G13.1	2822,3	2796,3	G13.2	2822,3	G13.3	2739,4
G14	2618,3	G14.1(1)	2863,3	2837,3	G14.2(1)	2863,3	G14.3(1)	2780,4
		G14.1(2)	3108,3	3082,3	G14.2(2)	3108,3	G14.3(2)	2942,5
G15	2577,3	G15.1	2822,3	2796,3	G15.2	2822,3	G15.3	2739,4
G16	2618,3	G16.1(1)	2863,3	2837,3	G16.2(1)	2863,3	G16.3(1)	2780,4
		G16.1(2)	3108,3	3082,3	G16.2(2)	3108,3	G16.3(2)	2942,5
G17	2472,3	G17.1(1)	2717,3	2691,3	G17.2(1)	2717,3	G17.3(1)	2634,3
		G17.1(2)	2962,3	2936,3	G17.2(2)	2962,3	G17.3(2)	2796,4
G18	1433,3							
G19	1556,8							
G20	1596,2							

Table 7.1 Summary of MALDI-TOF MS values of immobilized N-glycans (G1-G20) and their derivatives obtained after enzyme assays (Chapter 6.3.2); (G12(2)=bi-glycosylated product, G12(1)=mono-glycosylated product). For azido-derivatives (G1.1-G17.1), together to mass ions [M+Na]⁺, peaks obtained for in-source expulsion of N₂ as [M+Na-N₂]⁺ have been observed.

➤ MALDI-TOF mass spectra of immobilized N-glycan on NHS-activated surface:

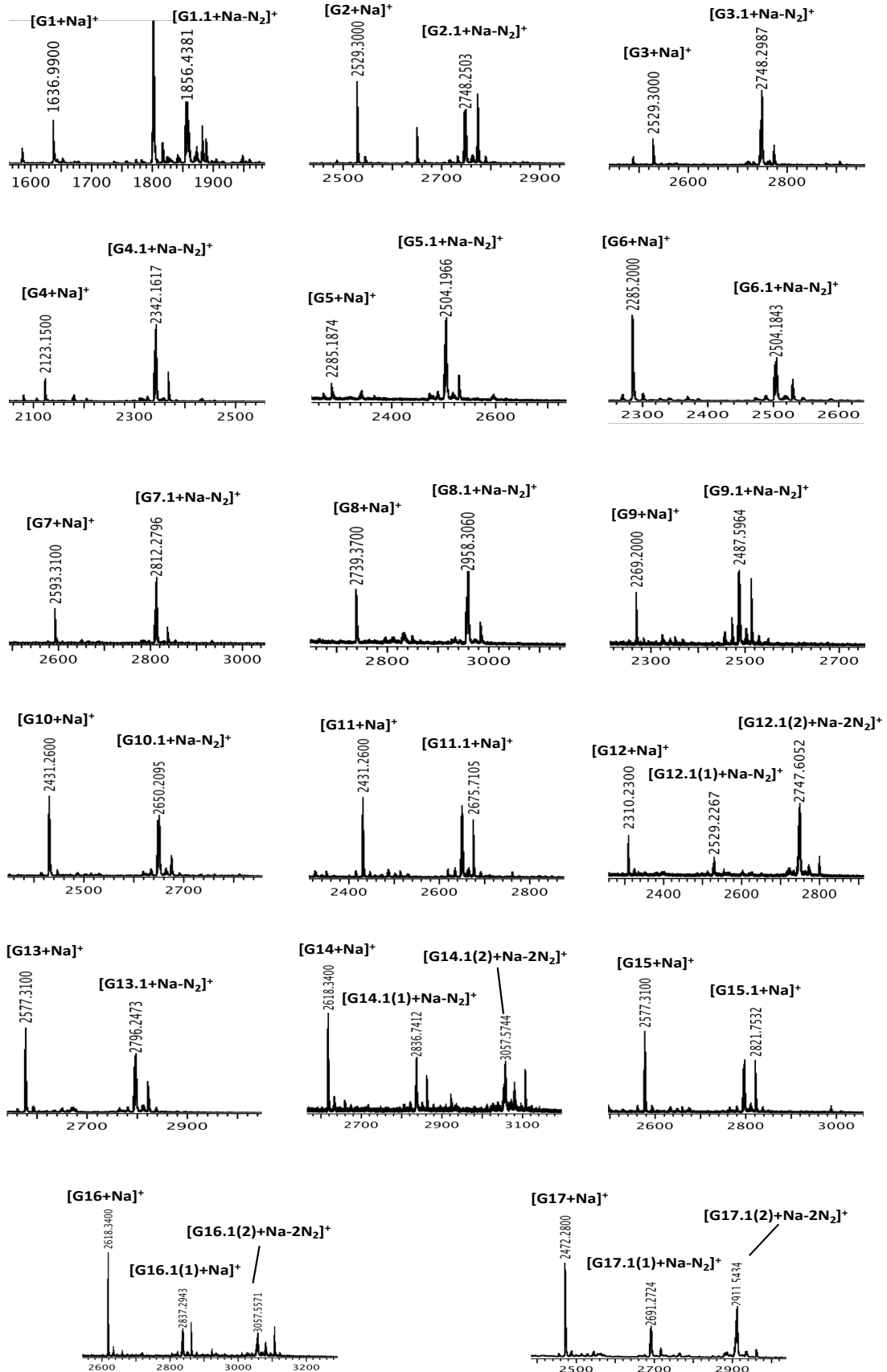


7. Appendix



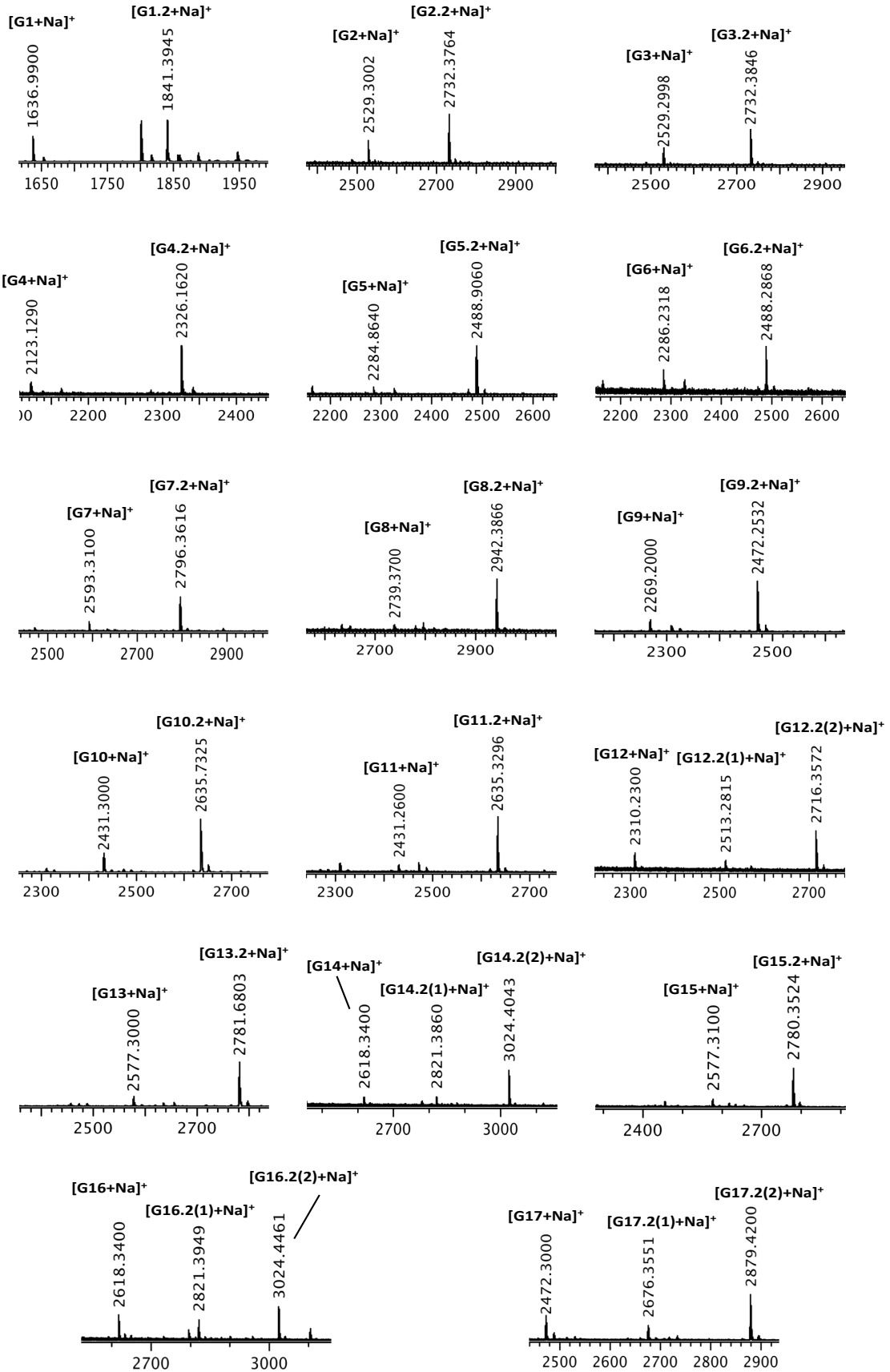
7. Appendix

- MALDI-TOF MS analysis of azido-N-Acetyl-D-galcosamine-derivatives (G1.1-G17.1) on NHS-activated surface:



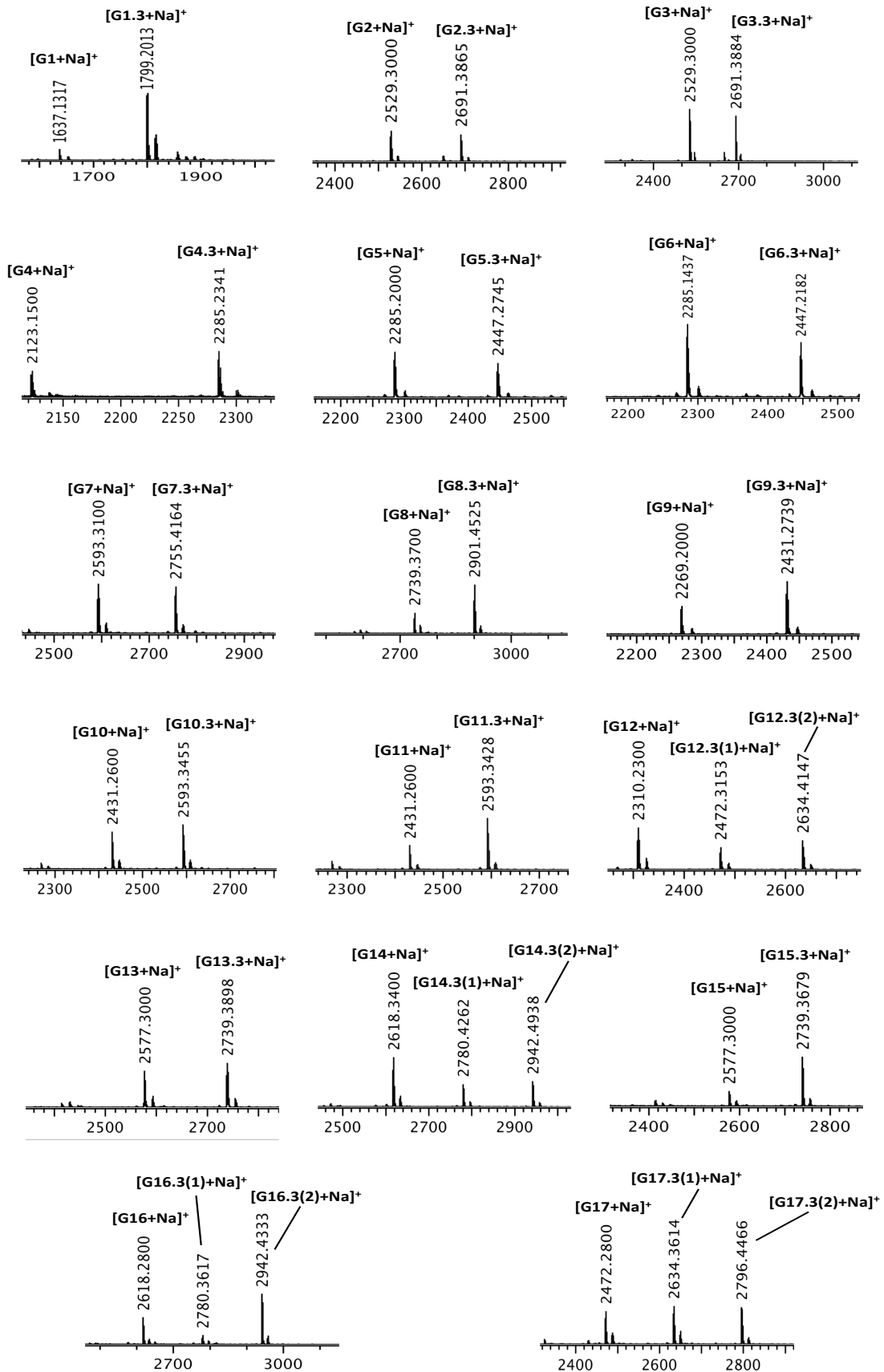
7. Appendix

- MALDI-TOF MS analysis of N-Acetyl-D-galcosamine-derivatives (G1.2-G17.2) on NHS-activated surface:



7. Appendix

- MALDI-TOF MS analysis of D-galcosamine-derivatives (**G1.3-G17.3**) on NHS-activated surface:



7. Appendix

7.3 Cu(I)-catalysed azide alkyne cycloaddition on the immobilized azido-N-glycans (G1.1-G17.1)

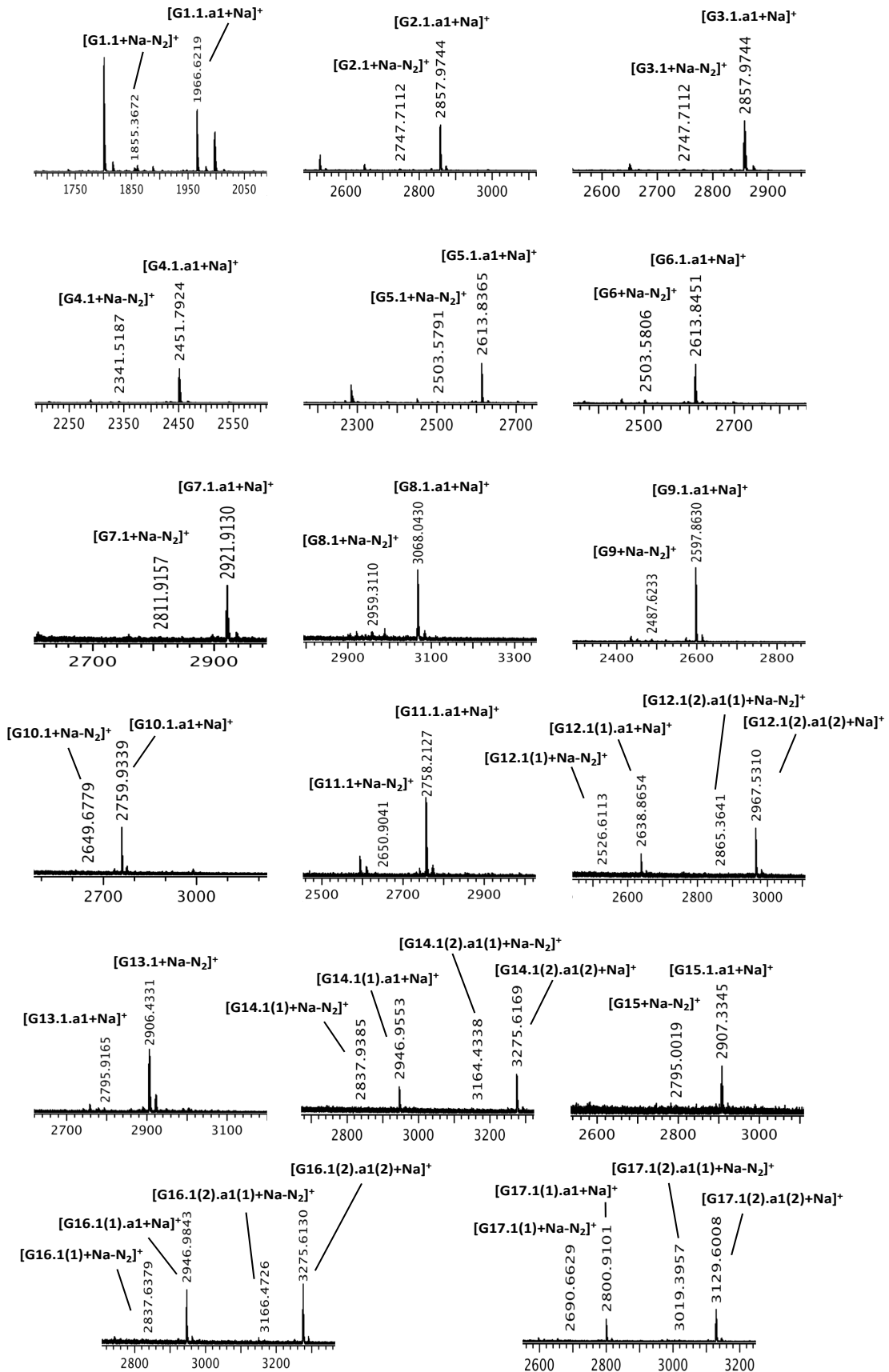
Theoretical m/z [M+Na] ⁺										
Azido-glycan	a1	a2	a3	a4	a5	a6	a7	a10	a11	a12
G1.1	1966,0	1985,0	1937,0	1998,0	2064,0	2004,0	2008,0	1938,0	1951,0	1948,0
G2.1	2858,3	2877,3	2829,3	2890,3	2956,3	2896,3	2900,3	2830,3	2843,3	2840,3
G3.1	2858,3	2877,3	2829,3	2890,3	2956,3	2896,3	2900,3	2830,3	2843,3	2840,3
G4.1	2452,2	2471,2	2423,2	2484,2	2550,2	2490,2	2494,2	2424,2	2437,2	2434,2
G5.1	2614,2	2633,2	2585,2	2646,2	2712,2	2652,2	2656,2	2586,2	2599,2	2596,2
G6.1	2614,2	2633,2	2585,2	2646,2	2712,2	2652,2	2656,2	2586,2	2599,2	2596,2
G7.1	2922,3	2941,3	2893,3	2954,3	3020,3	2960,3	2964,3	2894,3	2907,3	2904,3
G8.1	3068,4	3087,4	3039,4	3100,4	3166,4	3106,4	3110,4	3040,4	3053,4	3050,4
G9.1	2598,2	2617,2	2569,2	2630,2	2696,2	2636,2	2640,2	2570,2	2583,2	2580,2
G10.1	2760,3	2779,3	2731,3	2792,3	2858,3	2798,3	2802,3	2732,3	2745,3	2742,3
G11.1	2760,3	2779,3	2731,3	2792,3	2858,3	2798,3	2802,3	2732,3	2745,3	2742,3
G12.1(1)	2639,2	2658,2	2610,2	2671,2	2737,2	2677,2	2681,2	2611,2	2624,2	2621,2
G12.1(2)	2968,2	3006,2	2910,2	3032,2	3164,2	3044,2	3052,2	2912,2	2938,2	2932,2
G13.1	2906,3	2925,3	2877,3	2938,3	3004,3	2944,3	2948,3	2878,3	2891,3	2888,3
G14.1(1)	2947,3	2966,3	2918,3	2979,3	3045,3	2985,3	2989,3	2919,3	2932,3	2929,3
G14.1(2)	3276,3	3314,3	3218,3	3340,3	3472,3	3352,3	3360,3	3220,3	3246,3	3240,3
G15.1	2906,3	2925,3	2877,3	2938,3	3004,3	2944,3	2948,3	2878,3	2891,3	2888,3
G16.1(1)	2947,3	2966,3	2918,3	2979,3	3045,3	2985,3	2989,3	2919,3	2932,3	2929,3
G16.1(2)	3276,3	3314,3	3218,3	3340,3	3472,3	3352,3	3360,3	3220,3	3246,3	3240,3
G17.1(1)	2801,3	2820,3	2772,3	2833,3	2899,3	2839,3	2843,3	2773,3	2786,3	2783,3
G17.1(2)	3130,3	3168,3	3072,3	3194,3	3326,3	3206,3	3214,3	3074,3	3100,3	3094,3

Theoretical m/z [M+Na] ⁺									
Azido-glycan	a13	a14	a16	a17	a18	a20	a25	a26	a28
G1.1	1966,0	1965,0	1964,0	1980,0	1979,1	2020,0	1997,1	2014,0	2014,0
G2.1	2858,3	2857,3	2856,3	2872,3	2871,4	2912,3	2889,4	2906,3	2906,3
G3.1	2858,3	2857,3	2856,3	2872,3	2871,4	2912,3	2889,4	2906,3	2906,3
G4.1	2452,2	2451,2	2450,2	2466,2	2465,2	2506,2	2483,2	2500,2	2500,2
G5.1	2614,2	2613,2	2612,2	2628,2	2627,3	2668,2	2645,3	2662,2	2662,2
G6.1	2614,2	2613,2	2612,2	2628,2	2627,3	2668,2	2645,3	2662,2	2662,2
G7.1	2922,3	2921,3	2920,3	2936,3	2935,4	2976,3	2953,4	2970,3	2970,3
G8.1	3068,4	3067,4	3066,4	3082,4	3081,5	3122,4	3099,5	3116,4	3116,4
G9.1	2598,2	2597,2	2596,2	2612,2	2611,3	2652,2	2629,3	2646,2	2646,2
G10.1	2760,3	2759,3	2758,3	2774,3	2773,3	2814,3	2791,3	2808,3	2808,3
G11.1	2760,3	2759,3	2758,3	2774,3	2773,3	2814,3	2791,3	2808,3	2808,3
G12.1(1)	2639,2	2638,2	2637,2	2653,2	2652,3	2693,2	2670,3	2687,2	2687,2
G12.1(2)	2968,2	2966,2	2964,2	2996,2	2995,3	3076,2	3031,3	3064,2	3064,2
G13.1	2906,3	2905,3	2904,3	2920,3	2919,4	2960,3	2937,4	2954,3	2954,3
G14.1(1)	2947,3	2946,3	2945,3	2961,3	2960,4	3001,3	2978,4	2995,3	2995,3
G14.1(2)	3276,3	3274,3	3272,3	3304,3	3303,4	3384,3	3339,4	3372,3	3372,3
G15.1	2906,3	2905,3	2904,3	2920,3	2919,4	2960,3	2937,4	2954,3	2954,3
G16.1(1)	2947,3	2946,3	2945,3	2961,3	2960,4	3001,3	2978,4	2995,3	2995,3
G16.1(2)	3276,3	3274,3	3272,3	3304,3	3303,4	3384,3	3339,4	3372,3	3372,3
G17.1(1)	2801,3	2800,3	2799,3	2815,3	2814,4	2855,3	2832,4	2849,3	2849,3
G17.1(2)	3130,3	3128,3	3126,3	3158,3	3157,4	3238,3	3193,4	3226,3	3226,3

Table 7.2 Summary of MALDI-TOF MS values of N-glycan derivatives obtained after performing CuAAC with selected 19 alkynes (**Chapter 6.3.3**). (Gx.y(2) =bi-glycosylated product, Gx.y(1) =mono-glycosylated product).

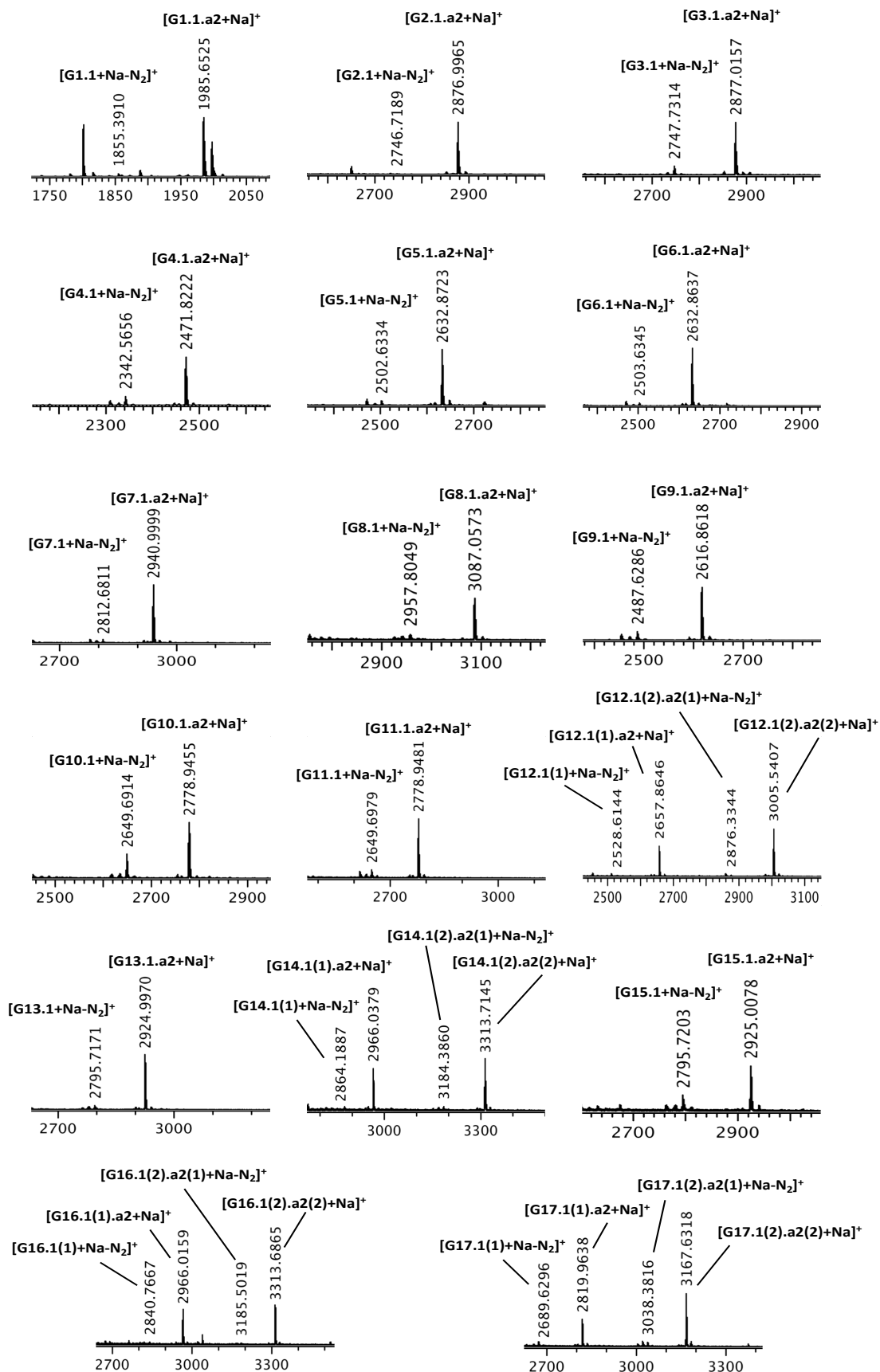
7. Appendix

- MALDI-TOF MS analysis of N-glycan derivatives achieved by coupling alkyne **a1** on azido-derivatives (**G1.1.-G17.1**):



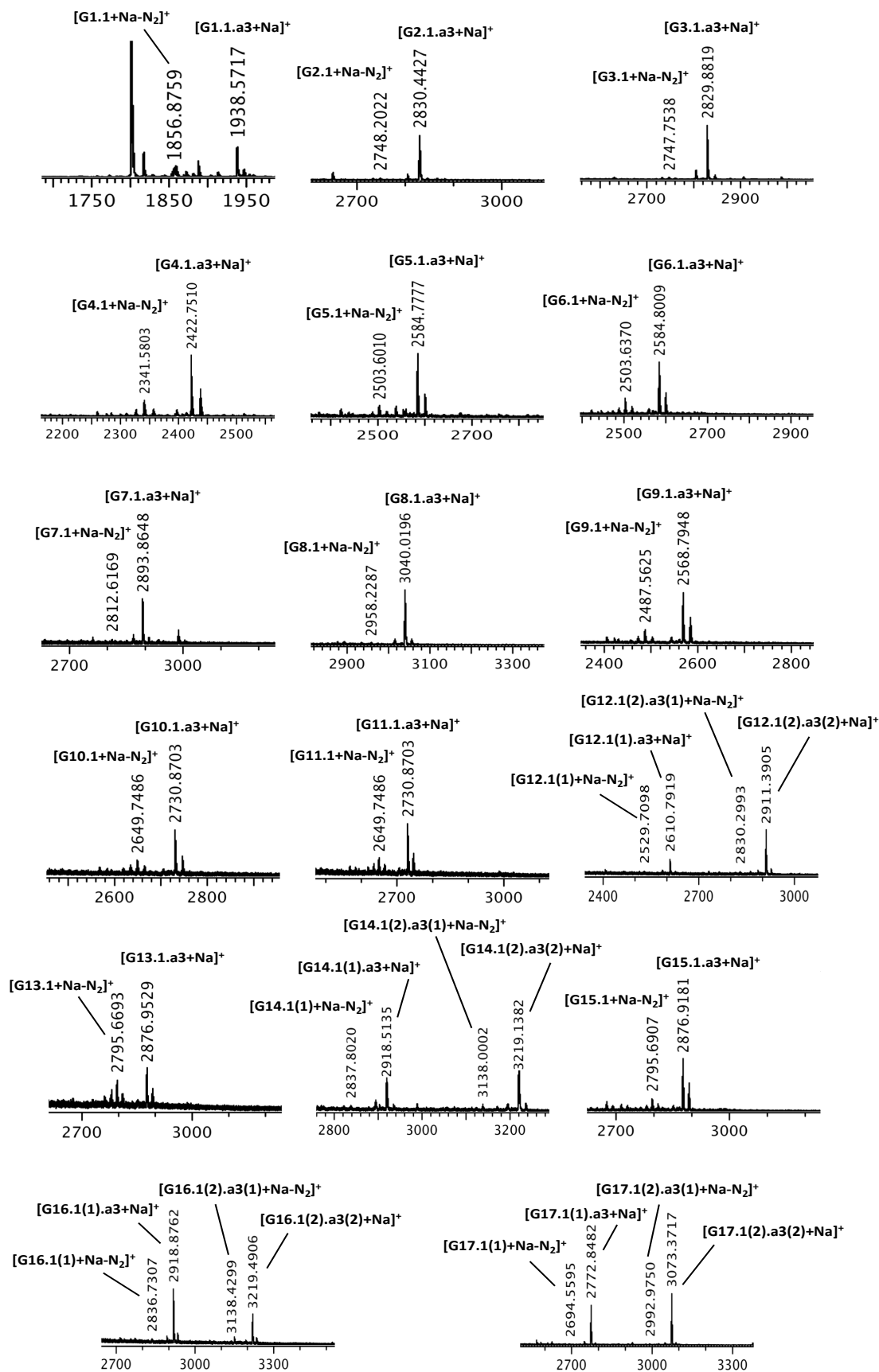
7. Appendix

- MALDI-TOF MS analysis of N-glycan derivatives achieved by coupling alkyne **a2** on azido-derivatives (**G1.1.-G17.1**):



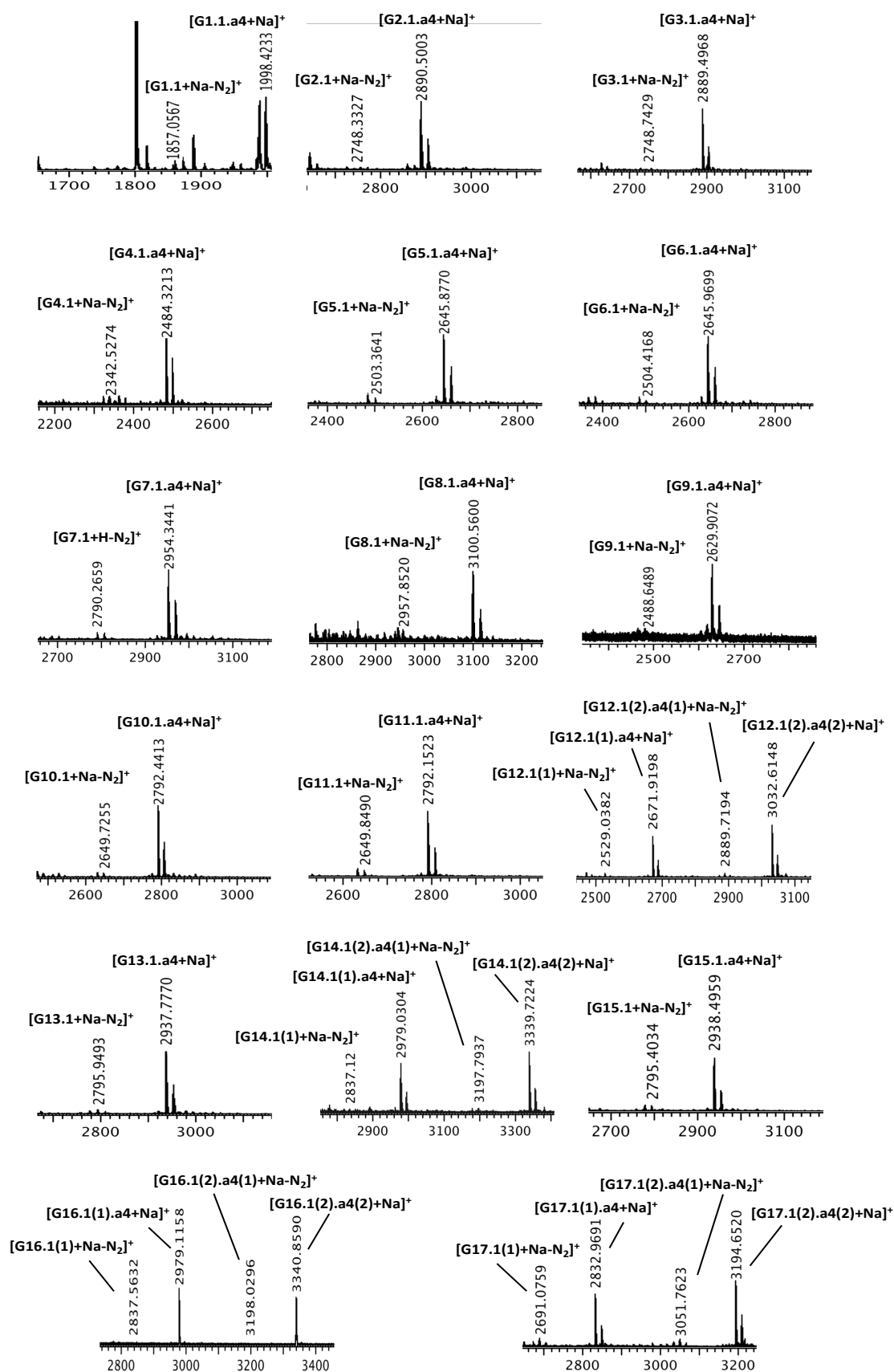
7. Appendix

- MALDI-TOF MS analysis of N-glycan derivatives achieved by coupling alkyne **a3** on azido-derivatives (**G1.1.-G17.1**):



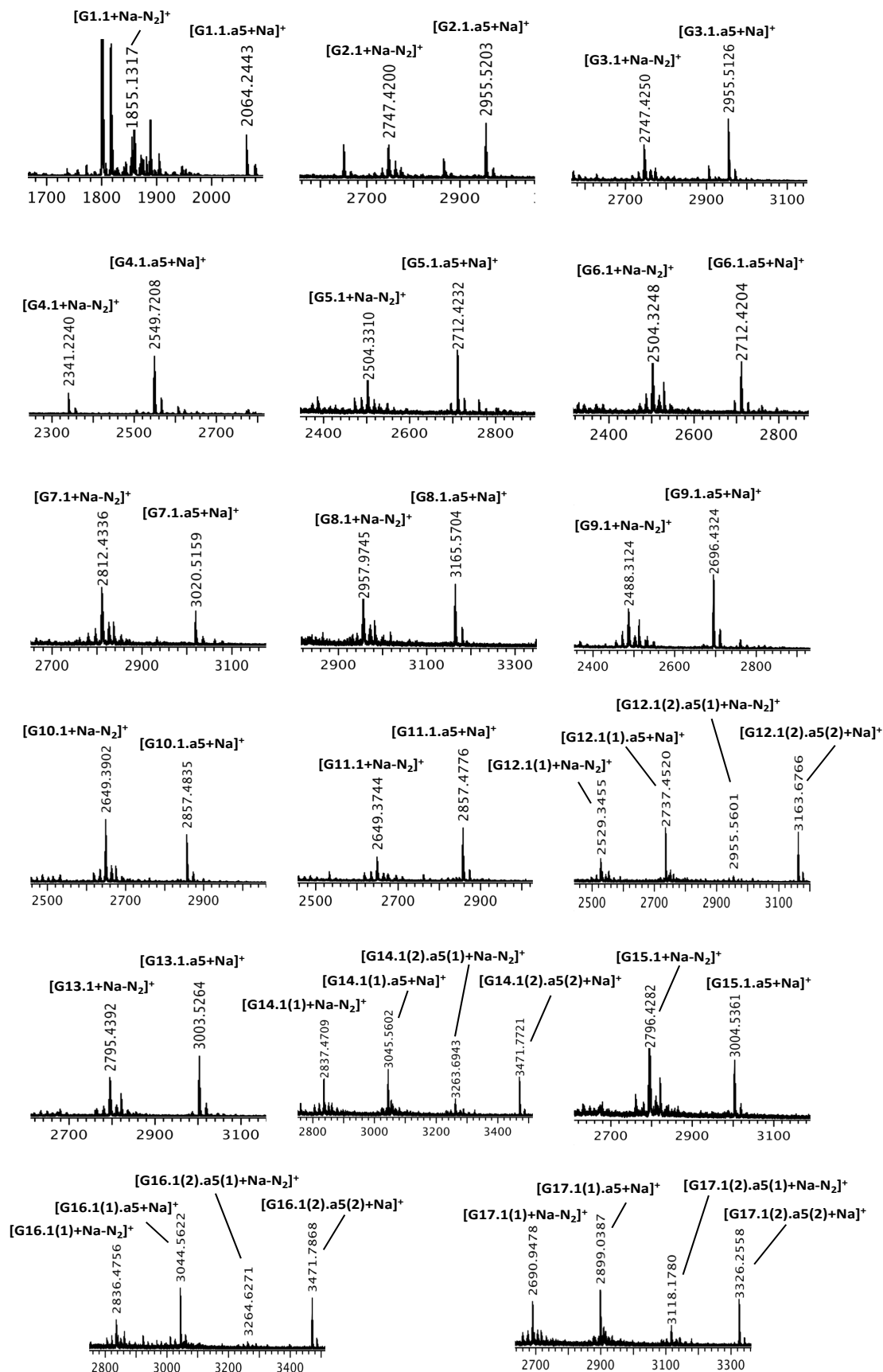
7. Appendix

- MALDI-TOF MS analysis of N-glycan derivatives achieved by coupling alkyne **a4** on azido-derivatives (**G1.1.-G17.1**):



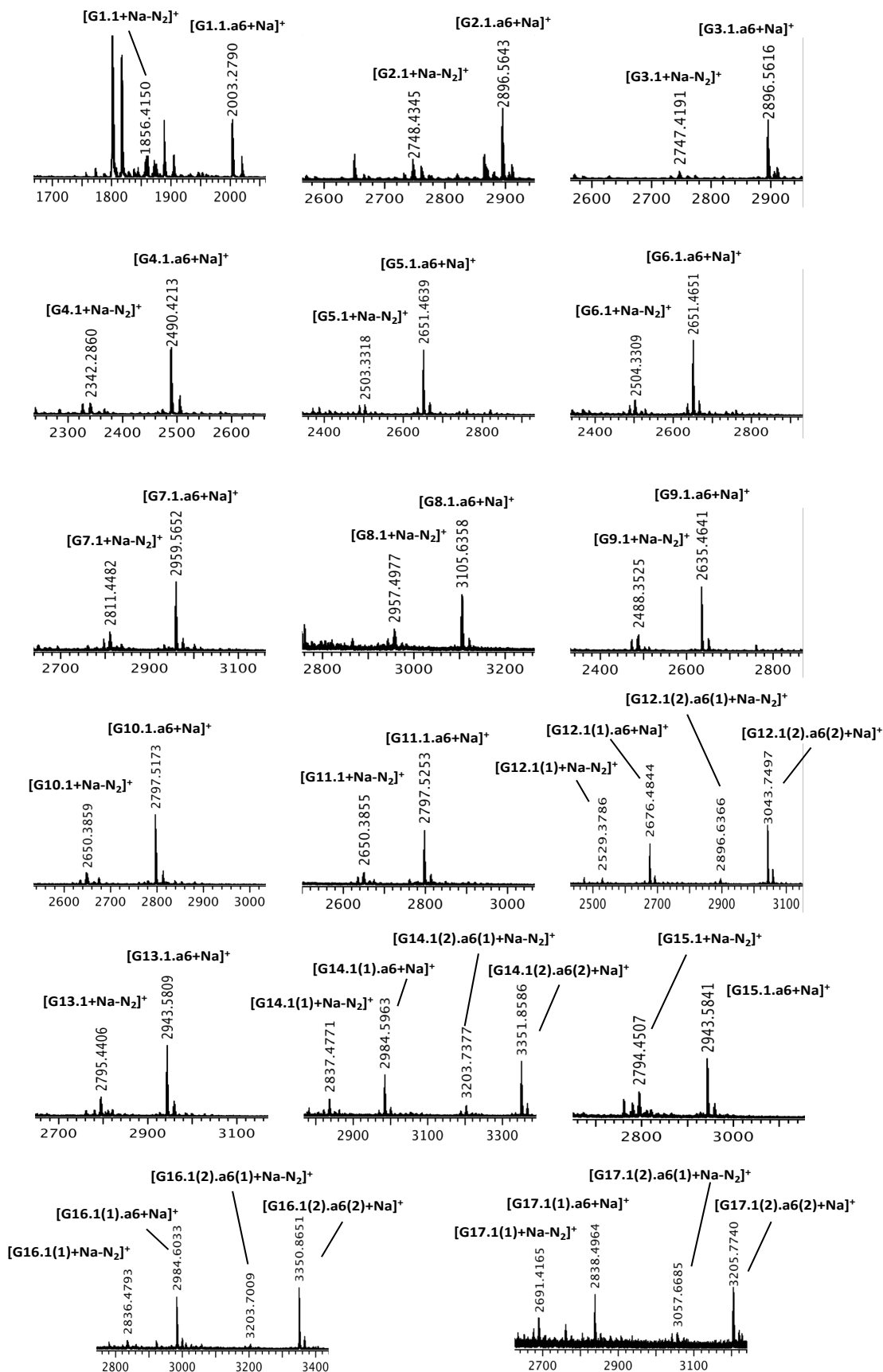
7. Appendix

- MALDI-TOF MS analysis of N-glycan derivatives achieved by coupling alkyne **a5** on azido-derivatives (**G1.1.-G17.1**):



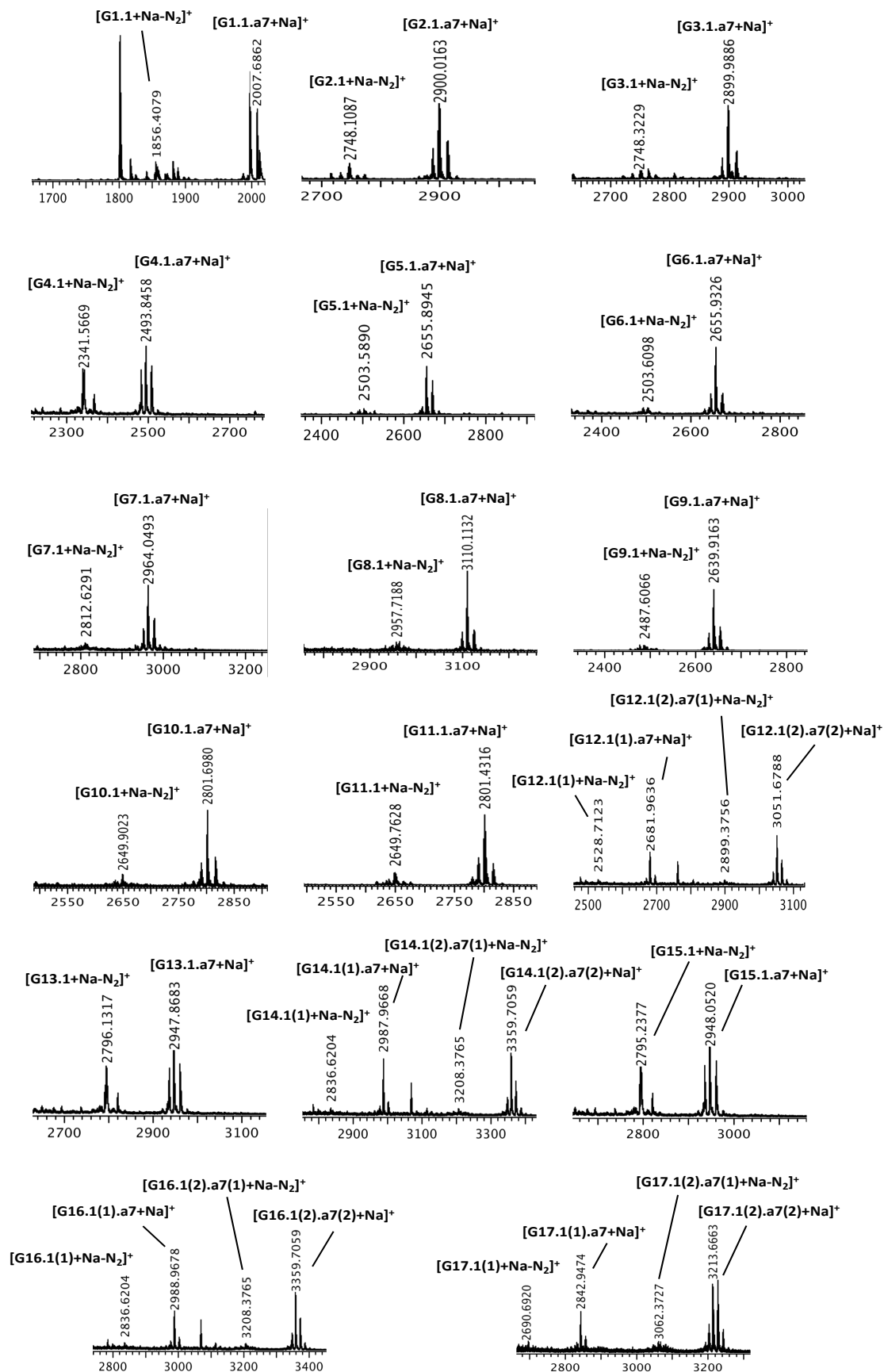
7. Appendix

- MALDI-TOF MS analysis of N-glycan derivatives achieved by coupling alkyne **a6** on azido-derivatives (**G1.1.-G17.1**):



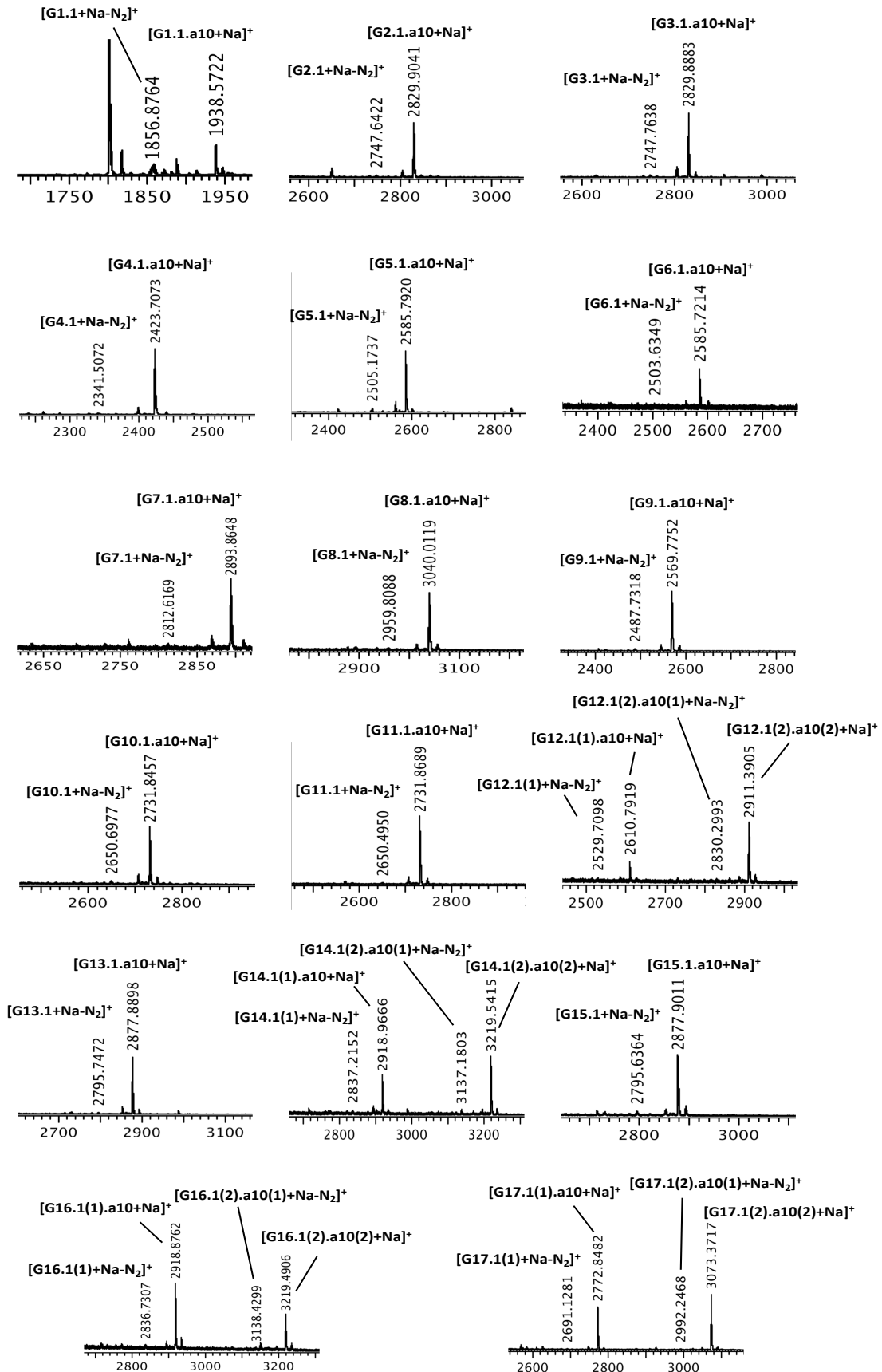
7. Appendix

- MALDI-TOF MS analysis of N-glycan derivatives achieved by coupling alkyne **a7** on azido-derivatives (**G1.1.-G17.1**):



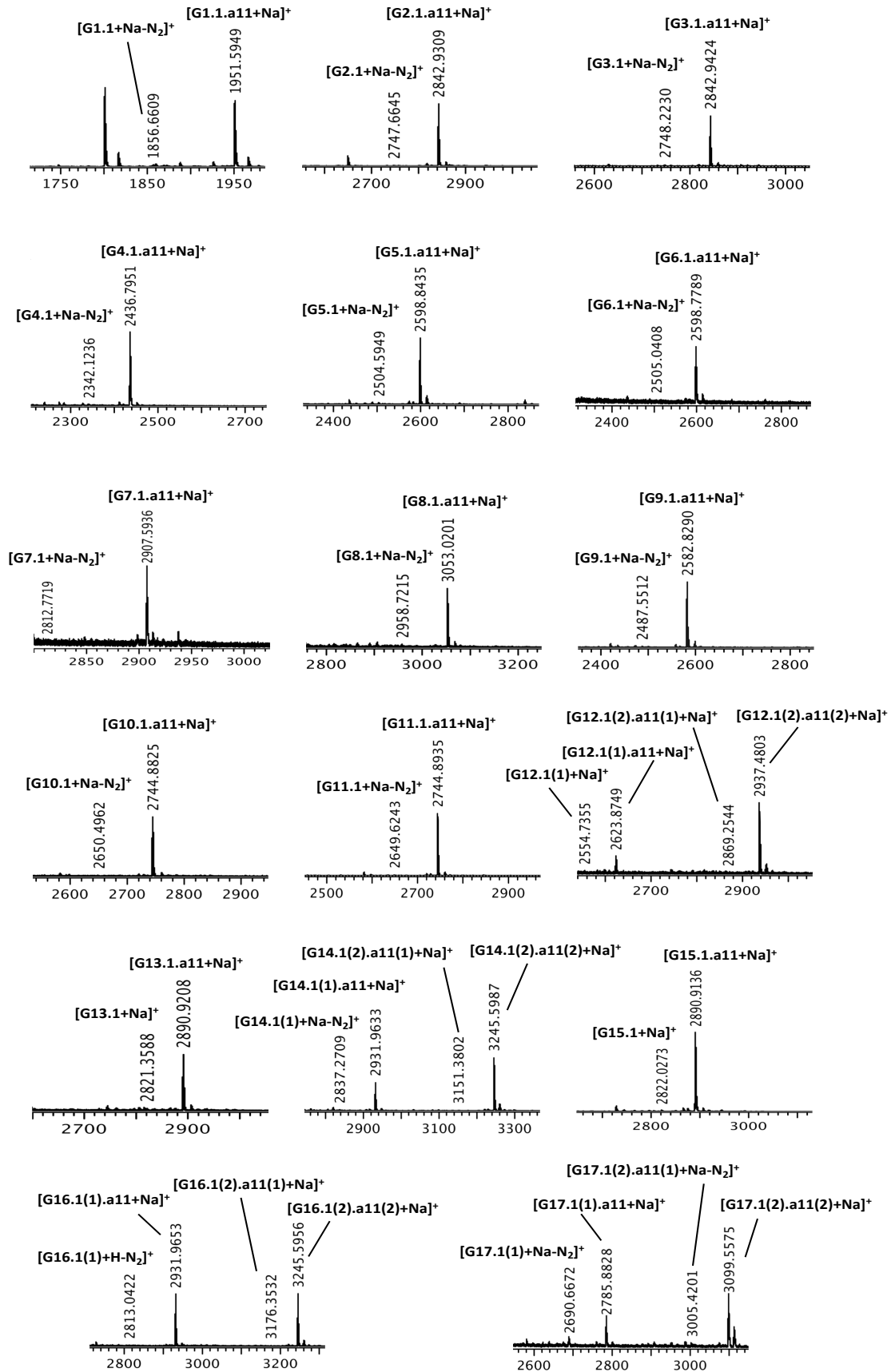
7. Appendix

- MALDI-TOF MS analysis of N-glycan derivatives achieved by coupling alkyne **a10** on azido-derivatives (**G1.1.-G17.1**):



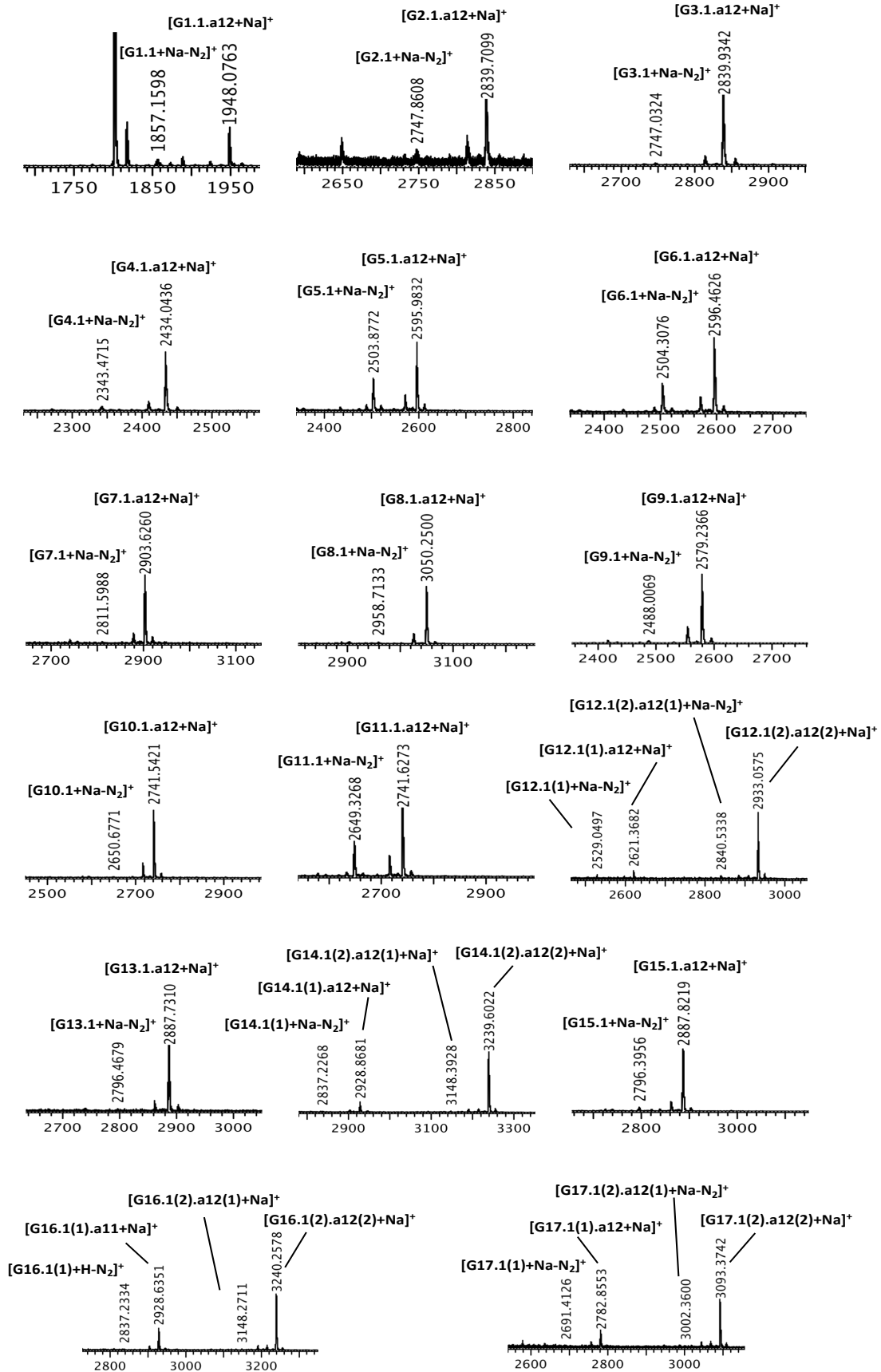
7. Appendix

- MALDI-TOF MS analysis of N-glycan derivatives achieved by coupling alkyne **a11** on azido-derivatives (**G1.1.-G17.1**):



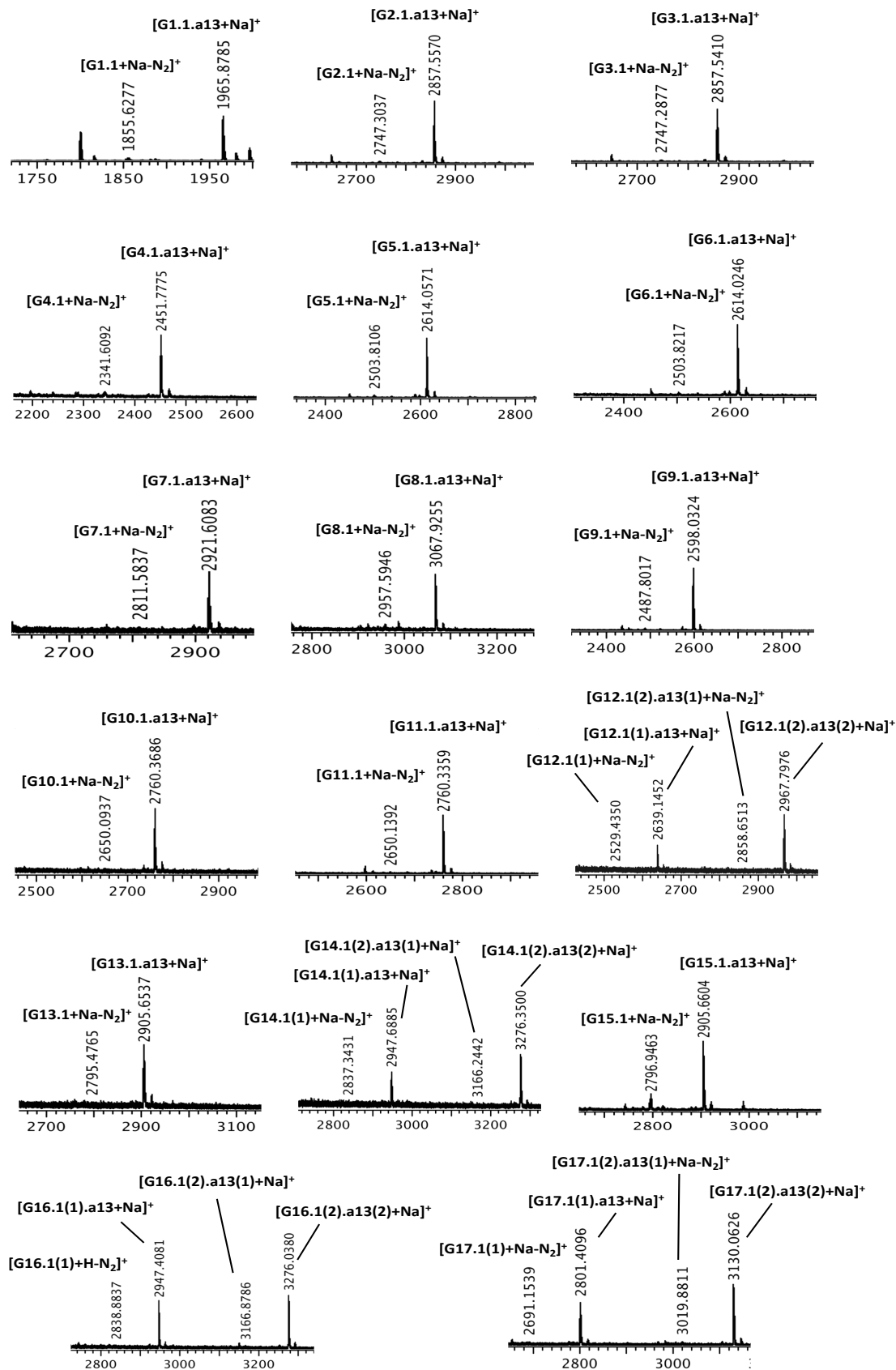
7. Appendix

- MALDI-TOF MS analysis of N-glycan derivatives achieved by coupling alkyne **a12** on azido-derivatives (**G1.1.-G17.1**):



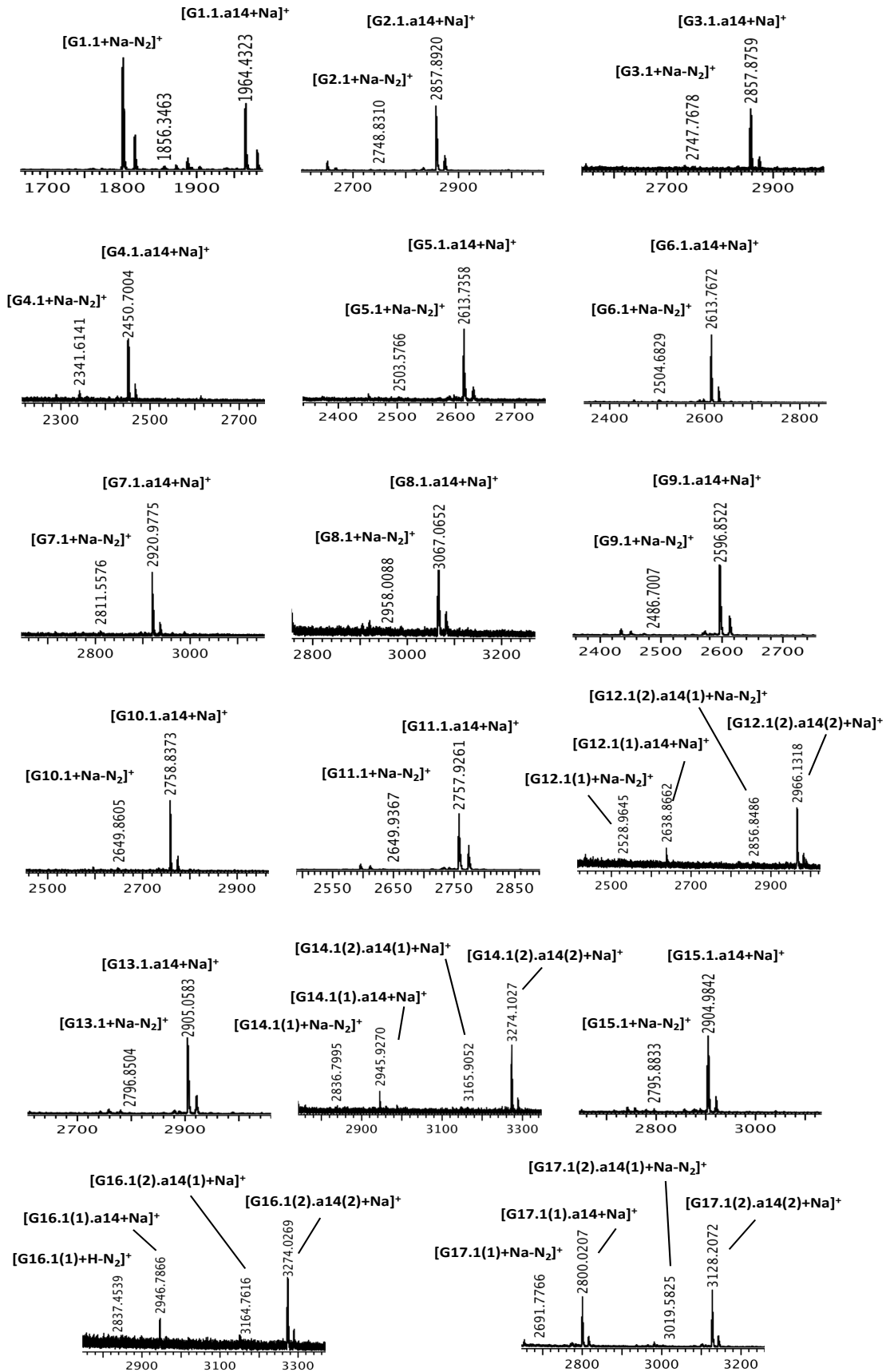
7. Appendix

- MALDI-TOF MS analysis of N-glycan derivatives achieved by coupling alkyne **a13** on azido-derivatives (**G1.1.-G17.1**):



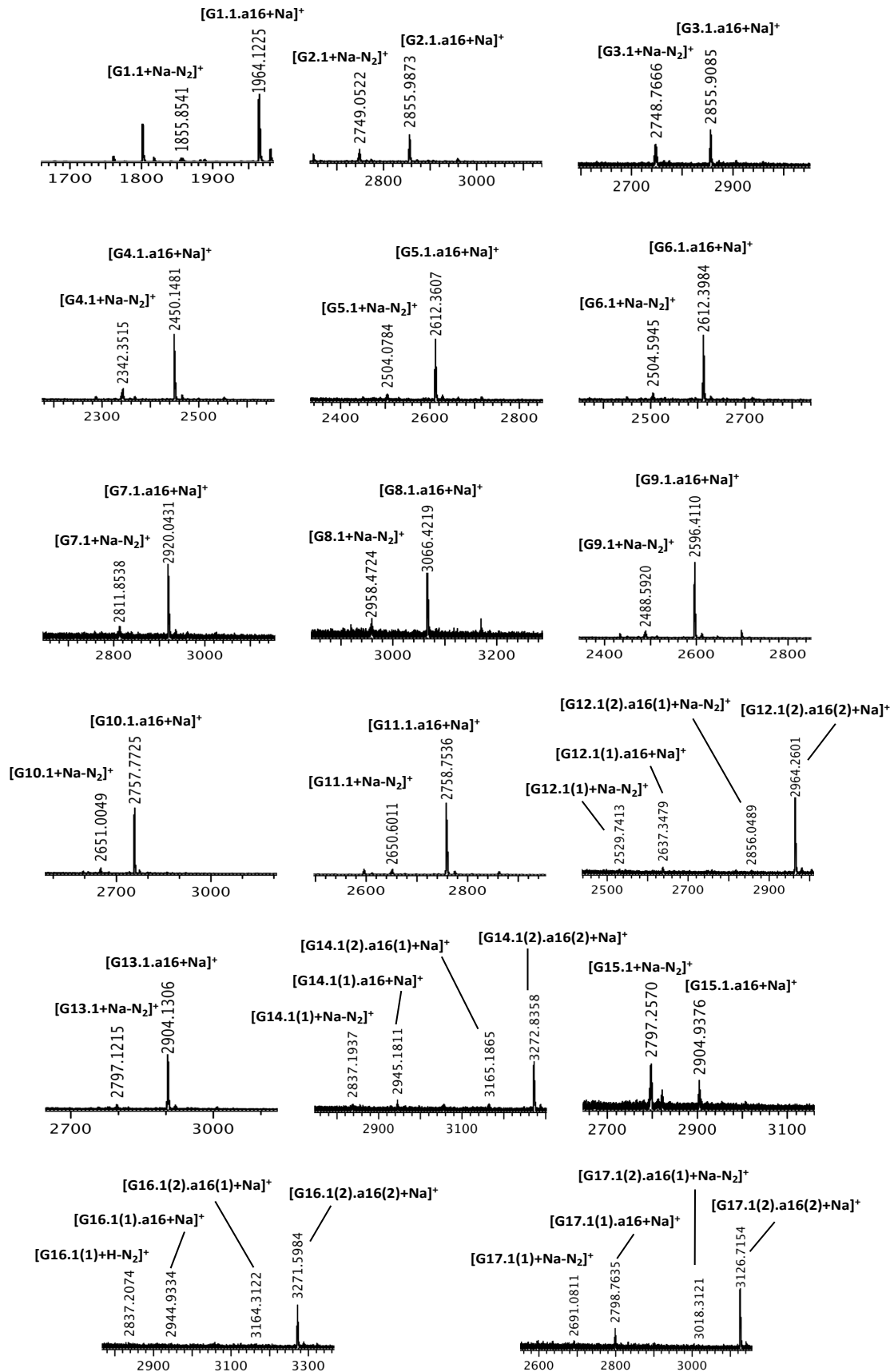
7. Appendix

- MALDI-TOF MS analysis of N-glycan derivatives achieved by coupling alkyne **a14** on azido-derivatives (**G1.1.-G17.1**):



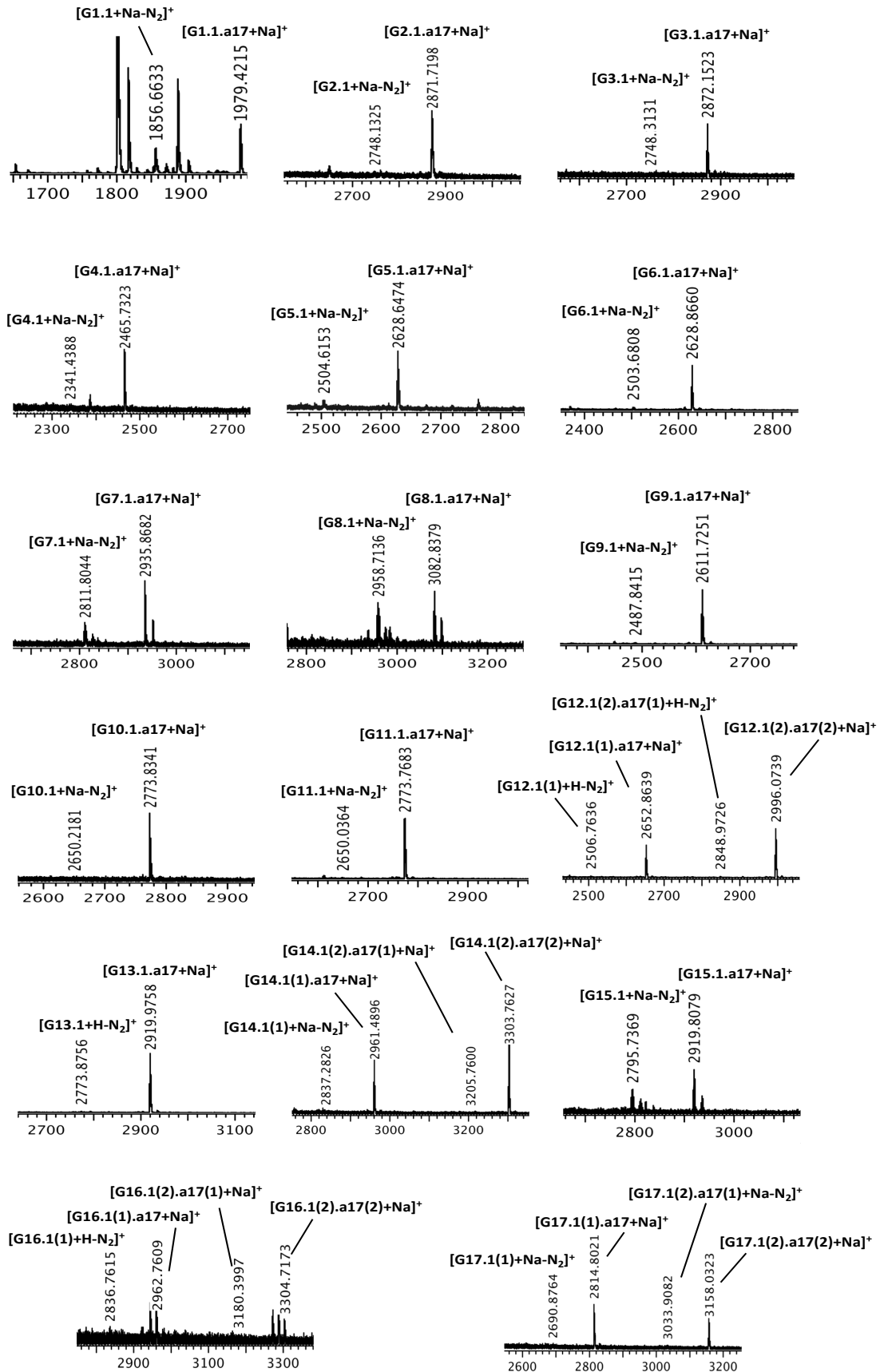
7. Appendix

- MALDI-TOF MS analysis of N-glycan derivatives achieved by coupling alkyne a16 on azido-derivatives (G1.1.-G17.1):



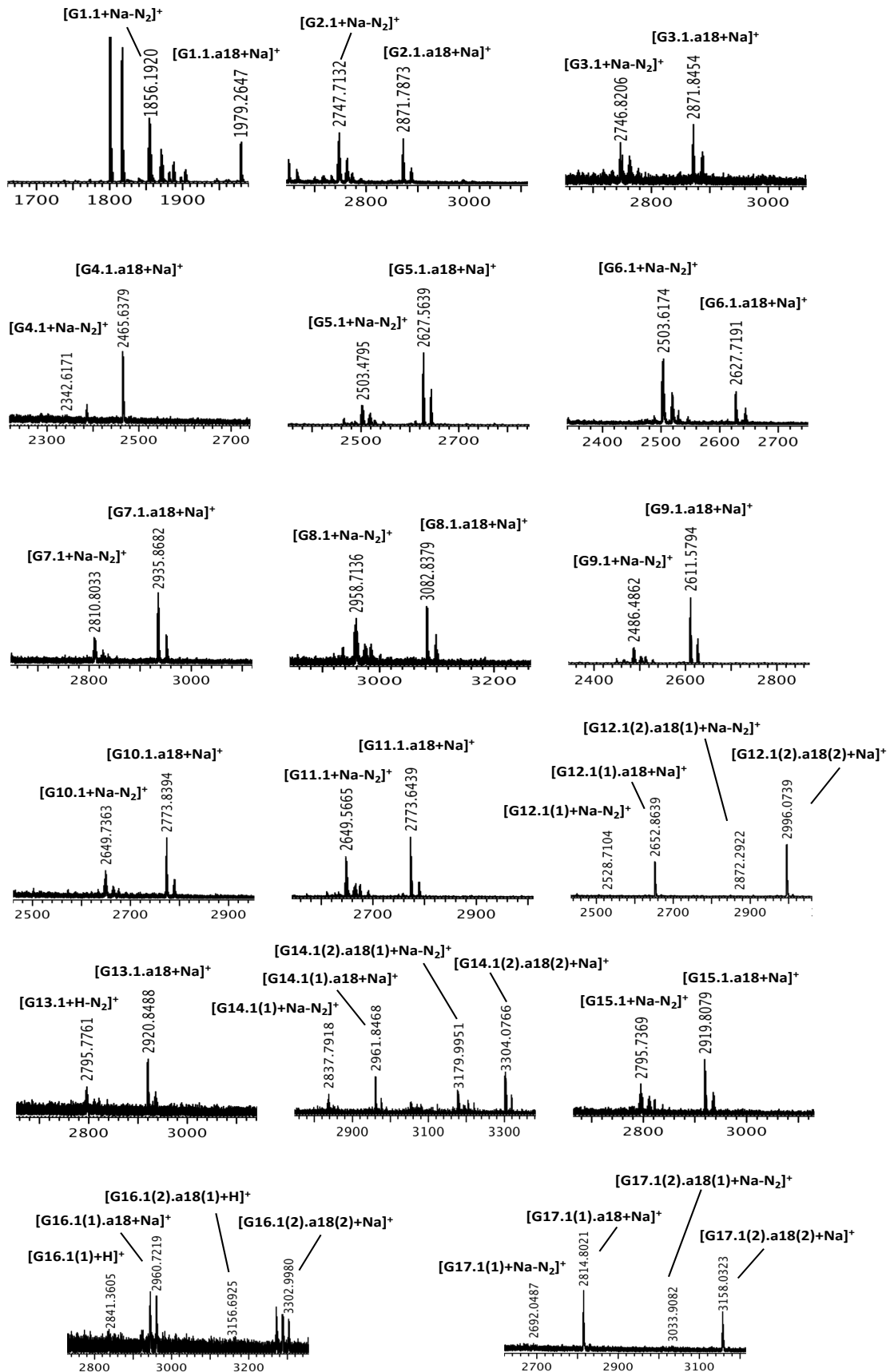
7. Appendix

- MALDI-TOF MS analysis of N-glycan derivatives achieved by coupling alkyne a17 on azido-derivatives (G1.1.-G17.1):



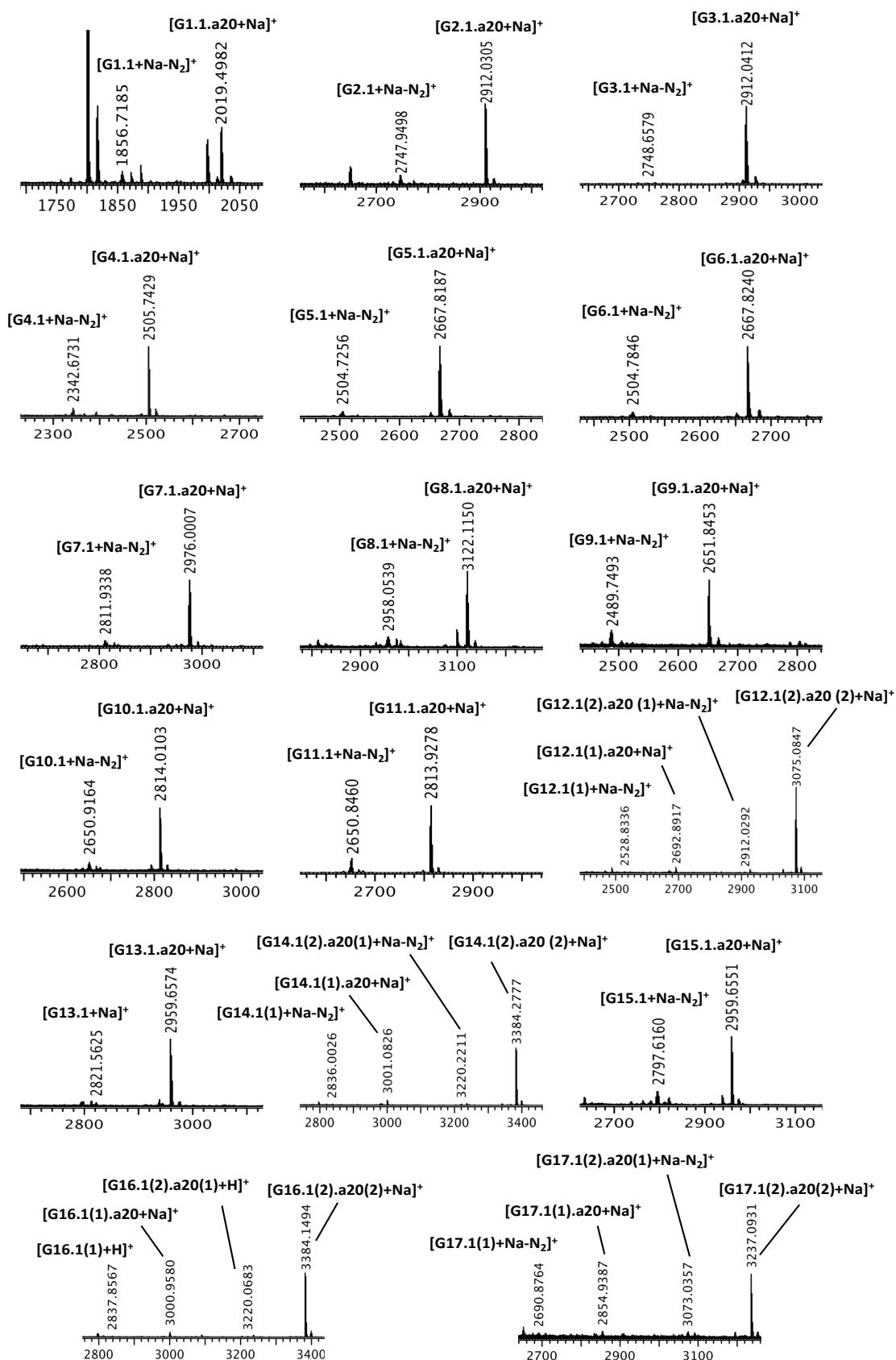
7. Appendix

- MALDI-TOF MS analysis of N-glycan derivatives achieved by coupling alkyne **a18** on azido-derivatives (**G1.1.-G17.1**):



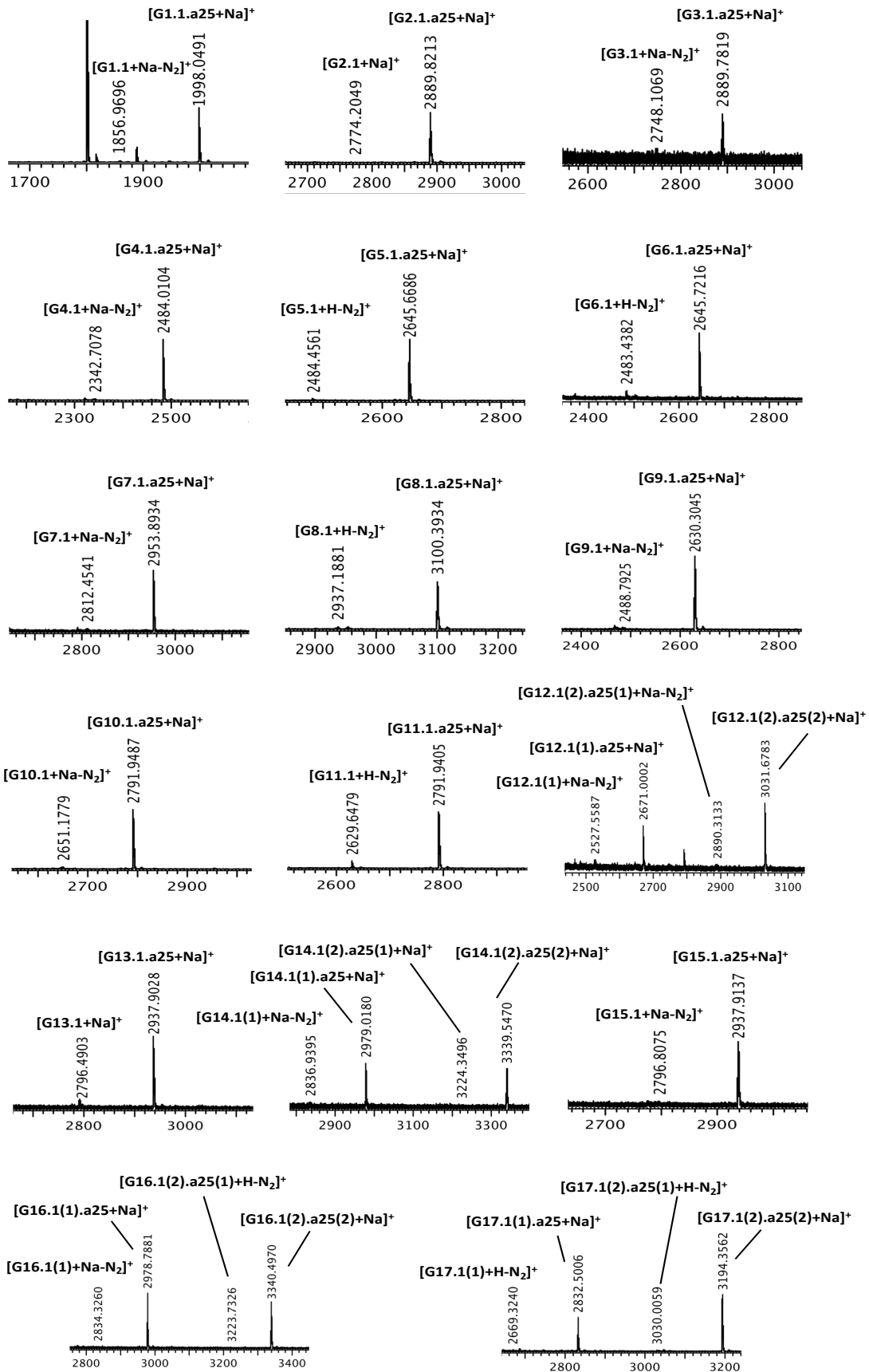
7. Appendix

- MALDI-TOF MS analysis of N-glycan derivatives achieved by coupling alkyne **a20** on azido-derivatives (**G1.1.-G17.1**):



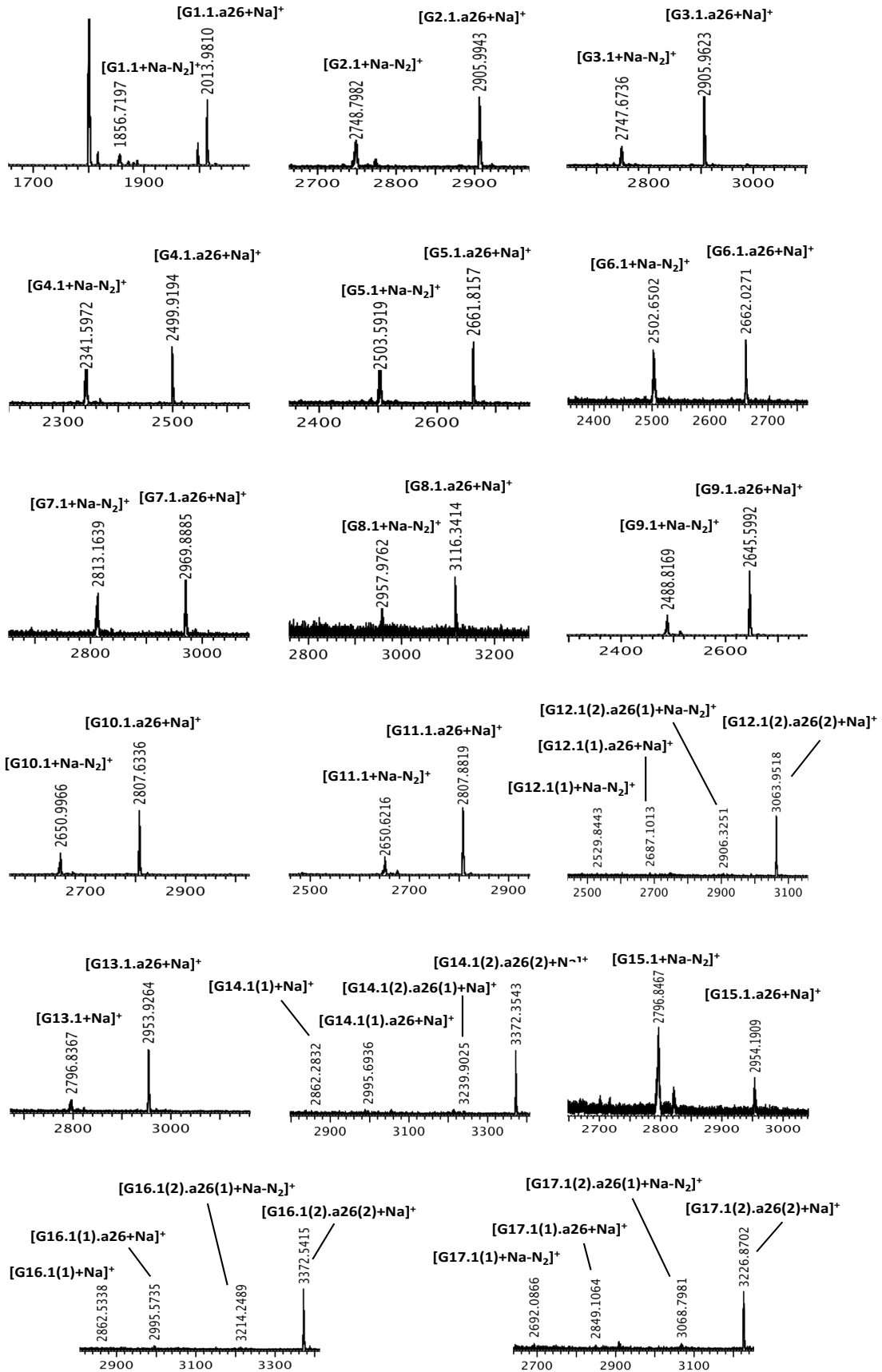
7. Appendix

- MALDI-TOF MS analysis of N-glycan derivatives achieved by coupling alkyne a25 on azido-derivatives (G1.1.-G17.1):



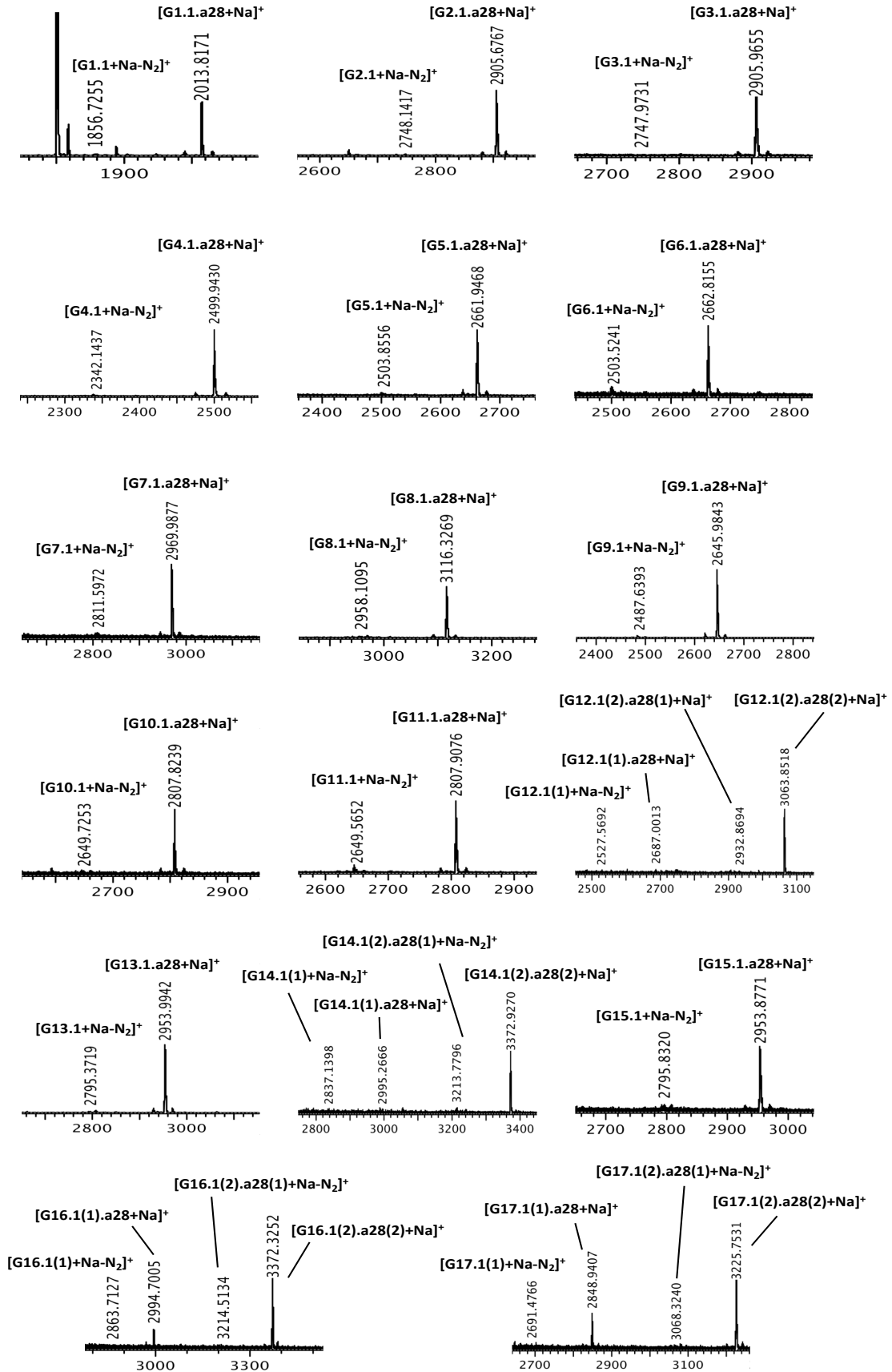
7. Appendix

- MALDI-TOF MS analysis of N-glycan derivatives achieved by coupling alkyne a26 on azido-derivatives (G1.1.-G17.1):



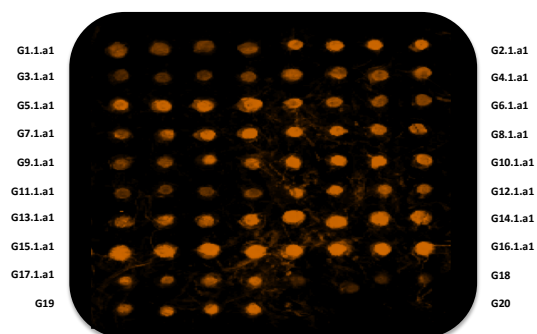
7. Appendix

- MALDI-TOF MS analysis of N-glycan derivatives achieved by coupling alkyne **a28** on azido-derivatives (**G1.1.-G17.1**):

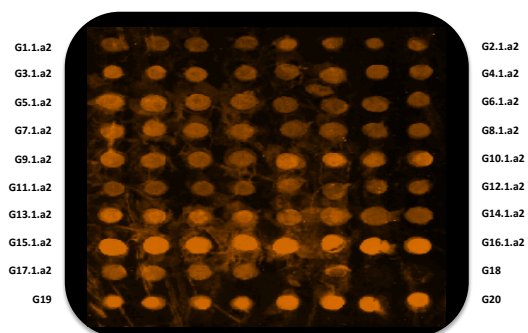


7.4 Binding assays of N-glycan mimetics with fluorescently labeled lectins

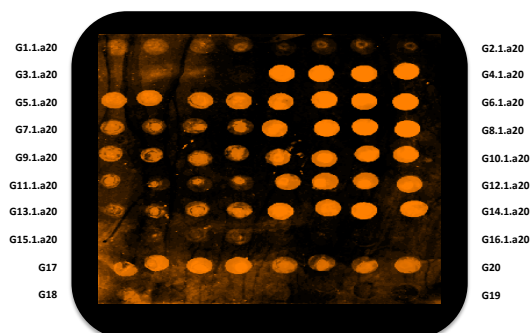
- Example of fluorescent image achieved after on-chip incubation of *Wisteria Floribunda Agglutinin-Alexafluor647* (1 $\mu\text{g}/\text{mL}$, DOL=0.71) with **G1.a1-G17.a1** derivatives array.



- Example of fluorescent image achieved after on-chip incubation of *Macrophage Galactose Lectin-Alexafluor555* (10 $\mu\text{g}/\text{mL}$, DOL=0.47) with **G1.1.a2-G17.1.a2** derivatives array.

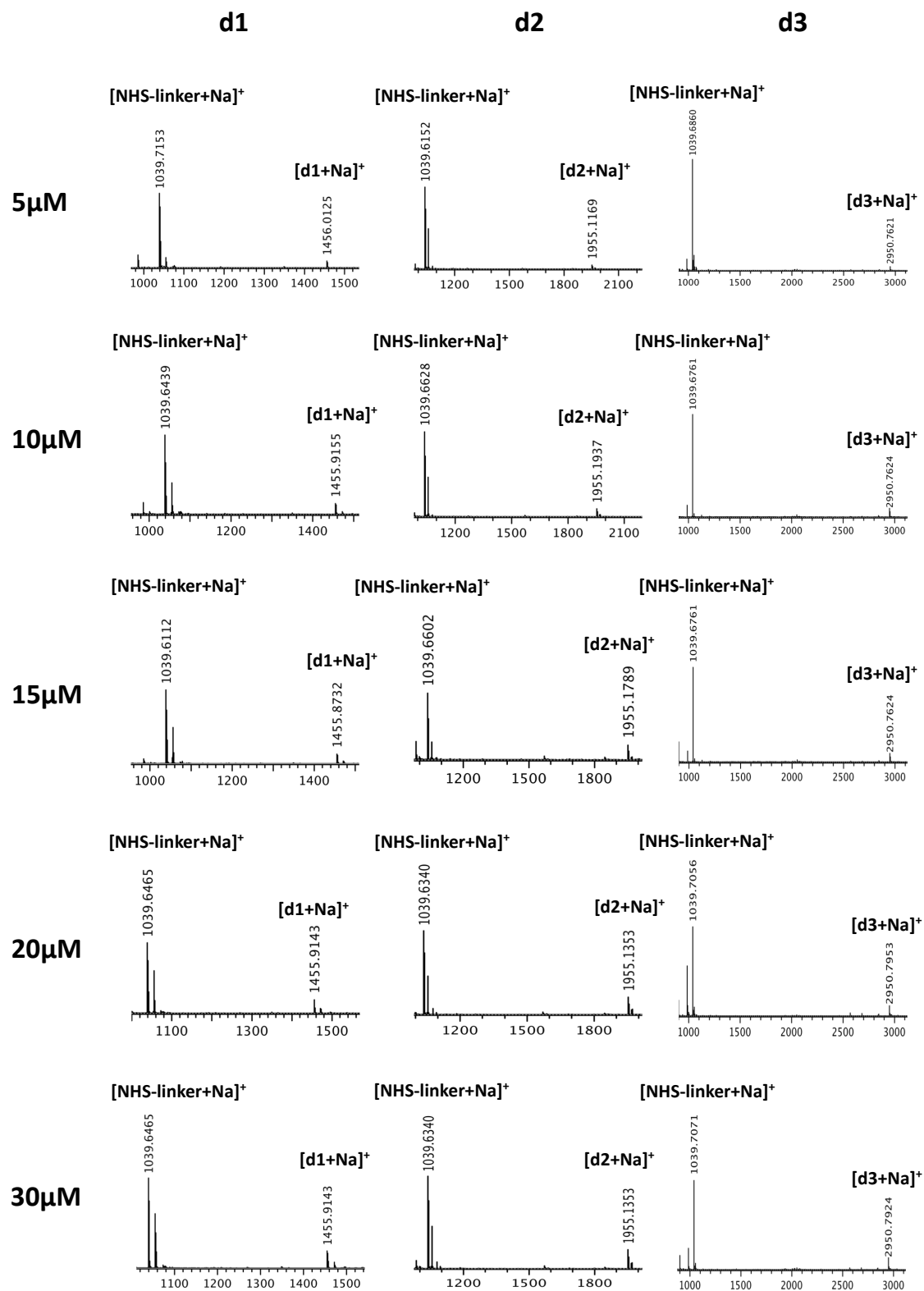


- Example of fluorescent image achieved after on-chip incubation of *Langerin ECD-Cy3* (10 $\mu\text{g}/\text{mL}$, DOL= 0.70) with **G1.1.a20-G17.1.a20** derivatives array.



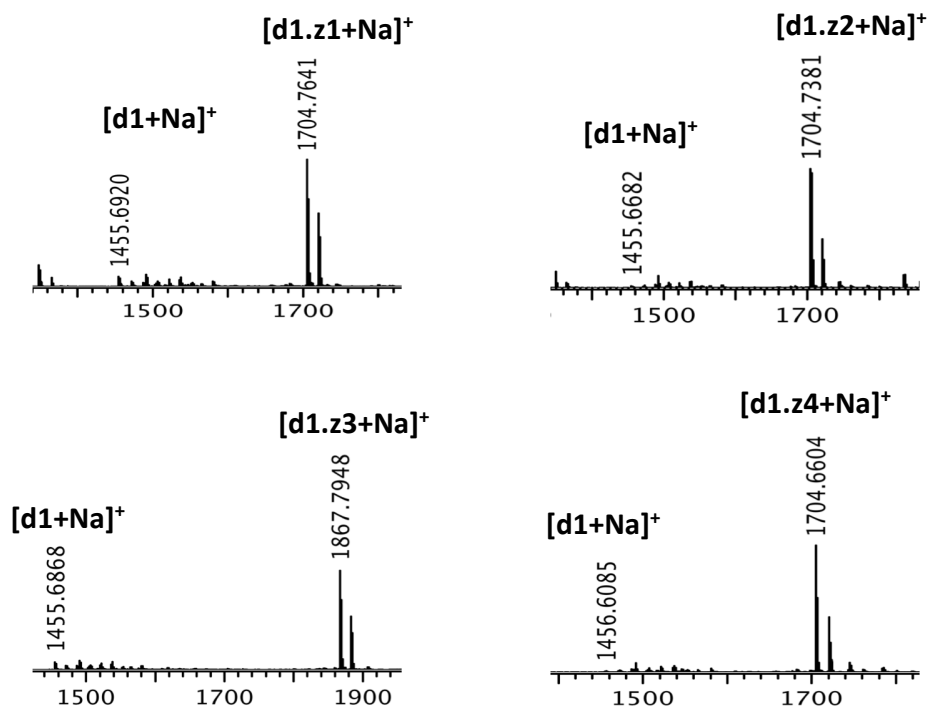
7.5 Cyclooctyne-dendrons immobilization

- MALDI-TOF MS analysis of immobilized cyclooctyne-dendrons (**d1-3**) by adopting different coating concentration

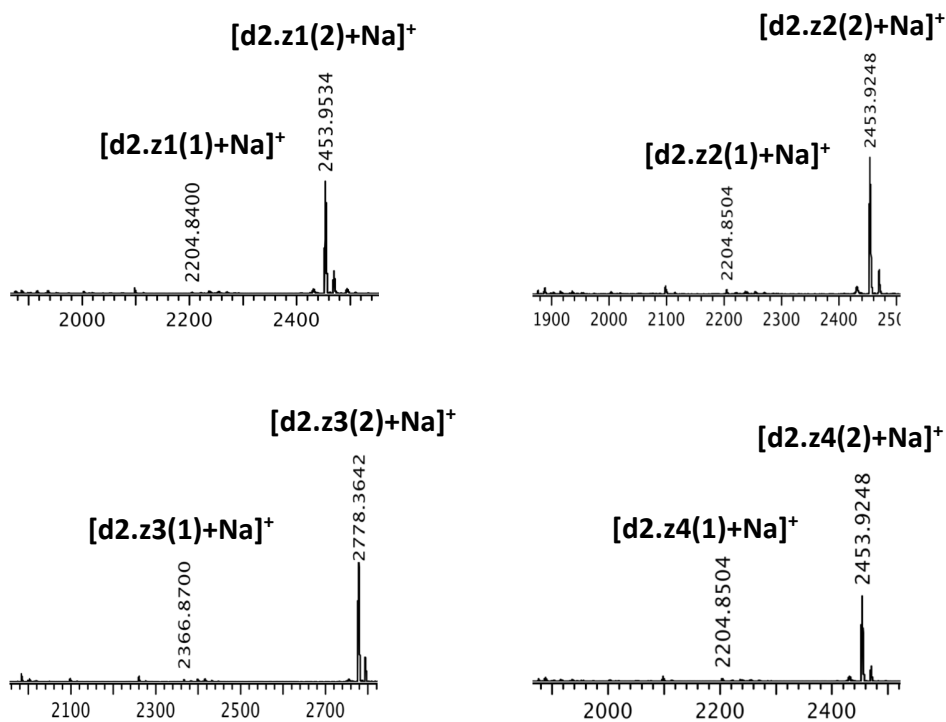


7.6 On-chip SPAAC on cyclooctyne-dendrons surfaces

- MALDI-TOF mass spectra detected after on-chip SPAAC with azidoethyl glucosides (**z1-z4**) on MONO-cyclooctyne surface (**d1**)

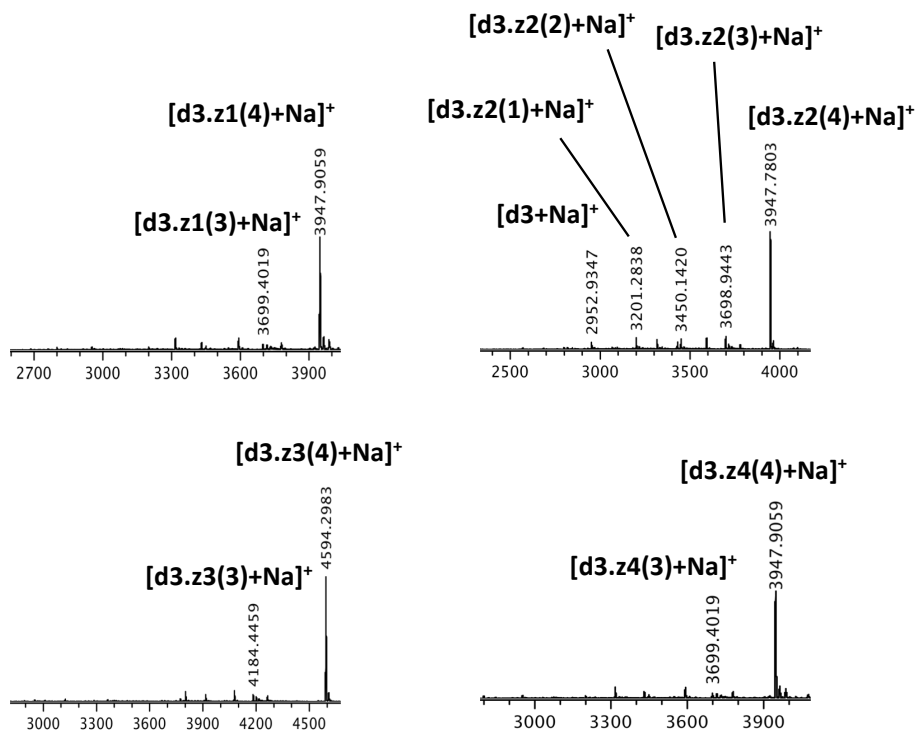


- MALDI-TOF mass spectra detected after on-chip SPAAC with azidoethyl glucosides (**z1-z4**) on BI-cyclooctyne surface (**d2**)



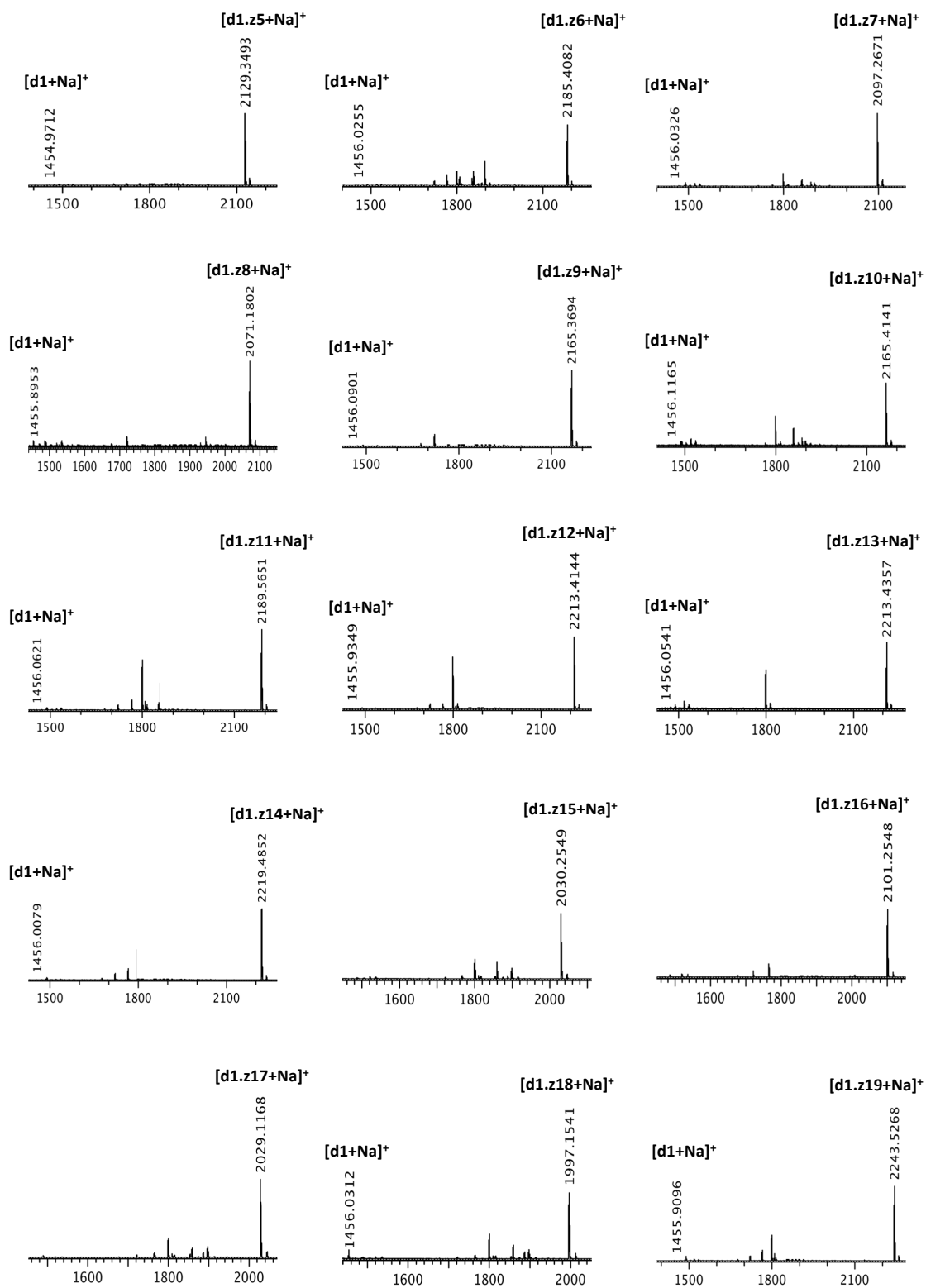
7. Appendix

- MALDI-TOF mass spectra detected after on-chip SPAAC with azidoethyl glucosides (**z1-z4**) on TETRA-cyclooctyne surface (**d3**)

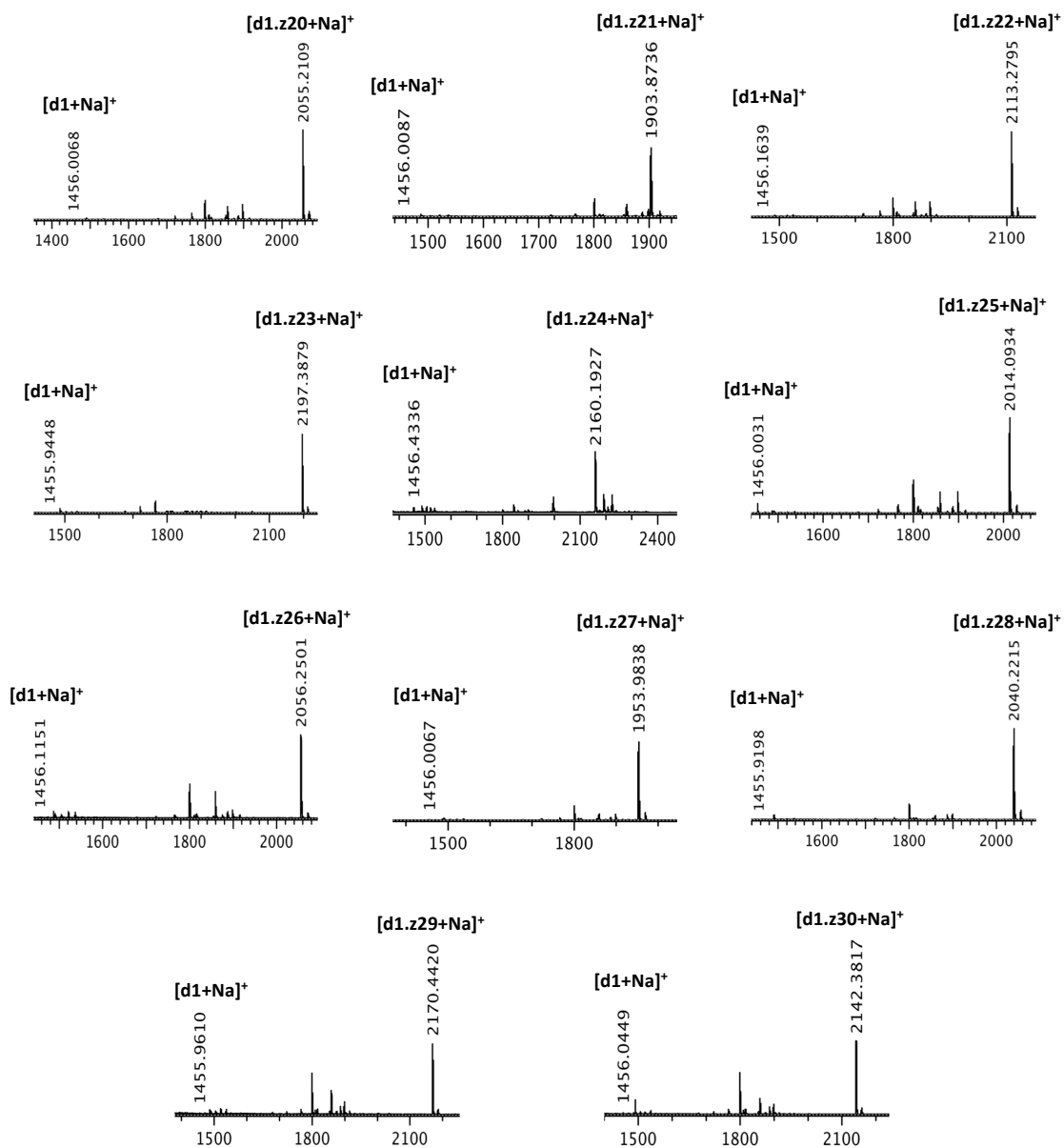


7. Appendix

- MALDI-TOF mass spectra detected after on-chip SPAAC with glycomimetic azides **z5-z30** on MONO-cyclooctyne surface (**d1**)

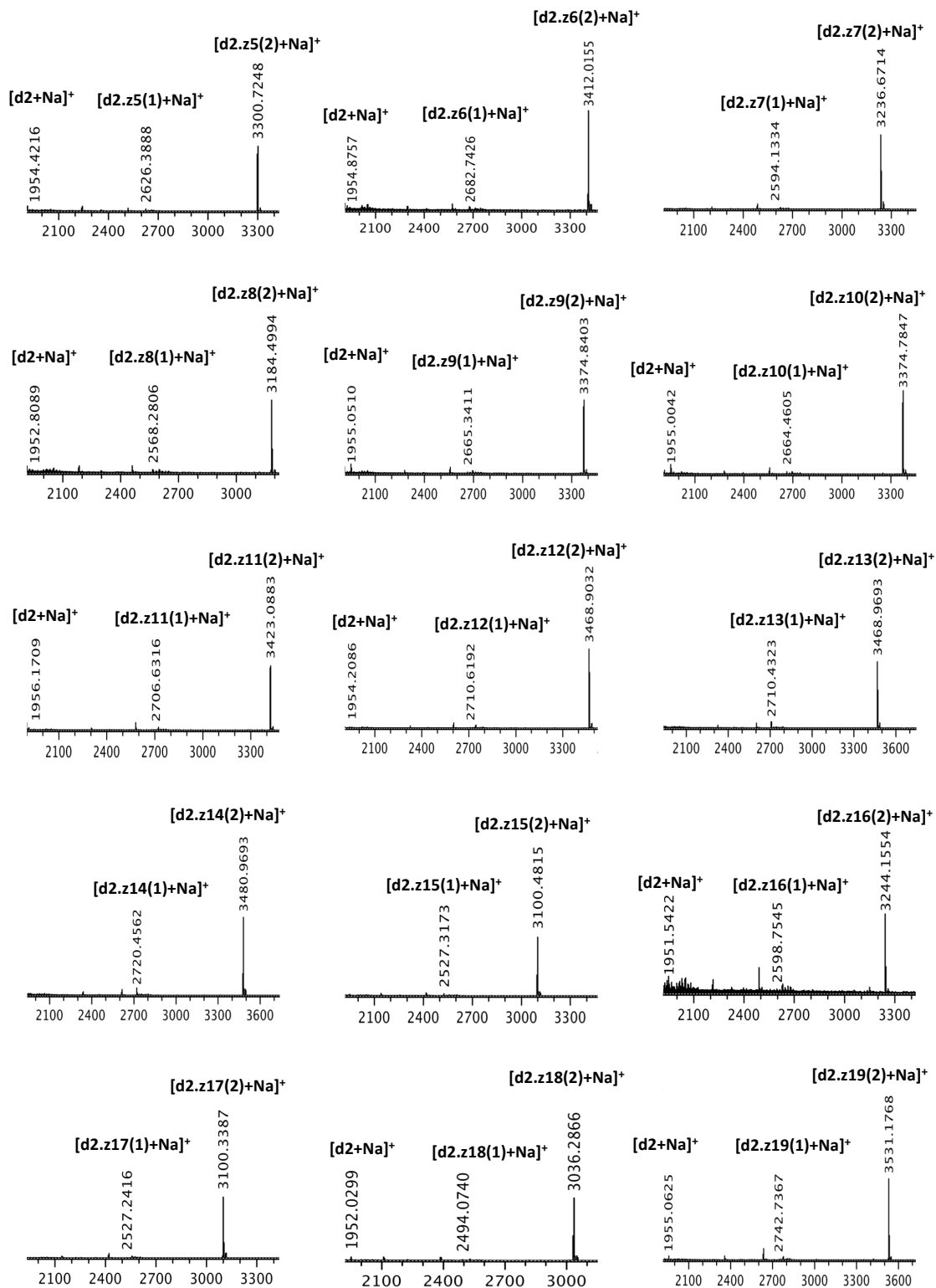


7. Appendix

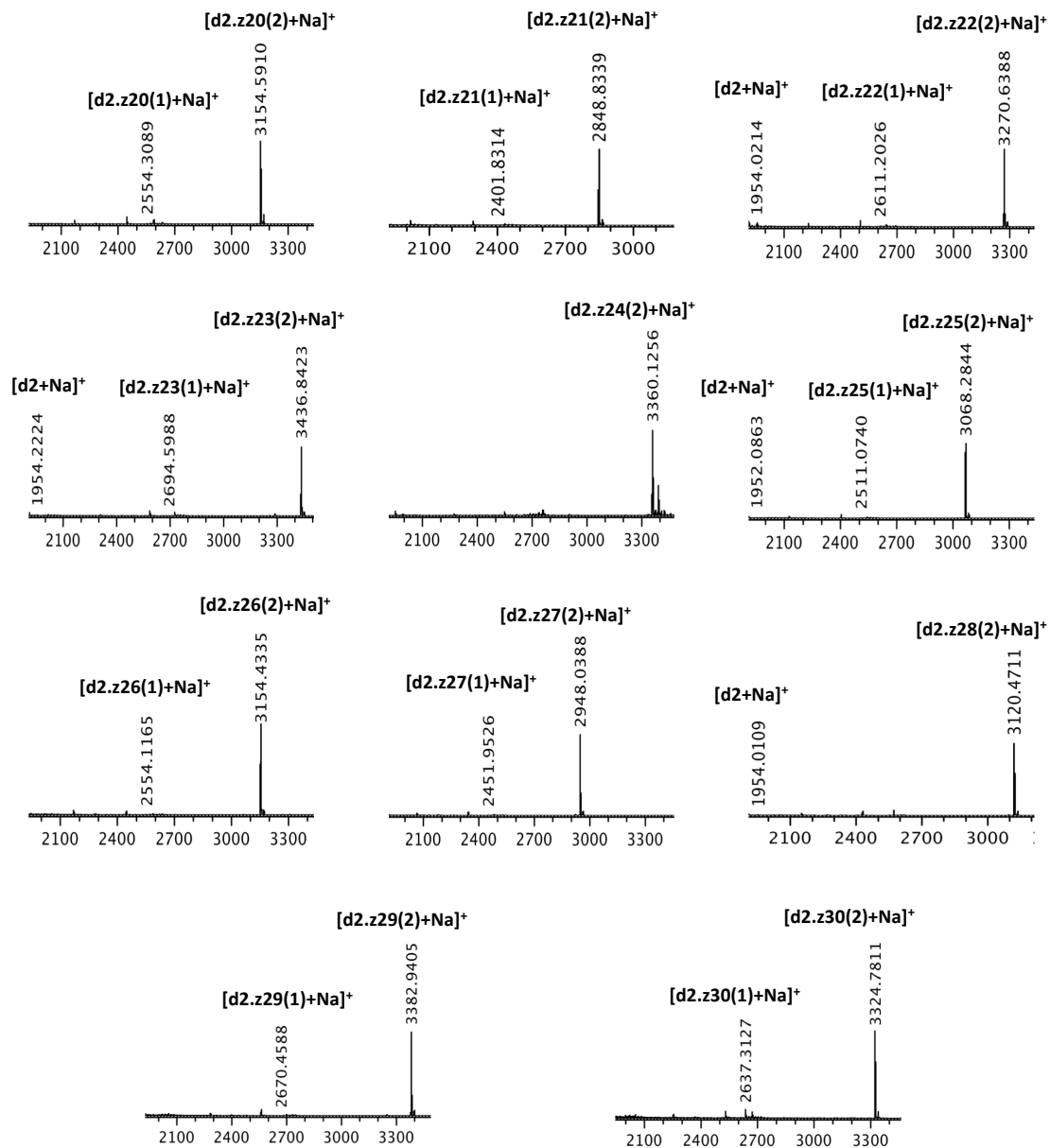


7. Appendix

- MALDI-TOF mass spectra detected after on-chip SPAAC with glycomimetics azides **z5-z30** on BI-cyclooctyne surface (**d2**)

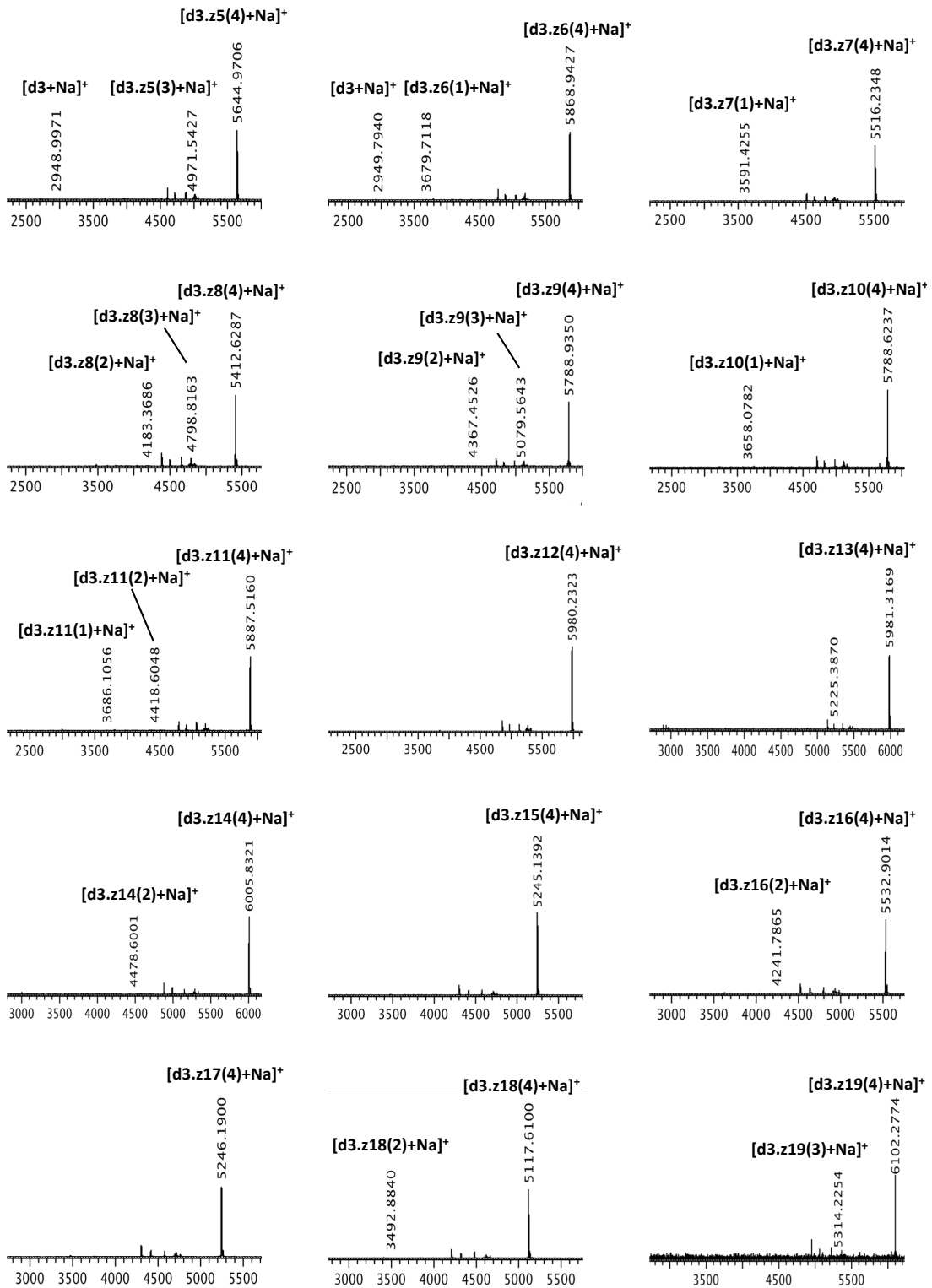


7. Appendix

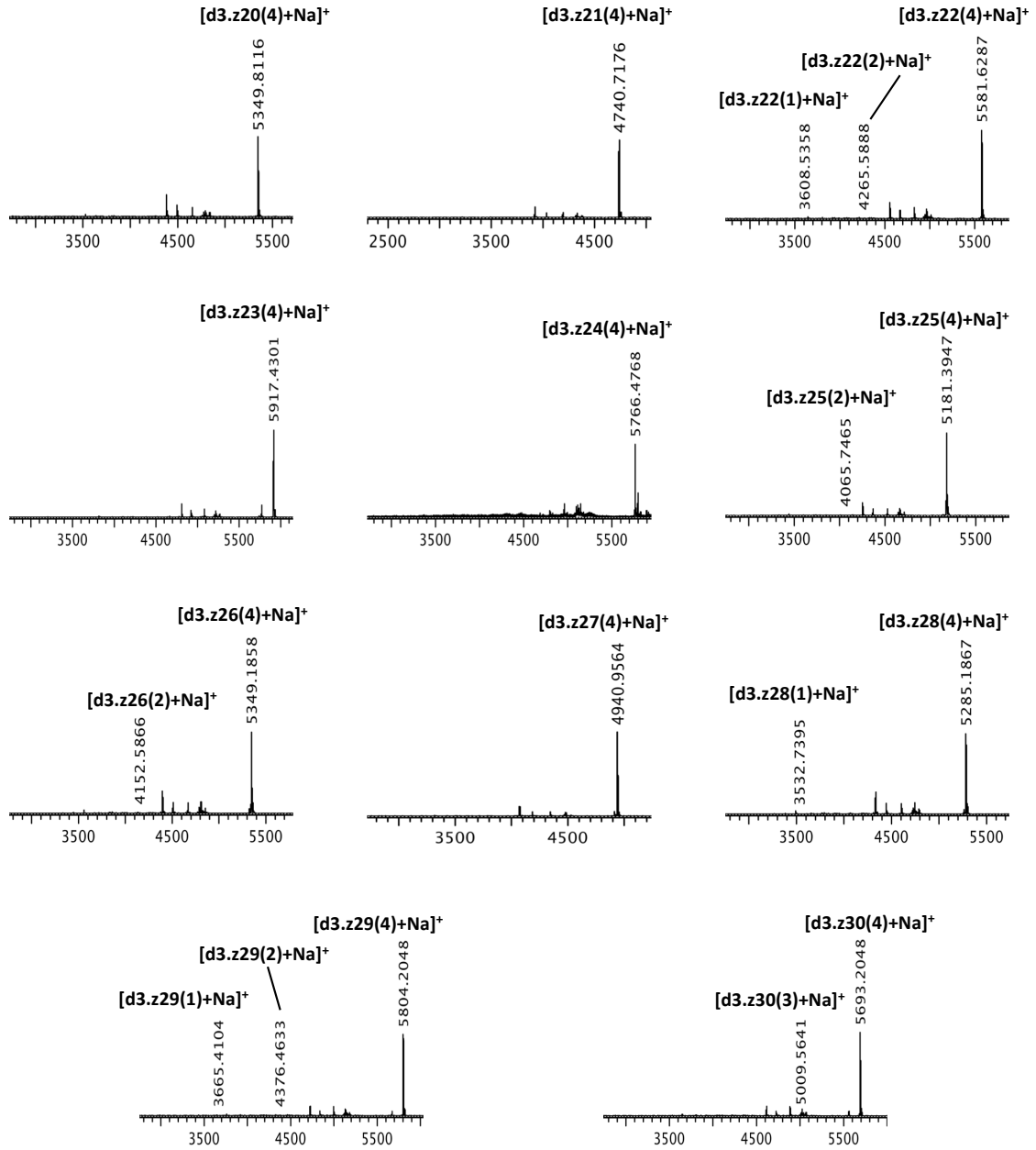


7. Appendix

- MALDI-TOF mass spectra detected after on-chip SPAAC with glycomimetics azides **z5-z30** on TETRA-cyclooctyne surface (**d3**)

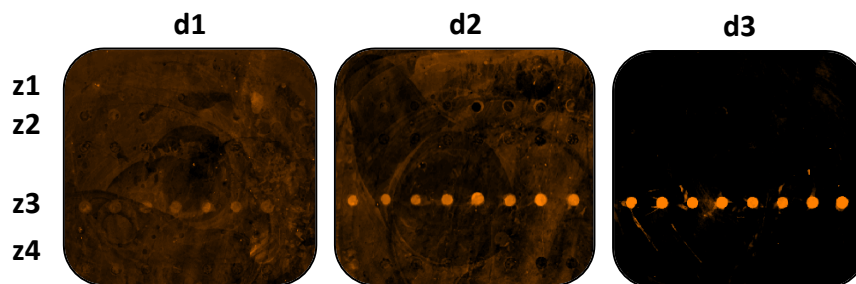


7. Appendix

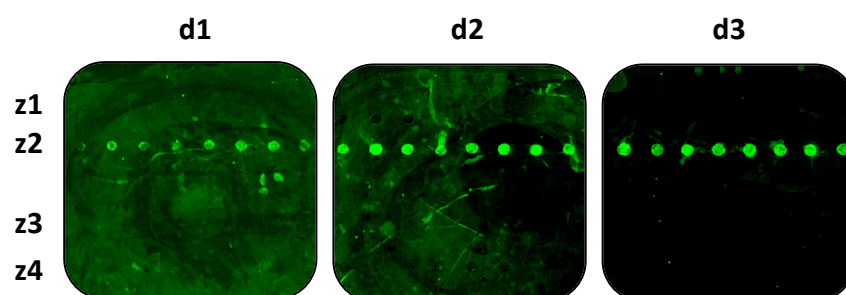


7.7 Binding assays of glycodendrons with fluorescently labeled lectins (Section 4.3)

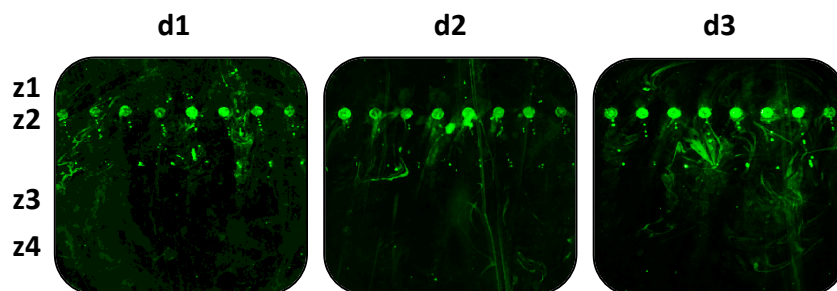
- Binding assays with *Pisum Sativum*-Alexafluor555 (50 μ g/mL, DOL=0.37)



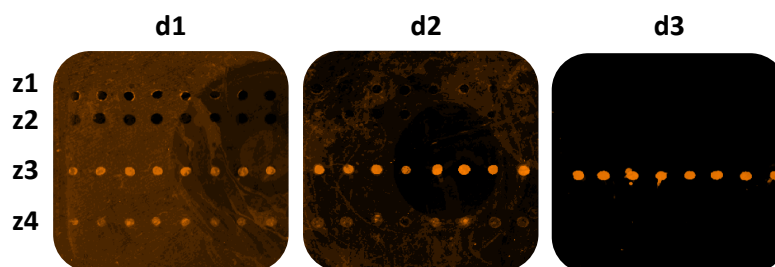
- Binding assays with *Wisteria floribunda*-Alexafluor647 (50 μ g/mL, DOL=0.71)



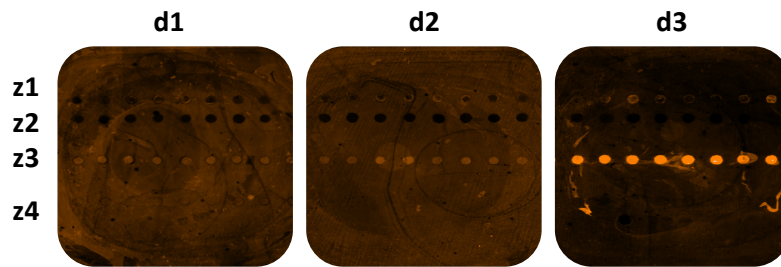
- Binding assays with *Pseudomonas Aeruginosa* I-Alexafluor555 (50 μ g/mL, DOL=0.36)



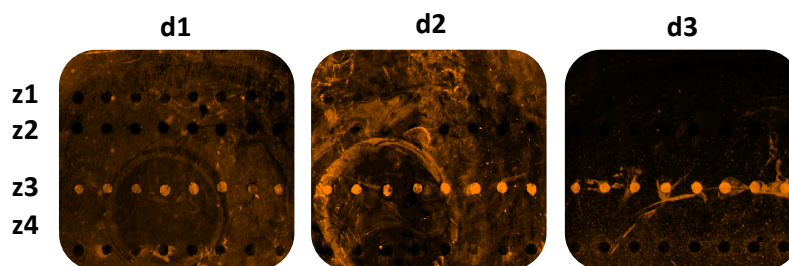
- Binding assays with *DCR ECD*-Cy3 (10 μ g/mL, DOL=0.40)



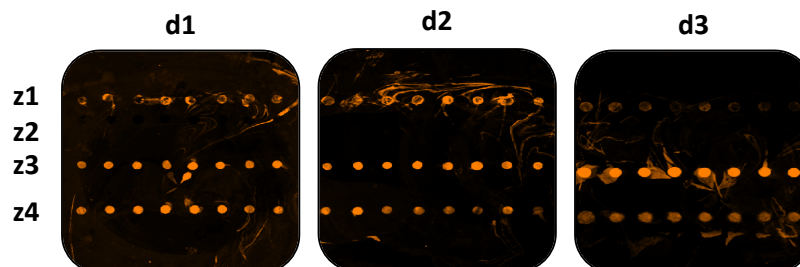
- Binding assays with *Langerin ECD-Cy3* (10 μ g/mL, DOL=0.70)



- Binding assays with *Dectin2 ECD-Cy3* (10 μ g/mL, DOL=0.40)

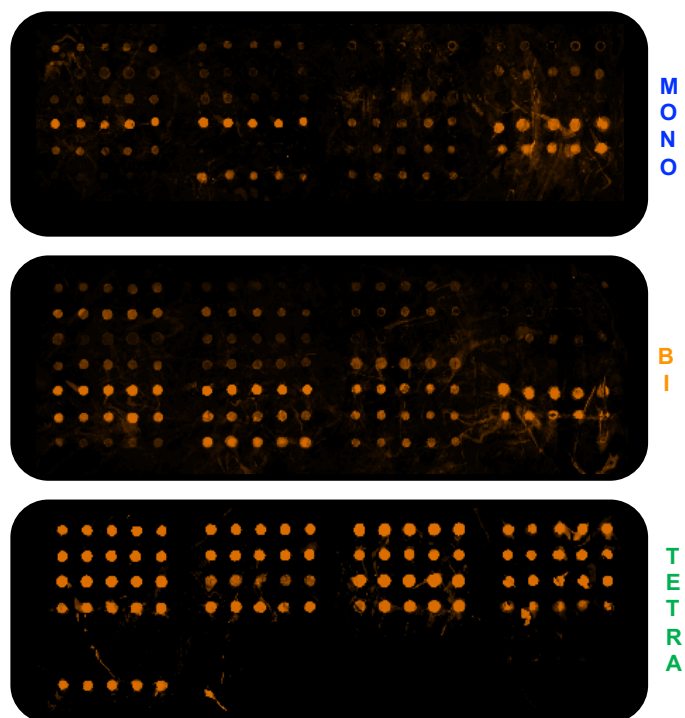


- Binding assays with *DC SIGN ECD-Cy3* (10 μ g/mL, DOL=0.95)

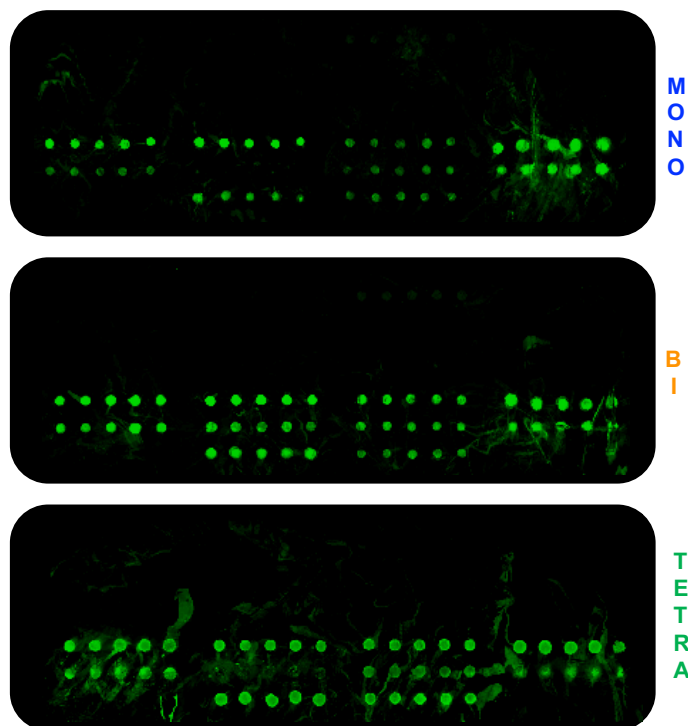


7.8 Binding assays of glycomimetic dendrons with fluorescently labeled lectins
(Section 4.4)

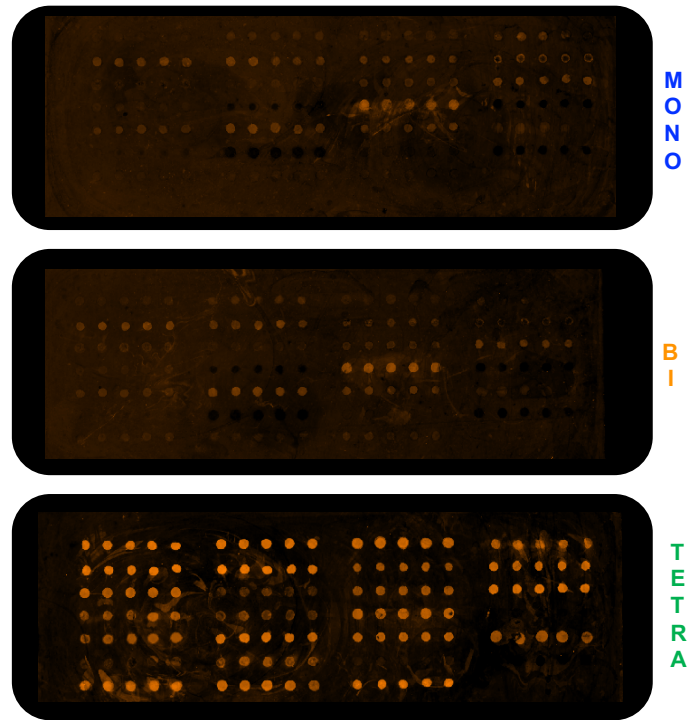
- Binding assays with Concanavalin A-Alexafluor647 (10 $\mu\text{g}/\text{mL}$, DOL=0.51)



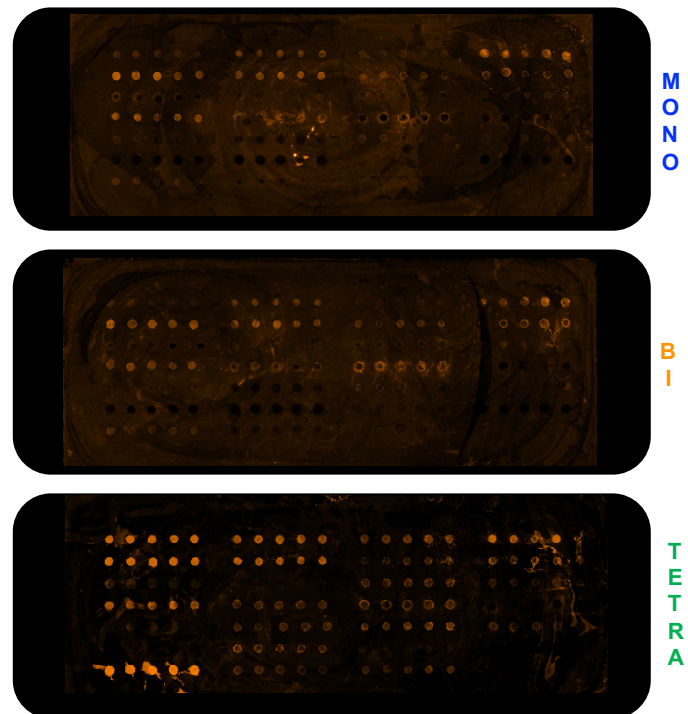
- Binding assays with Aleuria Aurantia Lectin-Alexafluor647 (1 $\mu\text{g}/\text{mL}$, DOL=1.07)



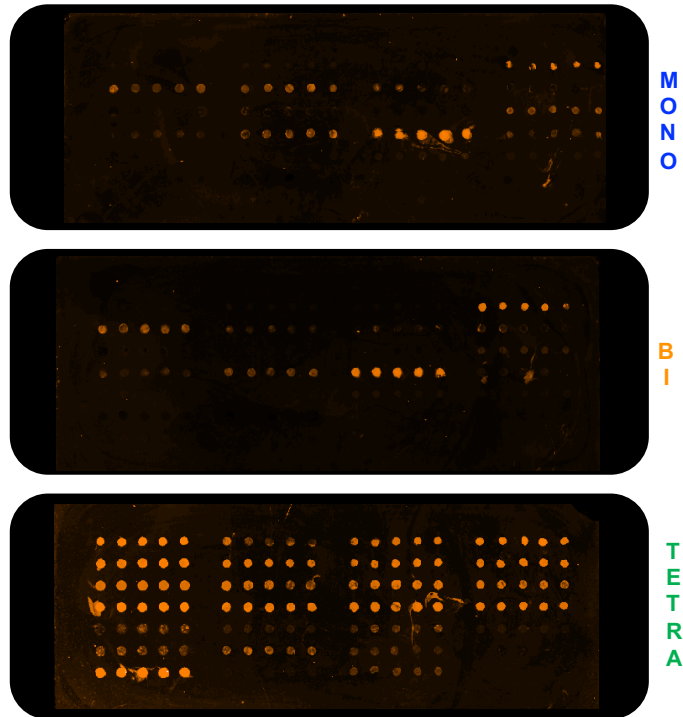
- *Binding assays with Langerin ECD-Cy3 (10 µg/mL, DOL=0.70)*



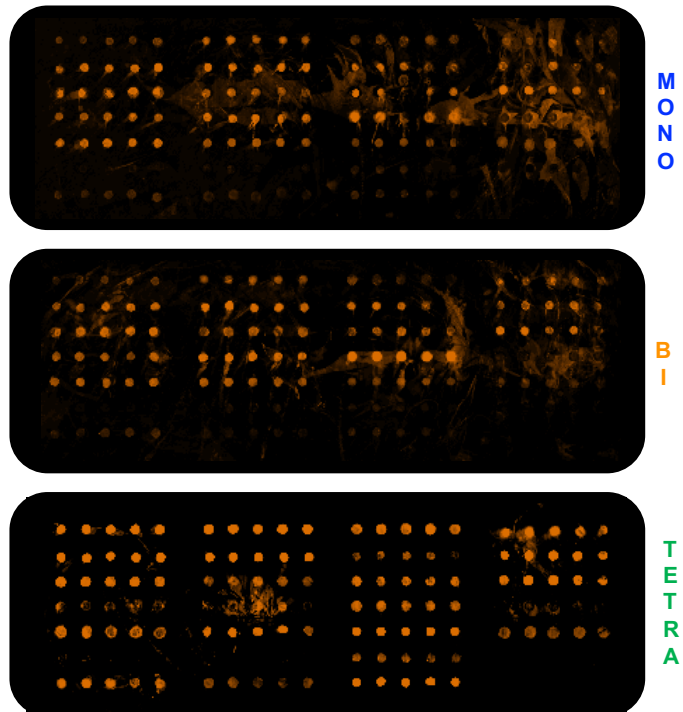
- *Binding assays with Dectin-2 ECD-cy3 (10 µg/mL, DOL=0.40)*

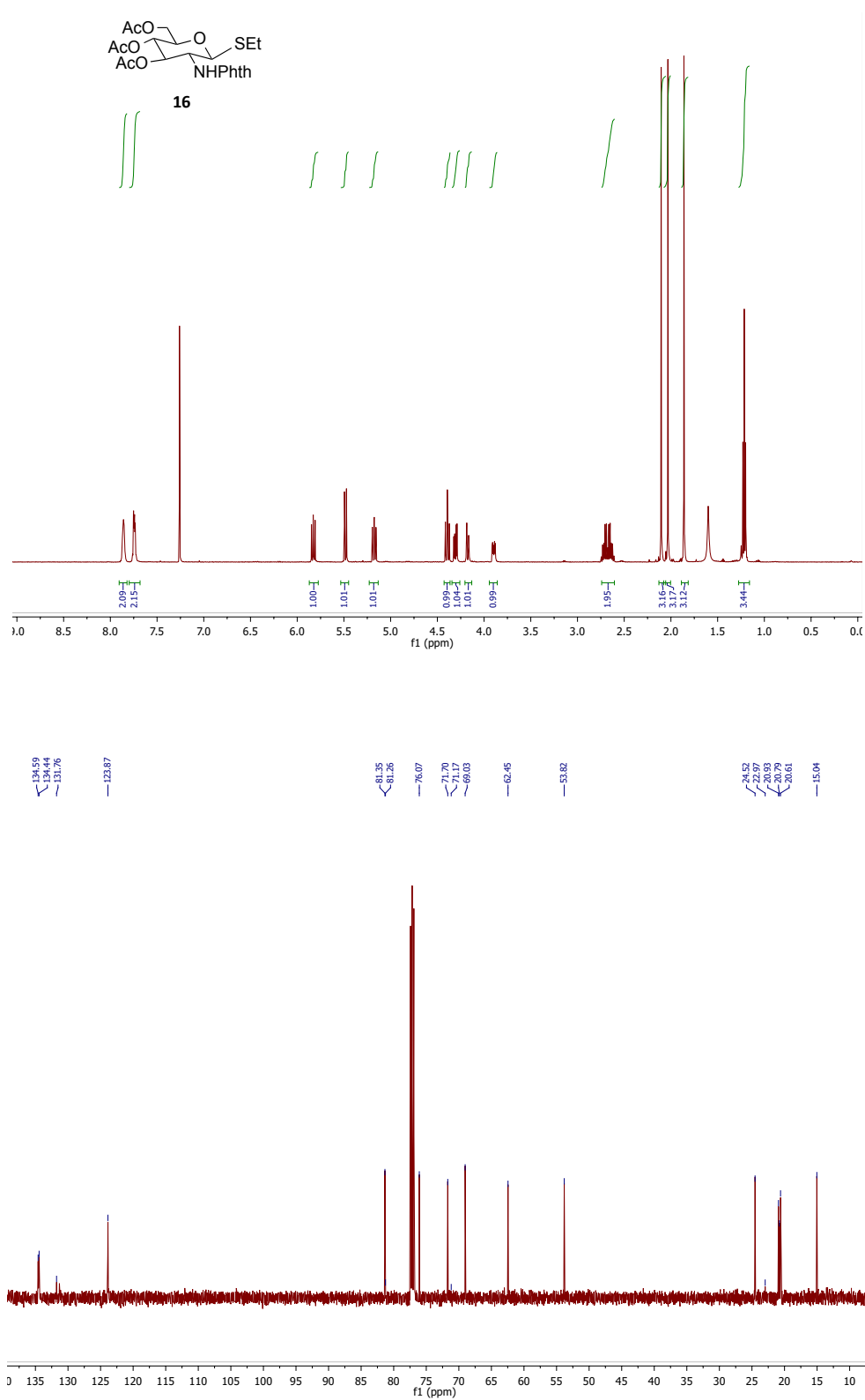


- *Binding assays with hMBL-Alexafluor555 (10 µg/mL, DOL=0,70)*

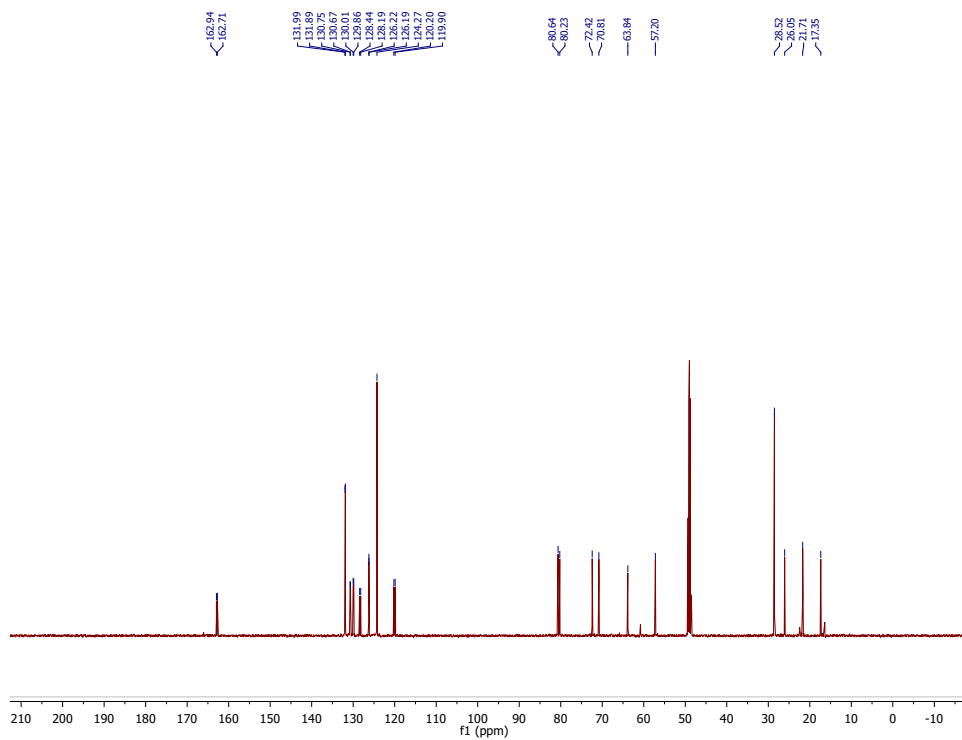
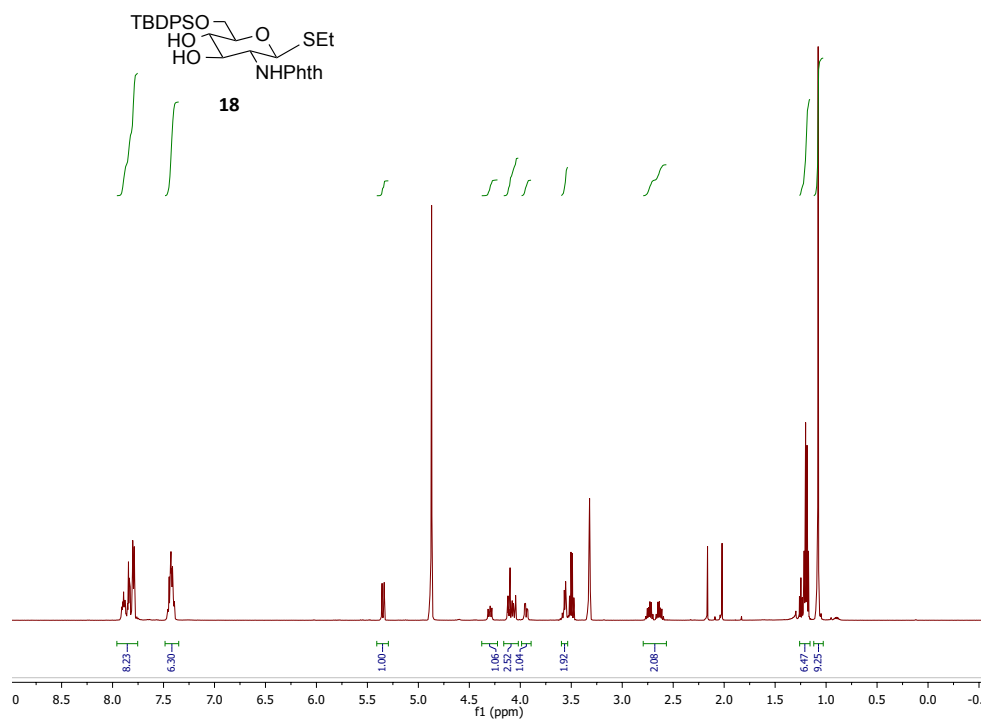


- *Binding assays with DCSIGN ECD-Cy3 (10 µg/mL, DOL=0,95)*

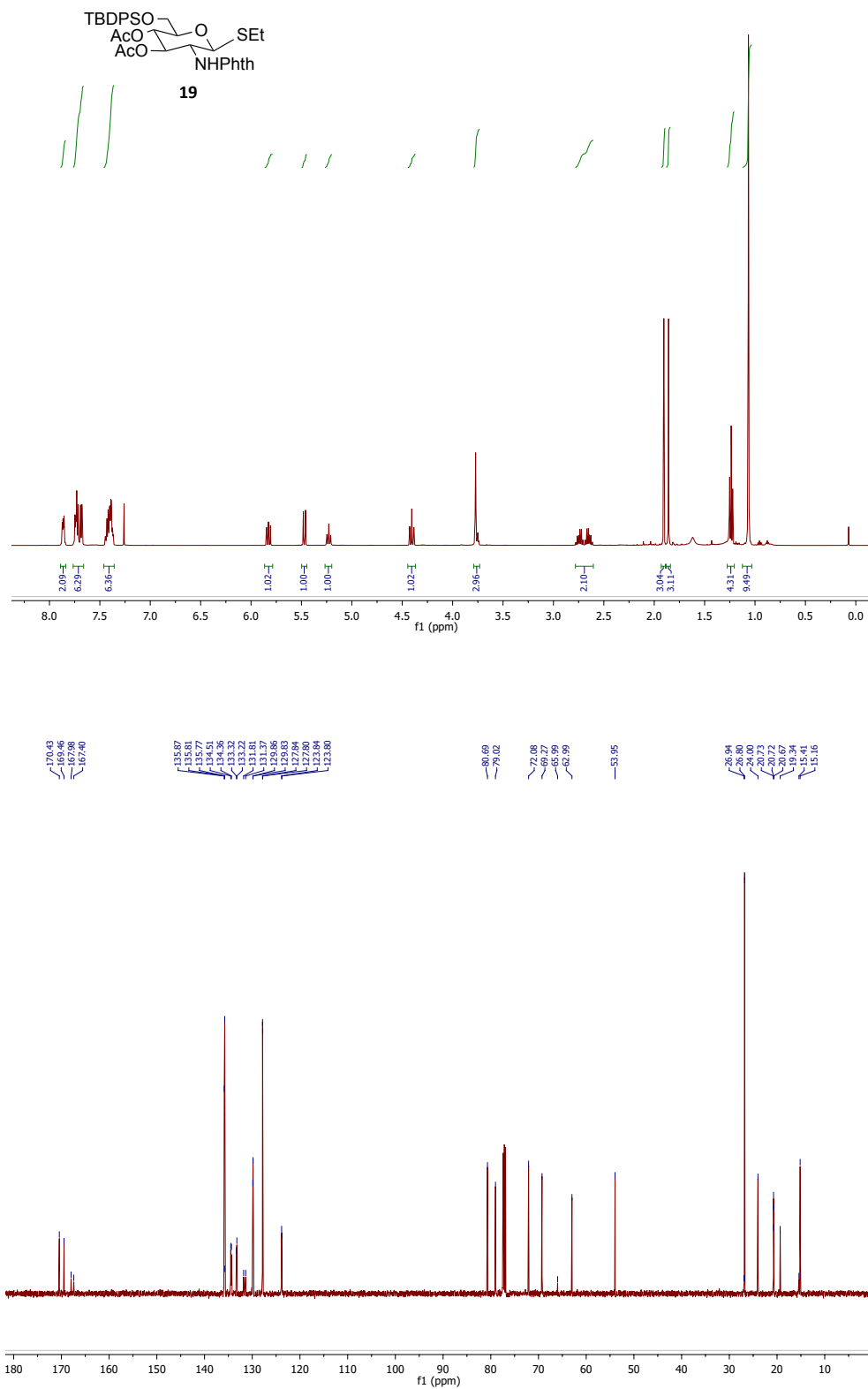


➤ Tioethyl 3,4,6-*O*-acetyl-2-phthalimido- β -D-glucopyranoside (**16**):

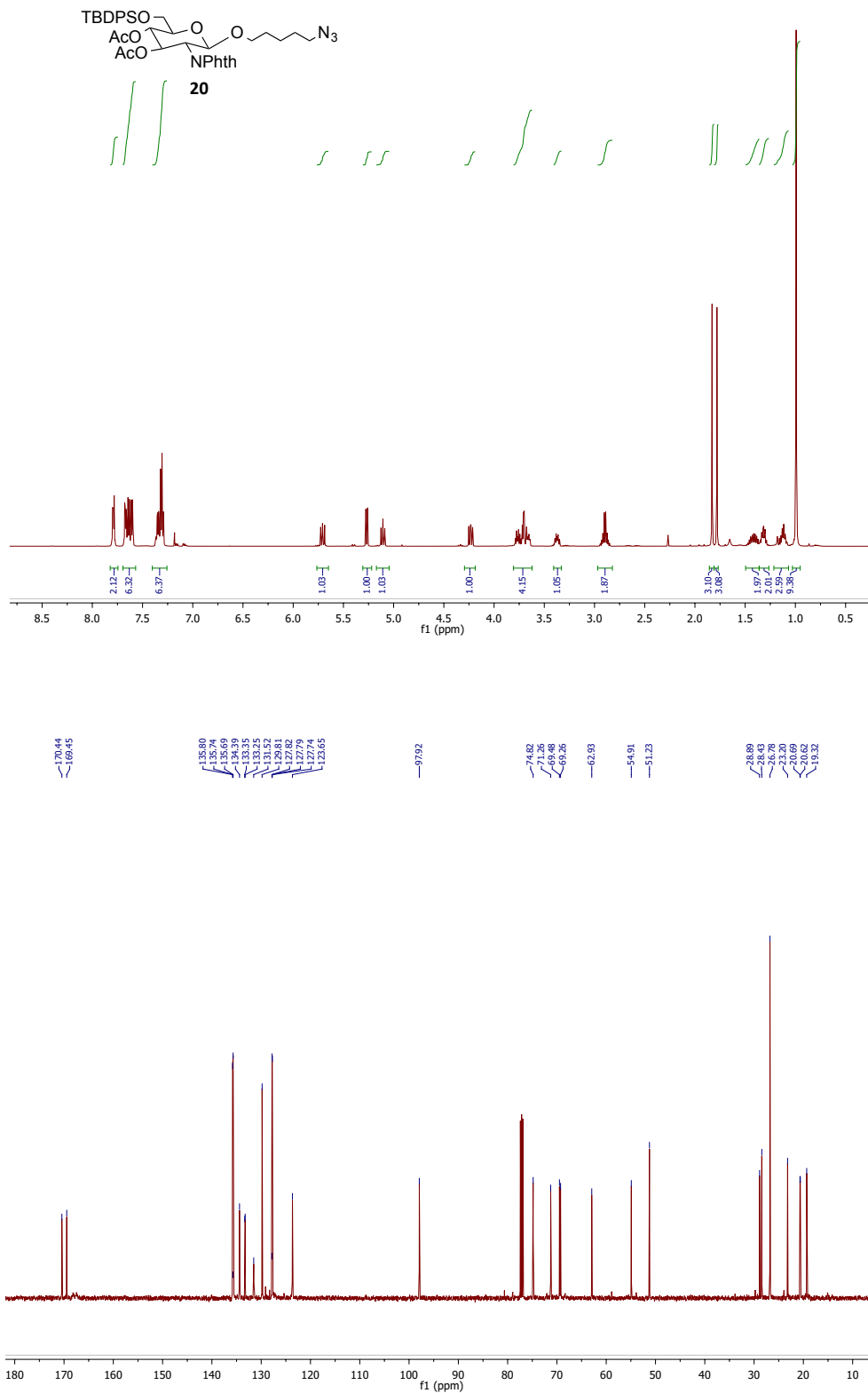
- Tioethyl 2-phthalimido-6-*tert*-butyldiphenylsilyl- β -D-glucopyranoside (18):



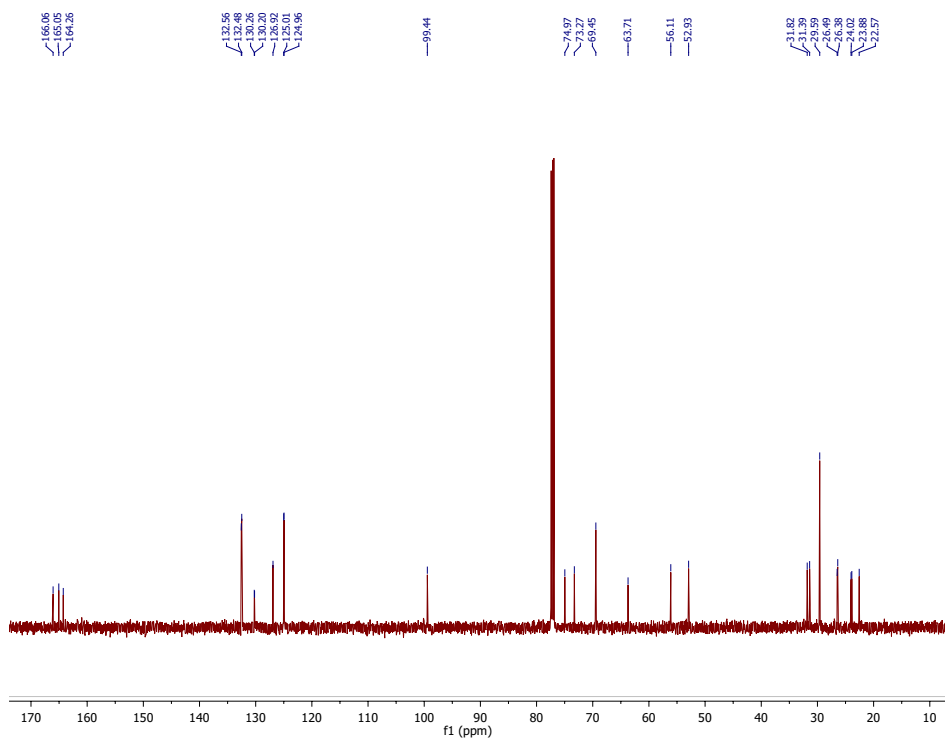
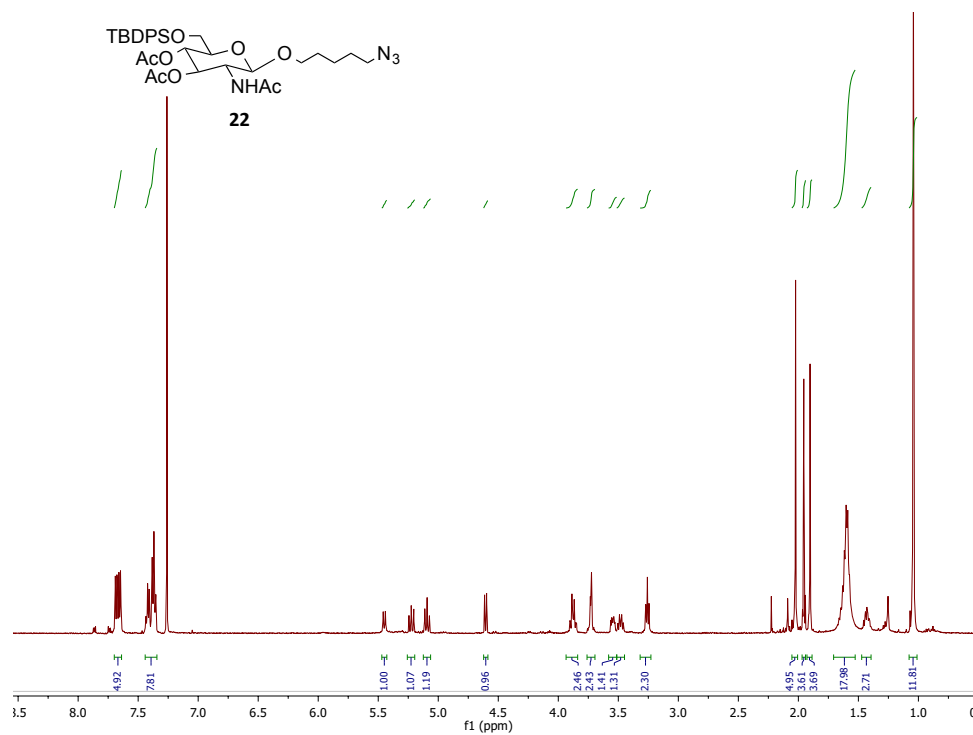
- Tioethyl 3,4-*O*-acetyl-2-phthalimido-6-*tert*-butyldiphenylsilyl- β -D-glucopyranoside (**19**):

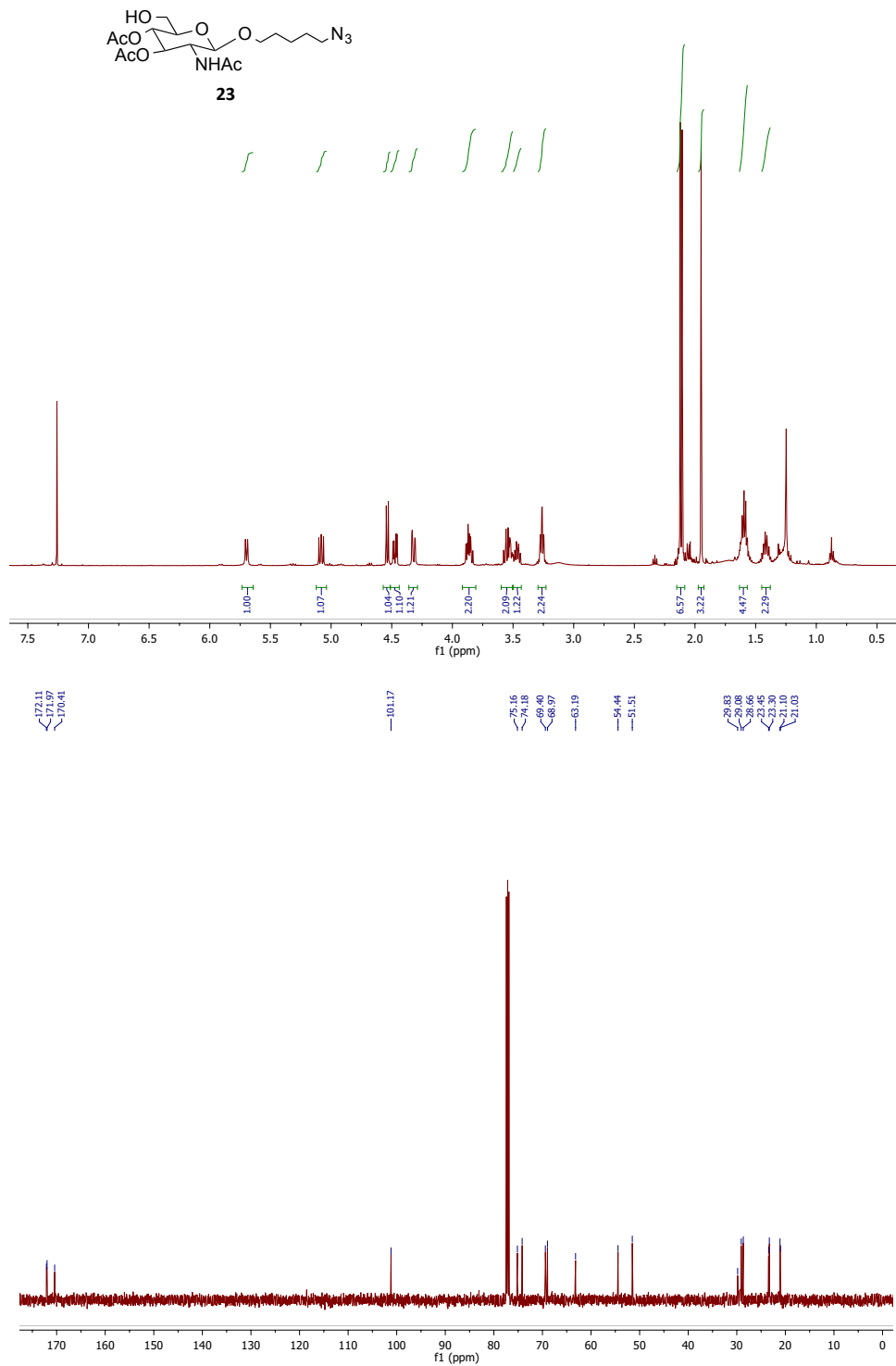


- Azidopentyl 3,4-*O*-acetyl-2-phthalimido-6-*tert*-butyldiphenylsilyl-β-D-glucopyranoside (**20**):

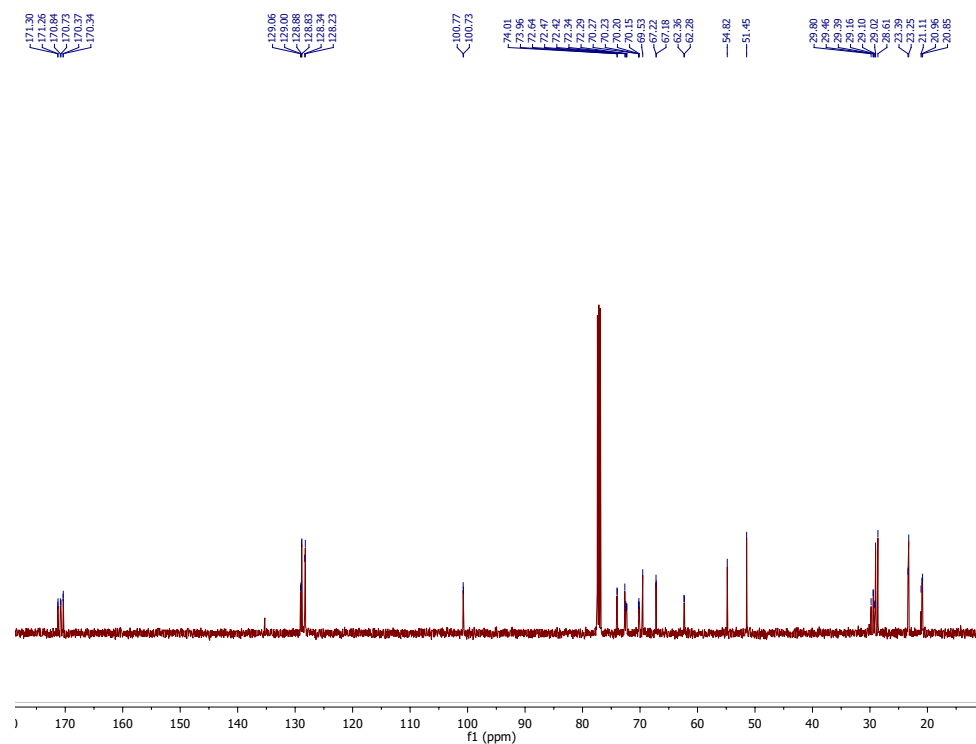
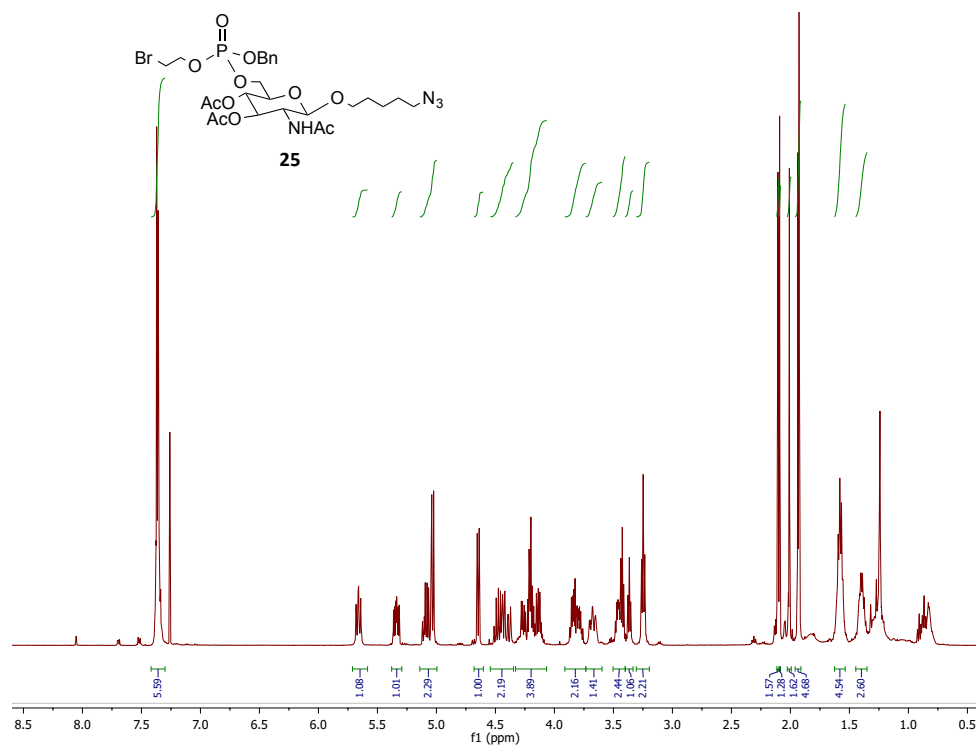


- Azidopentyl 3,4-*O*-acetyl-2-*N*-acetyl-6-*tert*-butyldiphenylsilyl- β -D-glucopyranoside (**22**):

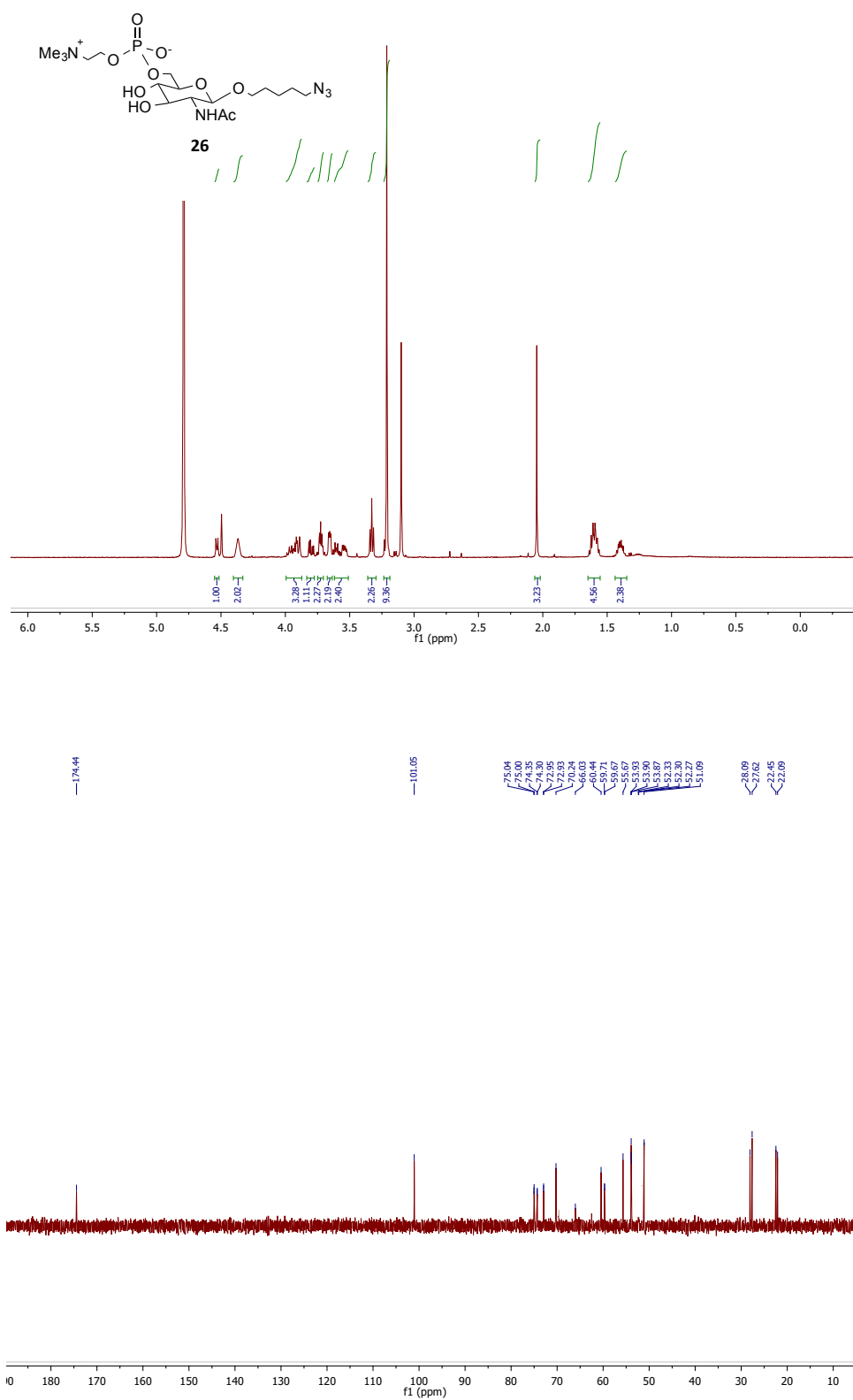


➤ Azidopentyl 3,4-*O*-acetyl-2-*N*-acetyl- β -D-glucopyranoside (**23**):

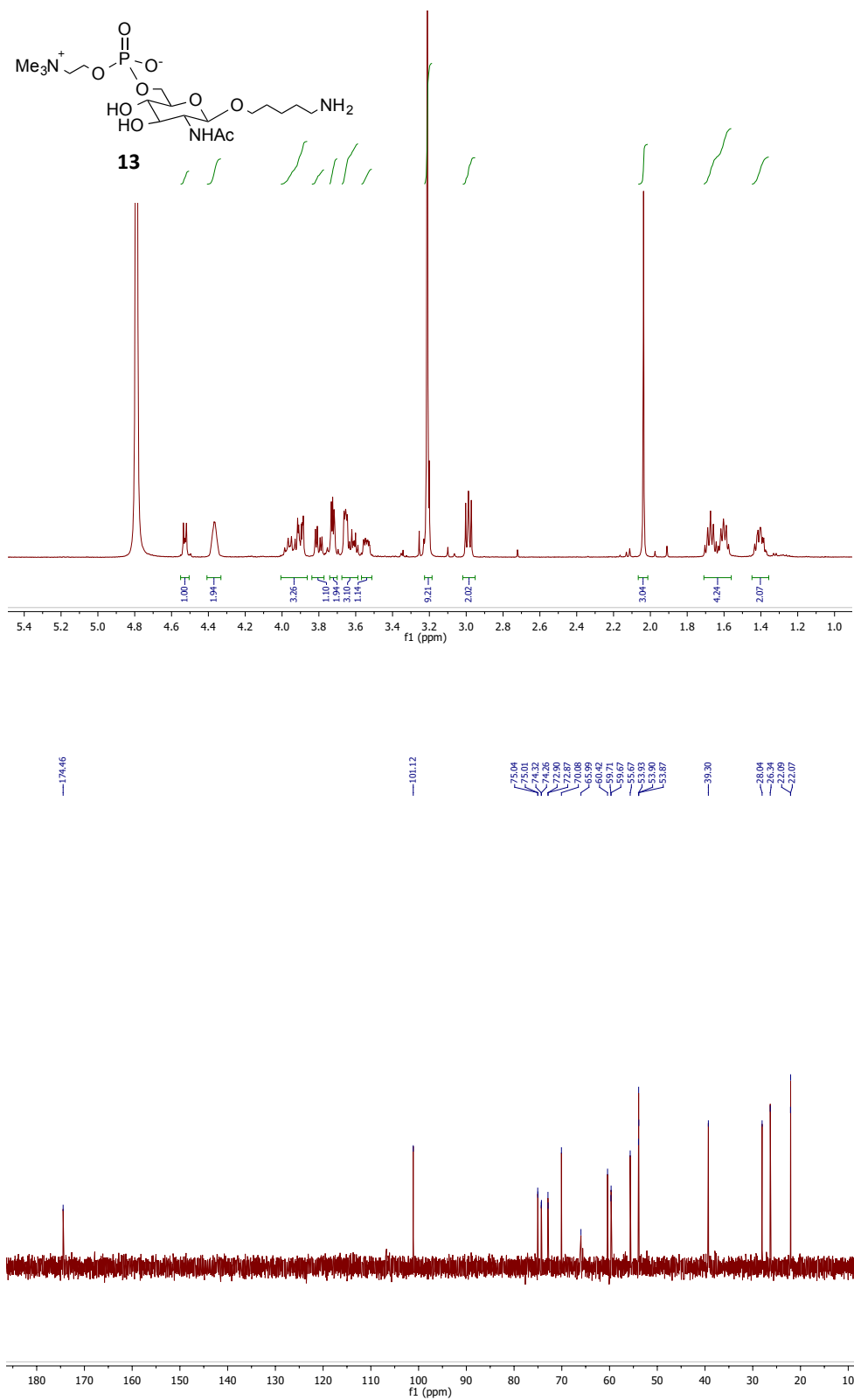
- *O*-((benzyloxy)(2-bromoethoxy)phosphoryl)-azidopentyl 3,4-*O*-acetyl-2-*N*-acetyl- β -D-glucopyranoside (**25**):



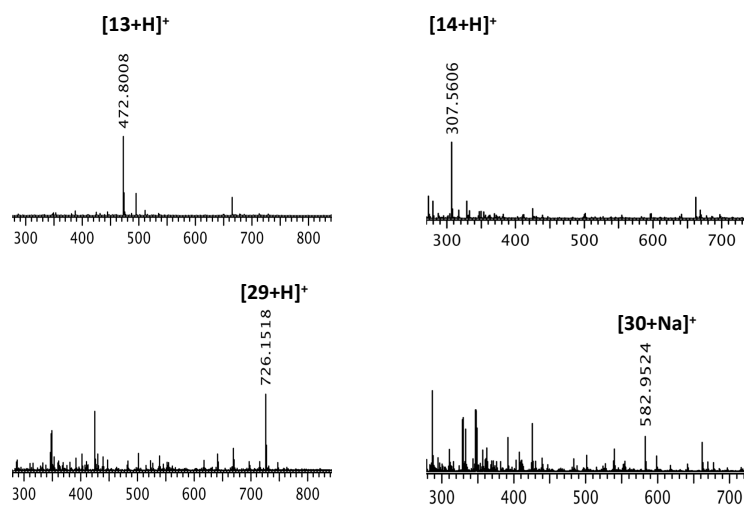
➤ Phosphatidylcholine azido-pentyl 2-N-acetyl-β-D-glucopyranoside
(26):



➤ Phosphatidylcholine amino-pentyl 2-N-acetyl-β-D-glucopyranoside (**13**):



- MALDI-TOF mass spectra of compounds **13** and **14** before and after performing activation with DSS-activated linker



- MALDI-TOF mass spectra of OVA-Alexafluor647 and OVA-based glycoconjugates:

